Fireside corrosion in oxy-fuel environments and the influence of fuel and ash characteristics on corrosion and deposition

Toor-E-Aiman Rizvi

Submitted in accordance with the requirements for the degree of

Doctor of Philosophy

The University of Leeds

Energy Technology and Innovation Institute

School of Chemical and Process Engineering

October, 2014

The candidate confirms that the work submitted is her own, except where work which has formed part of jointly-authored publications has been included. The contribution of the candidate and the other authors to this work has been explicitly indicated below. The candidate confirms that appropriate credit has been given within the thesis where reference has been made to the work of others.

Some of the work presented in Chapter 5 and Chapter 6 of this thesis forms part of the following publication:

Rizvi, T., Xing, P., Pourkashanian, M., Darvell, L.I., Jones, J.M., Nimmo,W. 2015. Prediction of biomass ash fusion behaviour by the use of detailed characterization methods coupled with thermodynamic analysis. *Fuel*, 141, 275-284.

- The candidate (T.Rizvi) was responsible for performing the experimental and modelling work presented in this paper as well as preparing the first and second drafts of the paper.
- W.Nimmo and M. Pourkashanian were the candidate's supervisors.
- Dr. Nimmo helped in planning the experiments, gave feedback to improve the first and second drafts of the paper and finalized the document for submission.
- J. Jones was in charge of the laboratory while P.Xing and L.Darvell instructed the candidate on the STA equipment.

Some of the work presented in Chapter 4 of this thesis forms part of the following paper submitted for publication:

Rizvi, T., Pourkashanian, M., Nimmo, W. 2014. A lab-scale study on the influence of SO_2 and deposits on fireside corrosion in oxy-fuel environments. *Energy and Fuels.* (Submitted).

- The candidate (T.Rizvi) was responsible for performing the experimental and modelling work presented in this paper as well as preparing the first and final drafts of the paper.
- W.Nimmo and M. Pourkashanian were the candidate's supervisors.
- Dr. Nimmo helped in planning the experiments, gave feedback to improve the first draft of the paper and finalized the document for submission.

Publications

Following is a list of outputs/publications based on this work:

Rizvi, T., Pourkashanian, M., Nimmo, W. 2011. Fireside corrosion in pulverised fuel boilers. (Oral Presentation to Drax Power Limited).

RizvI, T., Pourkashanian, M., Nimmo, W. 2014. Effect of gas and deposit composition on corrosion in oxy-fuel environments. 35th International Symposium on Combustion, San Franciso, California USA. (Poster Presentation).

Rizvi, T., Pourkashanian, M., Nimmo, W. 2014. Corrosion in oxy-fuel environments and the effect of coal and biomass ash deposits. 10th European Conference on Coal Research and its Applications, Hull, UK. (Oral Presentaion).

Rizvi, T., Xing, P., Pourkashanian, M., Darvell, L.I., Jones, J.M., Nimmo,W. 2015. Prediction of biomass ash fusion behaviour by the use of detailed characterization methods coupled with thermodynamic analysis. *Fuel*, 141, 275-284.

Rizvi, T., Pourkashanian, M., Nimmo, W. 2014. A lab-scale study on the influence of SO_2 and deposits on fireside corrosion in oxy-fuel environments. *Energy and Fuels.* (Submitted).

Dedication

To my parents-in-law, Uncle Zahoor and Mona Khala for their affection, kindness and remarkable support (both moral and financial) throughout the period of my post graduate study.

Acknowledgements

Firstly I thank Allah, The Most Gracious and Merciful, for His favours and endless blessings, without Whose help nothing would have been possible. May peace be upon His Messengers and upon Prophet Muhammad.

I would like to thank the University of Punjab for funding my PhD fees.

My earnest gratitude goes to Dr.Bill Nimmo, my primary supervisor, for his time, expert advice, immense support and encouragement, as well as the chance to learn from his vast experience and expertise. His door was always open for help and encouragement to keep me going. I am also thankful to my co-supervisors Dr.Lin Ma and Prof. Pourkashanian. I am particularly grateful to Dr.Kevin Hughes for introducing me to Chemkin and Factsage. Special thanks go to Mr.Robert Harris, Mr.Tarsem Hunjan and Mr.S.Terry for their technical assistance in setting up the corrosion rig and lending a hand in its subsequent maintenance whenever required. I would also like to acknowledge Mr.S.Lloyd and Dr.A.Cunliffe from the ERI Analytical Laboratories and Mr.J. Harrington and Mr.S.Micklethwaite from the Leeds Electron Microscopy centre (LEMAS) for their technical help. I am grateful to Dr.Leilani Darvell for the use of STA equipment.
Thanks are also due to Mr.Robert Ghent from Drax Power Limited.

I owe my lovely little boy, Ahmad, for his patience and understanding. I am indebted to my husband Asim for his love and appreciation. I would like to thank my sisters Naima, Asra, Hina and especially Zahra for seeing me through difficult times. This acknowledgement would be incomplete without thanking my dearest mum for her unconditional love and support. I would also like to make mention of my beloved dad, who had great aspirations for me and always believed in me.

Last but by no means least, I would like to thank all of my friends, relatives and well-wishers who extended to me their goodwill and hospitality during my stay at Leeds.

Abstract

The development of advanced techniques (such as carbon capture and storage) for future power plants and the implementation of retrofit technologies to existing ones (like biomass co-firing) in order to reduce pollutant emission, has raised several concerns for the power industry. One such problem, which also forms the basis of this thesis, is the effect of these measures on corrosion and deposition of the boiler heat transfer surfaces. This research work can be divided into two parts. The first part involved studying the corrosion behaviour of a typical waterwall and a superheater material under simulated oxy-fuel environments with and without the influence of an ash deposit. A custom-built, laboratory scale, corrosion rig with the ability to simulate a range of flue gas compositions and temperatures, in addition to generating a heat flux through the specimen, was set up for this purpose. The second part of this work deals with evaluating the properties of a UK power station coal and four biomass samples with the help of laboratory techniques and thermodynamic modelling in order to predict their fusion and deposit forming tendencies in combustion systems. A series of experiments were performed on the corrosion rig to assess the influence of individual variables on the rate of corrosion. The results indicated that the increased concentration of SO_2 in oxy fuel combustion due to recycling of the flue gas, can lead to an increase in corrosion rates especially in the presence of reactive alkali containing deposits. Under the conditions studied, the presence of a biomass ash deposit aggravated the corrosive propensity of the environment while coal ash lessened it. With regard to predicting the fusion behaviour of different ashes, the standard ash fusion tests proved inadequate for explaining the relationship between high alkali constituents in biomass ash and the expected higher slagging and fouling tendencies. Simultaneous thermal analysis was more useful in assessing the physical & chemical changes taking place in the ash. Prediction of the fuel behaviour using FactSage thermodynamic analysis showed that ash melting commences at much lower temperatures than those predicted from laboratory techniques. This would help to explain the increased risk of deposition and corrosion linked with burning high alkali containing fuels.

Table of Contents

List of Figures

List of Tables

Abbreviations

GHG   Greenhouse gas

CCS   Carbon Capture and Storage

IGCC   Integrated Gasification Combined Cycle

FGR   Flue gas recycle

PCC   Pulverised coal combustion

UNFCC   United Nations Framework convention on climate change

GNP   Gross National Product

PF   Pulverised fuel

GFC   Gas Flow Controller

T   Temperature (^{0}C)

p vapour pressure (mmHg)

q heat flux (kWm^{-2})

k   thermal conductivity (Wm^{-1}K^{-1})

MS   Mild steel

SS   Stainless steel

SEM   Scanning Electron Microscopy

EDX   Energy Dispersive X-ray

XRF   X-ray Fluorescence

TGA   Thermo gravimetric analysis

STA   Simultaneous Thermal Analysis

AFT   Ash Fusion Test

HHV   Higher heating value (MJkg^{-1})

FC   Fixed carbon

VM   Volatile matter

Chapter 1

Introduction

1.1 Thesis Overview

This thesis is divided into seven chapters. Chapter 1 provides a general introduction to power generation and material issues. Chapter 2 comprises of a detailed literature review pertaining to fireside corrosion and deposition problems and the possible mechanisms involved. Chapter 3 elucidates the procedures adopted for the setting up and operation of the corrosion rig and also gives details of associated experimental & analytical techniques employed for specimen preparation and analysis. Chapters 4, 5 and 6 are results and discussion chapters. Chapter 4 is based on the experiments performed on the corrosion rig. Chapter 5 presents details of fuel and ash characterization. Chapter 6 pertains to predicting the fuel ash behaviour using thermodynamic equilibrium modelling. Chapter 7 outlines the conclusions derived from the results obtained and also gives suggestions for future work.

1.2 Background

Power plants all over the world are under increasing pressures to enhance efficiency and reduce emissions. The global increase in demand for electricity is driven primarily by the rise in population, economic development and increase in standards of living (especially in the developing world). On the other hand, the drive to reduce emissions is necessitated by the increasing levels of greenhouse gases, (particularly CO_2), in order to avoid the most perilous effects of global

warming. The increasing energy demand along with stringent emission regulations poses several operational and economic problems for the power industry. One such problem is the corrosion and deposition experienced by various components of the power plant and will form the basis of this thesis.

1.3 Role of Fossil Fuels in Energy Generation and GHG emissions

Fossil fuels are the dominant source of energy generation in the world as shown in Fig.1 (IEA, 2012). However, fossil fuel combustion also contributes to the largest share of CO_2 emissions as shown in Fig.1.2. A reduction in CO_2 emissions from fossil fuel fired power plants is therefore required in order to meet the targets set by the United Nations Framework Convention on Climate Change (UN, 1998).
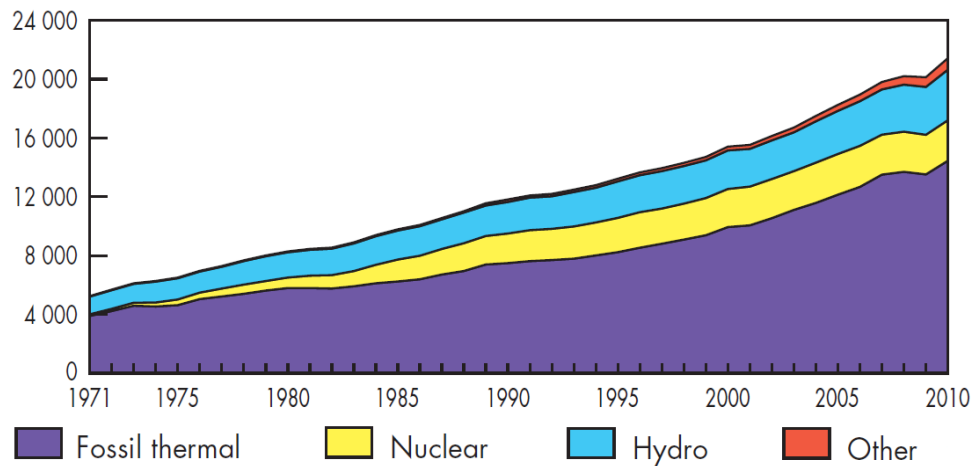
Figure 1.1 World electricity generation by fuel in TWh from 1971 to 2010 (IEA, 2012).
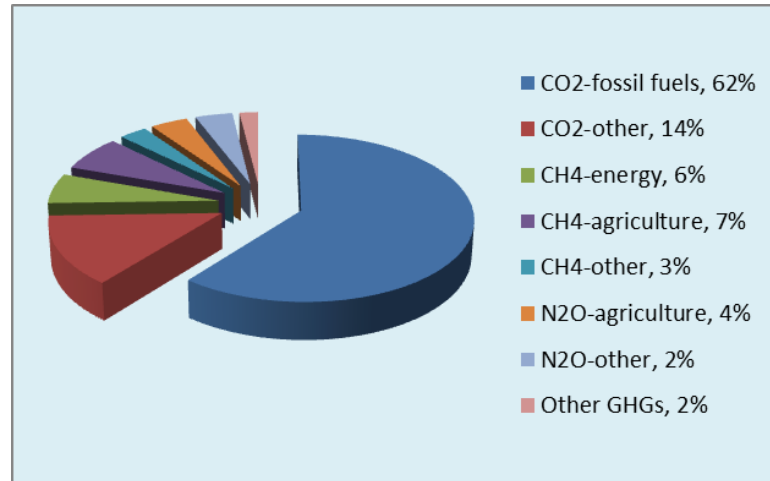
Figure 1.2 Global Anthropogenic GHG emissions for 2008 by type and source (Höök and Tang, 2013).

Carbon capture and storage (CCS) technologies, which involve the separation of carbon dioxide from large point sources and its subsequent transportation and storage in geological formations, has been proposed as an effective solution for the mitigation of CO_2 emissions The three options for CCS include pre-combustion capture, post-combustion capture and oxy-fuel combustion, illustrated in Figure 1.3. Pre-combustion capture is thought to be feasible for use with Integrated Gasification Combined Cycle (IGCC) power plants where coal is first gasified to produce a syngas containing CO, H_2 and CO_2. The CO is converted to CO_2 by the water gas shift reaction while the H_2 can be used for combustion. Post combustion capture aims at removing CO_2 from the flue gas of conventional pulverized fuel power plants. Recent developments and comparisons between these three technologies have been reviewed in considerable detail by several authors, including Gibbins and Chalmers (2008), Pires et al. (2011), Fu and Gundersen (2012).
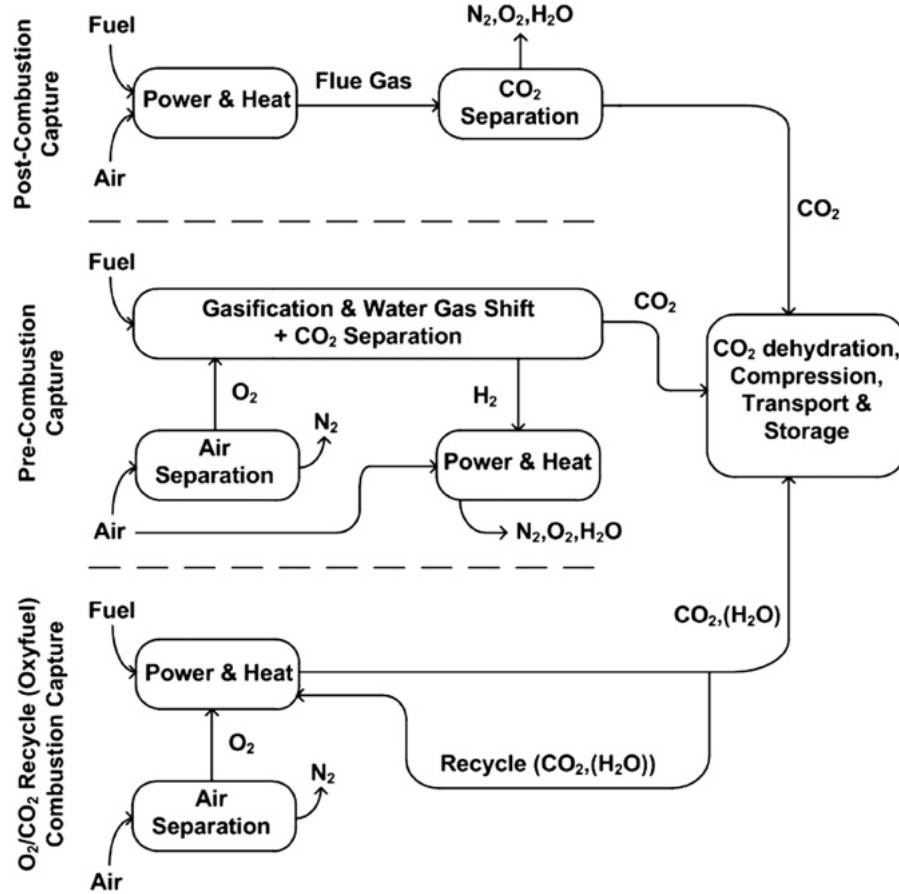
Figure 1.3 Possible, overall plant configurations for the three main categories of carbon capture technologies (Toftegaard et al., 2010).

1.4 Coal as a future energy source

Coal has been and continues to be the most widely used fuel for electricity generation, amounting to 40.6% of the total electrical energy generation in the world in 2010 as shown in Figure 1.4 (IEA, 2012). Figure 1.5 depicts the predicted increase in global coal consumption for electricity generation.

(a)

Hydro 21.0%
Other** 0.6%
Coal/peat 38.3%
Nuclear 3.3%
Natural gas 12.1%
Oil 24.7%

6 115 TWh

(b)

Hydro 16.0%
Other** 3.7%
Coal/peat 40.6%
Nuclear 12.9%
Natural gas 22.2%
Oil 4.6%

21 431 TWh

**Other includes geothermal, solar, wind, biofuels and waste.
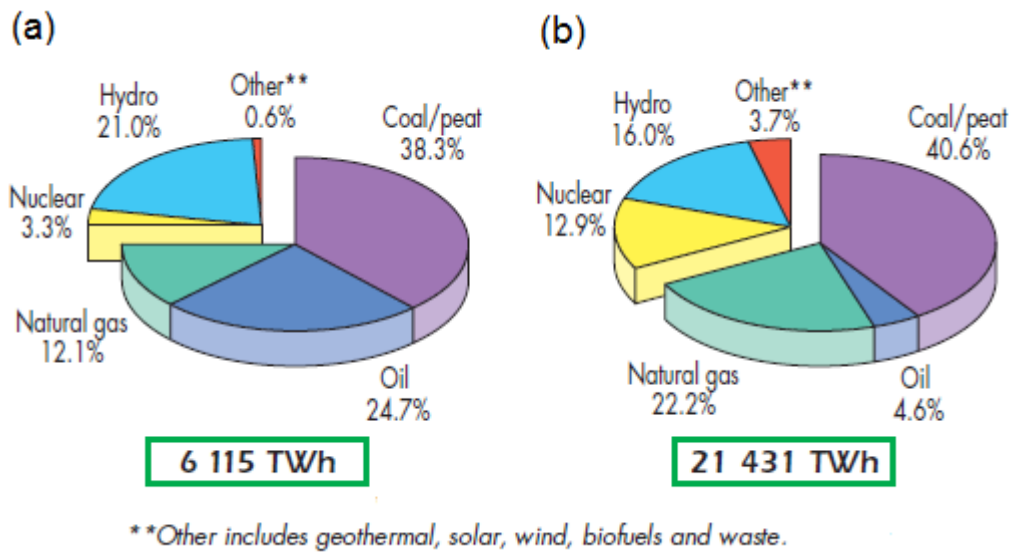
Figure 1.4   Share of global electricity generation by fuel in (a) 1973 and (b) 2010 (IEA, 2012).
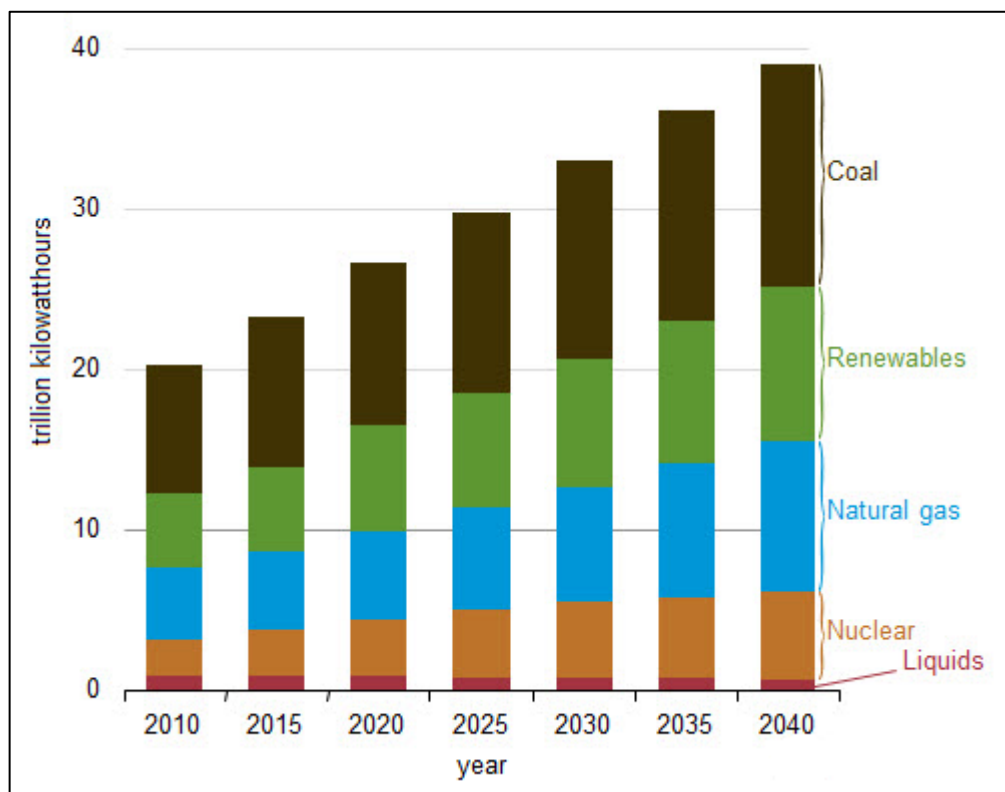
Figure 1.5 World net electricity generation by fuel, 2010-2040 (EIA, 2013).

Continued use of coal as a fuel therefore seems highly probable, given its abundant reserves (expected to be the only fossil fuel remaining after 2042 (Shafiee and Topal, 2009)). However, environmental constraints will only allow continued operation of current coal fired power plants if emission regulations are met. "*Oxy-fuel combustion and CO_2 capture from flue gases is a near-zero emission technology that can be adapted to both new and existing pulverised coal-fired power stations.*" (Buhre et al., 2005). While oxy-coal combustion and other long term CO_2 reduction and sequestration technologies are in the mid stages of development, co-firing of coal with biomass offers a near-term solution to reduce CO_2 emissions and has been adopted by a number of installations worldwide (Basu et al., 2011).

1.4.1 Oxy-fuel Combustion

Oxy-fuel combustion with flue gas recycle (FGR) is one of the three carbon capture and storage (CCS) technologies that are aimed at reducing carbon dioxide emissions from power plants. Oxy-fuel combustion differs from conventional air-firing by replacing the oxidizing stream with a mixture of pure oxygen and recycled flue gas. A schematic of this process is shown in Figure 1.6. The recent developments in this field have been reviewed by various researchers including Buhre et al. (2005), Wall et al. (2009), Toftegaard et al. (2010), Scheffknecht et al. (2011) and Chen et al. (2012). The possible effects on corrosion of boiler tubes when the combustion conditions are changed from air to oxy-firing are discussed in Section 2.3
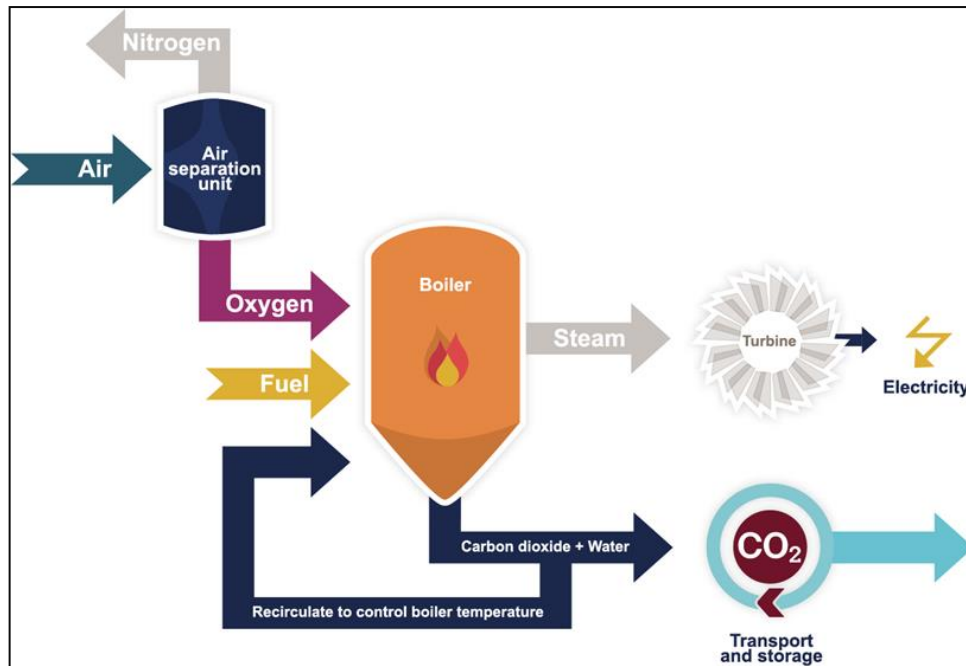
Figure 1.6 Schematic of the Oxy-fuel combustion process (ZEP, 2010)**.**

1.4.2 Biomass co-firing

Co-utilization of biomass with coal in power plants has gained increasing popularity during the past decade, following the need to reduce emissions and the increasing trend towards the application of renewable energy. Biomass co-firing has been successfully demonstrated in several installations, the worldwide distribution of which is shown in Figure 1.7. *"Experience with biomass co-firing in PCC boilers has demonstrated that co-firing woody biomass resulted in a modest decrease in boiler efficiency but no loss of boiler capacity."* (Al-Mansour and Zuwala, 2010). The major advantages of co-firing biomass with coal include reduced CO_2, SOx and NOx emissions (Spliethoff and Hein, 1998, Sami et al., 2001, Savolainen, 2003) which could in turn reduce the cost of flue gas cleaning.
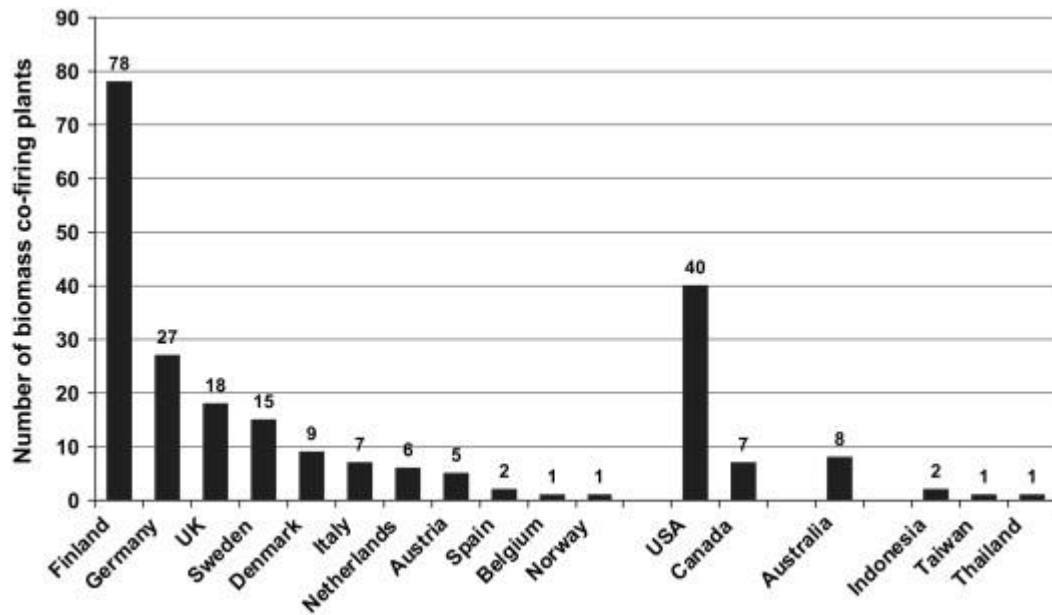
Figure 1.7 Worldwide distribution of biomass co-firing power plants (Al-Mansour and Zuwala, 2010).

However, the high content of chlorine and alkali metals in some types of biomass can lead to a higher risk of fireside corrosion and deposition (Demirbas, 2004, Malmgren and Riley, 2012). This is discussed in more detail in Section 2.4.

1.5 Pulverized Fuel Boilers

The purpose of the boiler is to generate steam (by burning fuel) that is then delivered to the turbine for generation of electricity. Pulverized fuel boilers are the most commonly employed form of utility boilers, especially where coal is used as fuel. A simplified schematic of a typical pulverized coal fired boiler is shown in Fig 1.8.

In the furnace region of the boiler, combustion of the fuel with air or combustion gas takes place. The furnace consists of a square or rectangular cross-section

enclosed by four walls (or waterwalls). The waterwall is comprised of vertical steel

tubes with a narrow plate (or membrane) connecting adjacent tubes. These tubes
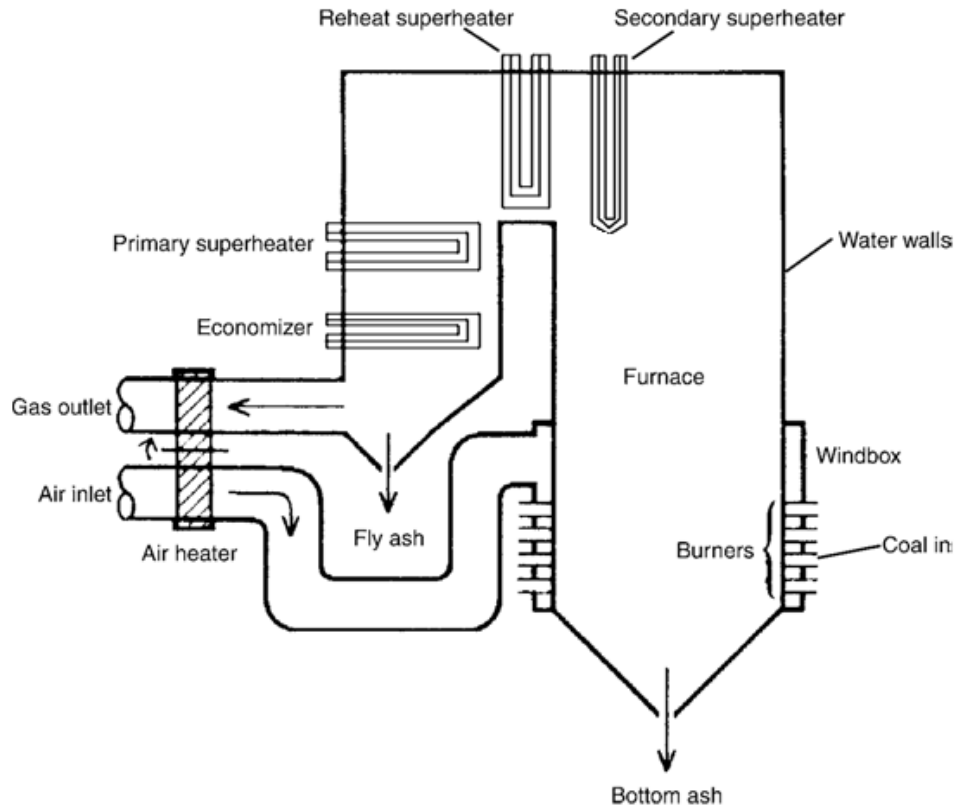
Figure 1.8 Schematic of a typical pulverized coal-fired boiler showing furnace
combustion section and heat transfer surfaces in the convection path (Lai, 2007).

absorb radiant heat from the combustion zone to convert the water rising through

them into steam. This steam first passes through a primary superheater, which is a

horizontal bank of heat exchanger tubes above the economizer, and then through

the secondary or platen superheater. From the secondary superheater, the steam,

after expanding through a high pressure gas turbine, is returned to the boiler to be

reheated in the reheater. The steam that has exhausted its useful energy is then

condensed back into water and the recycled to the boiler.

Continuous operation of the boiler requires regular maintenance through periodic, scheduled downtime, normally after 4 years or so. However, unscheduled plant shutdowns can and do occur resulting in loss of availability due to tube failure. One of the major challenges in this regard is the corrosion and deposition experienced by the boiler furnace heat transfer surfaces. Boiler tubes are susceptible to corrosion both from inside and from outside. The internal corrosion is largely driven by water chemistry while the external corrosion is driven by combustion conditions. Section 1.7 is an introduction to boiler related corrosion problems while Section 1.6 provides a general overview of the corrosion phenomena.

1.6 Corrosion and its implications

Corrosion is a widespread problem in various industries and can manifest itself in many forms. In the broadest terms, it can be defined as the deterioration of a material by chemical or electrochemical reactions with its environment. Corrosion has been classified in many ways depending on the environment, the type of corrosion products formed or the mechanism involved. It can take many forms which may result in general attachment over a large metal surface, in pinpoint penetration of the metal or in wastage of the metal. This section provides a general overview of the corrosion phenomena.

1.6.1 Cost of corrosion

The primary concerns associated with the corrosion phenomena are economics and safety. It is estimated that costs incurred from corrosion amount to 3-5% of the Gross National Product (GNP) of developed countries (Roberge, 2000). Table 1.1

shows the different cost aspects associated with corrosion. In addition to these cost related problems, some safety issues may arise from corrosion damage such as explosion in case of sudden failure, release of toxic product, etc. (Davis, 2000).

Table 1.1 Some elements of the cost of corrosion (Revie, 2011).

Capital costs
    Replacement of equipment and buildings
    Excess capacity
    Redundant equipment
Control costs
    Maintenance and repair
    Corrosion control
Design costs
    Materials of construction
    Corrosion allowance
    Special processing
Associated costs
    Loss of product
    Technical support
    Insurance
    Parts and equipment inventory

1.6.2 Factors affecting corrosion

The process of corrosion is highly complex and an understanding of the various phenomena involves consideration of several factors which affect the corrosion situation. According to Shreir (Shreir, 1976), the structural features of the metal, the nature of the environment and the reactions that occur at the metal/environment interface are the three most important factors in this regard. According to Landolt (Landolt, 2007), the corrosion behaviour of engineering materials is influenced by the following main factors:

- Chemical composition and microstructure of the metal

- Chemical composition of the environment

- Physical parameters such as temperature

- Mechanical forces including tensile stresses

1.6.3 General forms of corrosion

The eight well known forms of corrosion, as categorized by Fontana (Fontana and Greene, 1967) according to the appearance of the corroded metal, are shown in Figure 1.9. A brief description of each of these forms of corrosion is given below.

1.6.3.1 Uniform corrosion

Uniform corrosion is characterized by corrosive attack proceeding evenly over the entire surface area, or a large fraction of the total area, of the metal or alloy. Corrosion-resistant alloys and stainless steels become tarnished or oxidized due to reaction with air. If permitted to continue, surface corrosion may lead to roughness of the surface which in turn causes more serious types of corrosion to set in (Roberge, 2000).
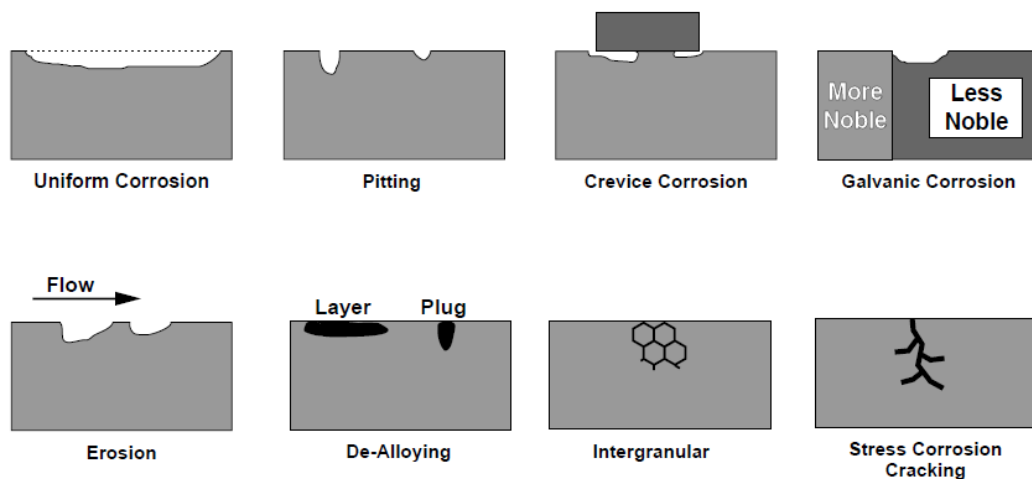
Figure 1.9 Forms of corrosion damage (Roberge, 2000).

1.6.3.2 Pitting corrosion

Pitting corrosion is a localized form of corrosion, which occurs when discrete regions of a material undergo a rapid attack while most of the adjacent surface remains virtually unaffected, causing the appearance of cavities in the material. Pitting usually requires a long initiation period but once the pit has started, the attack continues at an accelerating rate. Although the total metal loss may be small, the loss of effective cross-section decreases the strength of the material. Fatigue and stress corrosion cracking may then initiate at the base of the pit (Campbell, 2008).

1.6.3.3 Crevice corrosion

Crevice corrosion is a localized form of corrosion and it is usually associated with a stagnant solution on the microenvironmental level (Roberge, 2000). Such stagnant microenvironments tend to occur in crevices or shielded regions, such as those formed under gaskets, washers, insulating material, surface deposits, disbanded coatings, etc. Because oxygen diffusion into the crevice is restricted, a differential aeration cell is set up between the crevice (microenvironment) and the external surface (bulk environment) which is conducive to metal dissolution.

1.6.3.4 Galvanic corrosion

Galvanic corrosion occurs when dissimilar metallic materials are brought into contact in the presence of an electrolyte. An electrochemical cell is set up due to differences in the corrosion potential of the dissimilar materials. The more noble material acts as the cathode of the corrosion cell whereas the one with the higher corrosion potential is consumed by anodic dissolution.

1.6.3.5   Erosion corrosion

Erosion corrosion is the acceleration in the rate of deterioration or the attack on a metal because of the relative motion between a corrosive fluid and the metal surface (Fontana and Greene, 1967). The motion is usually one of high velocity with mechanical wear and abrasion effects and usually exhibits a directional plane. Erosion corrosion is found in systems such as piping, valves, pumps, nozzles, heat exchangers, turbine blades, baffles, mills, etc.

1.6.3.6   Selective leaching (or de-alloying)

Selective leaching refers to the selective removal of one element from an alloy, such as in the removal of zinc from unstabilized brass, whereby a weakened, porous copper structure is produced (Roberge, 2000). Similar processes occur in other alloy systems in which aluminium, iron, cobalt, chromium and other elements are removed.

1.6.3.7   Intergranular corrosion

Intergranular corrosion is a localized attack along the grain boundaries, or immediately adjacent to grain boundaries, while the bulk of the grains remain largely unaffected. Intergranular corrosion can be caused by impurities at the grain boundaries, enrichment of one of the alloying elements, or depletion of one of these elements in the grain-boundary areas (Fontana and Greene, 1967). There is an inherent tendency for impurities and alloying additions to segregate at grain boundaries. Depletion of chromium in the grain-boundary regions results in intergranular corrosion of stainless steels.

1.6.3.8 Stress corrosion cracking

Stress corrosion cracking refers to corrosion caused by the simultaneous presence of a tensile stress and a specific corrosive medium. It is characterized by fine cracks progressing through the metal or alloy. Depending on the environment or the metal structure, the cracks may be intergranular (along grain boundaries) or transgranular (without preference for boundaries) (Campbell, 2008).

1.6.4 Effect of metal structure on corrosion

A basic knowledge of the structural features of metals is useful in understanding the complex corrosion phenomena. The structural features of a metal or alloy and the heterogeneities associated with it, affect their properties and corrosion resistance.

1.6.4.1 Defects in crystal structure

All metals are crystalline in nature, a crystal being ideally defined as an orderly three-dimensional array of atoms. However, real crystals contain imperfections in their structure. Defects in crystal structures are responsible for solid state diffusion mechanisms. Since most chemical reactions and phase transformations in solids occur due to diffusion of atoms and ions, these defects play an important role by providing pathways for diffusion. In the case of corrosion, the form and concentration of these defects affect the morphology and microstructure of the oxide scale.

1.6.4.2   Grain boundaries and phase boundaries

Alloys are mixtures or solid solutions of two or more metals consisting of a number of crystals or grains. Microscopic analysis of polycrystalline substances reveals the appearance of grain boundaries. Since grain boundaries can be regarded as regions of disordered atomic arrangement possessing higher energies than the surrounding atoms, they are therefore preferential sites for chemical attack such as intergranular corrosion. The size and structure of the grains varies with the type of alloy and heat treatment, as does the morphology and structure of the intergranular attack (Béranger et al., 1996).

1.6.5   Types of steels and effect of alloying elements

Steels are essentially alloys of iron having a carbon content that varies from traces to about 2%. There are a number of classification systems for the various types of steels based on the composition, microstructure, application or specification. Steels can broadly be divided into plain carbon steels, low alloy steels and high alloy steels with several subclasses (Bramfitt and Benscotter, 2002). The properties of carbon steels are mainly due to the element carbon while the properties of alloy steels are due to the alloying elements present although the role of carbon is also significant (Sharma, 2005). Various alloying elements are added to steel for the purpose of attaining specific properties and characteristics. The most common of these include nickel, manganese, chromium, molybdenum, cobalt, aluminium and silicon. Most of the alloying elements form substitutional solid solutions with iron resulting in an increase of tensile strength and hardness. Some elements make the mechanical movement of dislocations much more difficult. Specific characteristics such as corrosion resistance and high yield strength can be achieved by alloying

elements. Creep strength, weldability, fireside corrosion resistance and steam side oxidation resistance are important features that dictate the selection of boiler tube materials. Waterwall tubes, in general, are made from mild steel or low alloy steel, while superheater tubes are made from high alloy steels which exhibit superior corrosion resistance at higher temperatures.

1.6.6 High Temperature Corrosion

High temperature corrosion, sometimes referred to as "dry corrosion" is the form of corrosion that occurs at high temperatures (above 300 ^{o}C), in the absence of an aqueous electrolyte (Landolt, 2007). High-temperature corrosion is an important problem in many technological activities such as energy production (gas turbines, combustion chambers, reactors, furnaces), transport (jet engines, diesel motors), chemical and metallurgical processing and waste incineration. This type of corrosion can take place in oxidizing or reducing environments. Oxidizing environments refer to high-oxygen activities with excess oxygen, while reducing environments are characterized by low-oxygen activities and the absence of excess oxygen.

1.6.7 Mechanisms of High Temperature Corrosion

The mechanisms of high temperature corrosion, briefly described below, include oxidation, sulphidation, carburization, nitridation, gaseous halogen corrosion and fuel ash or molten salt corrosion. A brief outline of these mechanisms are presented in the following paragraphs, the details of which have been discussed by several authors including Lai (1990), Meetham et al. (2000), Young (2008), Revie and Uhlig (2008).

Oxidation, the chemical reaction of a material with oxygen is generally regarded as the most commonly encountered form of high-temperature corrosion. The oxidation process itself is usually not detrimental. This is because most corrosion and heat resistant alloys rely on the formation of an oxide film (such as chromium or iron oxide) to provide corrosion resistance. However, in most industrial corrosion problems, oxidation does not occur in isolation; rather a combination of high-temperature corrosion mechanisms causes material degradation when contaminating species such as sulphur, chlorine, etc. are present in the atmosphere.

Sulphidation is a common high temperature corrosion-failure mechanism brought about by the presence of sulphur compounds. Localized pitting type attack is sometimes associated with sulphidation. Gaseous environments associated with sulphidation have been divided into three categories according to the type of sulphur compounds present in a specific environment. These include hydrogen-hydrogen sulphide mixtures or sulphur vapour of highly reducing nature, moderately reducing mixed gas environments that contain mixtures of hydrogen, water, carbon dioxide, hydrogen sulphide and sulphur dioxide or sulphur trioxide containing environments.

Carburization damage is mainly associated with high temperature exposure to carbon monoxide, carbon dioxide, methane and other hydrocarbons. Carbon from the environment combines primarily with chromium but also with any other carbide formers (Nb, W, Mo, Ti) present in the alloy to form internal carbides. Carbides formed in the microstructure can be complex in composition and structure and can be found to precipitate on the grain boundaries, or inside the

grains. The main undesirable effect of carbide formation is embrittlement and reduced ductility. Carburization also reduces oxidation resistance by tying up chromium in the form of chromium-rich carbides.

Nitridation usually takes place when carbon, low alloy and stainless steels are exposed to a nitrogen or ammonia bearing environment at elevated temperatures. In air or combustion atmospheres containing nitrogen, nitridation can occur under reducing conditions when oxide scales no longer provide protection. Under oxidation/nitridation conditions, nitrogen molecules permeate through cracks and pores in the oxide layer and reach the metal underneath the oxide scales, leading to the formation of nitrides.

Halogens and hydrogen halides contribute to high temperature corrosion by interfering with the formation of protective oxides, or breaking them down if already formed. In gas mixtures containing both chlorine and oxygen, simultaneous formation of metal oxide and metal chloride can take place followed by overgrowth of oxide scales that are porous and non-protective. Chlorine and chlorine containing compounds have a considerable influence on the fireside corrosion of boilers.

Fuel ash corrosion, particularly encountered in fossil fuel power plants, is caused due to the formation of low melting point compounds (such as sodium pyrosulphate) in ash deposits. These compounds initiate a fluxing mechanism whereby an otherwise protective oxide scale on the substrate surface dissolves at the oxide/salt interface and precipitates as non-protective particles within the salt

film. Metallographic examinations of corroded components show oxide particles dispersed in the adherent salt film.

1.7 Fireside corrosion, slagging, fouling in boilers

Corrosion of tubes due to chemical attack occurring on the furnace or fireside of heat exchanger surfaces in boilers is known as external or fireside corrosion. This topic is introduced here and discussed in greater detail in Chapter 2. Fireside corrosion has been among the leading causes of boiler tube failure for many years. "*Tubes affected by the fireside corrosion mechanism may lose 15 mils per year (mpy) and more in extreme cases*" (Koripelli et al., 2010). In addition to corrosion, boiler tubes are also susceptible to ash deposition. Two general types of ash deposition phenomena have been defined as slagging and fouling. Such deposits reduce the heat absorption capacity of tubes, which increases the downstream flue gas temperature and result in drop in steam output. The presence of deposits may also lead to increased corrosion of the underlying tubes in some cases (Bryers, 1996).

1.7.1 Fireside Corrosion

Fireside corrosion problems in boilers are encountered in the furnace combustion region (waterwalls) and also in the convective sections such as superheaters and reheaters. Corrosion of furnace and superheater tubes in pulverized fuel boilers may result from accelerated oxidation, localized reducing conditions, subsurface penetration by sulphides, attack by molten salts, or a combination of all these factors. The mechanisms which govern the corrosion of furnace wall tubes are not well understood. However, it is widely agreed that the corrosion behaviour is

closely linked to furnace design and operating parameters and the type of fuel used.

1.7.2 Slagging

Slagging is the formation of fused or partially fused deposits on furnace walls or tubes exposed to radiant heat (Zhang et al., 2010). Semi-molten ash may stick to the relatively cooler walls and cause the accumulation of deposits. The fusion temperature of the ash, which depends on its chemical composition, is an important factor contributing to the formation of slag deposits. The deposition and accumulation of fused, or partially-fused, slag deposits on furnace heat exchanger surfaces reduces furnace heat absorption by acting as an insulating layer on the tube surface (Bilirgen, 2014). This leads to increased flue gas temperatures, not only within the furnace but also at the furnace exit. In other words, it results in reduced thermal efficiency of the power plant.

1.7.3 Fouling

Fouling is defined as the formation, or accumulation, of ash deposits in the convective sections of boilers, such as superheaters and reheaters. It involves the formation of deposits in which the ash particles are bonded by low melting point compounds. Fouling, like slagging, results in reduced heat absorption but it is considered as a much slower process than slag formation. As the ash deposits grow over a period of time, they can form ash bridges between the tubes, resulting in channelling of the flue gas. Channelling causes localized increase in flue gas velocity which in turn can result in local overheating of the heat exchange tubes,

and in the localised damage of boiler tubes and other components by particle impact erosion (Stam et al., 2009).

1.8 Aims and objectives

The broader aim of this work is to gain a better insight into the process of corrosion in oxy-fuel environments and elucidate to some extent, the link between corrosion and deposition. This involves the setting up of a custom built laboratory scale corrosion test equipment in order to test boiler tube materials commonly used in air-fired units so as to assess their corrosion potential in retrofit environments.

The objectives include corrosion testing under different environments and deposits, characterizing the deposits and their parent fuels with the help of laboratory based tests and measurements, and assessing the deposition tendencies of the fuels with the help of the thermodynamic equilibrium software Factsage. The details of all these are presented in the proceeding chapters.

Chapter 2

Literature Review

2.1 Introduction

A general overview of fireside problems associated with industrial boilers has been presented in Section 1.7. This chapter considers in greater detail, the more specific aspects of fireside corrosion and deposition. A considerable amount of research available in the literature, pertaining to high temperature gas-side corrosion mechanisms in power boilers, is based on analysis of deposits and corrosion products found in various regions of boilers exhibiting high rates of metal wastage. Internal inspections of the boiler, in the past, required shutdown and scaffolding in order to measure metal loss and predict tube wall wastage leading to the next outage. Advances in technology have now enabled online measurements of corrosion rates with the help of corrosion probes and scanners. However, laboratory studies of simulated combustion systems, where accelerated corrosion can be made to occur, still remain a useful tool in predicting the corrosion behaviour of different boiler materials and the possible mechanisms involved. The proceeding sections provide a literature survey of the work of various authors contributing to the current state of understanding of this field of study.

2.2 Fireside corrosion in PF boilers

Fireside corrosion in pulverized fuel boilers can be broadly divided into two categories, as follows, according to the location:

- waterwall corrosion

- superheater/reheater corrosion

Different corrosion mechanisms operate on these surfaces depending upon the local chemistry of the combustion gases and deposits, the boiler tube compositions and the gas and metal temperatures. In addition, the corrosion behaviour is closely linked to furnace design and operating parameters and the type of coal/fuel used. Corrosion in the waterwall regions of the furnace occurs primarily due to the presence of reducing conditions and the presence of volatile species, such as chlorine, while in the superheater/reheater section, corrosion is due to the presence of low melting point deposits containing compounds such as sodium or potassium iron trisulphates or alkali metal sulphate (Labuda et al., 2000).

In the combustion zone of the furnace, the gas-side temperature ranges from 1370-1650^0C. The steam side temperature is much lower and this results in high heat flux across the waterwall tubes. Also, deposits on tube walls interfere with the heat transfer and act as a cover beneath which corrosion can occur. The combustion reactions are complete before the flue gas reaches the superhetaer/reheater section and as a result of the heat transfer in the furnace section, the temperature of the flue gas in this region is lower. The tempearture at the metal surface, however, is higher (about 650 ^{o}C) as compared to the waterwall section (around 450 ^{o}C) due to the higher steam temperatures in this region. Figure 2.1 shows a corroded waterwall tube due for replacement in a commercial boiler during plant mainteneance while Figure 2.2 represents corroded tubes in the superheater section of the boiler.

Figure 2.1 Photograph from a commercial boiler during plant shutdown showing corroded and replaced waterwall tubes.
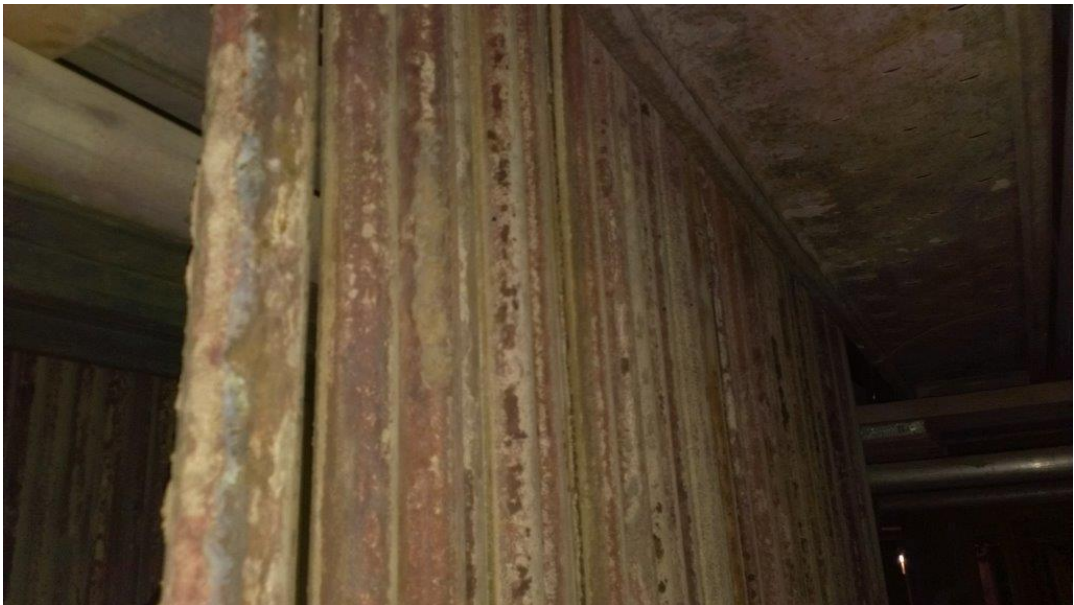
Figure 2.2 Photograph from a commercial boiler during plant shutdown showing corroded superheater tubes.

2.2.1 Waterwall corrosion

Corrosion of the furnace wall tubes is strongly linked to the presence of reducing conditions. Reducing conditions are associated with low oxygen concentrations,

increased levels of carbon monoxide and hydrogen sulphide in the gas phase and can prevail in configurations for low NOx formation with air staging and in cases where burners are firing off-line creating impingement and fluctuating local stoichiometrites in the region of water-wall tubes Carbon monoxide in the furnace flue gases is usually a result of imperfect mixing of air and coal particles in localized regions and in such low oxygen conditions, sulphur in the coal exists primarily as hydrogen sulphide in the gas phase. Manny & Bartok (Manny et al., 1978) observed severe corrosion, under a reducing environment, occurring on the side walls of a boiler burning high sulphur, high iron coal. Redistribution of the air flow so as to increase the local oxygen concentration resulted in alleviation of the problem.

Lees and Whitehead (1983) analysed corroded mild steel tube sections, with the assistance of Scanning Electron Microscope (SEM), to reveal a complex distribution of elements and phases, the most important features of which are shown in Figure 2.3. Examination of the microstructures showed poor scale adhesion with microchannels, pores and fissures (Fig.2.3(ix)). Intergranular attack, a few grain boundaries thick, was detected as shown in Figure 2.3(ii). It was found that at high corrosion rates, the scale was invariably separated from the metal by a chlorine rich phase. Lees and Whitehead (1983) also examined 25Cr-20Ni co-extruded mild steel tubes under the Scanning Electron Microscope to find that intergranular attack was more extensive in these tubes as compared to mild steel tubes and Cl, although similarly detected at the scale/metal interface was present in lower concentrations.

Clarke and Morris (1983) found that large concentrations of carbon monoxide (upto 4.3%) were present in a front wall fired boiler experiencing high corrosion rates. Furthermore, the hydrogen sulphide concentration became significant when
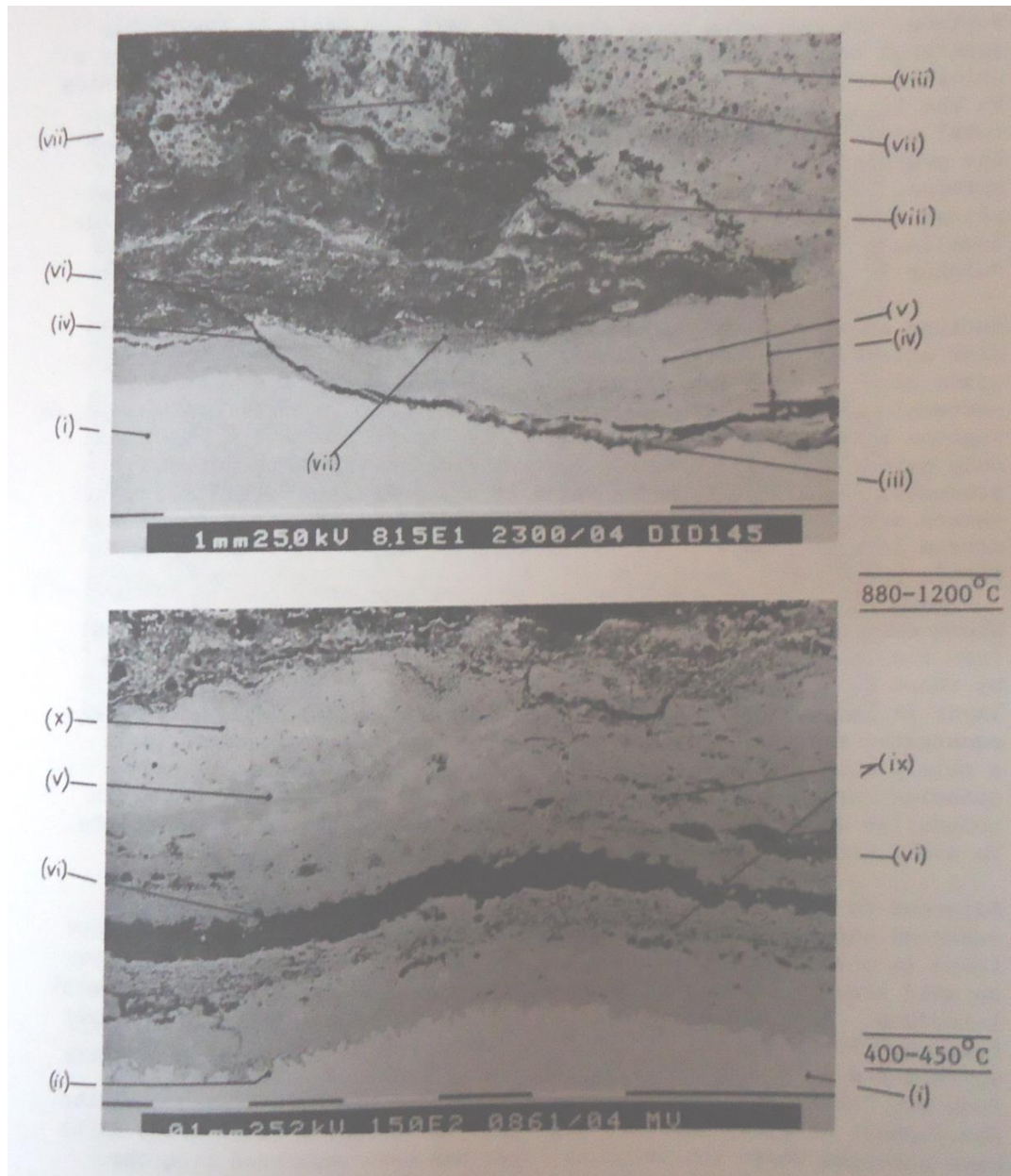
Figure 2.3. Scanning electron micrographs showing characteristic features of scale and deposit on corroded mild steel tube.(i) metal substrate, (ii) intergranular attack, (iii) Cl-containing phase, (iv) cracking, (v) compact iron oxide/sulphide, (vi) alkali metal sulphatic layer, (vii)solid combustion products, (viii) bulk iron sulphide, (ix) porosity, and (x) copper rich region (Lees and Whitehead, 1983).

the concentration of CO exceeded about 3%. They also found thick magnetite (Fe_3O_4)/sulphide scales with distinct sulphide bands in regions of furnace wall tubes exhibiting high corrosion rates as shown in Figure 2.4. Reid (Harb and Smith, 1990) reported the absence of corrosion in regions where the CO concentration was 0-0.2% while corrosion was observed in areas where the CO concentration ranged from 0.9-4.9%. Samms & Smith (Harb and Smith, 1990) analysed samples of the combustion gas taken from corrosion zones. The samples showed the presence of hydrogen sulphide, carbon monoxide, hydrogen and elemental sulphur.
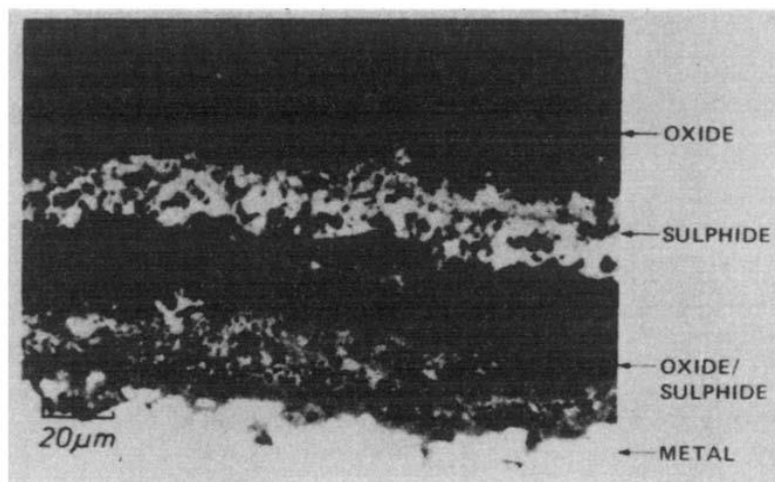
Figure 2.4 Oxide/sulphide corrosion scale from a region of high CO concentration (Harb and Smith, 1990).

When hydrogen sulphide (H_2S) is present in the flue gas, it preferentially reacts with iron in the waterwall tubes to form iron sulphide. In the presence of CO protective iron oxide scales can also be partially converted to FeS. Scales containing iron sulphide exhibit poor adhesion to the metal surface and this leads to higher rates of metal wastage. Based on a series of experiments in which various alloys were exposed to simulated reducing gas environments and a range of metal

temperatures (260 to 480 ^{o}C) typical for waterwalls regions of the boiler, Kung

(1997) developed a model to estimate the corrosion rate of carbon and low alloy

steels as a function of the metal temperature and H_2S concentration in the flue gas.

Figure 2.5 shows the predicted corrosion rate of a 0.5Cr-0.5Mo low alloy steel as a

function of the metal temperature. The figure clearly shows that the corrosion rate

increases with increasing temperature but the increase is sharper as the H_2S

concentration in the furnace gas increases.
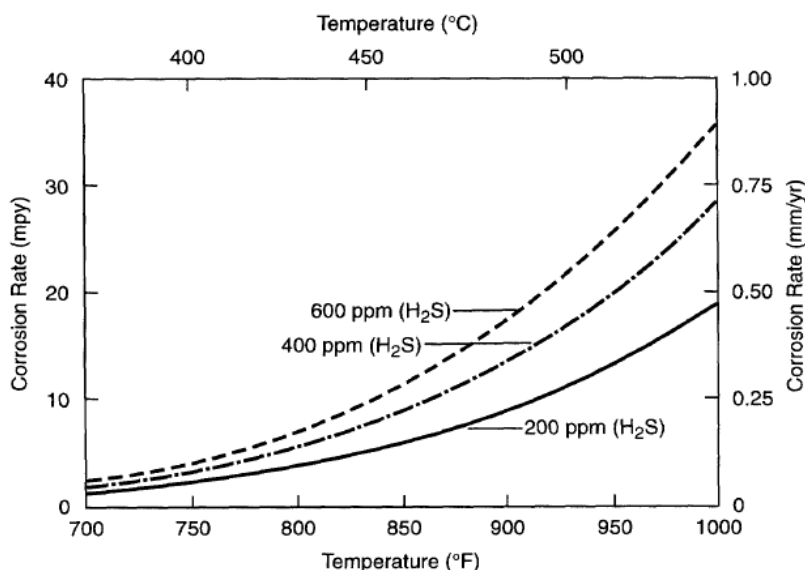
Figure 2.5 Predicted corrosion rate of low alloy steel in reducing flue gas
containing H_2S (Kung, 2006).

The implementation of NO_x control measures further aggravates the problem of

corrosion under reducing conditions. A number of low NO_x technologies have

been introduced in the past few decades, most of which depend on the strategy of

staged combustion to reduce the NO_x formation. In staged combustion, fuel is only

partially oxidized in the primary combustion zone while the remaining oxidation

takes place in the secondary zone. This delay in fuel/air mixing leads to the

enlargement of the flame zone and flame impingement. Flame impingement leads to severely reducing conditions and facilitates the transport of corrosive species to the tube surface (Bakker, 2003, Shim et al., 2008).

Extremely high wastage rates found on the furnace wall tubes of some coal-fired boilers retrofitted with low NOx burners were attributed to severe sulphidation caused by FeS rich ash deposits found on these tubes. FeS rich ash deposits are formed under reducing conditions in the furnace due to the partial oxidation of pyrite (FeS_2) present in the coal. Bakker & Kung (2000) exposed low alloy steel coupons to an environment simulating a 650MW boiler retrofitted with a low NOx burner system. The coupons were exposed to alternating oxidizing and reducing flue gas conditions, both with and without a FeS deposit. A 4-5 times increase in the corrosion rates was observed on coupons with FeS deposit. Based on further experiments, Bakker and Kung (2000) concluded that FeS deposits significantly increase the corrosion rates under alternating reducing and oxidizing conditions rather than reducing conditions alone. Their results are shown in Tables 2.1 and 2.2. Table 2.1 shows corrosion rates of low alloy steel exposed to reducing conditions and various FeS deposits at 427 ^{o}C. Table 2.2 shows the corrosion rates of the same steel under similar ash deposits at the same temperature, but alternating reducing and oxidizing environments. The authors proposed that once the FeS rich deposit is formed on the tubes under reducing conditions, it can be oxidized to produce iron oxide and elemental sulphur under subsequent oxidizing conditions. Below a temperature of about 444 ^{o}C, liquid sulphur is stable and a layer of elemental sulphur adjacent to the metal surface leads to much increased

rates of metal wastage as compared to gas phase H_2S induced corrosion in reducing environments (Kung, 2006).

Table 2.1 Corrosion rate of low alloy steel under various ash deposits in reducing conditions. (Bakker and Kung, 2000).

Ash Deposit	Corrosion rate (mm/yr)
No deposit	0.42−0.57
30% FeS, 70% fly ash	0.1−0.3
60% FeS, 40% fly ash	0.1−0.17
60% FeS, 20% carbon, 20% fly ash	0.2−0.6
30% FeS, 10% fly ash	0.1−0.27

Table 2.2 Corrosion rate of low alloy steel under various ash deposits in alternating reducing and oxidizing environments.(Bakker and Kung, 2000).

Ash Deposit	Corrosion rate (mm/yr)
No deposit	0.37−0.5
30% FeS, 70% fly ash	1.0
60% FeS, 40% fly ash	0.82
60% FeS, 20% carbon, 20% fly ash	1.2
30% FeS, 10% fly ash	1.2

Sulphidation attack is the most commonly accepted mechanism for fireside corrosion that can occur in both oxidising and reducing environments. In addition, volatile species such as hydrogen chloride, if present, increase the corrosive propensity of the environment. Damage may also be caused by low melting point compounds in ash deposits such as sodium pyrosulphate ($Na_2S_2O_7$). The role of

sulphur and chlorine species in corrosion is discussed in sections 2.3.1 and 2.3.2, respectively.

2.2.2 Superheater/Reheater corrosion

Corrosion of superheater and reheater tubes is attributed to the formation of deposits containing alkali iron trisulphates, i.e. sodium iron trisulphate ($Na_3Fe(SO_4)_2$) and potassium iron trisulphate ($Na_3Fe(SO_4)_2$). Severe metal loss occurs when these compounds are in the molten state (Srivastava et al., 1997). The corrosion rate follows a bell-shaped curve in this region derived from the melting temperatures of the complex sulphates and the thermodynamic stability of these compounds. The height of the curve depicting maximum metal loss varies with the tube material, depending on its corrosion resistance, as shown in Figure 2.6.
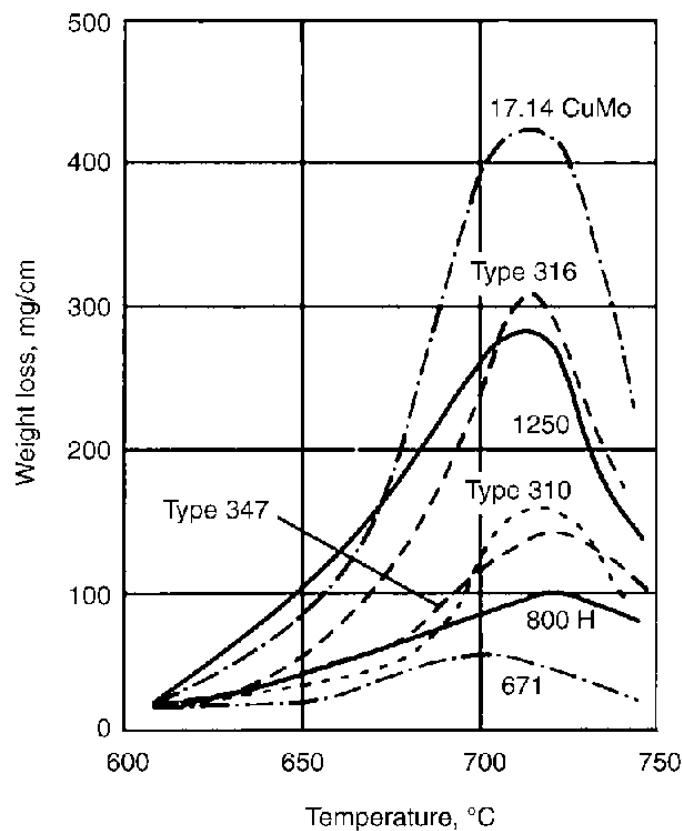
Figure 2.6 Bell shaped curve obtained from laboratory experiments simulating superheater conditions in the sulphate deposit range (Lai, 2007).

This shows that the severity of the attack varies with variation in material composition. The typical corroded superheater or reheater tube is characterized by two wastage flats at the 2 o'clock and 10 o'clock positions (when the flue gas impinges at 12 o'clock) as shown in Figure 2.7. At these two locations, the ash layer is relatively thin, because of erosion by the gas stream, resulting in a higher local heat flux and higher metal temperature, which in turn leads to the formation of a molten salt layer. At the 12 o'clock position, significantly lower wastage rates are observed due to sufficient thermal insulation being provided by the thick ash layer.
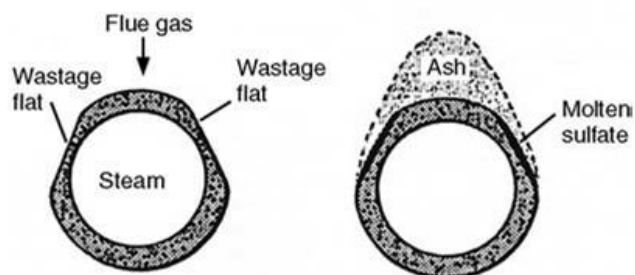
Figure 2.7 Typical wastage feature of a corroded superheater
tube from a coal-fired boiler (Lai, 2007).

2.3 Mineral matter in coal

Coal, in addition to carbon, hydrogen, nitrogen and oxygen consists of a variety of mineral impurities. These mineral impurities undergo transformations in the high temperature environments in the boiler to form corrosive species in the gas and deposit phase. Table 2.3 is a summary of the major mineral transformations in coal that lead to corrosion and deposition problems (Wall et al., 1979) Of the mineral

contents shown, aluminosilicates are mainly associated with slagging problems, while chlorine and sulpur are the major species contributing to corrosion.

Table 2.3 Principal reactions undergone by mineral matter in coal during combustion: oxidation, decomposition and vaporisation to ash gases and vapours (Wall et al., 1979).

Species	Reaction
Kaolinite $Al_2Si_2O_5(OH)_4$	$Al_2Si_2O_5(OH)_4 \rightarrow Al_2O_3 \cdot 2SiO_2 + 2H_2O$ $\downarrow$ $Al_2O_3 + 2SiO_2$
Pyrite FeS_2	$2FeS_2 + \frac{11}{2}O_2 \rightarrow Fe_2O_3 + 4SO_2$ $FeS_2 \rightarrow FeS + S$ $FeS_2(s) \rightarrow FeS_2(g)$
Sulphates $CaSO_4$ $MgSO_4$ $Fe_2(SO_4)_3$ Na_2SO_4	$CaSO_4 \rightarrow CaO + SO_3$ $MgSO_4 \rightarrow MgO + SO_3$ $Fe_2(SO_4)_3 \rightarrow Fe_2O_3 + 3SO_3$ $Na_2SO_4(l) \rightarrow Na_2SO_4(g)$
Carbonates $CaCO_3$ $CaMg(CO_3)_2$	$CaCO_3 \rightarrow CaO + CO_2$ $CaMg(CO_3)_2 \rightarrow CaO + MgO + 2CO_2$
Chlorides $NaCl$ KCl	$NaCl(l) \rightarrow NaCl(g)$
	$3NaCl + (Na, K)aluminosilicate \rightarrow (Na)alumino\ silicate + KCl(g)$ $NaCl + SiO_2 + H_2O \rightarrow Na_2SiO_2 + 2HCl$

2.3.1 Role of Sulphur

Sulphur is one of the impurities in coal that is most frequently associated with

corrosion and is present in coals in the form of pyritic sulphur, organic sulphur and sulphates. When combustion takes place in the presence of excess air or oxygen to ensure complete combustion, sulphur in the coal reacts with the oxygen to form sulphur dioxide and sulphur trioxide. A combustion atmosphere of this type is oxidizing in nature. In reducing conditions, sulphur assisted corrosion takes place due to the presence of hydrogen sulphide in the gas phase. Sulphidation in oxidizing environments, as well as in reducing environments, is frequently accelerated by other fuel impurities such as sodium, potassium and chlorine, which may react among themselves and/or with sulphur during combustion to form compounds that deposit on metal surfaces, resulting in an accelerated sulphidation attack (Kihara et al., 1992).

Corey (Reid, 1971) identified the presence alkali-iron trisulphates on the leading edge of the final superheater tube surface as being responsible for tube wastage. In both cases, the deposit consisted of a hard, white enamel-like material and corrosion was dependent on the existence of a molten phase. Both the formation of the alkali trisulphates and the formation of the pyrosulphates require the presence of a sufficient quantity of sulphur trioxide. Sulphur trioxide in the flue gas can be attributed to reactions within the flame, oxidation of SO_2 and the decomposition of sulphates (Cullis and Mulcahy, 1972).

Corey (Reid, 1971) proposed a mechanism of fireside corrosion which follows a series of steps, as illustrated in Figure 2.8. The first step is the formation of an oxide film on the tube surface followed by the formation of an alkali metal sulphate layer. The source of the alkali metals are volatile species formed in the
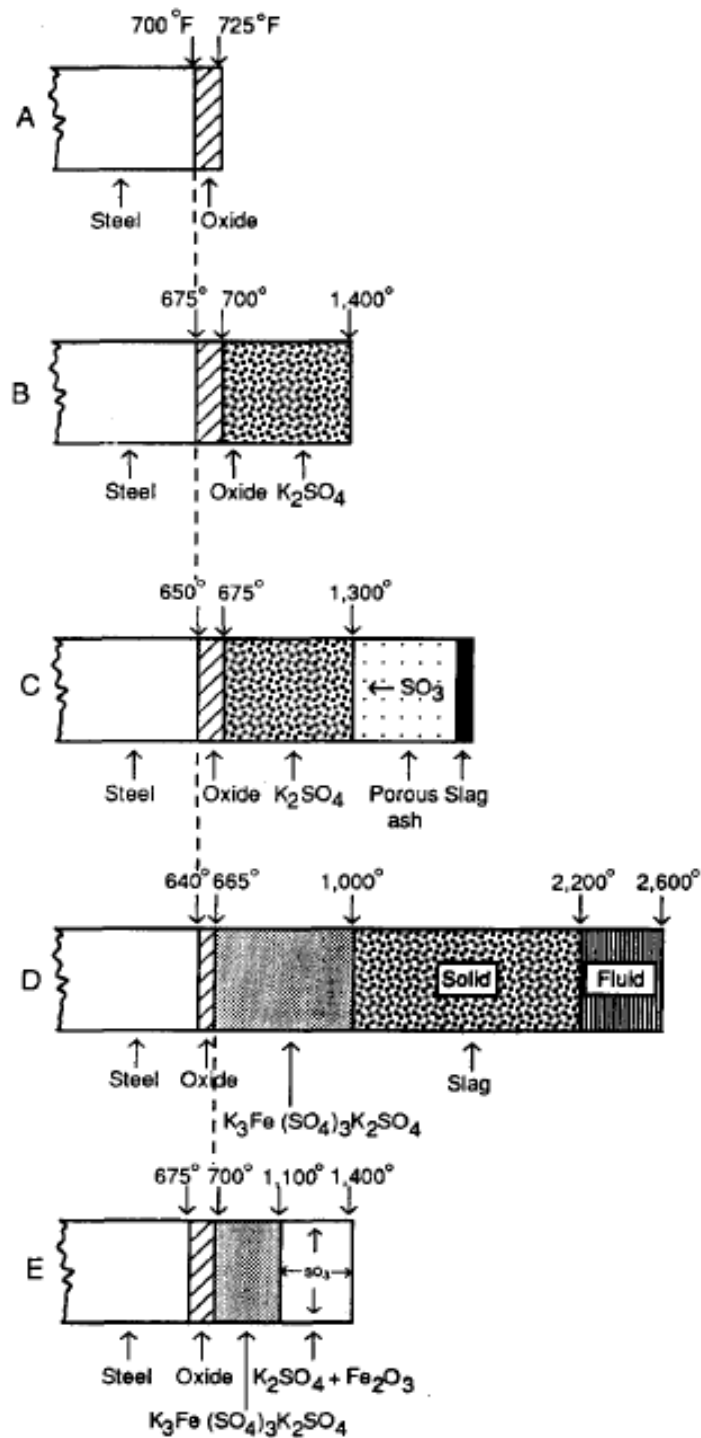
Figure 2.8.Proposed mechanism of corrosion of wall tubes by sulphate deposits
(Reid, 1971).

flame or from the molten slag. It was postulated that as the alkali sulphate layer thickened, the surface temperature would increase until ash began to stick to the surface and subsequently sinter to form a molten slag. Reactions in the ash during the melting process result in the formation of SO_3, which further reacts with sodium or potassium sulphate as follows :

$$3Na_2SO_4 + Fe_2O_3 + 3SO_3 \rightarrow 2Na_3Fe(SO_4)_3 \tag{2.1}$$

$$3K_2SO_4 + Fe_2O_3 + 3SO_3 \rightarrow 2K_3Fe(SO_4)_3 \tag{2.2}$$

The alkali iron sulphates thus formed act as flux progressively removing the protective oxide layer and resulting in further oxidation of the steel or alloy.

It has also been suggested that liquid pyrosulphates are formed on the surface of the tube by the following reactions:

$$Na_2SO_4 + 3SO_3 \rightarrow Na_2S_2O_7 \tag{2.3}$$

$$K_2SO_4 + 3SO_3 \rightarrow K_2S_2O_7 \tag{2.4}$$

Pyrosulphates ($X_2S_2O_7$) are likely to aggressively attack protective oxide films according to the following reactions :

$$3X_2S_2O_7 + Fe_2O_3 \rightarrow 2X_3Fe(SO_4)_3 \tag{2.5}$$

$$3X_2S_2O_7 + Fe_2O_3 \rightarrow 3X_2SO_4Fe_2(SO_4)_3 \tag{2.6}$$

$$3X_2S_2O_7 + Fe_2O_3 \rightarrow 4X_2SO_4 + FeSO_4 + Fe_2(SO_4)_3 \tag{2.7}$$
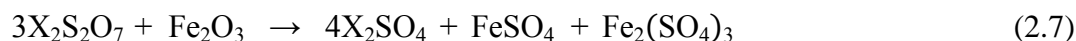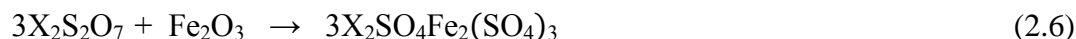
where X represents Na, K.

Lai reported the work of Blough (2007), aimed at studying the effect of increasing the sulphur dioxide content of a simulated flue gas and increasing the sulphate

content in the ash on the corrosion of several superheater/reheater materials at 650

°C.
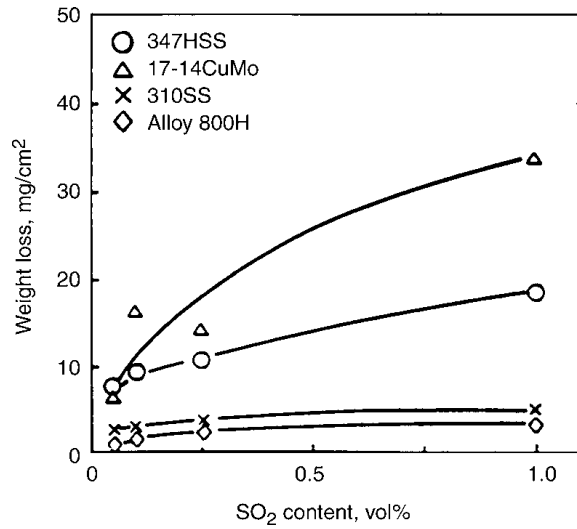
Figure 2.9 Effect of SO_2 content in flue gas on the corrosion of several superheater/ reheater materials at at 650 °C. Source: (Blough and Kihara, 1988).
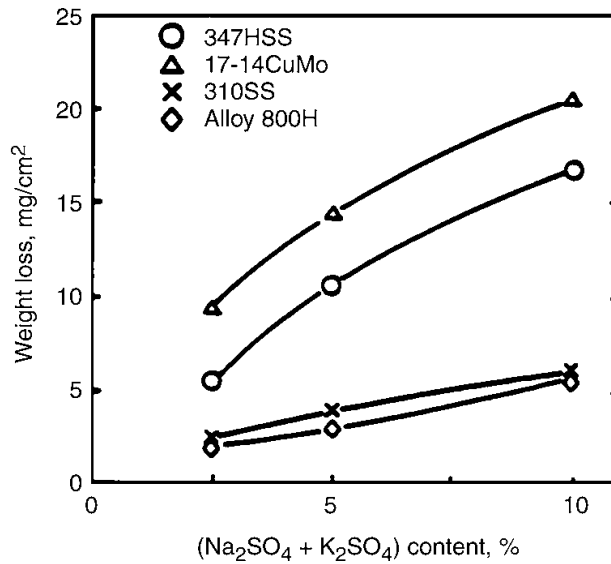
Figure 2.10 Effect of $Na_2SO_4+K_2SO_4$ content in synthetic ash on the corrosion of several superheater/reheater materials at 650 °C (1200 °F) in flue gas containing 0.25% SO_2. Source: (Blough and Kihara, 1988).

An increase in the corrosion rates was observed for both cases, as shown in Figure 2.9 and 2.10, respectively, showing the significance of both these factors in sulphate induced corrosion. The rate of increase varied with the alloy composition.

2.3.2 Role of Chlorine

Chlorine, which exists in varying concentrations in different types of coal, is among the most volatile of the trace elements and is known to contribute significantly to corrosion and deposition. Much of the concern about burning high chlorine coal in utility boilers and subsequent efforts to establish a link between fuel chlorine content and fireside corrosion began with burning high chlorine coal in different power plants in the UK. The impact of coal chlorine on fireside corrosion behaviour as documented from occurrences in CEGB and PowerGen stations in the UK has been reviewed by James and Pinder (1997). Preliminary data from experience in UK boilers indicated a linear increase in corrosion rates with increase in chlorine content and a chlorine content in excess of 0.2% resulted in severe corrosion attack. However, further investigations established that the relationship between chlorine content and rate of corrosion was influenced by several factors, such as combustion conditions, proximity of the corroding surface to the flame, the temperature and nature of the chlorine species in the vicinity of corrosive attack and so on.

The extent of the contribution of chlorine to the corrosion phenomena, among other combustion considerations, depends on the concentration and form of chlorine in the fuel (Tillman et al., 2009). Chlorine can influence the corrosion of tubes either directly as gaseous species by accelerating the oxidation of metal

alloys or in the form of deposits (solid or molten phase). The alkali and sulphur content of coal, oxygen concentration and temperature of the combustion environment also influences the formation of chlorine-based products of combustion. When the chlorine content of the coal is substantial, a significant amount of volatile HCl is present in the flue gas. It is estimated that for every 0.1% chlorine in coal, the HCl concentration in the flue gas is 80 ppm. In the molten or solid phase, alkali chlorides are thought to be responsible for aggressive corrosion attack.

Lees and Whitehead (Gupta et al., 1999) reported the presence of a chlorine phase that was almost always found on the surface of corroded tubes. Brooks and Meadowcroft (Meadowcroft and Manning, 1983) observed chlorine at the metal scale interface which resulted in an intergranular chloride attack of tubes. Manolescu and Thorpe (Harb and Smith, 1990) found that HCl adversely affects the integrity of the oxide layer, such that a 2% HCl gas completely destroys the continuity of the iron oxide layers. Flatley described a mechanism which postulated that HCl, by reacting with the outer grain boundaries of the previously protective oxide layer, creates microchannels which allow chlorine and sulphur containing species to gain access to the metal surface and cause accelerated corrosion (Harb and Smith, 1990).

Gaseous chlorine species present in combustion environments can accelerate the corrosion rate by diffusion through the protective oxide layer(originally formed by the reaction of metal with oxygen as a dense and stable oxide scale) to the scale-

metal interface to form volatile metal chlorides by the following reactions (Grabke et al., 2004):

$$M(s) + 2Cl(g) \rightarrow MCl_2(g)$$

(2.8)

$$M(s) + 2HCl(g) \rightarrow MCl_2(g) + H_2(g) \tag{2.9}$$

$$MCl_2(s) \rightarrow MCl_2(g) \tag{2.10}$$
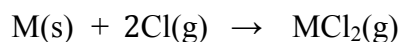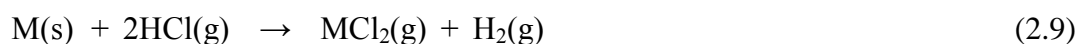
where M denotes Fe,Cr and Ni.

The volatile metal chlorides diffuse outward through the oxide scale and in oxidizing conditions, react with oxygen to form oxides by the following reactions:

$$3MCl_2(g) + 2O_2(g) \rightarrow M_3O_4(s) + 3Cl_2(g) \tag{2.11}$$

$$2MCl_2(g) + 1.5O_2(g) \rightarrow M_2O_3(s) + 2Cl_2(g) \tag{2.12}$$
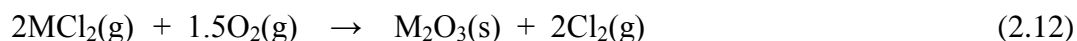
The resulting oxides that precipitate from this gas phase reaction form a loose and porous metal oxide layer, providing no protection against further attack. Also, the chlorine thus released is free to diffuse back to the metal surface, resulting in the process being cyclic (Antunes and de Oliveira, 2013). This process is shown schematically in Fig. 2.11.

Alkali chlorides in deposits can form low temperature melting eutectics (Tillman et al., 2009). The presence of chlorides in sulphate deposits lowers the melting temperature of the salt mixture, thus increasing the temperature range over which molten salt corrosion occurs. In other words, the presence of chlorine is likely to make the bell shaped curve wider and higher. In oxidizing environments
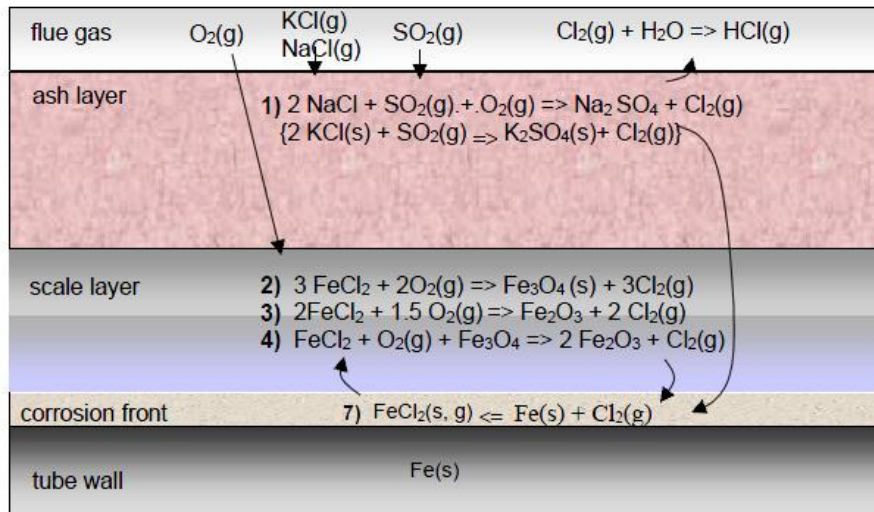
Figure 2.11 Principle mechanisms of Cl-induced corrosion (Reidl et al., 1999).

containing sulphur dioxide, alkali chlorides react to form sulphates releasing gaseous HCl or Cl_2 by the following reactions:

$$2KCl + 0.5O_2 + SO_2 + H_2O \rightarrow K_2SO_4 + HCl \qquad (2.13)$$

$$2KCl + O_2 + SO_2 \rightarrow K_2SO_4 + Cl_2 \qquad (2.14)$$

The chlorine containing gaseous species thus released have the ability to form volatile metal chloride according to reactions (2.8) and (2.9). The reactions of chlorides to form sulphates thus give way to corrosion by gaseous species but the solid sulphate deposit is much less corrosive than solid chlorides (Grabke et al., 1995).

2.4   Fireside corrosion in oxy-coal environments

Oxy-fuel combustion has been proposed as an effective means of controlling carbon dioxide emissions from coal-fired power plants. In oxy-coal combustion with flue gas recycle, an oxygen and carbon dioxide mixture, rather than air, is

used to burn the coal, thus facilitating the sequestering of carbon dioxide by minimizing the amount of nitrogen in the exit gas stream. Thus the oxy-fuel process differs from conventional air-fired systems by involving combustion atmospheres with reduced nitrogen and much increased levels of re-circulated flue gas. This difference also affects the formation and chemistry of deposits, and risk of corrosion on the fireside surfaces. The flue gas composition is significantly changed when combustion conditions are changed from air to oxy-fuel fired (Bordenet, 2008). The presence of higher levels of certain gases associated with oxy-fuel combustion, namely CO_2, SO_2 and H_2O is expected to have a negative impact on the corrosion of waterwalls, superheaters, reheaters and other boiler components in contact with the flue gas.

According to research carried out at the University of Utah (Ahn et al., 2010), a greater fraction of sulphur dioxide can be oxidized to sulfur trioxide in the flue gas due to the increased amount of oxygen in oxy-fuel combustion. The study based on a 5 MBtu/hr pilot scale combustor using high sulphur coal showed that, on average, the SO_3 concentration was four times higher during oxy-coal combustion as compared to air-fired conditions. Because sulphur trioxide is very corrosive, and can form sulphuric acid with water vapor in the flue gas, it can lead to an increased rate of corrosion, especially at temperatures below the acid dew point. Based on the findings of this study, that demonstrate the increased rate of production of sulphur trioxide due to high sulphur dioxide concentrations, it would be useful to study the corresponding effect, on corrosion, of these factors in oxy-coal environments.

Another study based on combustion tests in a 500 kW pulverized fuel combustion test rig followed by corrosion tests in laboratory furnaces at the University of Stuttgart (Stein-Brzozowska et al., 2011) compared the SO_2 content and its impact on corrosion between the two environments (air and oxy-fuel). The sulphur dioxide content was three times higher in the oxy-fuel environment accompanied by a higher rate of corrosion. The higher depth of corrosive attack observed after 350-hour exposure tests was attributed to higher SO_2 levels and increased sulphur-induced corrosion. An increase in the uniformity of the oxide layer was also observed with increase in the chromium content (from 18 to 25%) of the alloy under study.

Fry et al. (2011) performed real time corrosion rate measurements on one waterwall material and three superheater materials in a 1.5MW pilot scale PC-fired furnace in order to investigate the impact of oxy-coal retrofit on fireside corrosion. The gas phase sulphur dioxide concentration was also measured from burning three different coals. The SO_2 concentration obtained from oxy-firing was much greater than that from air-firing for all three coals. This was in conformity with the work of previous authors as was the reported increase in corrosion rates of the superheater tube materials when conditions were changed from air to oxy-firing. The waterwall probe, however, showed decrease in corrosion rates for all three coals.

Table 2.4 Pilot studies in oxy-fuel with reported sulphur effects (Stanger and Wall, 2011).

Facility	Focus of study	Sulphur related outcomes
1.2MW$_t$ Horizontal furnace, Japan	Flame speed in O_2/CO_2 mixes,Fuel-N conversion to NOx with reductive and oxidative conditions, and S deposition throughout equipment	−Sulphur balance not closed −O_2/CO_2 produced lower SO_2 output (kg/hr) −Higher SO_3 in ash for higher Ca coals
0.2MW$_t$ CANMET, Canada	NOx and SOx emissions in O_2/CO_2 mixes with pf combustion for flue gas and in-line burner measurements	−SO_2 emissions (mg/MJ) lower in recycled oxy-fuel −Fuel S conversion to SO_2 lower in recycled oxy-fuel mixes (91% air fired to 56-66% in oxy-fuel case) −Fuel S conversion to SO_2 independent of O_2 concentration, higher in-line sulphur deposition −Higher SO_3 in flue gas condensate (>3000mg/l) −Higher SO_2 concentration in oxy-fuel (1506-1778 ppm) than air-fired (598 ppm)
20kW 0.2MW$_t$ IVD-Stuttgart, Germany	SO_2 and H_2S profiles in Air/Oxyfuel furnace with direct SO_2 injection, SO_3 conversion fly ash deposition and composition	−Negligible sulphur deposition in radiative section of furnace (1150 ^{o}C) despite artificially high levels of SO_2 from direct injection −Large capture of sulphur in convective section of furnace (450-1150 ^{o}C) −H_2S levels higher in sub-stoichiometric stages of burner −H_2S levels doubled with higher SO_2 (3000 ppm) −SO_2 concentration higher in oxy-fuel (8 ppm air fired, 85 ppm oxy-fuel) −Evidence of sulphatisation and carbonisation in fly ash deposits −Higher SO_2 concentration (ppm) with oxy-fuel but lower emission rate (mg/MJ)
ANL-EERC USA	Furnace operating conditions, combustion process characteristics, flame spectral and flow properties, radiant heat transfer, stack emissions, wet and dry recycle	−SO_2 concentration in oxy-fuel higher depending on recycle conditions (1000-1640 ppm wet recycle, 550 ppm dry recycle) compared to air (280-338 ppm) −SO_2 emissions in oxy-fuel lower in dry recycle than wet recycle Both lower than air −SO_3 higher in oxy-fuel conditions, wet recycle higher than dry recycle
1MW$_t$ E.ON Test Facility, UK	Development and Testing update	−Elevated SO_2 levels in oxy-fuel (600 ppm air fired, 1750-2300 ppm oxy-fuel) −Lower SO_2 emissions (mg/MJ) in oxy-fuel

Table 2.4, taken from a review by Stranger and Wall (2011), summarizes the sulphur effects from different pilot scale oxy-fuel studies available in the literature. The outcome of nearly all these studies suggest an increase in sulphur dioxide concentrations in combustion gas, although the total sulphur dioxide emissions (mg/MJ) show a decreasing trend in most cases. This can be attributed to an increased capture of sulphur species in the ash.

Two separate pieces of experimental work, on the effect of oxyfuel environments on superheater corrosion published by NACE International show different results. The first study (Covino et al., 2008) conducted on different alloy materials at a superheater temperature of 675 $^{\circ}C$, both with and without ash coatings shows higher rates of corrosion of bare alloys in oxyfuel environments as compared to air combustion environments. However, under the influence of ash deposits, there was no noticeable difference in corrosion rates between the two environments. On the other hand, results of the second study (Pohjanne et al., 2010) showed that the oxidation rate of all the test materials was lower in the simulated oxyfuel environment than in the reference air combustion environment. Analysis of the causes of the different outcomes of the two studies showed that although the major constituents of simulated oxyfuel environments in both cases were CO_2, H_2O and O_2, a small proportion of SO_2 was also added to the simulated gas stream in the first case. Thus it can be inferred that increased CO_2 levels in the flue gas alone does not have a significant effect on the superheater corrosion, unless other impurities, such as acid gases are present.

Abang et al. (2013) carried out corrosion testing of five different superheater materials under simulated oxy-coal gas environments in a test tube furnace at 600 ^{o}C. The results indicated that metal wastage increased with decreasing chromium content. High amounts of sulphur in the oxide scale and inward penetration of sulphur into the base material due to sulphidation was observed for some alloys but no uptake of carbon (carburization attack) was observed for any of the materials tested.

Holcomb et al. (2012) carried out short-term (200hr) and long-term (1000hr) corrosion tests on different waterwall and superheater materials under varying laboratory conditions simulating oxy-coal and air combustion. They found that increased CO_2 content did not result in increased rates of corrosion of the alloys under long term exposure. However, short-term tests revealed increase in corrosion rates in CO_2 containing environments when the content of water vapour in the environment was also significant (30%).

Syed et al. (2012) carried out testing of various superheater and reheater materials in simulated air and oxy-fuel environments for co-firing coal and biomass at 600 and 650 ^{o}C. The corrosive environment was created in a vertical alumina lined furnace, both with and without the use of deposits. Comparison of metal loss for the materials showed that the wastage was greater in oxy environments as compared to air in all cases as shown in Fig. 2.12. The presence of deposits worsened the damage but damage was most severe under a deposit simulating undiluted alkali-iron trisulphate (37.5% Na_2SO_4, 37.5% K_2SO_4 & 25% Fe_2O_3).
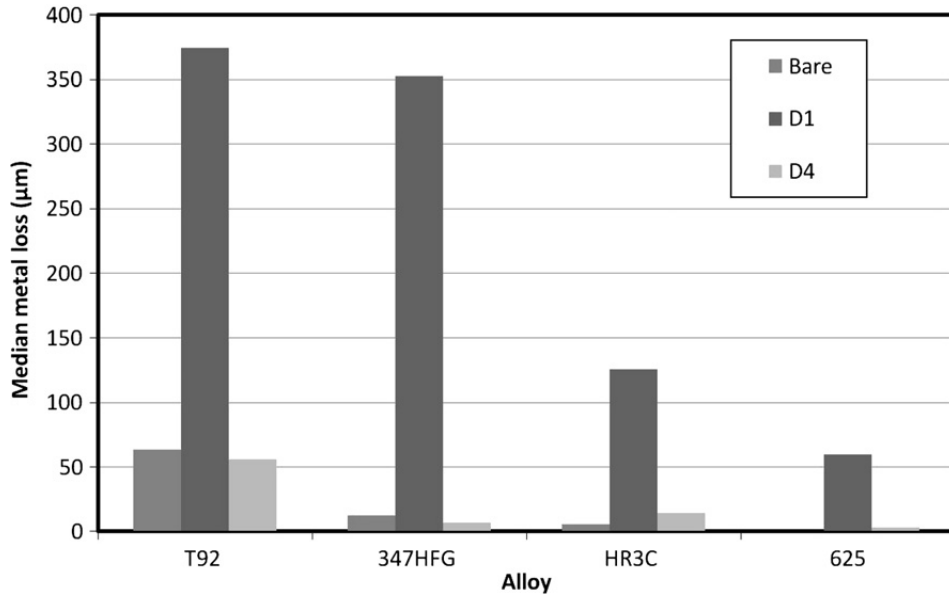
Figure 2.12 metal loss damage to bare alloys and alloys covered with deposits after exposure at 650 ^{o}C in a simulated oxy environment (Syed et al., 2012).

2.5 Effect of biomass firing and co-firing

In recent years, global warming concerns have led to increased interest in carbon neutral energy sources for power production, among which biomass is gaining an increasing importance. Biomass fuels are considered environmentally friendly because, firstly, there is no net increase in CO_2 as a result of burning biomass, secondly co-firing of biomass residues brings additional greenhouse gas mitigation by preventing CH_4 release from landfills, and thirdly most biomass fuels have very little sulphur content so SO_2 emissions can be reduced by co-firing biomass with coal, especially when burning high sulphur coals (Sami et al., 2001). However, biomass differs from coal in many important ways including organic, inorganic and energy content, physical properties, ash content, etc. The high potassium and chlorine contents associated with biomass fuels pose additional corrosion and deposition problems which is a major cause of concern when using biomass as a

fuel for energy production (Hughes and Tillman, 1998). Fig 2.13 provides a general indication of the type of corrosive species associated with biomass-firing or co-firing. The figure deals with K, S and Cl compounds where (g) represents gas phase and (c) represents condensed phase. It can be seen that potassium exists mostly as gaseous species in the furnace region and as silicates in the ash. With decreasing flue gas temperature (convective section), $KOH(g)$ is converted to $K_2SO_4(g,s)$ and $K_2CO_4(s)$ by gas phase reactions while $KCl(g)$ condenses to $KCl(s)$.
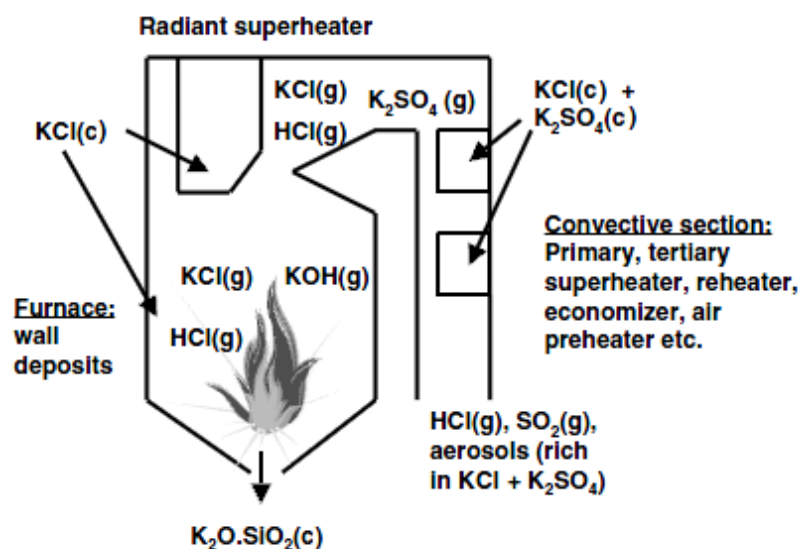
Figure 2.13 Principle pathways of potassium, sulphur and chlorine in a biomass fired boiler (Nielsen et al., 2000)

The mechanisms associated with potassium and chlorine-induced corrosion in biomass boilers are similar to those encountered in coal-fired boilers but the extent and severity of the problem is increased due to the presence of increased amounts of K and Cl in the fuel. Nielsen et al. (2000), in their review on the chlorine associated corrosion problems in biomass boilers, observed that the most severe

corrosion in biomass boilers can be attributed to the presence of alkali chloride in deposits and accelerated corrosion can occur well below the melting point of KCl. They also observed that chlorine in the gas phase may not lead to catastrophic corrosion in oxidising environments unless it is present in considerably high concentrations (above 1000ppm).

Uusitalo and his co-workers (Uusitalo et al., 2003, Uusitalo et al., 2002) performed a series of experiments to study the effect of chlorine on the corrosion behaviour of various boiler steels and coatings under synthetic atmospheres simulating combustion conditions encountered in boilers burning chlorine containing fuels. In the first case, different materials were subjected to corrosion under reducing conditions. The test environment consisted of 500 ppm HCl, 600ppm H_2S, 20% H_2O, 5% CO and Ar as a balance in a vertical test furnace at a test temperature of 550 ^{o}C. For ferritic steel of nominal composition 2.25Cr-1Mo, the corrosion products consisted of an outer layer consisting exclusively of iron and sulphur where extensive spalling was observed and an inner layer containing iron, chromium and molybdenum in addition to chlorine and sulphur. Internal attack by chlorine at the grain boundaries was also observed. The porous and lamellar nature of the non-protective scales was due to the presence of chlorine. The corrosion resistance of austenitic steel (nominal composition 27Cr31Ni3.5Mo) was better than ferritic steel but the internal attack by chlorine at the grain boundaries was also observed in this case. Under oxidizing chlorine containing environments, in the absence of hydrogen sulphide, the oxides formed were again observed to be porous and non-protective but no internal attack was observed in this case. Thus it was reiterated that the primary effect of gaseous chlorine species is to cause

repeated failure of a scale whose fast growth can be attributed to oxidation/sulphidation and chlorine induced corrosion damage is more pronounced under reducing conditions.

2.6 Ash deposition and corrosion

An introduction to the ash related problems in boilers is presented in Section 1.5. Deposits on boiler tubes not only hinder the heat transferred through the walls, but can also aggravate the corrosion of tube surfaces. Corrosion can be accelerated by certain chemical species in the deposits mainly Cl, S, K, Na, which have been discussed in the preceding sections. In the regions of the flame an initial sticky layer is usually attributed to an FeS deposit. On the other hand, condensing salts of Na and K are thought to contribute considerably in the initiation of ash deposition on superheater tubes as shown in Figure 2.14 (Tomeczek and Wacławiak, 2009).
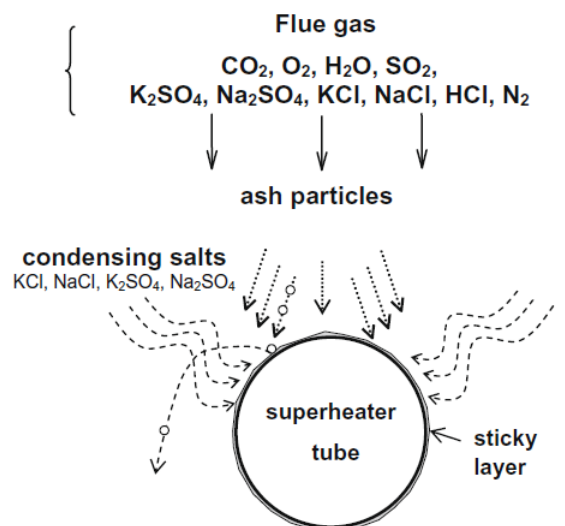
Figure 2.14 Schematic representation of ash particles deposition (Tomeczek and Wacławiak, 2009).

"Ash deposition phenomena are influenced by factors such as the type of coal (ash compositions, melting temperature and distribution of mineral matter), reaction atmosphere, particle temperature, surface temperature of heat exchanger tubes, tube materials, and flow dynamics." (Akiyama et al., 2011a). Current understanding in the literature, of ash deposition behaviour and related experiences from the laboratory to full scale have been reviewed by Bryers (1996) and Frandsen (2009).

While detailed study of deposit forming mechanisms in boilers is beyond the scope of this research, ash deposition characteristics have been studied primarily in the context of their relationship with under-deposit corrosion. In principle, corrosion and deposition can be regarded as two fundamentally distinct processes that are likely to occur simultaneously in corrosive environments containing solid particles and mineral species. It is in fact the mineral elements that provide a link between the two by affecting both the deposit forming tendencies of particulate matter in fuels as well as aggravating the corrosive propensity of the environment.

2.6.1 Ash forming elements in coal and biomass

Coal and biomass do not contain ash as such but, rather, mineral matter in various forms, most of which decomposes and/or reacts to form oxides during combustion. The mineral matter in fuels therefore effects the composition of ash formed. Ash forming constituents in coal are broadly classified as inherent and extraneous mineral matter, although clear distinction is difficult between the two as similar elements may be present in both. Inherent mineral matter is composed of chemical elements that were organically bound to the original plant tissues while extraneous

matter consists of inorganic species that mixed with the organic substance during the formation of coal either by sedimentation or contamination (Reid, 1971).

The mineral phases in biomass are much more diverse consisting of varying contents of inorganic and organic minerals that differ widely among different biomass groups and sub groups. Table 2.5 shows the occurrence of minerals in coal while Table 2.6 summarizes the mineral phases and components found in biomass.

Table 2.5 Occurence of minerals in coal (Reid, 1971).

Mineral	Formula
Shale group	$(K, Na, H_3O_3, Ca)_2(Al, Mg, Fe, Ti)_4(Al, Si)_8O_{20}(OH,F)_4$
Clay group	$Al_2O_3.2SiO_2.xH_2O$
(Kaolinite)	$Al_2O_3.2SiO_2.2H_2O$
Sulphur group	$FeS_2, FeSO_4, Na_2SO_4$
Carbonate group	$CaCO_3, CaCO_3.MgCO_3$
Associated minerals	
Quartz	SiO_2
Feldspar	$(K, Na)_2O.Al_2O_3.6SiO_2$
Garnet	$3CaO.Al_2O_3.3SiO_2$
Hornblende	$CaO.3FeO.4SiO_2$
Gypsum	$CaSO_4.2H_2O$
Apatite	$9CaO.3P_2O_5.CaF_2$
Zircon	$ZrSiO_4$
Epidote	$4CaO.3Al_2O_3.6SiO_2.H_2O$
Biotite	$K_2O.MgO.Al_2O_3.2SiO_2.H_2O$
Augite	$CaO.MgO.2SiO_2$
Prochlorite	$2FeO.2MgO.Al_2O_3.2SiO_2.2H_2O$
Diaspore	$Al_2O_3.H_2O$
Lepidocrocite	$Fe_2O_3.H2O$
Magnetite	Fe_3O_4
Kyanite	$Al_2O_3.SiO_2$
Staurolite	$2FeO.5Al_2O_3.4SiO_2.H_2O$
Topaz	$(Al,F)_2SiO_4$
Tourmaline	$MgAl_3(BOH)2Si_4O_{19}$
Hematite	Fe_2O_3
Penninite	$5MgO.Al_2O_3.3SiO_2.2H_2O$

Table 2.6 Phase and mineral composition of biomass (Vassilev et al., 2010).

Phases and components
− Structural ingredients namely cellulose, hemicellulose, lignin, extractives, others − Organic minerals such as Ca-Mg-K-Na oxalates, others − Mineral species from phosphates, carbonates, silicates, chlorides, sulphates, oxyhydroxides, nitrates and other mineral classes − Poorly crystallized mineraloids of some silicates, phosphates, hydroxides, others − Amorphous phases such as various glasses, silicates, others − Moisture, gas and gas-liquid inclusions associated with both organic and inorganic matter

2.6.2 Melting behaviour of ashes

Ash deposits and mixtures are known to melt over a wide temperature range, such that the difference in temperature where melting first starts and the temperature at which the ash is completely molten, may well be several hundred degrees. The fusibility characteristics of ash are commonly related to its composition, expressed as a function of the major oxides constituents. Table 2.7 shows the variation in composition ranges of these elements for coal and biomass ashes. It shows that while the major constituents in coal ash are SiO_2, Al_2O_3, Fe_2O_3 and CaO, biomass ashes contain a considerable proportion of calcium, potassium, magnesium and phosphorous oxides in addition to varying percentages of silica.

The melting behaviour of ash is considered as an important factor influencing the build-up of deposits in boilers with a melt phase of as little as 10% being sufficient to cause extensive deposit formation (Skrifvars et al., 1996). Compositional analysis of ash and Ash Fusion Temperature (AFT) tests have long been in use as laboratory techniques that attempt to predict the propensity of fuels to foul and slag

furnace heat transfer surfaces. A great variation exists in the fusion temperatures of

biomasses as compared to coal, as illustrated in Table 2.8. This is possibly due to

the diversity in composition of different biomasses as compared to coals.

Table 2.7 Typical composition of coal and biomass ashes expressed as percentage
of major oxide components (Seggiani, 1999).

Component	Coal ash (wt%)	Biomass ash (wt%)
SiO_2	≤ 72.5	1.5-39.5
Al_2O_3	≤ 46.8	0-12.9
TiO_2	0.0-2.5	0.0-11.2
Fe_2O_3	0.1-90.2	0.1-7.9
CaO	0.33-41.6	0.4-73.9
MgO	0.02-10.2	1.7-19.4
K_2O	0.0-6.0	0.0-24.2
P_2O_5	0.0-9.5	0.3-14.4
Na_2O	0.0-9.9	0.8-4.3
SO_3	0.0-24.3	0.4-7.0

Table 2.8 Ash fusion temperatures of biomass groups and coals with rank
(Vassilev et al., 2014).

Group, sub-group	DT	ST	HT	FT	Type[b]	Samples[c]
Biomass (all varieties)						
Mean	1105	1262	1318	1351	M	90
Minimum	670	795	975	1000	VL	90
Maximum	1505	1571	1665	>1700	VH	90
Natural biomass						
Mean	1103	1262	1319	1354	M	87
Minimum	670	795	975	1000	VL	87
Maximum	1565	1571	1165	>1700	VH	87
Coal						
Lignite (mean)	1147		1261	1286	M	5
Subbituminous coal (mean)	1218		1365	1389	M	10
Bituminous coal (mean)	1280		1404	1423	H	22
Coal (mean)	1251		1388	1411	M	37
Coal (minimum)	1105		1200	1205	L, M	37
Coal (maximum)	1525		1575	1585	H	37

[a] DT: initial deformation temperature, ST: spherical temperature, HT: hemispherical temperature,
FT: fluid temeperature

[b] Melting types based on HT: VL: very low (<1000 °C), L: low (1000-1200 °C), M: medium
(1200-1400 °C), H: high (1400-1600 °C), VH: very high (>1600 °C)

[c] Some of these data are mean values from numerous determinations for a given biomass variety

2.6.3 Corrosion under deposits

Skrifvars et al. (2008), carried out corrosion testing of different materials under various salt deposits in the temperature range 450-600 ^{o}C. The deposits containing sulphates and chlorides of sodium and potassium were composed in such a way that their first melting temperature was different for each salt mixture. The authors reported that the presence of melt in the salt deposit significantly increased the rate of corrosion but the corrosion could take place at temperatures below the melting point of salt deposits when chlorine was present. No corrosion was observed below the melting point if chlorine was absent in the salt. An important inference that can be made from this work is that if chlorine is present in the deposit, corrosion can occur under the deposit even without the formation of a melt phase, possibly due to the ability of chlorine molecules to channel through pores in the deposit structure to reach the metal surface.

Pettersson et al. (2009), studied the behaviour of carbon steel, low alloy steel and stainless steels in simulated biomass deposit conditions. They reported that although chlorides and sulphates of potassium in deposits lead to increased rates of corrosion, the increase is much less in stainless steels as compared to low alloy and carbon steel. The high temperature stainless steel S30815 showed a corrosion rate which was five times lower than carbon steel at 700 ^{o}C and twenty times lower at 550 ^{o}C. Type S30815 stainless steel showed a lower metal loss and lower amounts of chlorine in the scale compared to S30403. The better corrosion resistance was attributed to a 1.5% silicon addition in the alloy which formed silicon oxides in

internally oxidised regions and blocked the sites at which metal chlorides would otherwise form.

Yin and Wu (2009), conducted simulated corrosion experiments on TP316L stainless steel in the temperature range 500-600 ^{o}C. They found that the mass gain due to the formation of corrosion products is significantly increased with increase in temperature and the corrosion rates increased greatly with KCl in the ash deposit. Based on an XRD analysis of the samples, they concluded that increasing the SO_2 content in the gas phase has a positive influence on controlling corrosion due to chlorine species because of the formation of compact $FeSO_4$ scale on the metal surface and conversion of KCl to K_2SO_4 which is less corrosive. In other words, sulphur containing scales though less protective than a continuous oxide layer, can still provide some protection to the base metal by preventing the formation of highly volatile and non protective Cl containing scales.

2.7 Conclusions

Fireside corrosion and deposition are complex phenomena driven by multiple factors that often manifest their effect synergistically in a given environment. This makes it difficult to pinpoint the contribution of each factor on corrosion especially in multifarious systems, such as real boilers, where a wide variation in parameters exist among different regions. Small scale and laboratory studies are therefore useful for studying the effect of different parameters which are thought to increase the propensity for corrosion and deposition to take place. These studies can then be used to assess the corrosion behaviour of various materials at a larger scale,

providing the associated limitations are considered when assessment is made, given the somewhat simplified nature of the simulated environment. Oxy-fuel combustion and biomass firing are relatively new technologies and the effect of these conditions on corrosion is not well established. Also, most of the lab-scale studies, available in literature, have been carried out under isothermal conditions with no provision for heat flux to the samples. Since heat flux is an important parameter affecting the performance of boiler tubes, the inclusion of a heat flux into the simulated laboratory environment makes it a step closer to the real situation.

The use of biomass fuels for combustion has steadily increased over the past decade. However, research on understanding the combustion behaviour of biomass is still on going. Increased risks of deposition and corrosion have been associated with burning biomass. Owing to the wide variation in the different types of biomass and their associated characteristics, the need to examine the properties of individual fuels is important in order that data may be used in the assessment of suitability of commercially available biomass for use in power stations.

Chapter 3

Experimental setup and analytical techniques

This chapter describes in detail the experimental set up and materials used for carrying out the experiments. The techniques employed for analysing the specimen and the procedures adopted for specimen preparation are also highlighted.

3.1 Experimental setup for corrosion tests

The first half of the experimental work consisted of establishing an efficient and economic setup for the operation of the corrosion rig. This rig was purposefully designed for the University of Leeds with the help of Elite Thermal Systems in order to carry out fundamental corrosion studies on various boiler tube materials in simulated environments similar to those found in real boilers, but without the hazards associated with firing fuel in the laboratory. This rig combines simplicity of operation with the ability to generate a range of simulated environments in order to study the effect of various factors such as gas composition, temperature, deposit composition, type of material etc. on corrosion. The distinguishing feature of this rig, in which it differs from conventional lab scale corrosion equipment, is the provision of heat flux to the specimen.

Figure 3.1 is a simplified layout of the experimental setup while Figure 3.2 is a pictorial representation of the actual facility. The proceeding sections describe in detail the various components that were combined to set up the experimental
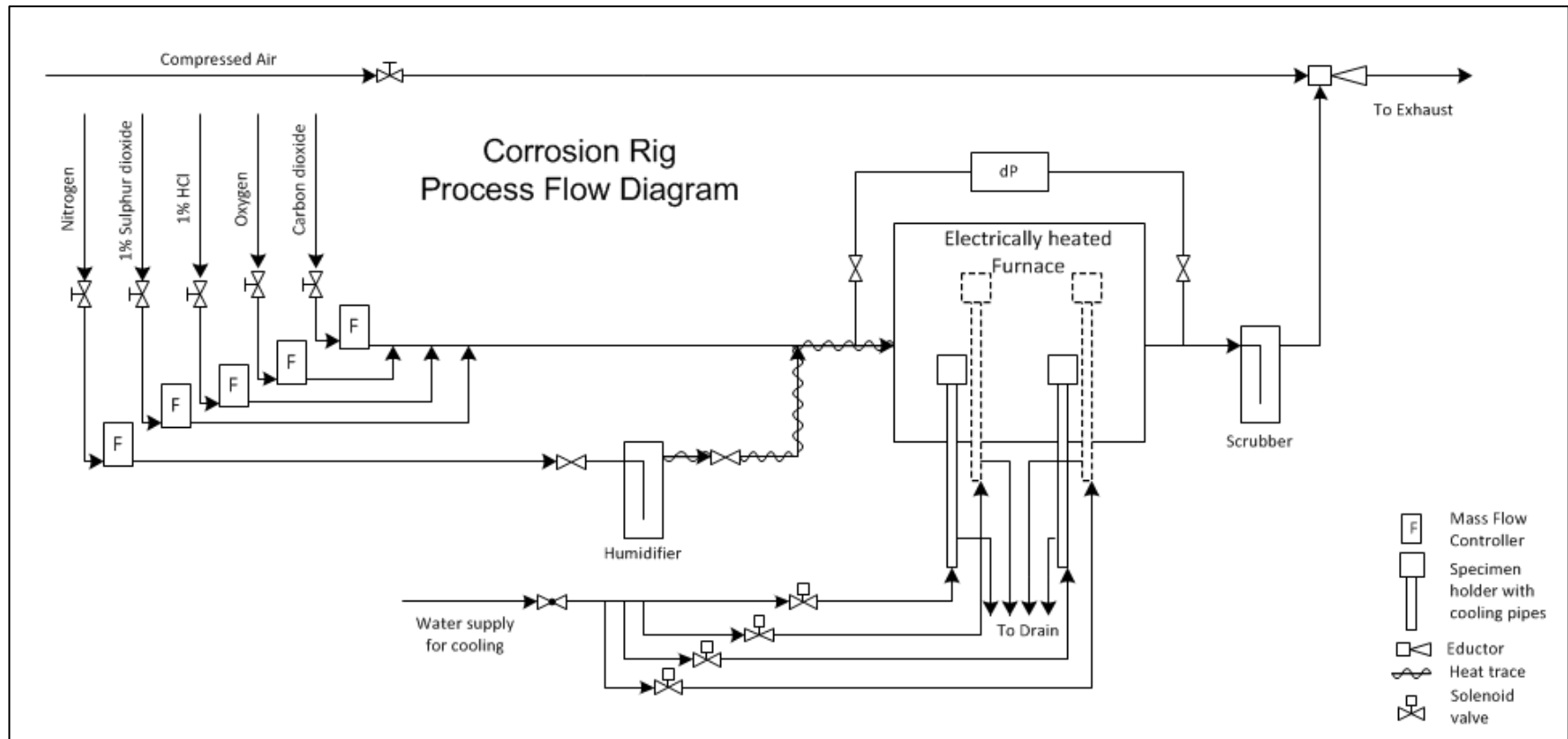
Figure 3.1 Simplified layout of the corrosion test facility.

facility in a dedicated laboratory area in the Energy Building at the University of Leeds.

Figure 3.2 Photograph of the experimental setup.

3.1.1 Corrosion Test Furnace

The corrosion test furnace is essentially a box type electrically heated furnace with a maximum power rating of 4.5KW and a maximum rated temperature of 1200^0C. It consists of an insulated steel casing enclosing a chamber where four corrosion samples can be loaded at any one time. The steel casing is split horizontally and lined with high temperature vacuum formed insulating board. The furnace is connected to the control panel via a 2m flexible conduit and cables. The temperature can be set at the desired set point with the assistance of temperature controllers mounted on the front of the control panel.

The top half of the furnace is hinged at the rear and held closed by front mounted overcentre catches. Gas springs assist with the opening and closing of the furnace

top. Heating is by six silicon carbide elements, mounted transversely over the chamber in the top half of the furnace (See Figure 3.3). The bottom half of the furnace consists of heavy gauge inconel plate and tubes, as shown in Figure 3.3, through which the sample carriers are loaded. The base plate is protected from excessive heat damage with the help of a ceramic plate with four openings for the sample carriers. The peripheries of the inconel plate form a powder trough system. A ceramic liner in inverted position with gas in and out pipes is placed on the metal trough system which provides a basic gas tight seal.
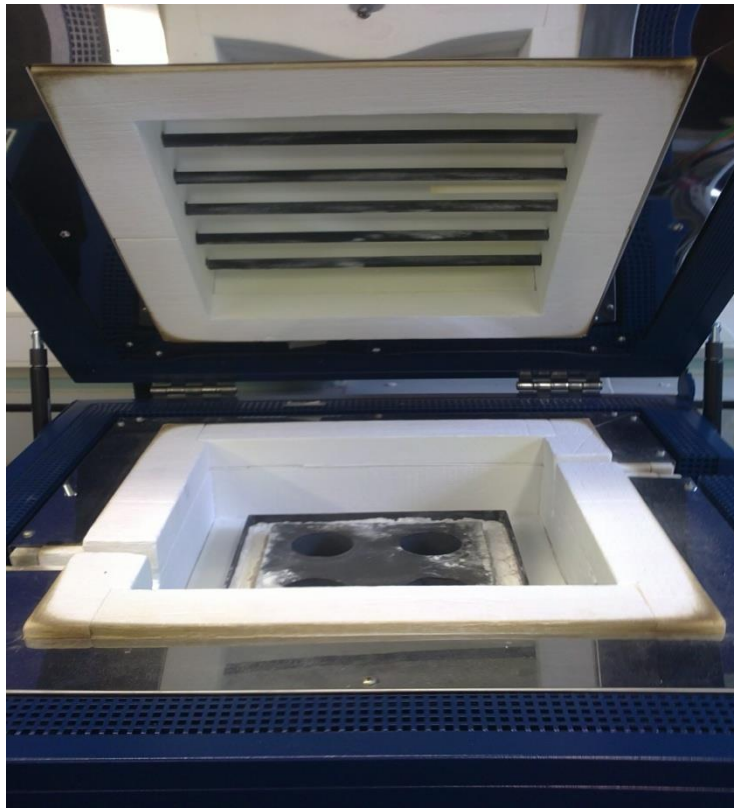
Figure 3.3 Photograph of the furnace showing the top and bottom halves.

The sample carriers are in the form of cooling bombs with water inlet and outlet pipes for cooling. The specimen sits on a 5mm thick, circular plinth machined on the anterior surface of the cooling bombs and having the same diameter as the base

of the specimen. The specimen was secured in position with a flange fastened to the cooling bombs with the help of four hex socket screws. The samples were machined from the specific tube material under study in the form of circular discs, 26mm in diameter and approximately 10mm in height. Figure 3.4 shows four samples loaded onto the sample carriers inside the furnace.

Figure 3.4 Four mild steel samples loaded inside the furnace before start up.

3.1.2 Gas Supply system

The simulated gas mixture entering the furnace was formed by combining five individual gas streams. The gases are supplied to the lab through their designated supply lines from gas bottle cylinders outside the lab via pressure regulators. Pressure gauges attached to regulating valves are also present inside the lab for fine control. For the purpose of safety, each of the gas supply lines were also fitted with quarter-turn valves which enable prompt gas shut off in case of emergency.

The flowrate of each of the gases was controlled by flow controllers of the type Aalborg GFC thermal mass flow controllers. Thermal mass flow controllers make

use of the heat conductivity of fluids, in this case gas, to determine the mass flow. Figure 3.5 is a schematic of a typical mass flow controller showing its essential components. In this instrument, metered gas is divided into two flow paths, one through the primary flow conduit and the other through a capillary sensor tube. Since both flow conduits are designed to ensure laminar flows, the ratio of their flow rates is constant. Two precision wound heater-sensor coils on the capillary tube are heated such that their temperature difference is zero at no flow conditions. When gas flows through the capillary, it carries heat from the upstream to the downstream section of the tube creating a temperature difference between the two sensor coils. This temperature difference is interpreted in the form of an electrical signal which is linearly proportional to the mass flow. The Aalborg flow controllers generate output signals of 0-5Vdc and 4-20mA. An electromagnetic valve combined with an appropriate orifice constitutes the flow control element and the mass flow output through the controller is maintained at the set flow rate with the help of a built-in closed loop control circuit. Each of the flow controllers was calibrated by the supplier for the specific gas it monitors.
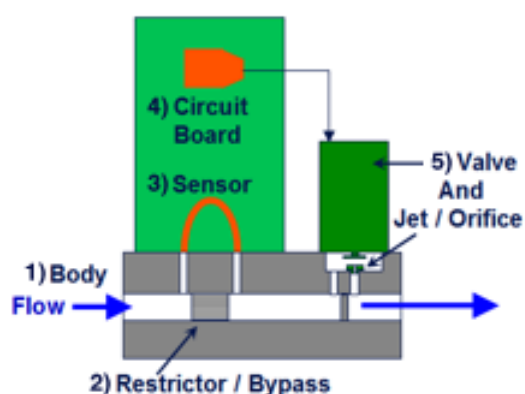
Figure 3.5 Schematic representation of a typical mass flow controller showing its essential components.

The five metered gases included carbon dioxide, oxygen, nitrogen, 1% hydrogen chloride in nitrogen and 2% sulphur dioxide in nitrogen. Water vapour was introduced into the system with the help of a humidifier arrangement which is explained in the next section. The moisture laden nitrogen was coupled with the rest of the gases downstream the humidifier to prevent premature mixing of the acid gases with water.

Since the operating flowrates are very low (approximately 600mL/min), a very slight negative pressure differential (0.06-0.08 mbar) was maintained across the rig to ensure continuous flow of the gases. This was achieved by using a compressed air venturi vacuum generator, or simply an air mover to drive the exhaust gases out of the system. The air mover was selected for this purpose because, as opposed to a pump, it is easy and inexpensive to install and does not require much maintenance due to the absence of moving parts. Its working is based on the Bernoulli principle. When compressed air is forced through a restricting nozzle, it expands and increases in velocity on exiting the restriction. This sudden change in velocity induces a vacuum or suction which helps to entrain the exhaust gases with the air stream which then exit the system via a specially designed flue. The flue was lined with ceramic and resistant to corrosion. However, the gas was scrubbed before exhaust (see Section 3.1.4).

The differential pressure across the rig was monitored with the help of a differential pressure manometer so as to maintain the pressure drop during operation to prevent air leakage. This was achieved by carefully controlling the suction pressure at the outlet with the help of a quarter turn plug valve and a needle

valve each attached to a bleed line. A pressure transducer fitted in the compressed air line was connected to the power source supplying the mass flow controllers. The signal from the pressure transducer serves as a trip to the power supply in case the compressed air flow rate falls or the air supply is cut off. This was a safety measure incorporated into the system in order to prevent the accumulation of exhaust gases in the laboratory.

3.1.3 Humidifier

Water vapour, which is a key component of the simulated environment, is introduced into the system with the help of a humidifier arrangement. Since it was important to prevent premature mixing of the acid gases with water vapour, it was added to the gas mixture immediately before it enters the furnace. This was achieved by bubbling a fixed quantity of nitrogen gas through distilled water in a dreschel bottle at a fixed temperature. The water was heated to a constant temperature with the help of a hot plate which is calibrated for corresponding water temperature for a fixed quantity of nitrogen passing through it. The moisture laden nitrogen stream was then combined with the rest of the gases through a heated pipe section to prevent condensation in the gas line.

Pre-determined amount of moisture can be added to the system by calibrating the humidifier. The calibration procedure was performed before commissioning the rig. For this purpose, 100mL/min of nitrogen was bubbled through a known amount of water in the humidifier at a given hot plate temperature. The water temperature was also recorded. After the water temperature had reached steady state, the amount of water vapour carried over by nitrogen was determined by recording the rate of loss in mass of water after every hour for at least 5 hours and

taking an average of the readings. This procedure was repeated for 200mL of nitrogen at four different water temperatures. It was found that the amount of water vapour accompanying the carrier nitrogen stream was proportional to the initial amount of nitrogen and varied only with temperature. The readings obtained from the calibration experiments agreed closely with the theoretical values as illustrated in Figure 3.6.
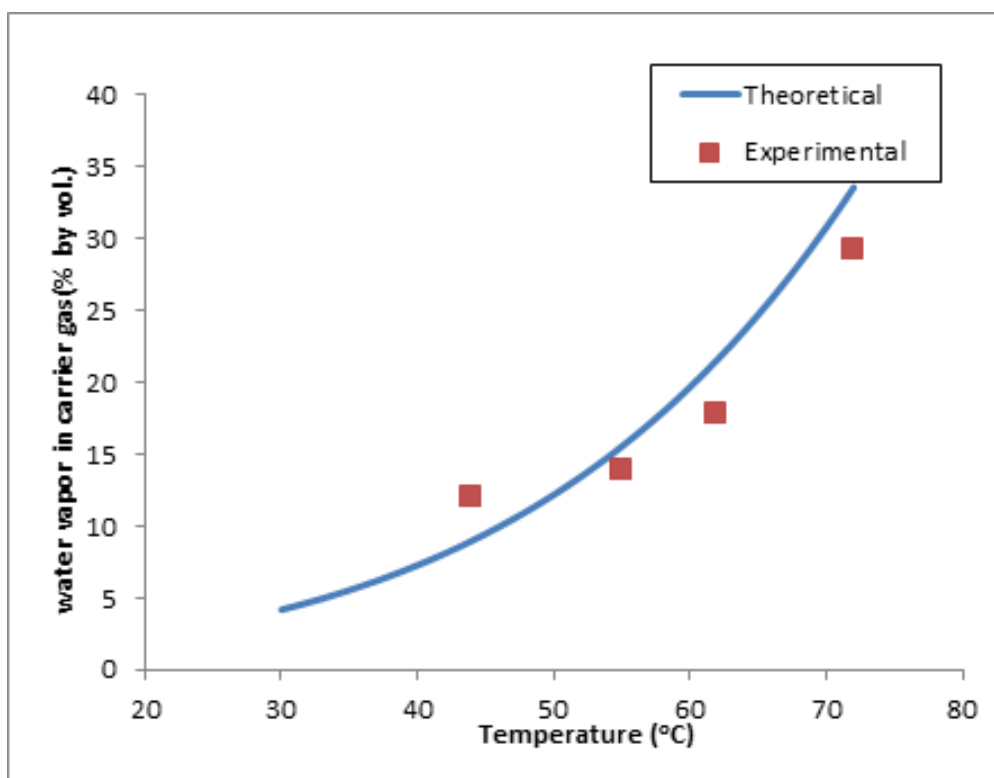
Figure 3.6 Relation between temperature and water vapour picked up by N_2 gas.

The theoretical values were obtained by using Bartlett's relation (1927), assuming that the ideal gas law is applicable to both the gas and vapour. According to this relation, the volume percent of water vapour at temperature T in a non-reactive gas at any pressure can be calculated by using the equation:

$$(\text{Volume percent of water vapour})_T = (100p)/(760P)_T \qquad (3.1)$$

where p is the vapour pressure of water in mmHg at temperature T and P is the total pressure in atmospheres (the mixture is assumed to be at atmospheric pressure).

3.1.4 Scrubber

The exit gas leaving the furnace was scrubbed with a basic solution in order to remove acid gas constituents before leaving the system through the extraction hood. This was achieved by bubbling the gas through a sodium hydroxide (NaOH) solution which results in neutralization of the HCl and SO_2 gas by the following neutralization reactions:

$$HCl(g) + NaOH(aq) \rightarrow Na.Cl(l) + H_2O(l) \tag{3.2}$$

$$SO_2(g) + 2NaOH(aq) \rightarrow Na_{-2}SO_4(l) + H_2O(l) \tag{3.3}$$
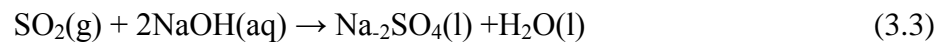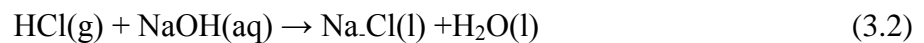
These balanced reaction equations were used to calculate the amount of NaOH required to neutralize known quantities (in moles) of HCl and SO_2 in the exit gas using ideal gas law relations.

3.1.5 Cooling water system

In order to create a heat flux through the samples, water had to be circulated through the cooling bombs. This enabled the specimen to be cooled to the desired temperature as the water takes up heat from the specimen. The lower surface of the specimen was in contact with the cooling bomb. The upper surface of the sample was in contact with the hot simulated gas environment. This corresponds to the difference in the inner and outer temperatures of superheater and reheater tubes in boilers arising due to the difference in temperature of the flue gas (in contact with the outer tube surface) and steam (in contact with the inner surface of the tube).

The temperature at the lower surface of the specimen was controlled by connecting the lower thermocouple to a temperature controller connected to a solenoid valve via an electrical circuit which controls the flow of water through the cooling bomb. There are four sets of temperature controllers and solenoid valves: one for each cooling bomb for independent operation. The temperature controllers are responsible for initiating the opening and closing of the solenoid valve through a simple ON/OFF control mechanism. The solenoid valves are normally closed until the temperature approaches the desired set point. This activates the circuit and initiates the flow of water through the valves. The water was supplied from the mains at a controlled flow rate via a flow control valve which ensured continuous flow of water to the solenoids. Figure 3.7 is an illustration of the cooling water

Figure 3.7 Cooling Water Circuit

circuit. During commissioning it was observed that rapid cooling of the specimens occurred when temperature exceeded the set point. The cause was cited in the high pressure of the water coming from the mains supply. The problem was solved by reducing the water pressure from the mains supply with the help of four pressure reducing valves plumbed in place before each of the solenoids.

3.1.6 Data Logging

The temperatures and flow rates were continuously logged and monitored with the help of National Instruments PC-based hardware and software. The hardware consists of a data acquisition device (compact DAQ chases) and a thermocouple and analogue input module. The software consists of a LabVIEW programme specifically tailored for the corrosion rig. Figure 3.8 is a typical screenshot of the output from the LabVIEW programme.
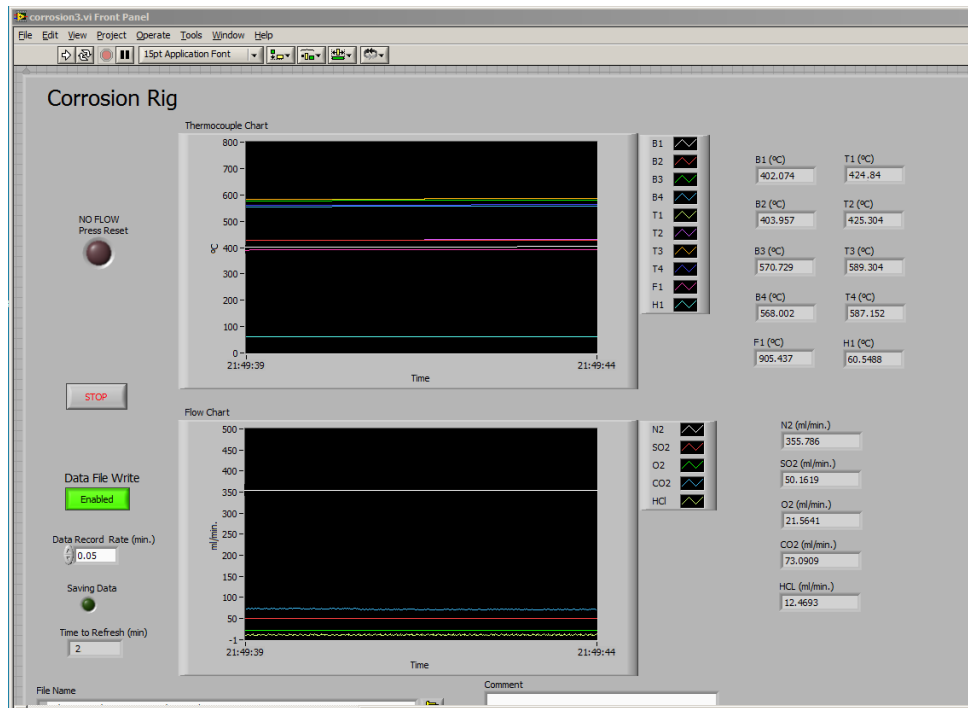
Figure 3.8 Screenshot of logged temperatures and flowrates in LabVIEW.

3.1.7 Temperature and heat flux measurements

Two temperature measurements can be made through the samples with the help of 1mm thick, calibrated k-type thermocouples. The thermocouples are embedded in thermowells inside the specimen 5mm apart as shown in Figure 3.9.
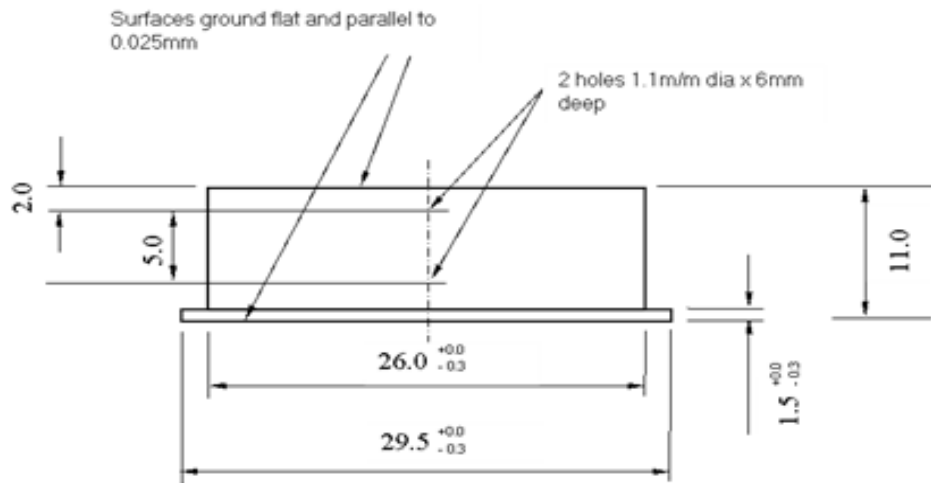
Figure 3.9 Cross-sectional sketch of the sample showing its dimensions.

Figure 3.10 is a typical example of plotted data showing the time-temperature history of the hot and cold side of an A210 specimen as it reaches steady state. From the difference in temperature between the two thermocouples, the temperature at the surface can be calculated by extrapolation. The heat flux can be calculated through the specimen of known thermal conductivity using the following forms of Fourier's law :

$$Q = kA\left(\frac{\Delta T}{x}\right) \qquad (3.4)$$

Or

$$q = k \left(\frac{\Delta T}{x} \right) \tag{3.5}$$

where Q is the conductive heat transfer through the specimen in kW, q is the heat

flux through the specimen in kWm^{-2}, k is the thermal conductivity of the material

from which the specimen is machined (Wm^{-1}K^{-1}), A is the heat transfer area of the

specimen, ΔT is the difference in temperature between the upper and lower surface

and x is the thickness of the specimen.
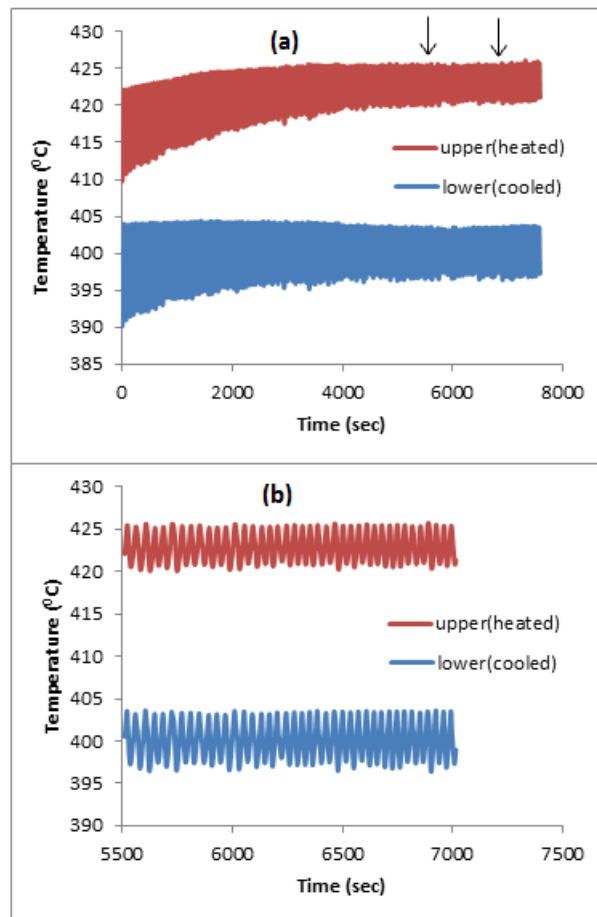
Figure 3.10 Historical temperature data (a) and inset (b) showing approach of steady state temperatures for an A210 specimen.

Example 3.1 Determination of heat flux through the specimen.

(a) Material : mild steel (A210)

Thermal conductivity, $k = 39 \text{Wm}^{-1}\text{K}^{-1}$

Temperature, hot side $= 423^0\text{C}$

Temperature, cold side $=400^0\text{C}$

Thickness, $x = 5.00\text{E-}03$ m

$q = 39 \ (23/5.00\text{E-}03) \ \text{kWm}^{-2}$

$q = 179.4 \ \text{kWm}^{-2}$

(b) Material : stainless steel (AISI310)

Thermal conductivity, $k = 21 \text{Wm}^{-1}\text{K}^{-1}$

Temperature, hot side $= 589^0\text{C}$

Temperature, cold side $=570^0\text{C}$

Thickness, $x = 5.00\text{E-}03$ m

$q = 21 \ (19/5.00\text{E-}03) \ \text{kWm}^{-2}$

$q = 79.8 \ \text{kWm}^{-2}$

By plotting a graph between temperature, T, and thickness, x, of the specimen, the temperature at the surface can be estimated by extrapolation assuming the temperature varies linearly with the distance. An example of this graph is shown in Figure 3.11, where T_1 is the temperature measurement on the cold side, T_2 is the temperature on the hot side and T_s is the surface temperature obtained by linear extrapolation.
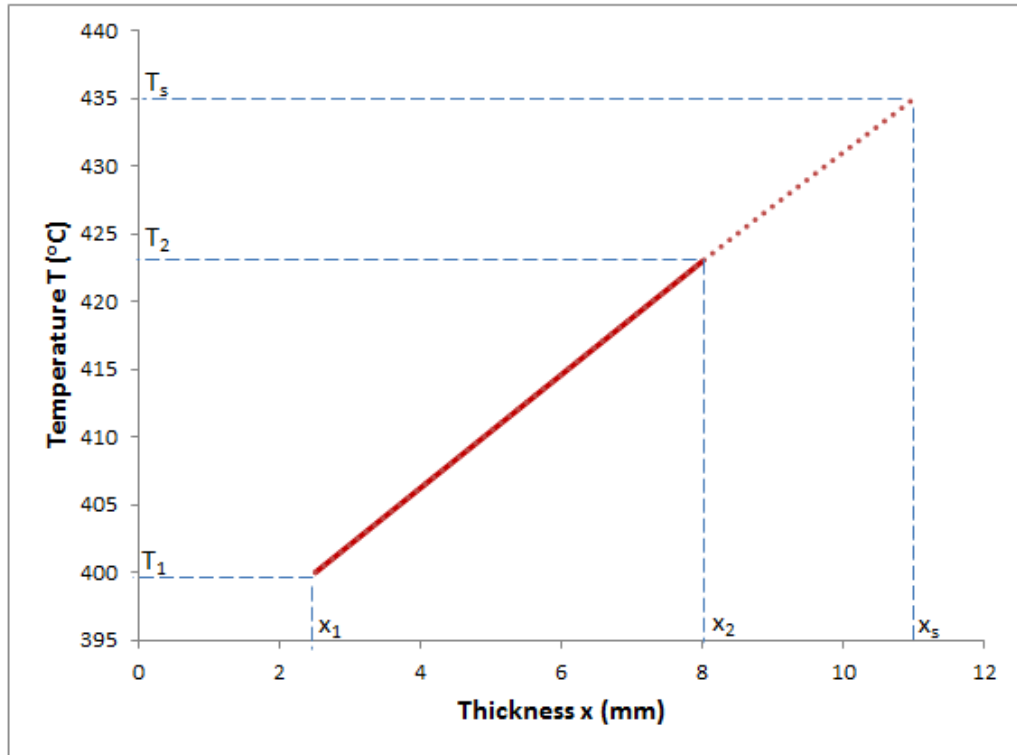
Figure 3.11 Graph showing the surface temperature obtained from extrapolation.

3.2 Experimental Materials and Specimen preparation

The experimental materials used for corrosion testing and their compositions are shown in Table 3.1. These materials were obtained in the form of round bars which were then machined at the university workshop according to the dimensions given in Figure 3.9.

Table 3.1 Materials used for corrosion testing.

Material/	Nominal composition (wt%)						
Designation	C	Si	Mn	P	S	Cr	Ni
Mild (low carbon) steel/ A210	0.18	≤ 0.55	1.22	0.02	≤ 0.025	–	–
Stainless Steel/ AISI310	0.08	≤ 1.5	≤ 2	≤ 0.035	≤ 0.015	24	19

The following techniques were adopted for pre and post exposure analysis of the machined specimen.

3.2.1 Pre-Exposure

Before being exposed to the corrosive environment, the specimen were first ground to a uniform surface roughness using Buehler P600 Silicon Carbide (SiC) paper & dry polishing with 6, 3 and 1μm diamond paste. After cleaning, a digital micrometer with a resolution of ±0.001mm was used to acquire 10 point measurements across the diameter of the specimen. The initial specimen thickness was then obtained by taking a mean of these measurements. The specimens were then conditioned in the furnace for 2hrs at 200 ^{o}C. For those tests in which the effect of ash coating on the specimen was studied, each specimen was coated with 0.2g of laboratory prepared ash to give a uniform ash layer approximately 1mm thick. A few drops of ethanol added to the ash helped to coat the specimen uniformly. The specimens were then dried in a specimen dryer at room temperature to evaporate the ethanol.

3.2.2 Post-Exposure

After each run, the specimens were carefully extracted from the furnace and the mean post-exposure thickness recorded by taking 10 point measurements as before. The specimens were then transferred to a desiccator to be further analysed with the help of SEM/EDX analysis (explained in Section 3.3) to study the surface morphology and composition of the corroded specimen. Surface and cross-sectional analysis each requires a different specimen preparation technique outlined below:

For surface analysis, the specimens were mounted on aluminium stubs with the help of double sided adhesive, conductive carbon tape. This secures the sample to the sample holder and allows a path for the electrons to travel and connect with ground. The specimen was then coated with gold or platinum using the Agar High Resolution Sputter Coater connected to an Agar Thickness Monitor.

Cross sectional analysis involved sectioning of the corroded specimen using Buehler's Isomet Low Speed Saw. The specimen was first encapsulated in cold setting epoxy resin using Buehler's Cast N Vac equipment with a curing time of at least 12 hours. The encapsulated specimen was then sectioned by cutting along a line perpendicular to the specimen surface using Buehler's Isomet Low speed saw with a diamond blade and an oil based lubricant. The sectioned piece was then ground with SiC paper and polished to a mirror finish using successive grades of 6, 3, 1 and ¼ micron diamond paste. It was then mounted onto aluminium stubs and coated with platinum in order to prevent charging and distortion of the image.

3.2.3 Ash preparation

The ashes and ash mixtures used for studying the effect of corrosion under the influence of ash deposits were prepared in controlled laboratory conditions using British Standards BS EN 14775:2009 for biomass and BS ISO 1171:2010 for coal. The coal and wood samples were both obtained from Drax. The ash obtained in each case was analysed for elemental content using EDX and XRF analysis.

3.3 Analysis techniques

This section describes the various analysis techniques/equipment used in this project. These include Scanning Electron Microscopy with Energy Dispersive X-

ray Spectroscopy (SEM/EDX), X-ray Florescence (XRF) Spectroscopy, Thermogravimetric analysis (TGA), standard proximate analysis, CHNS analysis, Simultaneous thermal analysis coupled with mass spectroscopy (STA-MS) and ash fusion testing (AFT).

3.3.1 SEM/EDX analysis

Scanning Electron Microscopy was used to obtain images of the sample by scanning it with a focused beam of electrons. Figure 3.12 is a schematic of a typical Scanning Electron Microscope showing its main components. The electrons interact with atoms in the sample, to produce different signals that can be collected
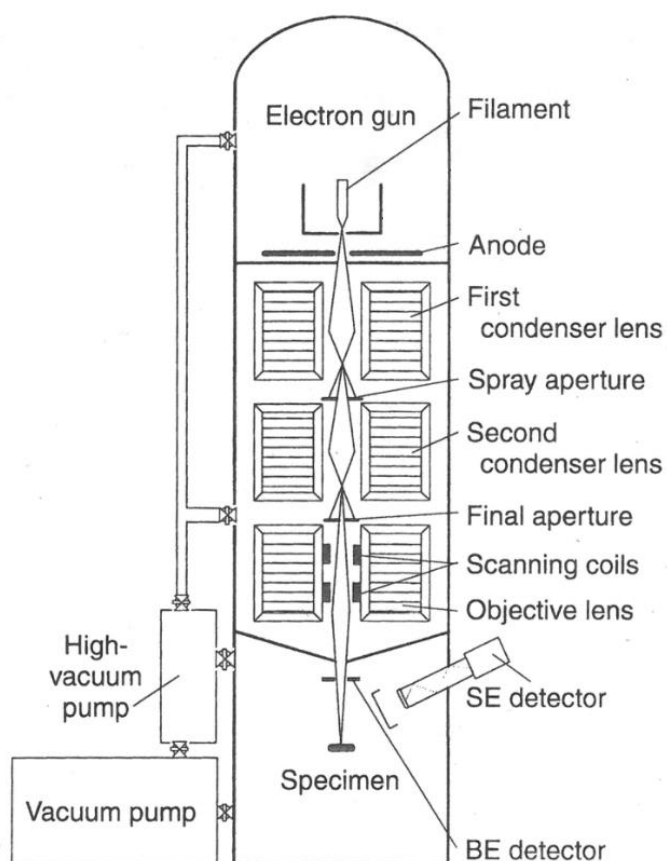
Figure 3.12 Schematic of a Scanning Electron Microscope.

by suitable detectors. These signals contain information about the sample's surface and composition. The secondary electron signal (SE) is produced as a result of the ejection of low energy electrons from the specimen atom by inelastic scattering interactions with beam electrons. If the incoming beam of electrons interacts with the atoms of the specimen and is backscattered with negligible loss of energy (elastic scattering), a Backscattered Electron (BSE) Image is obtained. Energy Dispersive X-ray (EDX) signals are generated when the electron beam removes an inner shell electron from the atom, causing an electron from a higher energy orbital to take its place and emit characteristic X-rays. These characteristic X-rays are used to identify the composition and measure the abundance of elements in the sample. The main SEM equipment used in this study was Philips EVOMA 15 shown in Figure 3.13.
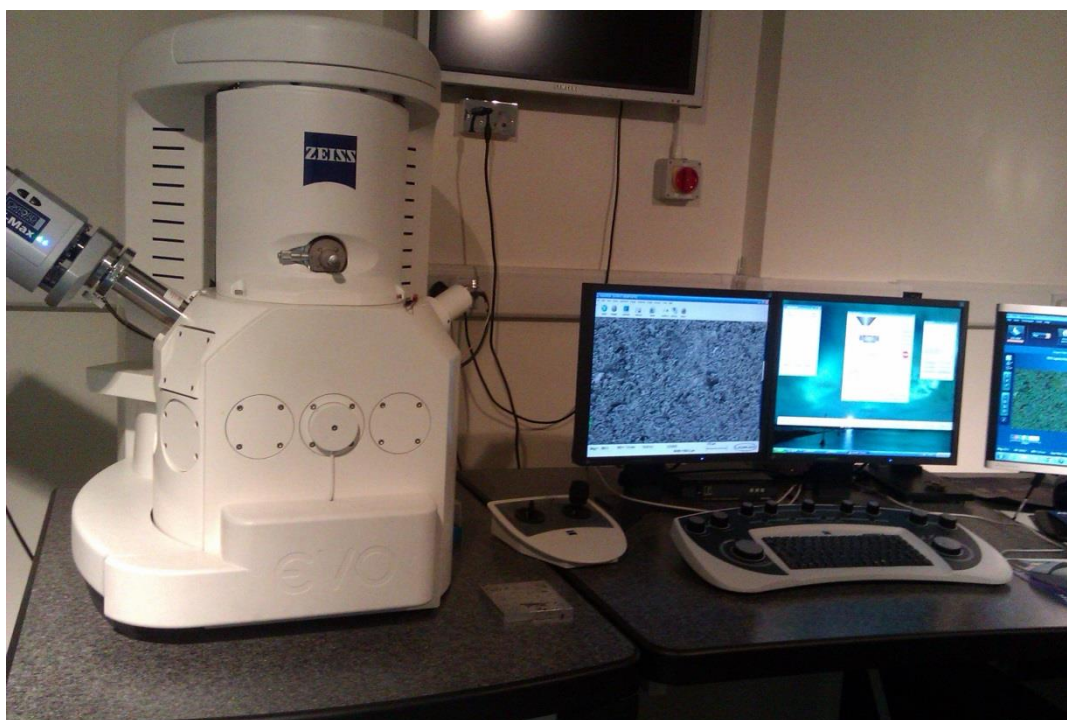
Figure 3.13 Philips EVOMA 15 Scanning Electron Microscope.

3.3.2 XRF analysis

X-Ray Fluorescence (XRF) analysis is based on the emission of fluorescent or secondary X-rays from a material that has been excited by bombarding with high-energy electromagnetic radiation (X-rays or γ-rays). This technique was used to determine the elemental composition of the various ashes used in this work. For this purpose, XRF specimens in the form of fused beads were prepared from laboratory prepared ash in a dedicated high temperature furnace using a platinum crucible and mould. The procedure involved dissolving 0.5g of ash in 5g lithium tetraborate at 1250 ^{o}C. The lithium tetraborate acts as a fluxing agent. A minute quantity of lithium bromide (0.05g) served as an antiwetting agent, preventing the ash from sticking to the platinumware. Extreme caution should be exercised during weighing and especially heating and transferring the reagents inside the furnace due to the extremely reactive nature of lithium tetraborate. The prepared specimen were then given to the technician for analysis in a Thermoadvent XP sequential XRF analyser.

3.3.3 Standard proximate analysis

The proximate analysis of the fuels in terms of moisture, volatile matter and ash was carried out using British Standards BS ISO 17246:2010 for coal and BS EN 14774-3:2009, 15148:2009 and 14775:2009 for biomass. The following is a brief description of the procedures followed for determining the moisture, volatile matter and ash content. The fixed carbon was calculated by difference.

Determination of the moisture content involves heating a minimum of 1g of ground sample in an oven at 105±2 ^{o}C for at least two hours. The difference in weight of the sample before and after heating gives its moisture content.

The volatile matter of the fuels was determined by heating a minimum of 1g of sample in a covered crucible in a furnace at 900 ± 10 ^{o}C for seven minutes. By subtracting the moisture content of the sample from the loss in its weight before and after heating, the amount of volatile matter is obtained.

Determination of the ash content involves heating a minimum of 1g of sample in a furnace at a specified temperature for upto 12 hours or until the sample attains constant weight. The specified temperature for biomass is 550 ^{o}C while that for coal is 850 ^{o}C. Subtracting the moisture content from the mass loss upon heating gives the amount of ash in the sample.

3.3.4 Thermogravimetric analysis

Thermogravimetric analysis involves testing the weight changes in a known amount of sample during programmed heat treatment. The basic advantage of this technique is that it allows proximate determination in a single operation. The equipment used for determining the proximate content of the fuel samples was a Shimadzu TGA-50 Thermogravimetric Analyser, shown in Figure 3.14. It essentially consists of an electric oven fitted with a thermo-balance and temperature controller, also permitting controlled flow of gas through the system.

The proximate programme employed consisted of initial heating of the sample to 110 ^{o}C at a heating rate of 10 ^{o}C/min in nitrogen at 50mL/min and holding for 10 min. The resultant weight loss is associated with the removal of moisture. The heating rate was then increased to 25 ^{o}C/min until the temperature reached 910 ^{o}C with a holding time of 10min. The weight loss corresponding to this step is due to the release of volatiles by pyrolysis. In the final step, air was introduced into the

oven at 910 $^{\circ}$C for 10 min to allow for oxidation of fixed carbon, leaving behind a residue consisting mostly of ash.

Figure 3.14 Shimadzu TGA-50 Thermogravimetric Analyser.

3.3.5 Ultimate Analysis

The carbon, hydrogen, nitrogen and sulphur content of the fuels was determined using a Thermoscientific Flash 2000 Organic Element Analyzer shown in Figure 3.15. The equipment takes advantage of the tendency of combustible materials to react with oxygen at high temperatures to produce gaseous species which can be quantified with the help of gas chromatography to identify the elemental composition of combustibles present in the original sample. About 2.5 mg of moisture-free samples encapsulated in tin capsules are introduced into the furnace

at 900 ^{o}C where they are injected with pure O_2 for 10 seconds. This causes the samples to undergo flash combustion along with the tin. The evolved gases then pass through a reactor consisting of an oxidizing and reducing section to form CO_2, H_2O, SO_2 and N_2 which are then separated with gas chromatography and their amounts determined.

Figure 3.15 Thermoscientific Flash 2000 Organic Element Analyzer.

3.3.6 Simultaneous thermal analysis coupled with mass spectroscopy

Simultaneous thermal analysis coupled with mass spectroscopy (STA-MS) was used to characterise the behaviour of laboratory prepared fuel ashes in order to obtain information regarding their melting behaviour and gas phase release as a function of temperature. STA equipment enables thermogravimetric analysis

(TGA) to be performed simultaneously with differential scanning calorimetry (DSC). While TGA provides information regarding the change in weight of the sample with respect to a controlled heating programme, DSC enables the detection of heat flow through the sample during the process. This is done by comparing the sample temperature to the temperature of an inert reference material, to subsequently quantify the energy associated with any heat producing or heat consuming processes occurring in the sample. Heat consumption is associated with physical changes taking place in the sample while heat producing processes are linked to chemical changes. Melting is regarded as the main endothermic reaction occurring in the ash on heating. The ash samples were analyzed using a Netzsch STA 449C coupled with a Netzsch QMS (Quadrupole Mass Spectrometer) 403C Aeolos equipment linked to computer controlled detection and analysis software. The equipment is pictured in Figure 3.16.

Figure 3.16 Netzsch STA 449C and Netzsch QMS 403 Aeolos analyser.

In each case, 10mg of ash was heated from 30 ^{o}C to 1400 ^{o}C in a 12.5% O_2/He environment at a constant heating rate of 10 ^{o}C/min. The gas outlet at the furnace of the thermobalance was connected to the gas inlet at the mass spectrometer through a heated fused silica capillary tube. This enabled the detection of gas species such as carbon dioxide, sulphur dioxide, chlorine and water vapour, evolved during the heating process.

3.3.7 Ash fusion Tests

Ash fusion tests were carried out in a Carbolite Ash Fusion furnace (shown in Figure 3.17) fitted with a camera and image processing software designed to capture images at preset temperature intervals.

Figure 3.17 Carbolite Ash Fusion furnace.

The fusion samples were prepared by carefully adding a few drops of demineralised water to form a paste of suitable consistency. They were then moulded into compact cylinders 5mm (height) and 5mm (dia) and allowed to dry for a few hours. The ash test pieces were then mounted on porcelain slabs and placed inside the furnace and heated in an oxidising environment (air) at a constant heating rate of 10 ^{o}C/min from 550 ^{o}C to 1500 ^{o}C. The digital probe fitted inside the furnace enabled image capture at every 5^{0}C rise in temperature. The key stages in the deformation and flow of the sample cylinders were determined using British Standards (DD CEN/TS 15370 – 1:2006). The shrinkage temperature (ST) is defined as the temperature at which the area of the test piece reduces to 95% of the original area. The temperature at which the first signs of rounding of the edges occur, marks the deformation temperature (DT). The hemispherical temperature (HT) is the temperature at which the height becomes approximately half of the base diameter such that the test piece forms a hemisphere. At the flow temperature (FT), the height of the melting ash layer becomes approximately half the height at the hemispherical temperature.

Chapter 4

Corrosion experiments

4.1 Introduction

This chapter includes the results obtained from performing a series of experiments on the corrosion rig, the operational details of which have been presented in Chapter 3. The corrosion damage experienced by the different specimens was quantified in terms of average thickness loss which was measured as described in Section 3.2.1. Elemental mapping and surface morphology of corroded specimen was studied with the help of SEM/EDX analyses. The typical duration for an experimental run was 350hrs. This long duration of the tests was a major limiting factor in obtaining experimental data in bulk.

It is pertinent to mention here that technical and safety issues relating to the new building led to a number of aborted runs resulting in early shutdown of the rig/experiment. For all such occurrences, the particular run had to be started afresh (in order to avoid the introduction of thermal cycling as an additional factor affecting the rate of corrosion). The specimens from these aborted runs were not considered for inclusion in the results presented. However, it was observed that where the aborted test runs lasted a period of 240 hours or less, thickness measurements did not reveal any metal loss. This observation can be used to emphasize the importance of a minimum exposure duration that is required before measurable corrosion rates can be recorded.

4.2 Results and Discussion

It has been discussed in Chapter 2 that the rate of corrosion is controlled not by one but by multiple factors which makes it difficult to ascertain the effect of individual variables. Keeping this in view, the corrosion experiments were designed such that the effect of certain factors on corrosion in an oxy-fuel environment could be studied by minimising the effect of other variables. The parameters that were kept constant for all the test runs included gas and specimen temperatures which in turn helped in maintaining a fairly constant heat flux through the specimen. The control temperature for the mild steel specimen was set at 400^0C while that for the stainless steel was set at 570 ^oC.The average temperature difference measured across the mild steel specimens was 23 ^oC, giving a heat flux of ~180kW/m^2 while the average temperature difference across the stainless steel specimens was 19 ^oC, giving a heat flux of ~80kW/m^2. The metal surface temperature for the mild steel and stainless steel specimen were approximated at 435 ^oC and 600 ^oC, respectively. The gas temperature was controlled at 900±5 ^oC with an average exposure time of 350hrs.

4.2.1 Baseline experiments

4.2.1.1 Significance of fuel ash

The first set of baseline experiments were performed in an oxy fuel environment consisting of N_2, 3% O_2, 64% CO_2, 10% H_2O, 1000ppm SO_2 and 250ppm HCl. Duplicate samples of the given mild steel (A210) and stainless steel (AISI310) specimen were prepared for these tests in order to check the repeatability of the measurements. The materials were exposed to the corrosive gas environment both

with and without the presence of an ash coating. The deposit used for the baseline experiments consisted of wood ash prepared under standard laboratory conditions as laid out in Section 3.2.3. The gas and metal temperatures were held constant as described in Section 4.2. The measured values of thickness loss and calculated rate of corrosion for mild steel and stainless steel are shown in Table 4.1 and Table 4.2 respectively. For the sake of convenience, the mild steel specimens are denoted by MS and stainless steel as SS. The results showed good agreement between metal loss values for duplicate samples and also emphasized the importance of the effect of an ash layer on the rate of corrosion. For the current type of ash, the metal loss exhibited by ash coated specimen was considerably higher than the corresponding type of specimen where no ash coating was applied. Also, it can be observed that the metal loss rates exhibited by the mild steel specimen are much higher as compared to the stainless steel, as expected. This is due to the high chromium content of stainless steel which is linked to increased corrosion resistance.

Visual observation of the corroded specimen revealed scales for the mild steel specimens which were poorly adherent and spalled easily during extraction from the furnace. On the other hand, the corrosion scales for stainless steel were much less conspicuous demonstrating superior corrosion resistance and hence lower values of metal loss. For all types of specimen coated with ash, the ash layer above the corroded specimen appeared to have fused and re-solidified acquiring a lighter, whiter appearance. This indicates the possible formation of a melt phase which is linked to higher rates of corrosion and will be discussed in further detail in Section 4.2.2.

Table 4.1 Metal loss for duplicate mild steel(A210) specimen under oxy fuel environment with and without an ash deposit for an exposure time of 380hrs.

Specimen designation	Ash coating	Average initial thickness (mm)	Average final thickness (mm)	Mean metal loss (mm)
MS_1	None	10.985	10.9762	8.8E-03
MS_2	None	10.9834	10.9744	9.0E-03
MS_3	coated	10.9414	10.9318	13.3E-03
MS_4	coated	10.9842	10.9712	13.0E-03

Table 4.2 Metal loss for duplicate stainless steel(AISI310) specimen under oxy fuel environment with and without an ash deposit for an exposure time of 360hrs.

Specimen designation	Ash coating	Average initial thickness (mm)	Average final thickness (mm)	Mean metal loss (mm)
SS_1	None	11.0983	11.0937	4.6E-03
SS_3	None	10.9923	10.9876	4.7E-03
SS_3	coated	10.9867	10.9797	7.0E-03
SS_4	coated	11.0154	11.0085	6.9E-03

4.2.1.2 Air case

The flue gas environment during oxy-fuel combustion differs considerably from air firing. To serve as a simplified basis for comparison between air and oxy fuel, bare and ash coated specimen of mild and stainless steel were subjected to a gas environment containing N_2, 3% O_2, 14% CO_2, 10% H_2O, 1000ppm SO_2 and 250ppm HCl. Note that the basic difference in composition for this case as compared to the one in Section 4.2.1.1 is between the nitrogen and carbon dioxide contents, while the concentration of other gas constituents is similar. For actual combustion systems, this similarity in the percentage of water vapour and acid gas constituents for air and corresponding oxy firing can only occur if the recycle stream in oxy fuel is taken after the condensation and flue gas desulphurisation units.

Table 4.3 shows the measured metal loss experienced by the mild steel and stainless steel specimen. Table 4.4 shows the rate of corrosion (expressed in nm/hr) observed in this case compared to the simulated oxy fuel gas mixture in the previous section. The results indicate that there is little difference in the rate of corrosion when the carbon dioxide content of the flue gas is increased in oxidizing environments. This leads to the inference that increased CO_2 content alone may not result in increased corrosion rates and is in agreement with the observations of Holcomb et al. (2012) and Abang et al. (2013). Furthermore, it points towards the significance of other constituents in the flue gas such as SO_2, HCl and water vapour. Among these factors, the effect of increasing the sulphur dioxide content of the simulated oxy fuel gas mixture both with and without the presence of fuel ash deposits was considered in detail and is presented in the next section.

Table 3.3 Measured metal loss for mild(A210) and stainless(AISI310) steel in a
simulated air environment for an exposure time of 360hrs.

Specimen designation	Ash coating	Average initial thickness (mm)	Average final thickness (mm)	Mean metal loss (mm)
MS$_1$	none	10.9393	10.931	8.3E-03
MS$_2$	coated	10.9416	10.9292	12.4E-03
SS$_3$	none	10.685	10.6804	4.6E-03
SS$_4$	coated	10.9585	10.9515	7.0E-03

Table 4.4 Comparison of corrosion rates between simulated air and oxy for
(a) mild steel and (b) stainless steel.

(a)

Ash coating	Gas comp.	Rate of corrosion (nm/hr)
non-coated	Air	23.1
	Oxy	23.7
coated	Air	34.4
	Oxy	35

(b)

Ash coating	Gas comp.	Rate of corrosion (nm/hr)
non-coated	Air	12.7
	Oxy	13.0
coated	Air	19.2
	Oxy	19.4

4.2.2 Effect of variation of SO₂ content and deposit composition

In order to assess the effect of increasing the sulphur dioxide content on the rate of corrosion for both mild and stainless steel, a series of experiments were performed. In addition, the effect of an ash layer on the rate of corrosion was also studied. The elemental composition of ashes, denoted by D1, D2 and D3 used for coating the specimen is shown in Table 4.5. D0 refers to the bare specimen where no ash coating is applied. D1 is a UK coal ash, D2 is a biomass (pine wood) ash while D3 is a mixture of 50% D1 and 50% D2 on a weight basis. Table 4.6 is a simplified

Table 4.5 Elemental composition of ash used for coating the specimen.

Element (wt%)	Type of ash coating		
	D1 (Coal ash (Potland Burn UK))	D2 (Biomass ash (Pine Wood))	D3 (50% coal 50% pine ash)
O	53.1	42.1	47.6
K	1.7	9.6	5.6
Na	0.4	1.2	0.8
Ca	0.7	18.0	9.3
Fe	5.7	4.0	4.8
Mg	1.1	5.7	3.4
Si	19.6	10.1	14.8
Al	14.9	4.7	9.8
Cl	0.07	0.2	0.13
Others	Bal.	Bal.	Bal.

Table 4.6 Matrix of conditions studied for the effect of SO₂ and deposit composition.

SO₂(ppm)	Material	Ash coating			
		D0	D1	D2	D3
1000	MS	✓	✓	✓	✓
	SS	✓	-	✓	-
2000	MS	✓	✓	✓	✓
	SS	✓	-	✓	✓
3000	MS	✓	✓	✓	✓
	SS	✓	✓	✓	✓

matrix of the test conditions used to study the effect of increasing the sulphur dioxide content of the flue gas on the rate of corrosion. The gas and metal temperatures, heat flux and concentration of the remaining gases including carbon dioxide, oxygen, water vapour and hydrogen chloride were held fairly constant for all the cases.

The rate of corrosion computed from the measured values of metal loss for mild steel corresponding to different SO_2 concentrations and various ash deposits are shown in Figure 4.1. It can be seen that the specimens coated with ash D2 exhibit the highest rates of corrosion and the rate of metal loss increases with increase in SO_2 concentration. A similar trend of increase in rate of corrosion with increasing SO_2 content is observed for specimen coated with deposit D3 but the rate of metal loss is lower than that for specimen coated with D2. A slight increase in the rate of
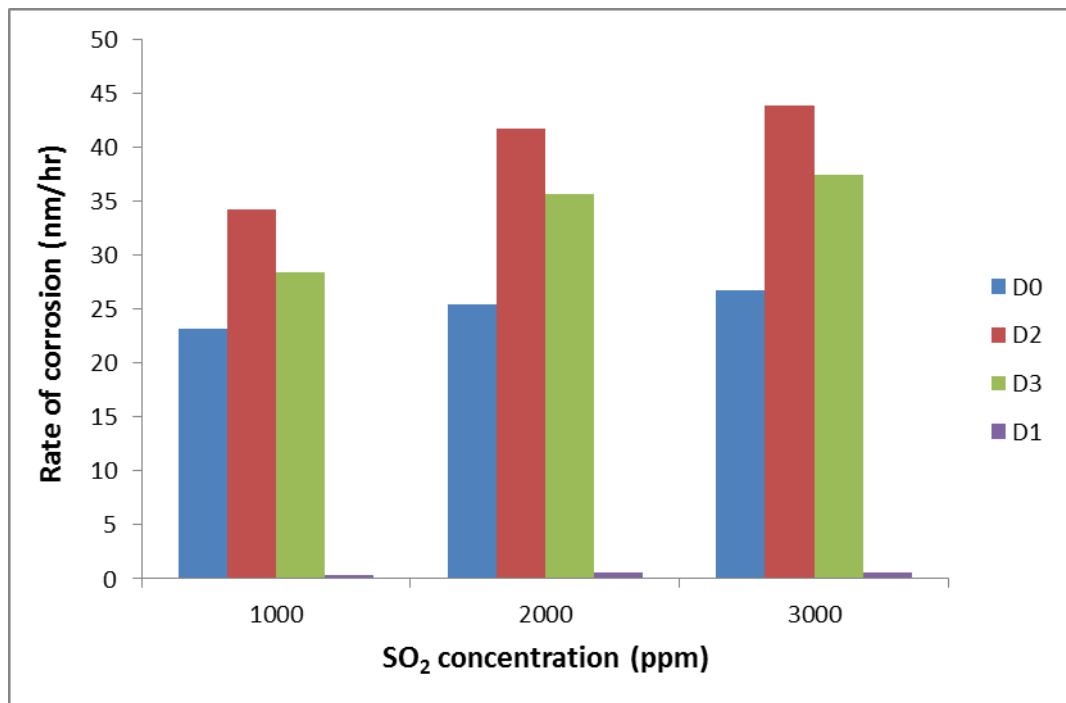
Figure 4.1 Rate of corrosion corresponding to different SO_2 concentrations and deposits for mild steel.

corrosion for bare specimen (D0) is observed while negligible corrosion occurs for specimen coated with ash D1 for all concentrations of SO_2.

The rate of corrosion for stainless steel specimen corresponding to different SO_2 concentrations is shown in Figure 5.2. Here again the highest rates of corrosion are observed for specimen coated with biomass ash (D2) and the rate of corrosion increases with increase in SO_2. Negligible increase in the rate of corrosion with respect to increase in SO_2 content is seen for the non-coated specimen. The effect of mixed ash (D3) on the rate of corrosion, studied for two concentrations of SO_2 showed that the behaviour of mixed ash resembled that of biomass ash in causing increased rates of corrosion compared to blank specimen. The influence of coal ash tested at 3000ppm SO_2, again proved to be protective.
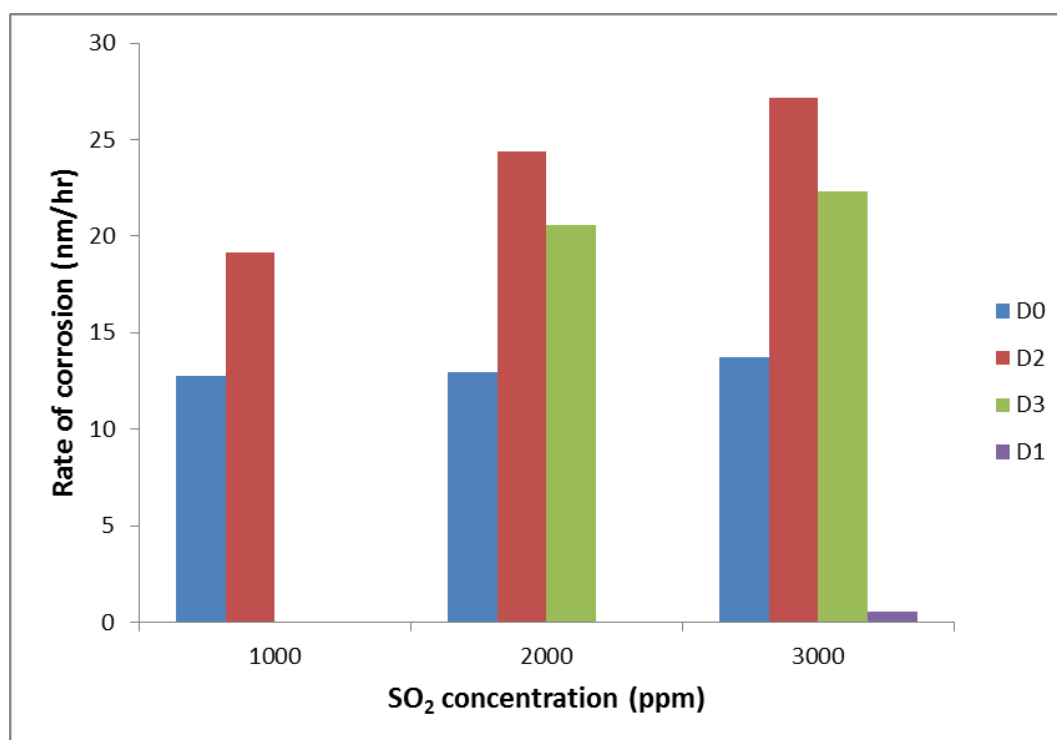

Figure 4.2 Rate of corrosion corresponding to different SO_2 concentrations and deposits for stainless steel.

This shows that the general trend followed by the given mild steel and stainless steel specimens is the same except that the rate of corrosion exhibited by stainless steel is much lower than mild steel. The lower values of metal loss observed for stainless steel as compared to mild steel are due to its superior corrosion resistance which is expected due to its high chromium content. However, the similarity in the observed trends for both materials suggests that the mechanisms by which corrosion occurs are similar. The results show that at the given conditions of the experiment, the coal ash (D1) acts as an inert layer, not reacting with the gas components and also preventing the metal from being attacked by corrosive species in the gas phase. On the other hand, the biomass ash (D2) greatly expedites the rate of corrosion. Based on this, it would be reasonable to deduce that in the case of mixed ash (D3), the biomass content serves as the reactive part of the ash.

EDX spectra of the surface of bare corroded specimen after the corrosion scale had been removed, showed considerable O and S in addition to the main oxide forming constituents as shown in Figures 4.3, 4.4, 4.5 and 4.6. This indicates that the corrosion of bare specimen is primarily due to a combined oxidation and sulphidation mechanism for both the mild and stainless steel. EDX maps showed that the spread of S on the surface was more or less uniform for stainless steel specimen as seen in Figure 4.5 and Figure 4.6. However, this was not the case for mild steel (Figures 4.3 and 4.4), where S was found to be concentrated more in some areas as compared to others exhibiting a more localized form of sulphur attack.

It is generally accepted that an initial, uniform oxide layer formed on the surface of a metal or alloy offers resistance to further attack of the underlying metal. The main oxide forming component in mild steel is iron (Fe) while stainless steels form oxides containing both chromium (Cr) and iron (Fe). Gleeson (2004) noted that even in multi-oxidant environments, alloys often exhibit an initial period of protective oxidation preceding breakaway corrosion. Once the integrity of the initial oxide scale is destroyed, corrosion proceeds by combined oxidation and sulphidation. This means that oxides with intermittent sulphides would be formed which are more liable to spall due to additional stresses resulting from the difference in growth rates of oxides and sulphides. Hsu (1987) proposed that the nucleation and growth of iron and/or chromium sulphides in mixed gas environments is initiated by the penetration of sulphur bearing species through the initial oxide layer by diffusion along oxide grain boundaries or molecular transport through mechanical defects such as cracks and pores in the oxide. The more localized sulphur attack seen in mild steel suggests that penetration of gaseous sulphur species may have occurred primarily through cracks and pores on the initial oxide surface leading to higher sulphur activity in these areas.

Figure 4.3   Electron image, spectrum and maps for bare MS at 1000ppm SO_2.
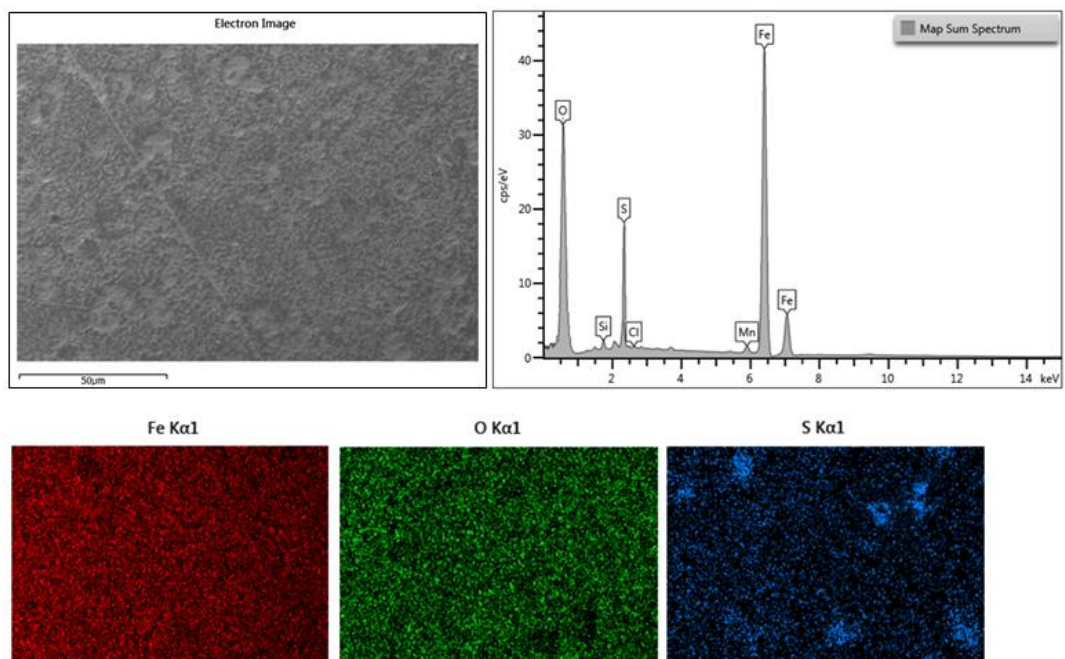
Figure 4.4   Electron image, spectrum and maps for bare MS at 2000ppm SO_2.

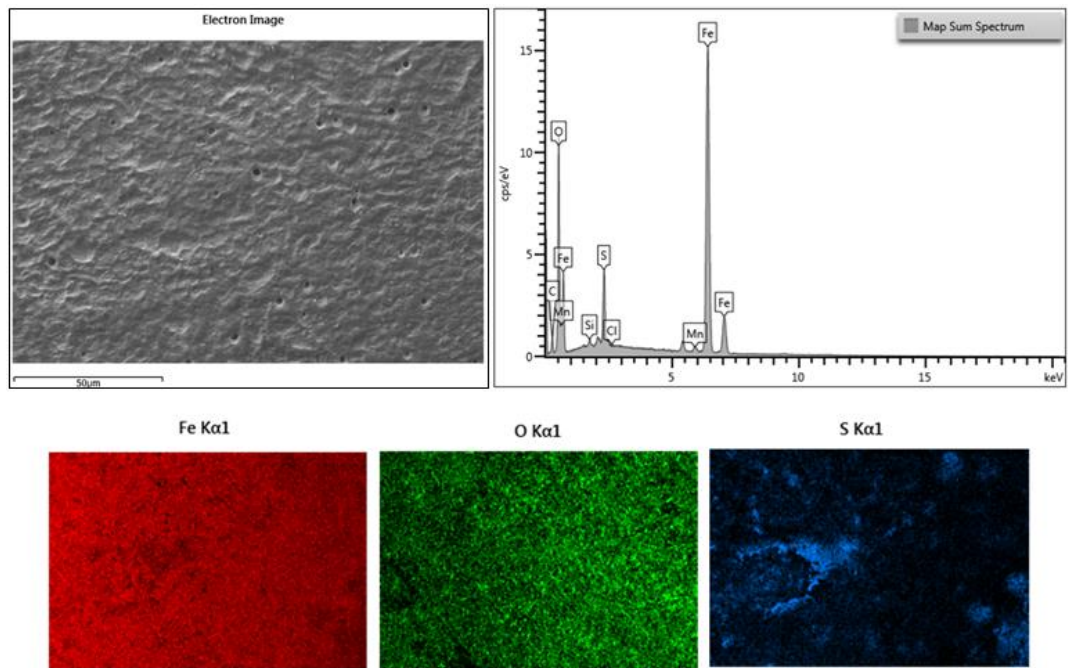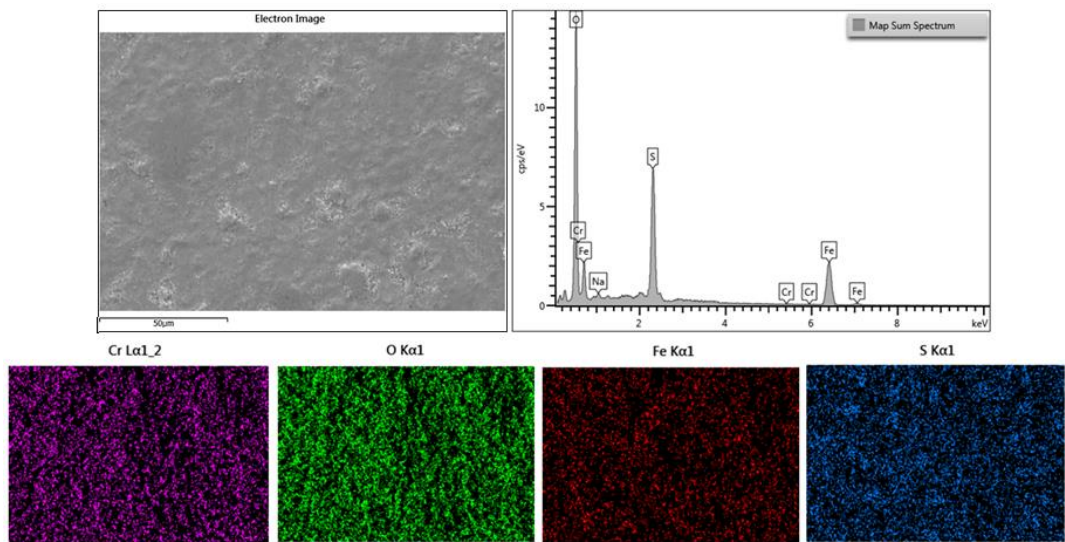Figure 4.5   Electron image, spectrum and maps for bare SS at 1000ppm SO_2.
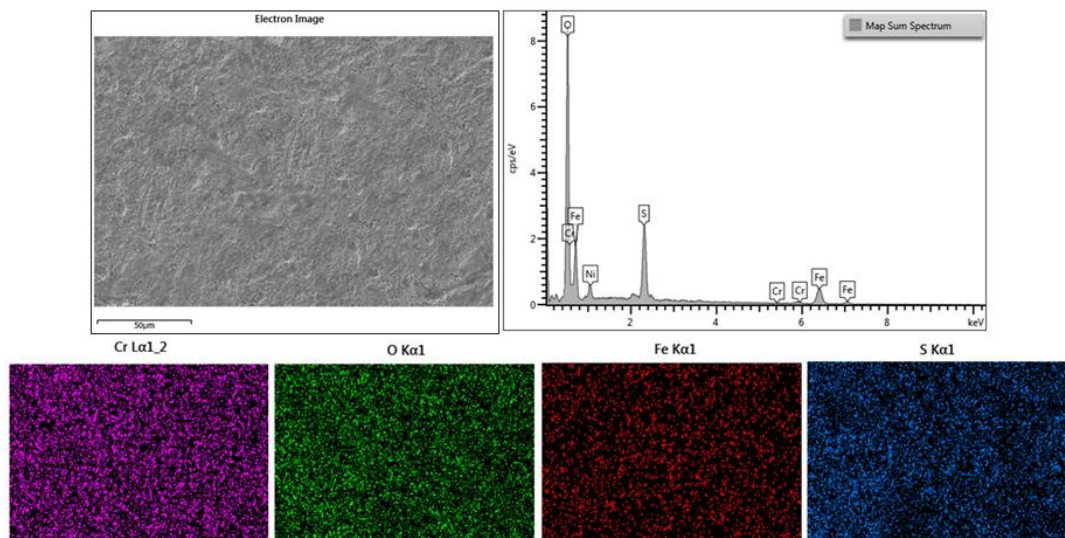
Figure 4.6   Electron image, spectrum and maps for bare SS at 2000ppm SO_2.

The considerably higher rates of corrosion in the presence of deposits containing biomass ash compared to bare specimen points towards the existence of a melt phase since reactions involving a liquid phase are much faster than gas-solid interactions (Rapp and Zhang, 1994). The formation of a melt phase can be attributed to the presence of reactive alkali components in the biomass ash. The alkali oxides in the ash can react with sulphur species in the gas to form sulphates (Spliethoff and Hein, 1998). This was evidenced by the enrichment of sulphur in the recovered biomass deposits observed by EDX analysis as shown in Figure 4.7. Negligible uptake of S was observed for the recovered coal ash as seen in Figure 4.8, showing its non-reactive nature.
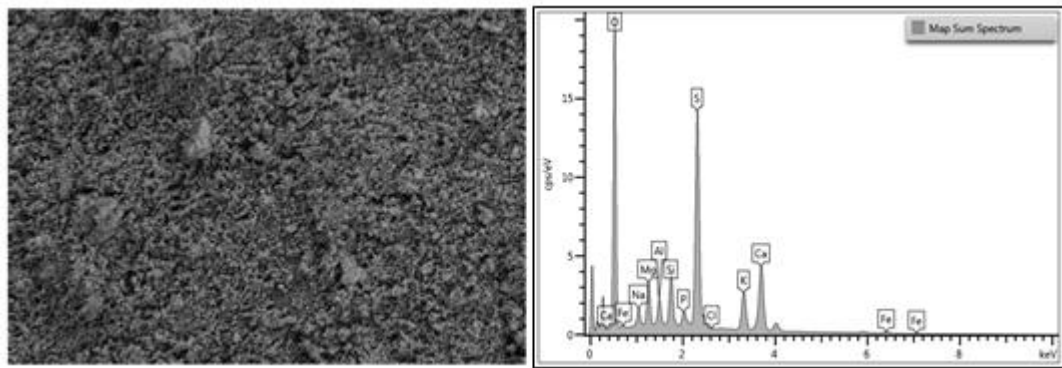
Figure 4.7 Electron image and spectrum of biomass ash recovered from SS specimen after exposure at 3000ppm of SO_2.

Figure 4.8 Electron image and spectrum of coal ash recovered from SS sample after exposure at 3000ppm of SO_2.

EDX analysis of the surface of the specimen coated with deposits containing biomass ash also showed enrichment of S in addition to alkali components, mainly K, Na and Ca as shown in Figure 4.9. The acceleration of corrosion under the influence of reactive alkali deposits containing sulphates is linked to the formation of a melt phase on the surface of the alloy and has previously been associated with high rates of corrosion (see Section 2.3.1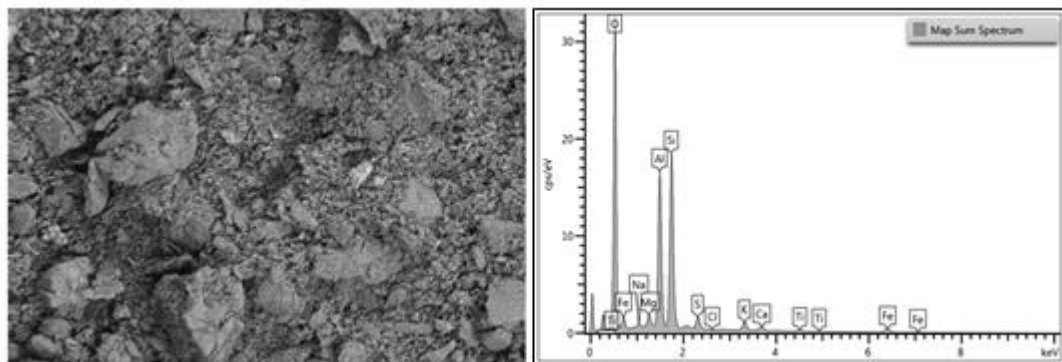). Based on the results and observations presented and the studies available in literature, the following simplified mechanism for corrosion of the specimen under the influence of deposits containing biomass ash (D2 and D3) is proposed:

i.   The alkali oxides in the biomass ash react to form sulphates either by the combined action of SO_2 and O_2 or by reacting directly with SO_3. SO_3 is expected to be present in oxidising environments containing SO_2 and its formation is enhanced due to the catalytic effect of iron in the ash.

ii.   The sulphates formed then diffuse to the metal/deposit interface and react further to form molten alkali iron trisulphates or pyrosulphates.

iii. Dissolution of the metal oxide in contact with the melt at the oxide/melt interface.

iv.   Reaction of underlying metal with sulphates and diffusing gas species (combined gas and deposit induced damage) to form oxides and sulphides below the melt causing further degradation.

Figure 4.10 represents a cross-section through a mild steel specimen corroded under the influence of biomass ash at 1000ppm SO_2 showing the main features of corrosion damage.
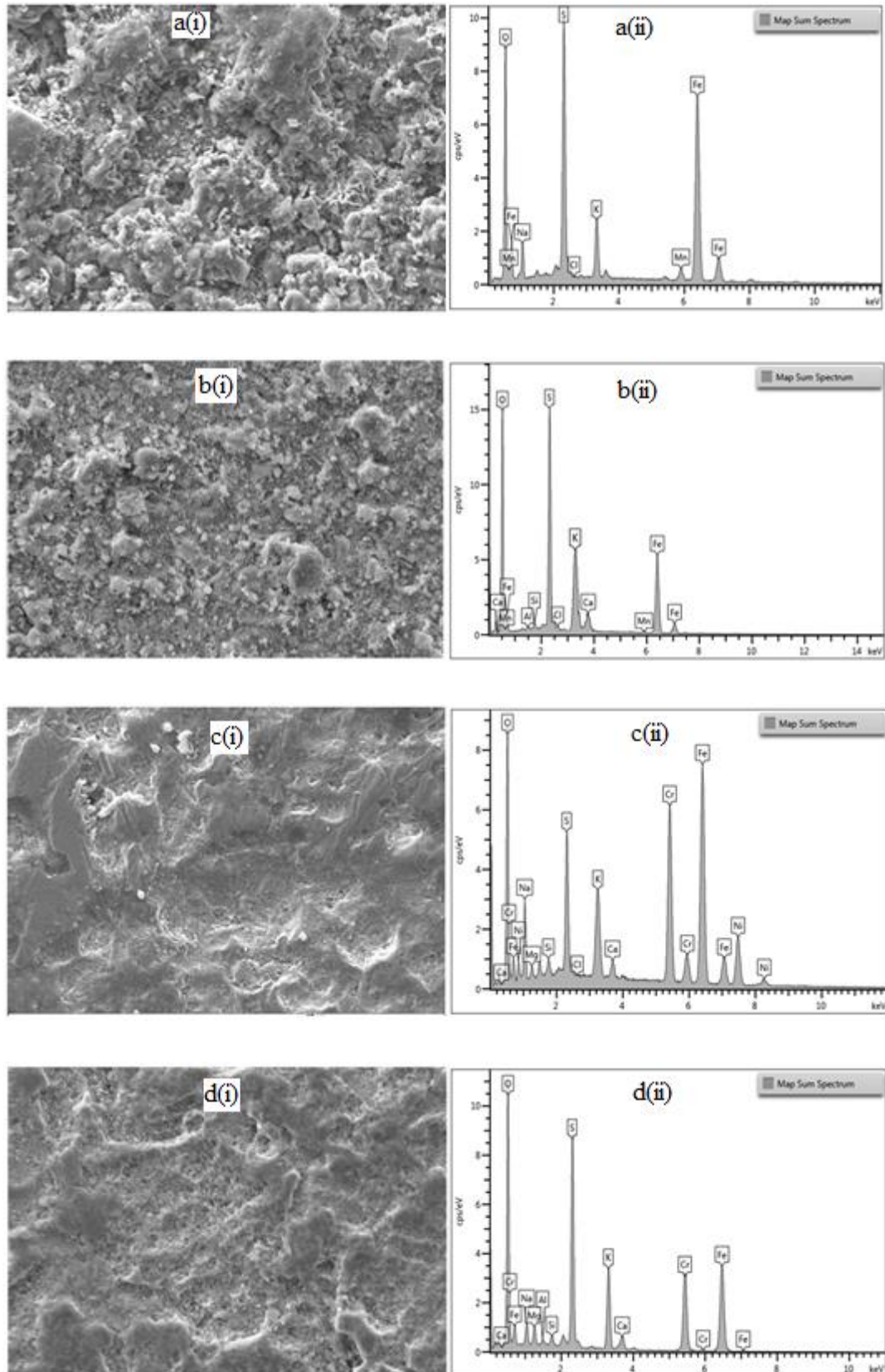
Figure 4.9(i) Electron image and (ii) EDX spectra of the corroded surface of deposits containing biomass ash (a)MS/D2 at 2000ppm SO_2, (b)MS/D3 at 2000ppm SO_2, (c)SS/D2 at 1000ppm SO_2, (d)SS/D2 at 3000ppm SO_2.
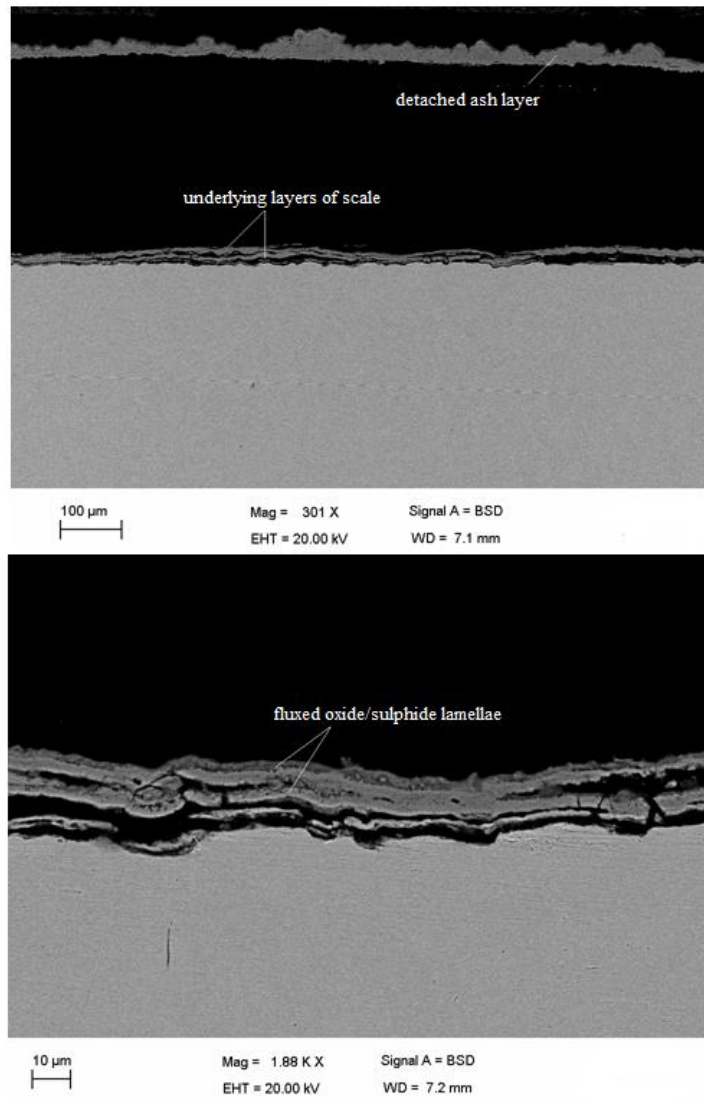
Figure 4.10 Cross-section through corroded mild steel under the influence of a biomass ash deposit at 1000ppm SO_2 showing fluxed layers of scale.

It has been suggested that during molten sulphate corrosion, SO_3 from the gas phase acts as the main oxidizing species in addition to SO_2 and O_2 owing to its higher solubility in the melt compared to SO_2 and O_2 (Harb and Smith, 1990). In other words SO_3, if present in the gas environment, contributes to increased corrosion in the presence of a sulphate melt. In order to validate this, a chemical kinetic study was performed to assess the formation of SO_3 in the gas phase under the conditions of the experiment. This is presented in the next section.

4.2.3 Prediction of sulphur trioxide formation using chemical kinetic analysis

The importance of sulphur trioxide in contributing towards corrosion under deposits, seems significant as has been discussed in the previous section. In order to assess the different parameters effecting the formation of SO_3, a chemical kinetic modelling approach was applied to the given system. This was done with the help of a Windows executable version of Senkin. Senkin is a Fortran computer programme that can be used to compute the evolution of chemical species over time in a closed, homogeneous reaction system (Lutz et al., 1988). It works in conjunction with the Chemkin software package which permits the formation, solution and interpretation of problems involving elementary gas phase chemical kinetics (Robert, 1989). The mechanism employed is the SOx extension to the Leeds Oxidation Mechanism. The Leeds oxidation mechanism, consisting of 37 species and 351 irreversible reactions, was first developed by Hughes et al. (2001) to describe comprehensively the oxidation of methane based on gas kinetic measurements and evaluated rate parameters and was thereby extended to other fuels. The SOx extension accounts for all the reactions leading to the oxidation of sulphur containing species and the following reactions can be regarded as being most significant for the conversion of SO_2 to SO_3:

$$SO_2 + O = SO_3 \tag{4.1}$$

$$SO_2 + OH = HOSO_2 \tag{4.2}$$

$$HOSO_2 + O_2 = SO_3 + HO_2 \tag{4.3}$$

Since the simulated gas also contains HCl, it called for the inclusion of the relevant chlorine species and reactions into the mechanism, in order to accommodate all the components in the oxy fuel mixture as reactants in the programme. For this purpose, the following elementary reactions were introduced into the existing mechanism in Chemkin :

$$HCl \; + \; OH \;\; = \;\; H_2O + \; Cl \tag{4.4}$$

$$HCl \; + \; O \;\; = \;\; OH \; + \; Cl \tag{4.5}$$

The thermodynamic and kinetic data for these reactions were obtained from Burcat's thermodynamic data (Burcat et al., 2009) and the NIST chemical kinetic database (NIST, 2013), respectively.

A series of computations were then performed based on the assumption that the furnace acts as a homogenous reactor and the reactants remain in the furnace for a fixed residence time (290 s) during which no in flow or out flow occurs. The residence time was calculated based on the total volume of the reactor (furnace) and the flow rate of the gases through the furnace using the following relation:

$$t_R = \frac{V}{F} \tag{4.6}$$

where t_R is the residence time in seconds, V is the total volume of the reactor in cubic centimeters ($2.9E+03 \; cm^3$) and F is the volumetric flow rate of the simulated gases entering the furnace ($1.0E+02 \; cm^3 s^{-1}$).

The predicted concentration of SO_3 that are expected to be formed at different temperatures with respect to the three inlet concentrations of SO_2 are shown in

Figure 4.11. It is clear that the SO_3 concentration increases with the increase in the concentration of SO_2 in the oxy fuel mixture, showing a parabolic trend with temperature. It is interesting to note that the curves peak around 900^0C which is the gas temperature used in the experiments. This shows that the formation of sulphur trioxide depends strongly on the gas temperature. It also leads to the possibility that lower corrosion rates might be observed for corrosion tests above and below this temperature. Further investigation is required in order to assess the effect of gas temperature on the rate of corrosion under deposits.
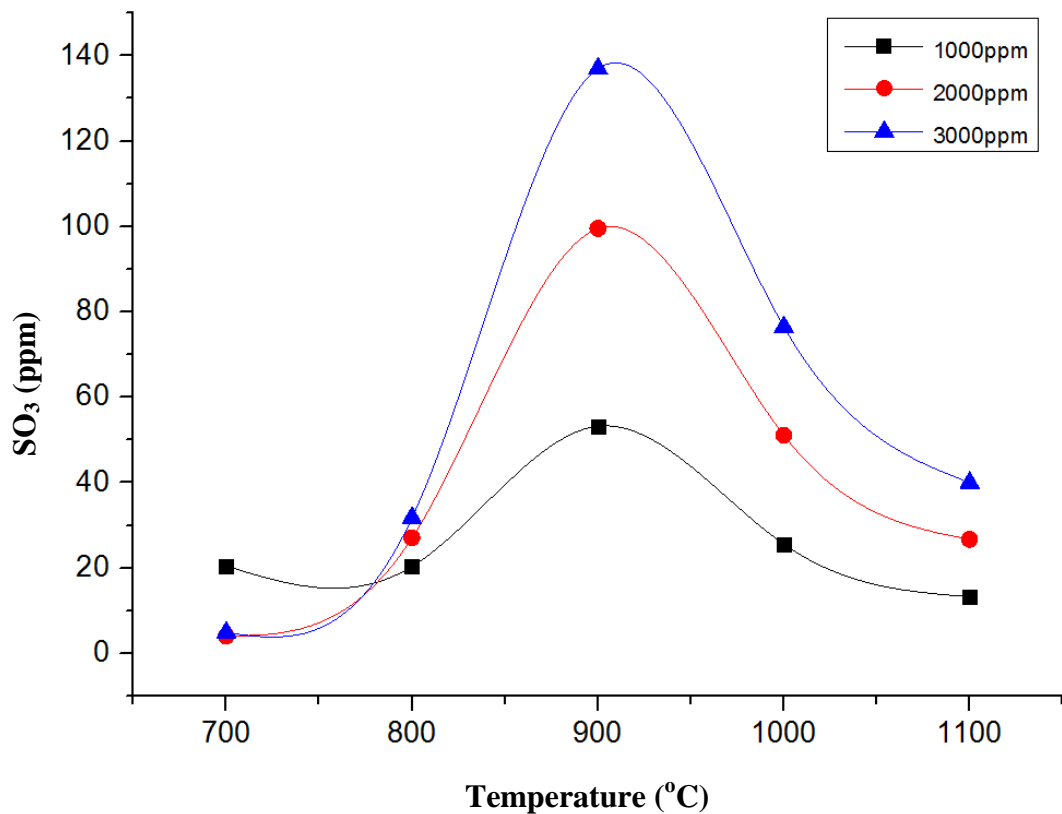

Figure 4.11 Effect of temperature and SO_2 content on the formation of SO_3.

4.2.4 Effect of HCl on the rate of corrosion

For the SO_2 tests presented in Section 4.2.2, the HCl concentration was held constant (~250ppm) for all the cases. Gaseous chlorine species can contribute to increase in the rate of corrosion by a mechanism known as active oxidation (Refer to Section 2.3.2). However, Cl could not be detected in noticeable amounts from EDX analysis. There could be several reasons for this, apart from the high volatility of metal chlorides which are expected to form by reaction with chlorine containing species. Valente (2001) showed that a minimum HCl concentration is required before gas phase chlorine attack can propagate and others have supported this view. However, this minimum can be expected to vary depending on the competition provided by other corrosive species in the gas phase. Some researchers have argued that the presence of Cl_2 and not HCl is responsible for aggressive gas phase attack in oxidising environments (Abels and Strehblow, 1997). Neilson (2000) reviewed that HCl concentrations as high as 1000ppm may not cause significant gas phase attack unless reducing conditions are present.

Due to the long duration of the tests and the high operating costs associated with running the rig, it was not possible to test a range of conditions for evaluating the influence of varying the HCl concentration. However, in order to serve as a basis for comparison, the effect of minimising the HCl content in the flue gas was studied for a test case. For this purpose, the test conditions were chosen similar to the one for intermediate SO_2 concentration (2000ppm) but the only difference was that the HCl content was set at 50ppm. The average rate of corrosion for bare specimen and specimen coated with deposit D2 are presented in Table 4.7 along with the corresponding values for higher concentration of HCl (250ppm).

Table 4.7 Comparison of corrosion rates for varying the HCl content of the simulated gas at 2000ppm SO_2 for (a) mild steel and (b) stainless steel.

(a)

Ash coating	HCl (ppm)	Rate of corrosion (nm/hr)
non-coated	50	23.2
	250	25.1
coated	50	41.2
	250	41.5

(b)

Ash coating	HCl (ppm)	Rate of corrosion (nm/hr)
non-coated	50	12.8
	250	13.0
coated	50	19.2
	250	19.4

The results showed a decrease in the rate of corrosion for bare mild steel specimen but little effect on the rate of metal loss was observed for stainless steel and both types of specimen coated with ash. It is possible that the concentration of 250ppm is already low enough to cause noticeable effect on the rate of corrosion, given the high SO_2 concentration. Clearly, further investigation is required in order to assess the relative importance of HCl in oxy-fuel environments containing high concentration of SO_2 and vice versa.

4.3 Conclusions

The metal loss rates under simulated oxyfuel environments for a typical waterwall (A210) and superheater material (AISI310) were studied in a custom built laboratory corrosion rig. It was found that the presence of an ash deposit plays a significant role in increasing or decreasing the rate of corrosion. For the conditions studied, the presence of a coal ash deposit acted as a protective layer preventing metal loss while the influence of a biomass ash deposit was to significantly

increase the rate of metal loss. The corrosion damage under these conditions worsened with the increase in SO_2 content of the gas for both the mild and stainless steel under deposits containing biomass ash but had little influence on the corrosion of bare specimens where no ash coating was applied. EDX analysis indicated that the metal loss of bare specimen was due to a combination of sulphidation and oxidation while in case of specimen coated with deposits, alkali content of the biomass, was responsible for the increased rates of corrosion under the influence of a melt phase. The suggested mechanism of attack under deposit included the formation of SO_3 in the gas phase which was supported by chemical kinetic modelling.

The present study indicates that the increased concentration of SO_2 in oxy fuel combustion environments, due to recycling of the flue gas, can lead to considerable increase in corrosion rates especially in the presence of reactive alkali containing deposits. Under the conditions studied, biomass ash was found to be efficient in capturing sulphur from the gas, leading to molten sulphate type corrosion. On the other hand, the coal ash acted as an inert layer. Further testing is required to assess the relative influence of other constituents in the flue gas and how their effect varies with flue gas temperature. The data generated from these experiments is the first series of results obtained from this rig and will serve as a basis for further testing by subsequent users.

On the whole, it can be concluded that when assessing the implications of oxy fuel environments on corrosion, considering the influence of individual parameters on the rate of corrosion serves as a useful approach for laboratory testing. If the

influence of individual parameters and their relative importance is known, this knowledge can then be applied for assessment to a larger scale. Ultimately, this would help to pinpoint regions in the boiler that are likely to undergo severe corrosion attack and consequently implement suitable corrosion inhibition strategies.

Chapter 5

Fuel and ash characteristics and their effect on slagging and fouling propensities

5.1 Introduction

The type of fuel and its characteristics is an important parameter affecting the formation of deposits and corrosive species in a boiler during combustion. Some of the chemical elements in fuels that affect deposit formation on heat transfer surfaces can also affect the corrosion experienced by the same, and has been discussed in detail in Section 2.5. The propensity of fuels to slag and foul boiler heat transfer surfaces can be predicted by means of laboratory based tests and measurements. Although most of these techniques were originally developed for coals, they have since been extended to other types of fuels. There is considerable concern regarding high rates of deposition associated with burning biomass fuels in boilers. Due to the wide variation in the different types of biomass and their associated characteristics, the need to examine the properties of individual fuels is important in order that data may be used in the assessment of suitability of commercially available biomass for use in power stations.

The following sections present the results and discussion from the various analytical techniques employed for evaluating the characteristics of fuel samples and their ashes. The fuel samples were obtained from Drax power station. Among these was a high sulphur coal (Potland Burn UK) and four types of biomass namely wood (pine), miscanthus, peanut shells and sunflower husks. Out of these biomass samples, soft wood (pine) is a typical example of sustainably produced

woody biomass from managed forests and forestry residues. Peanut and sunflower husks represent agricultural residues and by-products of food production that are readily available. Miscanthus is an example of short rotation energy crop that is planted specifically for the purpose of producing energy. The fuels were first analyzed for their moisture, volatile, fixed carbon and ash content as well as elemental composition in terms of percentage carbon, hydrogen, nitrogen and oxygen. Ash characterization involved XRF analysis, ash fusion tests and simultaneous thermal analysis coupled with mass spectroscopy. Ash obtained from some of these fuels was utilized for corrosion experiments presented in Chapter 4.

5.2   Results and Discussion

5.2.1   Ultimate analysis

Elemental analysis of the fuels was carried out using a Thermoscientific Flash 2000 analyzer as described in Section 3.3.5. Table 5.1 shows the carbon, hydrogen, oxygen, nitrogen and sulphur content of the fuels evaluated on a dry basis.

It can be observed that the biomass samples exhibit lower carbon content than the given coal, higher hydrogen content, varying amount of nitrogen and much higher oxygen content and lower sulphur content. This is in agreement with the general trend regarding the key differences in properties of biomass as compared to coal reviewed by Emami-Taba et al. (2013). However, the high sulphur and ash content of the coal suggests that this type of coal would not be fired alone but as a blend with other coals or possibly biomass to control sulphur emissions and ash handling problems (refer to Section 1.4). With regards to the nitrogen content of the biomass

Table 5.1 Elemental analysis of fuels evaluated on a dry basis.

Fuel Sample	Elemental Analysis (wt %)				
	C	H	N	O^d	S
Coal (Potland Burn UK)	54.32	4.26	1.13	16.34	2.06
Wood (Pine)	47.37	5.35	0.66	44.72	<1*
Peanut Shell	45.98	5.46	2.3	43.06	<1*
Sunflower husk	49.1	5.6	1.65	40.96	<1*
Miscanthus husk	46.82	5.42	1.01	43.15	<1*

[d] calculated by difference
[*] below instrument detection limit

samples, it is clear that wood contains the lowest nitrogen content, followed by miscanthus whereas the nitrogen content of sunflower and peanut are high. This trend is similar to that observed by Obernberger et al. (2006), who reviewed the nitrogen content of a number of biomass types to conclude that coniferous and deciduous wood have the lowest nitrogen content and the value becomes higher for short rotation crops and agricultural residues. It can be seen that the biomasses contain considerable carbon content. While the carbon content of the biomass contributes positively towards the heating value, the high oxygen content has a negative influence. This is demonstrated by the lower calorific values of biomass as compared to coal (Lackner et al., 2010).

5.2.2 Proximate analysis

The percentage of moisture, fixed carbon, volatiles and ash in fuels can be determined using available standards (most commonly British (BS) or American (ASTM) standards) or alternatively by instrumental techniques such as thermogravimetric analysis (TGA). However, a variation in the values obtained from various methods can be expected owing to the empirical nature of these tests. Standard testing procedures have long been in use for the determination of proximate content of coal and similar procedures are being developed for solid biofuels based on the presumption that "*the methodology and logic from coal experiments can be applied to biomass*" (Vassilev et al., 2010). TGA equipment offers the advantage of proximate determination in a single operation. However, while proximate analysis using TGA is quite well validated for coals, the same cannot be stated for the case of biomass (Lackner et al., 2010). This is because biomass combustion being a relatively new technology in power plants compared to coal, there are still grey areas in understanding its characteristics. Nevertheless, TGA techniques have found extensive use in reactivity studies of different materials.

The proximate analysis of the fuels, evaluated on an as received basis, by employing the British Standard methods (See Section 3.3.3) are shown in Table 5.2. The results show that the biomasses are high in moisture and low in ash content. This is typical for biomass fuels as is the high volatile matter. Proximate assessment with the help of a TGA programme using a Schimadzu TGA-50 analyser, (presented in Section 3.3.3.4) is shown in Table 5.3. It can be seen that variations exist between the values obtained from these two techniques. This can

be attributed to the difference in the specific environments and heating rates associated with each of these two methods. Considering the importance of heating

Table 5.2 Proximate analysis determined using British Standard methods.

Fuel Sample	Moisture (% AR)	Volatile Matter (% AR)	Fixed Carbon (% AR)[d]	Ash (% AR)
Coal (Potland Burn UK)	4.89	25.24	47.98	21.89
Wood (Pine)	7.45	72.14	18.51	1.9
Peanut Shell	7.74	71.26	17.8	3.2
Sunflower husk	8.68	70.38	18.25	2.69
Miscanthus husk	6.97	74.57	14.85	3.61

[d] calculated by difference

Table 5.3 Proximate analysis using TGA

Fuel Sample	Moisture (% AR)	Volatile Matter (% AR)	Fixed Carbon (% AR)	Ash (% AR)
Coal(Potland Burn UK)	3.78	26.65	45.05	24.52
Wood(Pine)	6.37	71.31	14.2	8.12
Peanut Shell	6.35	67.18	18.65	7.82
Sunflower husk	7.46	69.18	17.86	5.5
Miscanthus husk	5.35	74.3	15.15	5.2

rate, time and temperature on heat transfer and reaction rates of different fuels, it would not be appropriate to perform a direct comparison between the values obtained from these two techniques. However, it is possible to draw a few inferences based on these results. The significantly lower values of moisture content obtained from TGA suggests that the holding time of 10min employed in the TGA programme is not sufficient for complete removal of moisture. Although there is a possiblility that the values of moisture content obtained from the standard oven drying method may be slightly over estimated, they can still be deemed as being the more reliable of the two. This is supported by the measurements of Samuelsson et al. (2006), who found that the quantity of emitted low temperature volatile species during oven drying of different biomass samples was quite low, mostly below 1% of the moisture content.

The volatile matter content in biomass results from the pyrolysis or thermal degradation of structural components including lignin, cellulose and hemicellulose. Studies (Angın, 2013, Mimmo et al., 2014) have shown that temperature and heating rate of pyrolysis effects the composition of char produced which would in turn affect its reactivity. The lower values of moisture and volatile content obtained from TGA are carried over in the form of high ash content. It is interesting to note that the percentage of unreacted residue obtained from TGA measurements as compared to the ash yield obtained from the standard method is particularly large for the biomass fuels as compared to coal. One reason for this could be that the char obtained after pyrolysis is not completely oxidized at the end of the oxidation step, and considerable unburnt material remains in the residue. This possibility is minimised when using the standard method since it can

accommodate long reactions times by continued heating in air until negligible change in mass is observed. Also, the temperature at which the ash is obtained is also important as demonstrated by the work of Llorente and García (2006), who studied the ash produced from woody and herbaceous biomass samples at different temperatures ranging from 400-800^{0}C to conclude that temperatures from 500-550^{0}C are most suitable for obtaining ashes without organic carbon.

On the whole, it can be concluded that a TGA programme that gives reasonable values of proximate analysis for coals may lead to erroneous results for biomass. The determination of the proximate content of biomass by using TGA requires a series of trials in order to evaluate what conditions are best suited to define the moisture loss, devolatilization and oxidation steps for biomass. Mayoral et al., (2001) demonstrated that the specific conditions in the TGA programme (heating rates, final temperature, holding times) can be optimized to give values that are only marginally different than those obtained from standard measurements. Since reactivity studies are not included in the objectives of this work, alternative TGA programmes employing different temperatures and heating regimes were not tested.

5.2.3 Characterization of ash

For experiments involving the characterisation of ash, the standard ashing temperature of 550^{0}C (for biomass) and 850^{0}C (for coal) was used for preparing the ash samples by employing the British Standards BS EN 14775:2009 and BS ISO 1171:2010.

5.2.3.1 XRF analysis

The elemental analysis of the fuel ashes in terms of the oxides of aluminium, silicon, potassium, sodium, titatnium, calcium, magnesium, iron, phosphorous and sulphur as obtained from X-Ray fluorescence (XRF) analysis is given in Table 5.4. A bar chart of these values, presented in Figure 5.1, illustrates the wide variation in composition of the different ashes. The coal is a typical high alumina (49.48%), high silica (30.95%) type with considerable iron oxide (9.52%). Out of the four biomasses, wood and miscanthus are high in silica content at 45.23 and 49.55% respectively followed by peanut husk at 35.26%. The alumina content of all the biomasses is low, while the potassium content is considerably high as would be expected for biomass fuels. All of the biomasses also possess considerable calcium content. Sunflower husk is the only low silica biomass (less than 4%) but contains appreciable amounts of potassium, calcium and magnesium. The high potassium

Table 5.4 Major oxide composition of ash using XRF analysis.

Ash sample	% constituent in ash									
	SiO_2	Al_2O_3	Fe_2O_3	K_2O	CaO	MgO	P_2O_5	SO_3	Na_2O	TiO_2
Coal (Potland Burn UK)	49.48	30.95	9.52	2.56	2.36	1.63	0.19	1.16	1.01	1.15
Wood (Pine)	45.23	10.6	5.93	9.76	20.04	4.55	1.29	0.54	1.42	0.64
Peanut Shell	35.26	8.19	3.22	30.88	9.92	5.12	4.49	0.77	1.32	0.82
Sunflower husk	3.21	0.48	0.84	45.1	27.16	15.24	5.3	2.43	0.21	0.03
Miscanthus husk	49.55	0.45	0.41	30.49	7.95	2.86	5.76	0.13	2.39	0.01

content in agricultural residues is attributed to the use of fertilizers in agricultural farms (Werther et al., 2000).
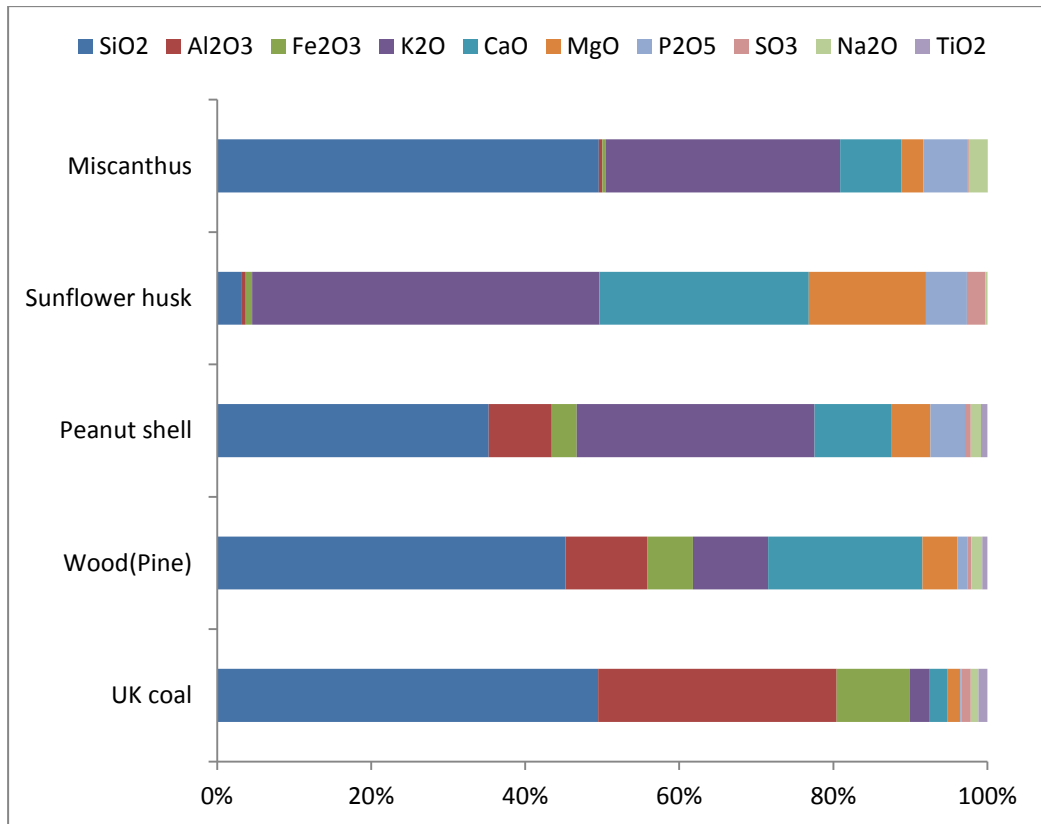

Figure 5.1 Bar chart illustrating the compositional variation of the fuel ashes.

5.2.3.2 Ash Fusion Tests

The ash fusion tests were performed using Carbolite Ash Fusion furnace under oxidizing conditions (Please refer to Section 3.3.7). The shrinkage temperature has not been reported due to the difficulty in discerning accurately such a small change in area due to poor luminosity at lower temperatures resulting in images with very low contrast ratio. Out of the three key stages in melting of the samples reported in Table 5.5, the deformation temperature in terms of first rounding of the edges was the most difficult to ascertain especially where shrinkage of the test pieces was observed. Hemispherical and flow temperatures were easier to assess and based on

the height to diameter ratio determined with the help of image processing software, to minimize discrepancies resulting from visual observation. It follows that consistent values of hemispherical and flow temperatures were observed for duplicate samples with little variation (≤ 5 ^{o}C), whereas the variation in the observed deformation temperatures for similar samples was much higher (≤ 45 ^{o}C). Similar problems in determining the initial deformation temperatures have previously been observed by several researchers (Gupta et al., 1998, Wall et al., 1998, Pang et al., 2013).

Table 5.5 Ash fusion temperatures of fuel ashes.

Sample	DT (^{o}C)	HT (^{o}C)	FT (^{o}C)
UK coal	1165	1470	1495
Wood (Pine)	1095	1210	1235
Peanut shell	1080	1250	1265
Sunflower	1225	1515	1560
Miscanthus	835	1020	1040

Table 5.5 shows the ash fusion temperatures of the five fuels. It can be observed that the wide variation in the composition of biomass is depicted in the values of their fusion temperatures which are significantly different from each other. While coals are known to deform at high temperatures, the values of fusion temperature for peanut and sunflower exceeds even that for the given coal. The lowest fusion temperatures are observed in the case of miscanthus. The unusually large differences in the fusion temperatures of different types of biomass has been reported in a recent review by Vassilev et al. (2014), who compared fusion data of

72 biomass species (see Section 2.5.2). It is interesting to note that the fusion temperatures for miscanthus are significantly lower than peanut although they possess similar potassium content. Futhermore, sunflower exhibits the highest fusion temperatures despite possessing the highest potassium content. This shows that, contrary to the proposition of Werther et al. (2000), lower laboratory ash fusion temperatures cannot be explained by higher potassium content alone. In other words, a high potassium content in the initial ash mixture does not necessarily mean that potassium will contribute significantly to the melt phase when the ash is subjected to higher temperatures. If a significant amount of potassium partitions into the vapour phase on heating, the ash mixture left behind will be low in potassium. In addition, the influence of other components in the ash needs to be considered. For instance, calcium, magnesium and aluminium have all been found favourable for increasing the ash melting temperatures (Obernberger et al., 2006, Werther et al., 2000, Akiyama et al., 2011b). In this case, miscanthus ash which displays the lowest fusion temperatures, possesses the lowest percentage of calcium, magnesium and aluminium among the biomasses. Similarly, the high calcium and magnesium content in sunflower ash can be held responsible for its high melting temperatures. Yu et al. (2014), demonstrated that the softening temperatures of biomass can be correlated with the percentage of the oxides Na_2O, MgO, Al_2O_3, SiO_2, K_2O, CaO and Fe_2O_3 in the ash.

Nonetheless, it is evident that the ash fusion test is far from being sufficient to explain the various physical and chemical changes taking place in the ash upon heating. In addition, the subjective nature of the test adds to the difficulty in discerning the different stages in melting of the ash. Alternative techniques such as

simultaneous thermal analysis, presented in the next section, may provide a better insight into the behaviour of ash on heating.

5.2.3.3 Simultaneous Thermal Analysis coupled with Mass Spectroscopy

The results obtained from STA-MS tests from UK coal, wood, peanut, sunflower and miscanthus ash are presented in Figure 5.2, Figure 5.3, Figure 5.4, Figure 5.5 and Figure 5.6 respectively. The mass loss and DTA curves are representative of physical and chemical changes taking place in the sample (see Section 3.3.6).

It is evident that all of the samples show distinct regions of mass loss. In the low temperature window (below $500^{0}C$), coal, wood and sunflower ash samples do not exhibit any significant mass loss. The mass loss associated with peanut and miscanthus ash in this temperature range is accompanied by corresponding H_2O peaks indicating the evaporation of equilibrium moisture from the samples. This is owed to the presence of hygroscopic compounds like potassium carbonate and calcium chloride that are likely to be present in biomass ash.

In the temperature region $500\text{-}1000^{0}C$, mass loss is most likely to be due to the thermal decomposition of carbonates particularly $CaCO_3$ between $600\text{-}850^{0}C$, according to the reaction:

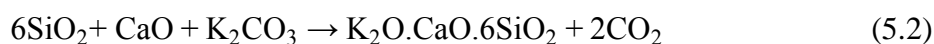$$CaCO_3 \rightarrow CaO + CO_2(g) \tag{5.1}$$
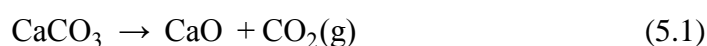
This is evidenced by the corresponding CO_2 peaks in both wood and sunflower and based on the assumption that the ash does not contain any residual unburnt carbon. However, this cannot be generalized for all the ashes since only a very slight CO_2

peak is observed for the peanut ash and none for miscanthus. For these ashes mass loss could be due to the evaporation of other species either by reactions within the ash or volatilization of active compounds. For instance, KCl is known to evaporate above 700^0C and was found to be one of the main crystalline species present in high potassium containing biomass ashes by Du et al., (2014) Unlike the biomasses, the coal ash does not exhibit any noticeable mass loss upto 1000^0C.

In the high temperature range (above 1000^0C) CO_2 and H_2O are progressively released into the gas phase for all the ashes. The remarkable similarity in the trend of the signal intensities for all cases suggests their release from similar reactions. One probability could be the dehydroxylation and decarbonotation of lattice compounds in complex mineral species and the destruction of their structure, that can occur at high temperatures (Pansu and Gautheyrou, 2007).

An increase in the SO_2 signal, as well as that of Cl can also be observed in all cases, mainly above 1200^0C. This can be attributed to their release from the breakdown or transformation of complex high temperature mineral and inorganic species in the ash. Also, SO_2 and CO_2 may also be released by the reaction of potassium sulphate (K_2SO_4) and carbonate (K_2CO_4) with silica containing species in the ash (Niu et al., 2013), typically above 1000^0C by reactions such as follows :

$$6SiO_2 + CaO + K_2CO_3 \rightarrow K_2O.CaO.6SiO_2 + 2CO_2 \tag{5.2}$$

$$Ca_2SiO_4 + 2K_2SO_4 + SiO_2 \rightarrow 2K_2CaSiO_4 + 2SO_2 + O_2 \tag{5.3}$$

$$CaSiO_3 + 2K_2SO_4 + 2SiO_2 \rightarrow K_4CaSi_3O_9 + 2SO_2 + O_2 \tag{5.4}$$

$$2K_2SO_4 + 2MgO + 10SiO_2 \rightarrow 2K_2MgSi_5O_{12} + 2SO_2 + O_2 \tag{5.5}$$

The minimum endothermic temperatures for the ashes as estimated from the DTA curves are shown in Table 5.6. The upward slope of the STA curve represents exothermic reactions while the downward sloping section is attributed to endothermic processes. The shift from exothermic to endothermic conditions on the curve is indicative of melting. The minimum endothermic temperatures evaluated in this way are much lower than the corresponding initial deformation temperatures obtained from ash fusion tests. This is in agreement with the findings of Wall et al. (1998), who used alternative laboratory techniques to conclude that the initial deformation temperature cannot be regarded as the lowest temperature for ash to soften. On the other hand, the minimum endothermic temperature cannot automatically be assumed to represent the temperature where melting first starts. Since it represents the initiation of net endothermic conditions, the probability of simultaneous exothermic and endothermic reactions below this temperature and vice versa cannot be disregarded.

Table 5.6 Minimum endotherm temperatures from DTA curves

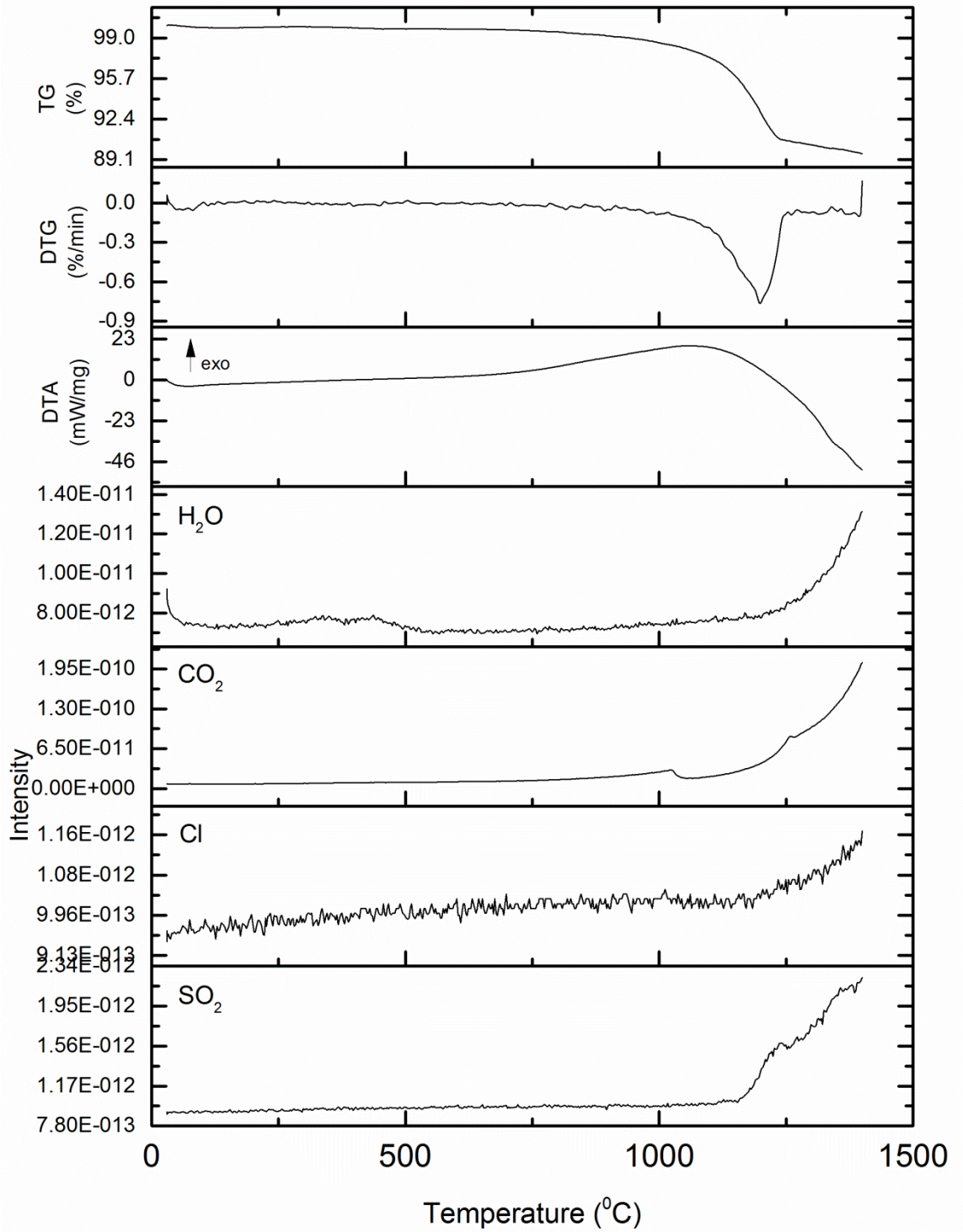| Ash Sample	Minimum Endothermic Temperature (^0C)
Uk coal	1070
Wood(Pine)	980
Peanut shell	1060
Sunflower husk	940
Miscanthus	750

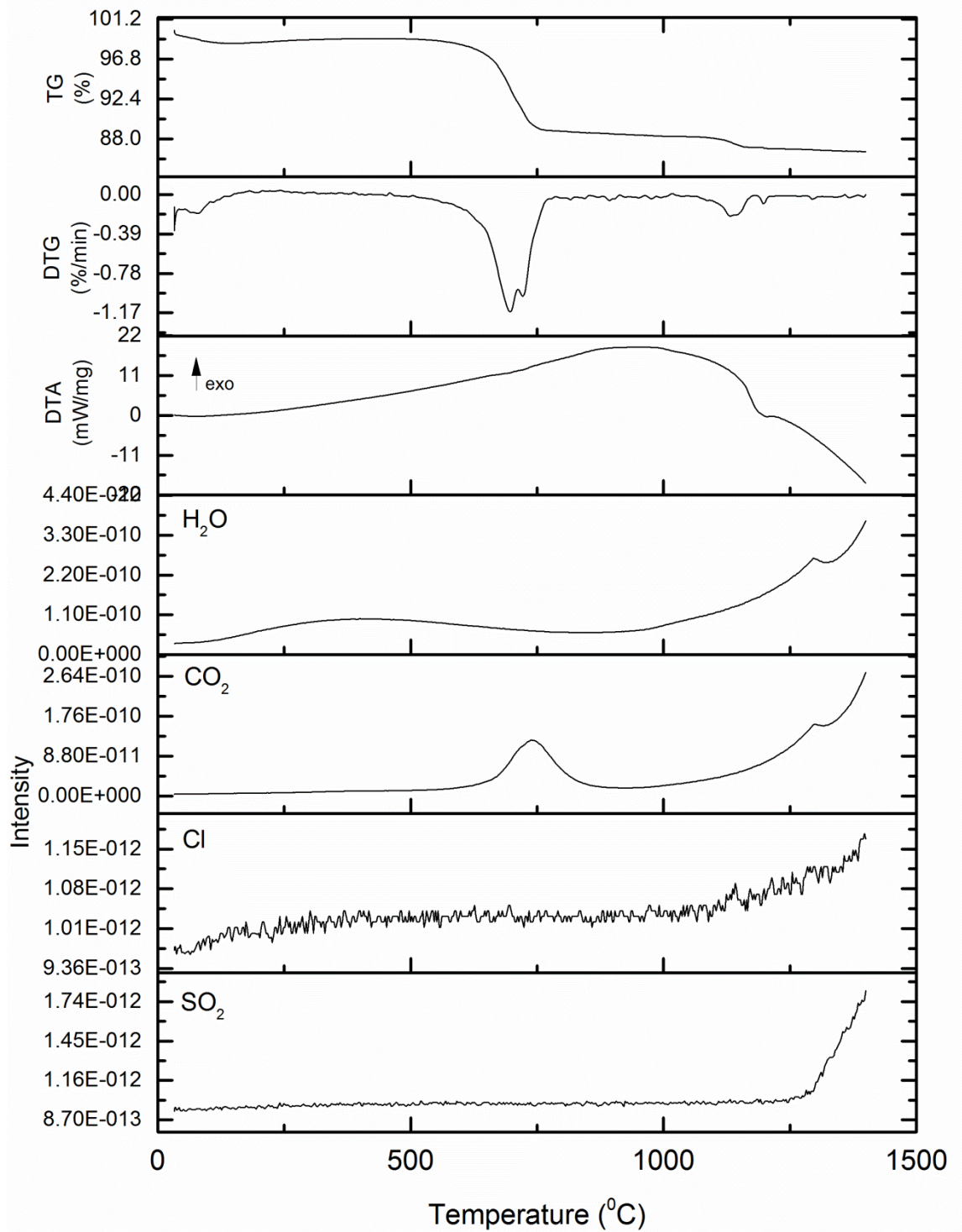Figure 5.2 STA-MS curves for coal ash.

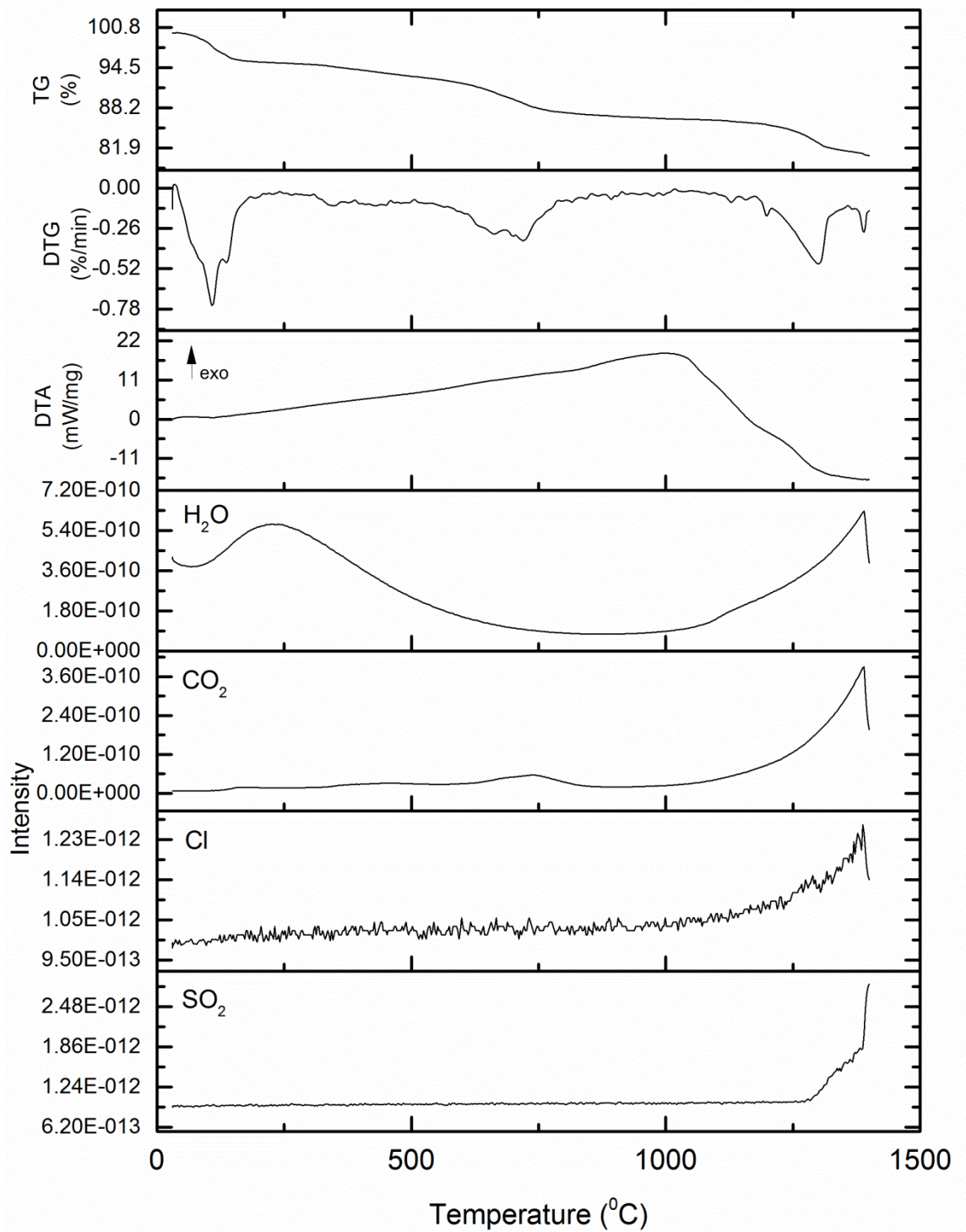Figure 5.3 STA-MS curves for wood ash.
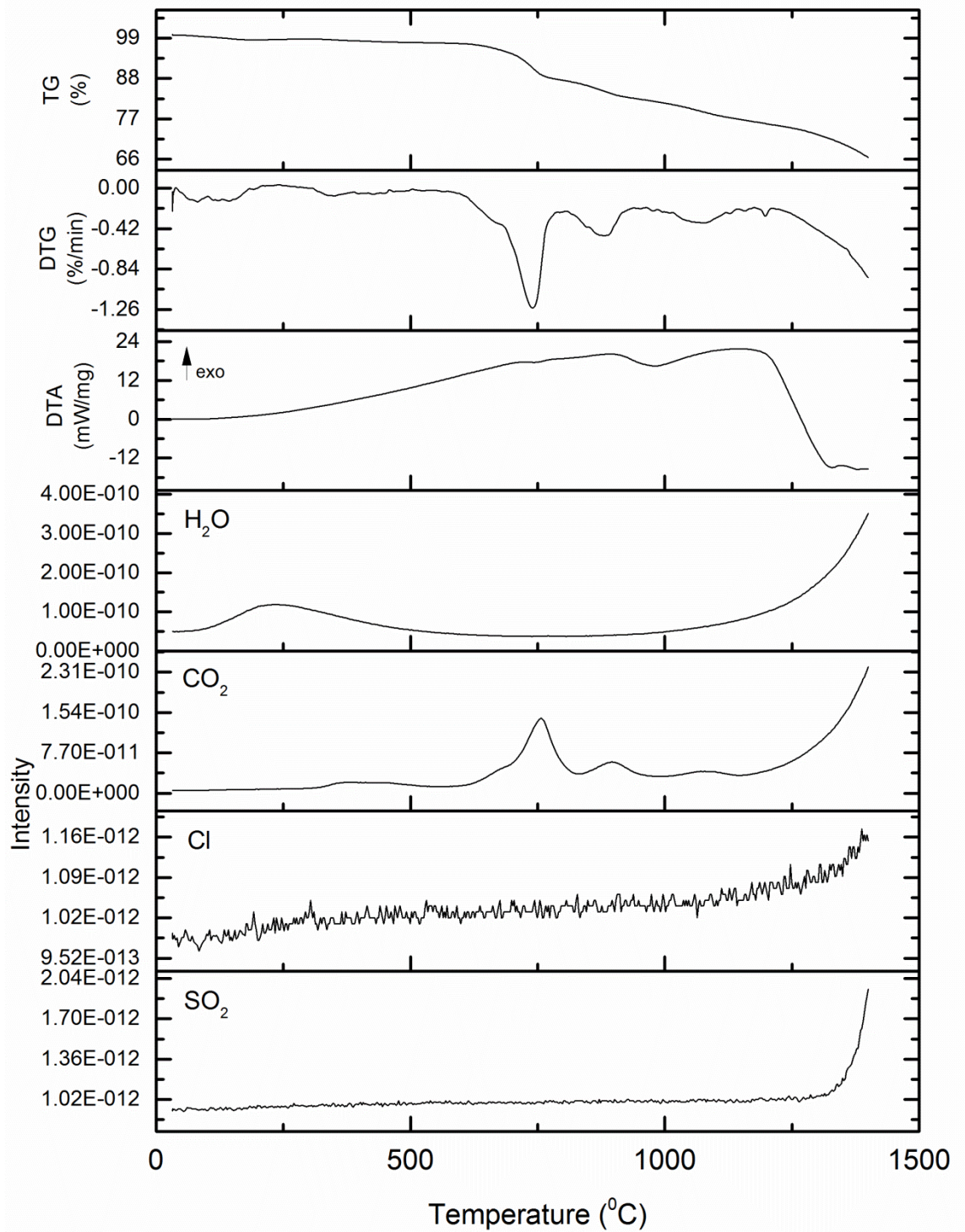
Figure 5.4 STA-MS curves for peanut ash.
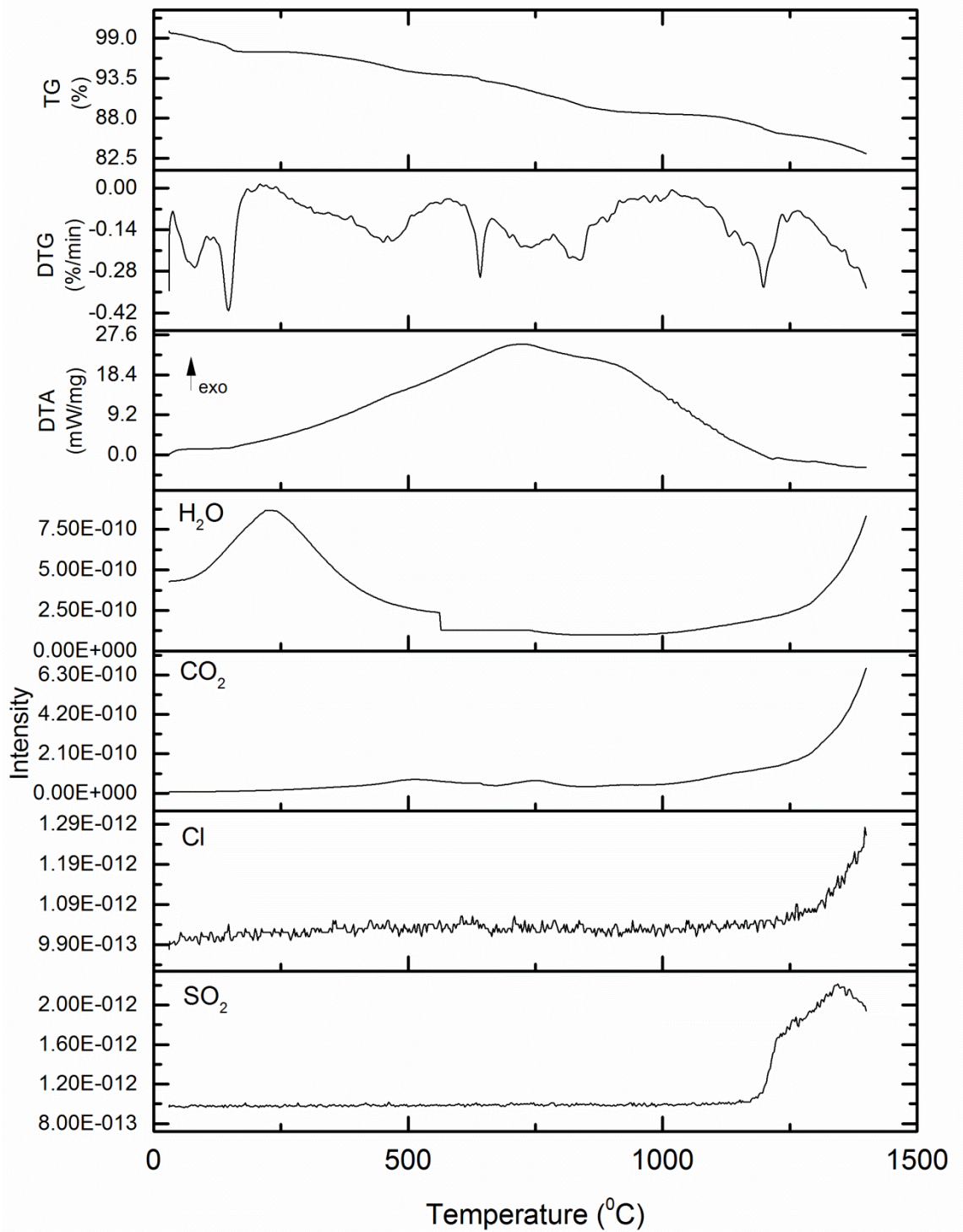
Figure 5.5 STA-MS curves for sunflower ash.

Figure 5.6 STA-MS curves for miscanthus ash.

5.2.4 Slagging and Fouling propensities

The mineral element composition of the ashes shown in Table 5.4 can further be utilized to predict slagging and fouling behaviour of these fuels under combustion conditions. Slagging and fouling indices have long been in use to assess deposit forming tendencies of fuels and detailed accounts are available in the literature (Bryers, 1996, Couch, 1994) It is worth mentioning that most of the slagging and fouling indices were originally developed for reference coals under specific boiler operating conditions, which may result in discrepancies when extending these to alternative fuels and boiler configurations. However, an overall prediction as to the slagging and fouling behaviour based on the relative consistency between the indices seems justified.

Table 5.7 Fusibility correlations and index ranges (Bryers, 1996, Couch, 1994, Pronobis, 2005, Barroso et al., 2007).

Index	Formula	Slagging and fouling propensity		
		Low	Medium	High to Severe
$R_{B/A}$	$\dfrac{Fe_2O_3 + CaO + MgO + Na_2O + K_2O}{SiO_2 + Al_2O_3 + TiO_2}$	< 0.2	$0.2\text{-}0.4$	$0.4\text{-}0.9$
S_R	$\dfrac{SiO_2}{SiO_2 + Fe_2O_3 + CaO + MgO} \times 100$	>72	$65\text{-}72$	≤ 65
F_U	$R_{B/A} \times (Na_2O + K_2O)$	≤ 0.6	$> 0.6, \leq 1.6$	$1.6\text{-}40$
Fe-Ca	$\dfrac{Fe_2O_3}{CaO}$	$<0.3, >3$		$0.3\text{-}3.0$
AI	$\dfrac{kg(Na_2O + K_2O)}{GJ}$	<0.17	$0.17\text{-}0.34$	≥ 0.34

Table 5.7 summarises the fusibility correlations employed in this study as well as the index ranges depicting the severity of slagging and fouling. The index ranges have further been colour coded green, yellow and red according to the low, medium and high propensities of slagging and fouling, respectively.

The base to acid ratio is the most commonly used index based on the ratio of basic to acidic oxides defined as follows:

Base to acid ratio (Bryers, 1996):

$$R_{B/A} = \frac{Fe_2O_3 + CaO + MgO + Na_2O + K_2O}{SiO_2 + Al_2O_3 + TiO_2} \tag{5.6}$$

where basic and acidic oxides are expressed as weight percentages. The base to acid ratio considers basic oxides as fluxing agents which tend to reduce ash melting temperature while acidic oxides tend to increase it (Pronobis, 2005).

The slag viscosity index defined by the equation below, correlates the slagging propensity of ash to the silica ratio.

Slag viscosity index (Pronobis, 2005):

$$S_R = \frac{SiO_2}{SiO_2 + Fe_2O_3 + CaO + MgO} \times 100 \tag{5.7}$$

High silica ratio corresponds to high ash viscosity and low slagging inclination.

The fouling factor is essentially the base to acid ratio multiplied by the sum of alkali elements (expressed as a weight percentage) as shown in the following equation.

Fouling index (Pronobis, 2005):

$$F_U = R_{B/A} \times (Na_2O + K_2O) \tag{5.8}$$

This expression of the fouling factor introduced by Pronobis (Pronobis, 2005) serves as an improvement on the original fouling factor proposed by Couch (1994) which only incorporated percent sodium content in the multiplication factor. Alkali compounds containing sodium and potassium compounds are known to be major constituents in fouling deposits found in boilers and can react to form low temperature species as discussed in Section 2.5. While sodium content is more relevant for coal, the major alkali constituent in biomass is potassium. Therefore the above form of fouling index which includes potassium oxide may help to extend its suitability for application to biomass.

The iron to calcium ratio is defined as follows:

Iron to calcium ratio (Barroso et al., 2007):

$$\frac{Fe_2O_3}{CaO} \tag{5.9}$$

It predicts slagging potential based on the identification of various iron containing complexes in boiler deposits (see Section 2.1.1), which are linked to increased slagging by increasing the sticking tendency of the ash. Iron to calcium ratio between 0.3-3.0 is thought to increase the presence of a slag phase in ash due to the formation of low melting point eutectics (Barroso et al., 2007).

The alkali index is given by Equation 5.10.

Alkali Index (Miles et al., 1996):

$$AI = \frac{kg(Na_2O + K_2O)}{GJ} \qquad (5.10)$$

It is the most popularly used slagging and fouling indicator for biomass adapted from the coal industry (Miles et al., 1996). It involves calculating the weight of alkali oxides per unit of fuel energy (HHV expressed in GJ/kg).

The HHV of the fuels was calculated by using the following correlation developed by Parikh et al. (2005) :

$$HHV = 0.3536\ FC + 0.1559\ VM - 0.0078\ ASH \qquad (5.11)$$

The major advantage of using this correlation is that the HHV of any fuel can be calculated simply from its proximate analysis. It is applicable to the entire spectrum of carbonaceous materials including hard coal, lignite and various types of biomass with a proximate content ranging from 1.0-91.5% FC, 0.92-96% VM and 0.12-77.7% ash.

The values of the aforementioned slagging and fouling indices and their predicted tendencies for the given fuels are presented in Table 5.8.

Table 5.8 Predicted slagging and fouling tendencies.

Sample	Slagging and Fouling Indices				
	$R_{B/A}$	S_R	F_U	Fe/Ca	AI
UK coal	0.21	79	0.75	4	0.08
Wood (Pine)	0.74	59	8.25	0.30	0.12
Peanut shell	1.14	65	36.7	0.32	0.57
Sunflower	23.75	7	1076	0.03	0.64
Miscanthus	0.88	81	29	0.05	0.65

It can be seen that the biomasses exhibit consistently high to severe slagging and fouling inclinations based on base to acid ratio and fouling index. The relatively lower alkali content in wood ash compared to the other biomasses results in its low alkali index. Since slagging from sticky iron containing complexes is usually encounterd in radiant sections of the boiler near the regions of the flame, low iron to calcium ratio for sunflower and miscanthus indicates low slagging in this area. Low silica ratio in miscanthus suggests slag of relatively low viscosity but the increased presence of fluxing agents indicates rapid accumulation of deposits. The coal exhibits considerable lower values of slagging and fouling suggesting problems with accumulation of deposits on the boiler walls are expected to be manageable in this case.

5.3 Conclusions

The properties of four different types of biomass and a coal have been studied with the assistance of various laboratory techniques in order to assess their behaviour during combustion. Preliminary analysis of the fuels suggests that the amount of ash and its possible composition depends on the combustion conditions and heating regime. The properties of the biomass samples were in agreement with the general trend reported in the literature in terms of high volatile matter and low ash content. The high sulphur and ash content of the coal suggests it would be more appropriate for use in blends, either with other coals or co-fired with biomass. XRF analysis of the ashes showed that they varied widely in composition although the biomass ashes did show high alkali and alkaline earth metal content typical of biomass fuels. The wide variation in the ash composition was also illustrated in the

difference in their ash fusion temperatures. Improved knowledge of change in mass of the ash on heating, gas phase release, melt formation was obtained by simultaneous thermal analysis coupled with mass spectroscopy. The fusion temperatures evaluated from this technique were significantly lower than the initial deformation temperature obtained from AFT suggesting that visual observations based on change in shape of the specimen do not provide reliable information regarding the onset of the melting process. Furthermore, the mass loss and evolution profiles obtained from STA-MS were used to predict the reactions taking place in the ash. While STA analysis proved useful for studying the behaviour of ash prepared under specified laboratory conditions, there are limitations associated with extending this data to predict the behaviour of ash in boilers. One deficiency is that it does not take into account interactions between ash particles and flue gas. The slagging and fouling propensities of the fuels evaluated with the help of a number of indices predicted low to medium slagging and fouling inclination of the coal but mostly severe slagging and fouling consequences for the biomasses. The high deposit forming tendencies for biomass could in turn lead to higher risks of tube wastage due to corrosion under deposits as demonstrated in Chapter 4.

Chapter 6

Prediction of fuel ash behaviour using thermodynamic modelling

6.1 Introduction

Thermodynamic modelling is an important tool which is useful for predicting the chemical behaviour of complex systems and has found application in the fields of combustion, gasification, metallurgy, glass technology, ceramics. Since thermodynamic models are based on the assumption that equilibrium is attained within the system, difficulty arises when adequate thermodynamic data is not available for all the species in the system or some of the reactions are kinetically controlled. Despite the inherent constraints associated with thermodynamic models, their role in contributing to the body of knowledge cannot be regarded as trivial. This is because they predict thermodynamic limits of a system that can serve as a guide to process evaluation, design and improvement.

This chapter presents the results and discussion derived from the application of various thermodynamic modelling techniques to the fuels presented in chapter 5 in order to assess the behaviour of ash forming species during combustion. While other researchers have employed this technique to predict coal ash fusibility mineral element evaporation and so on (Zhao et al., 2013, van Dyk et al., 2006, Otsuka, 2002, Li et al., 2006), there is a scarcity in the available literature on its applicability to biomass ash and blends. Also, the wide variation in the different types of biomass and their associated compositions and characteristics, makes it

difficult to generalize the results obtained from assessing the behaviour of a particular type of biomass. It therefore seems more appropriate to evaluate the behaviour of individual fuels in order to assess their performance on a larger scale. For this purpose, a series of computations were performed with the help of thermodynamic analysis software FactSage 6.3.

FactSage is one of the largest fully integrated database computing systems in chemical thermodynamics developed by Thermfact/CRCT (Montreal, Canada) and GTT-Technologies (Aachen, Germany) by the fusion of the FACT-Win/F*A*C*T (Facility for Analysis of Chemical Thermodynamics) and ChemSage thermochemical packages (Bale et al., 2009). FactSage consists of a series of information, database, calculation and manipulation modules that simplify the computation of multicomponent, multiphase equilibria. The Equilib module is of particular interest as it calculates the concentration of chemical species produced from the reaction of given amounts of elements or compounds by retrieving data from specified databases, based on the principle of Gibbs free energy minimisation. The Phase Diagram module permits users to calculate and plot multicomponent phase diagram sections by making use of available thermodynamic databases. These modules of the FactSage programme package were employed for the current thermodynamic analysis.

6.2 Results and Discussion

6.2.1 Prediction of melt phase formation

The importance of an initial melt phase or liquid slag formation in contributing to the increased rate of deposition has been discussed in Section 2.5. However, accurate assessment of the temperature at which the melting process commences is difficult by using laboratory techniques alone as demonstrated in Chapter 5. Alternative methods to assess the fusion behaviour of ash may therefore lead to more accurate predictions by coupling the computed values with laboratory data. To this end, a series of computations were performed in order to predict melt phase formation with respect to temperature for the given fuels. This entailed the use of the Equilib module in FactSage along with the FToxid and FactPS databases. The C,H,N,O and ash content of the fuels in terms of major oxides Al_2O_3, SiO_2, K_2O, CaO, Fe_2O_3, Na_2O, MgO, TiO_2, P_2O_5, SO_3, were used as inputs in the Reactants window of the programme. The calculations were carried out under oxidizing conditions such that V/V_0 (ratio of actual to theoretical air input) was set at 1.15 for all the cases. The temperature range of 700^0C to 1500^0C was selected yielding 9 subsets of data for each fuel at a temperature interval of 100^0C.

Figure 6.1 shows slag liquid formation for coal and Figure 6.2 shows the relative amounts of liquid slag formation for the biomass fuels. A couple of generalized observations can be made here regarding the difference in behaviour of coal and biomass. Firstly, while the initiation of a melt phase for coal occurs at 800^0C, all of the biomasses show the presence of a liquid slag even below 700^0C. Secondly, while the coal shows increased amounts of slag formation with respect to

temperature, this is hardly the case for the biomass fuels. For miscanthus it increases upto to 1000^0C, remains constant from 1000-1100^{0}C and then decreases. For peanut shells, it remains constant till about 900^0C, decreases till 1400^0C and then increases again. For wood it remains fairly constant until 1200^0C, increasing sharply at 1300 and becoming stable again with a slight increase at 1400^0C. The most unusual results are encountered in the case of sunflower husk which shows a peak at 900^0C but negligible liquid slag at 1100^0C.
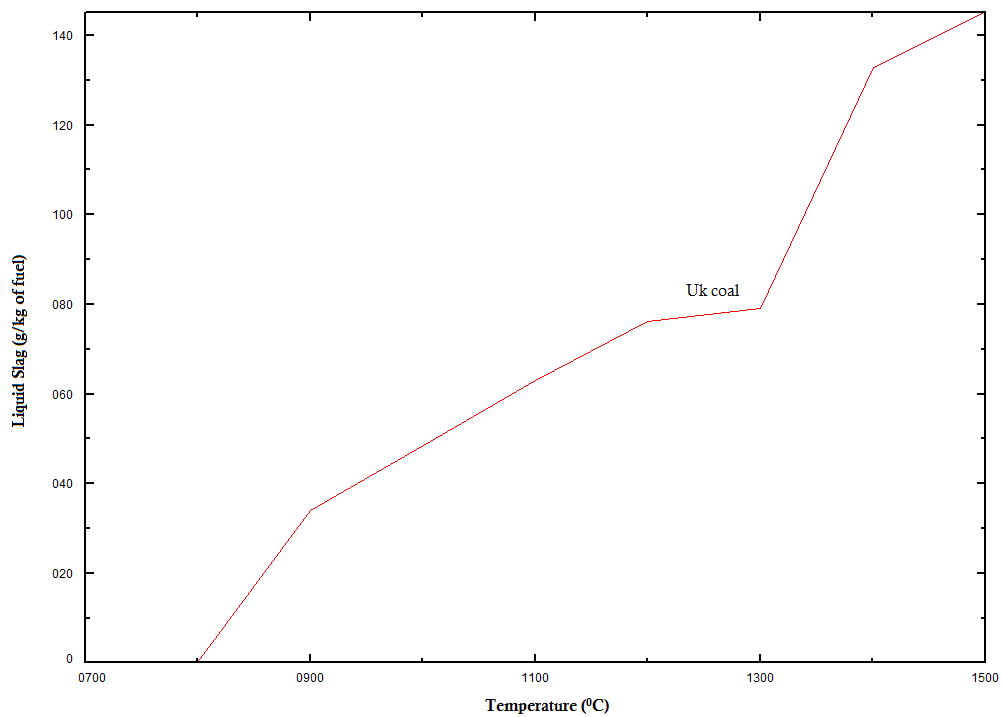
Figure 6.1 Liquid slag formation at different temperatures for coal ash.
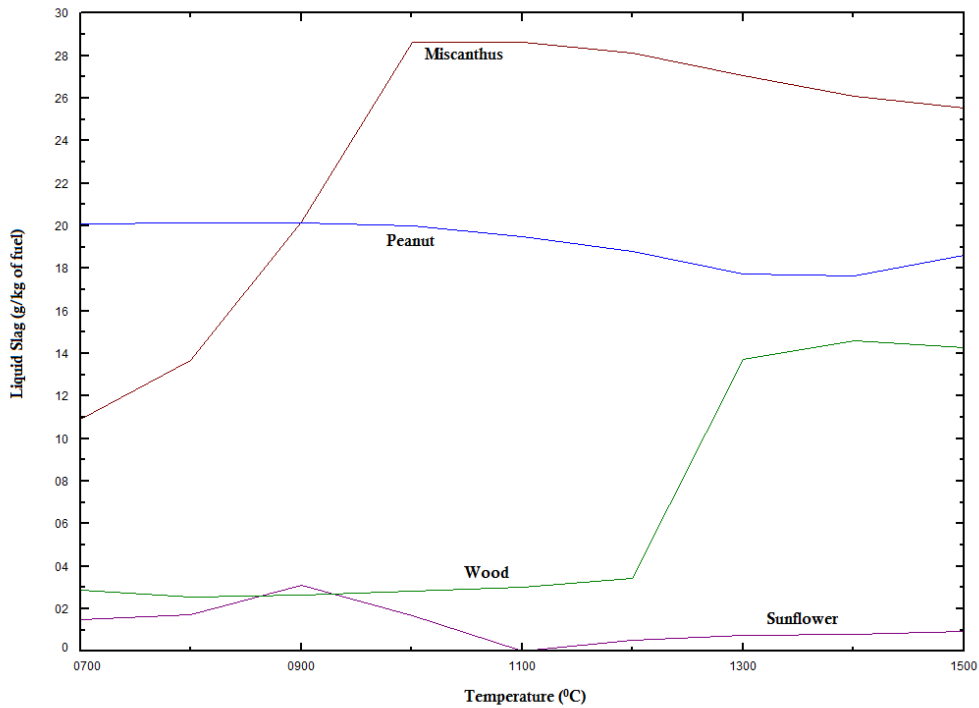
Figure 6.2 Liquid slag formation at different temperatures for biomass ash.

Figure 6.3(a-e) represents the proportion of major oxides in the slag phase with respect to temperature. The results show that silica is the core component of the slag. While the melting temperature of SiO_2 itself is high, oxides, hydroxides or metallo organic compounds of alkali metals potassium and sodium react to form low melting eutectics with silicates (Miles et al., 1996). Similar eutectics can be formed with iron and calcium but with higher melting temperatures. This trend can be seen by the results shown for all the fuels where potassium and/or sodium form the main oxide constituents of the slag with silica at lower temperatures while CaO and FeO appear in the slag at higher temperatures. It can also be observed that as CaO in the molten phase increases, it causes a corresponding decrease in the amount of K_2O in the melt. This trend is very clear for coal, peanut, miscanthus

and to some extent for wood and is in agreement with the experimental findings of Thy et al.(2000), who concluded that the inclusion of CaO into the melt phase drives the potassium out of the melt into the vapour phase. The partitioning of potassium into the vapour phase occurs because it is not easily accommodated into the melt structure. The high affinity for K_2O to be lost into the vapour phase can be used to explain the dip in the amount of slag at 1100^0C for sunflower ash. In addition, the very low silica content of sunflower ash is unlikely to support the retention of K_2O in the slag in the form of silicates.

Figure 6.4(a-e) represents the major solid phases in equilibrium with the slag phase at different temperatures. It can be observed that while solid potassium compounds mostly exist below 1100^0C for most of the fuels, Ca and Mg bearing phosphates and silicates are the main solid species in equilibrium with the slag at high temperatures (above 1300^0C). Some of the reactions associated with the formation of complex high temperature calcium magnesium silicates are given below (Niu et al., 2013):

$$2CaSi_2 + 5O_2 \rightarrow 2CaSiO_3 + 2SiO_2 \qquad (6.1)$$

$$2CaSiO_3 + MgO \rightarrow Ca_2MgSi_2O_7 \qquad (6.2)$$

$$2CaSi_2 + MgO + 5O_2 \rightarrow Ca_2MgSi_2O_7 + 2SiO_2 \qquad (6.3)$$

$$14CaSi_2 + 2MgO + 35O_2 \rightarrow 2Ca_7Mg(SiO_4)_4 + 20SiO_2 \qquad (6.4)$$

$$14CaSiO_3 + 2MgO + 21O_2 \rightarrow 2Ca_7Mg(SiO_4)_4 + 6SiO_2 \qquad (6.5)$$
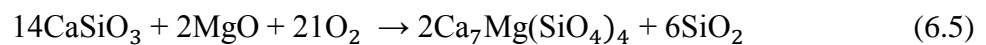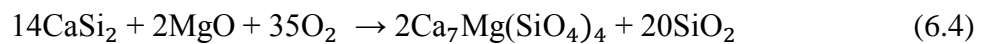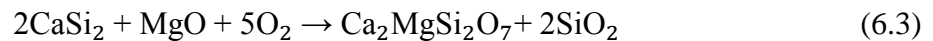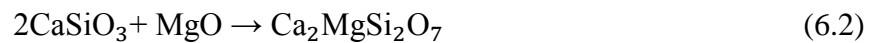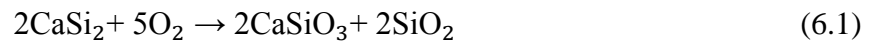
 The role of phosphorous in ash melting behaviour is considered important by many researchers. While some suggest phosphorous as having a positive influence towards decreasing the fusion temperature of ash, Zhang et al., (2013) found that phosphorous only helps to lower the melting temperature if the A/CNK ratio ($Al_2O_3/CaO+Na_2O+K_2O$) is more than 1. Since the A/CNK ratio is less than one for all the biomass samples used in the present study, the presence of solid phosphorous bearing species at high temperatures, as evaluated by Factsage, seems justified.
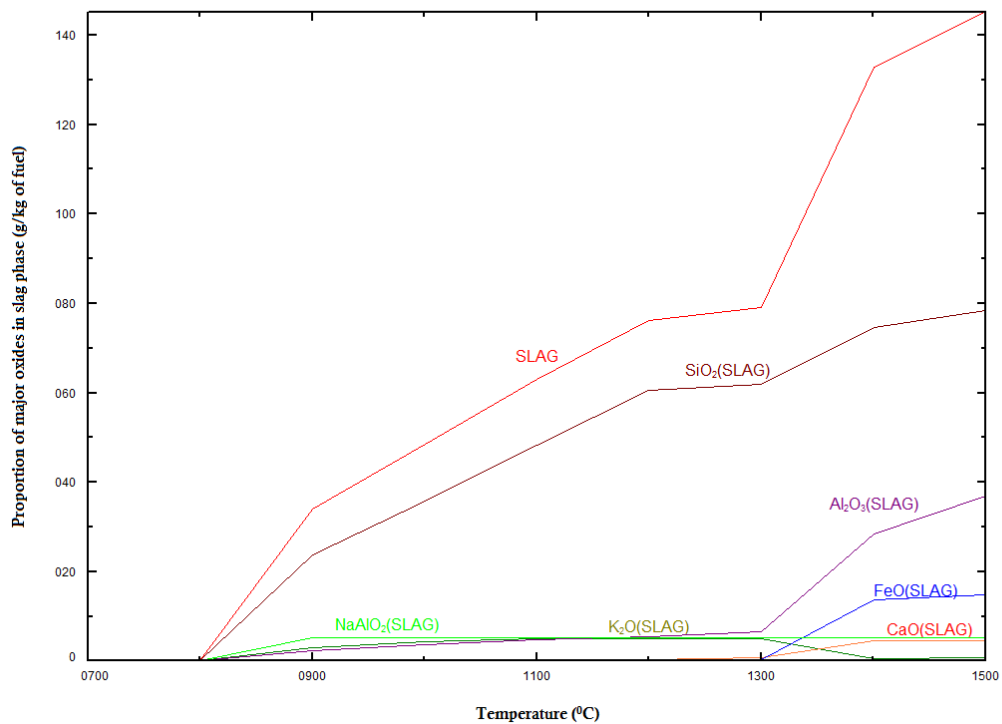
Figure 6.3(a). Proportion of major oxides in the slag phase for coal ash.
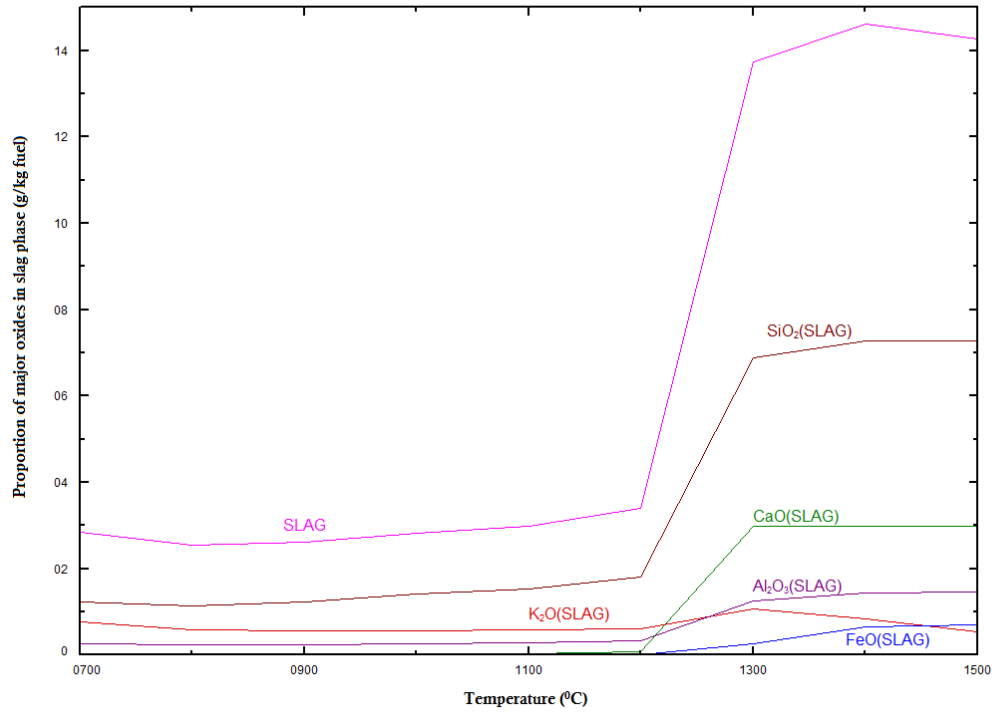
Figure 6.3(b). Proportion of major oxides in the slag phase for wood ash.
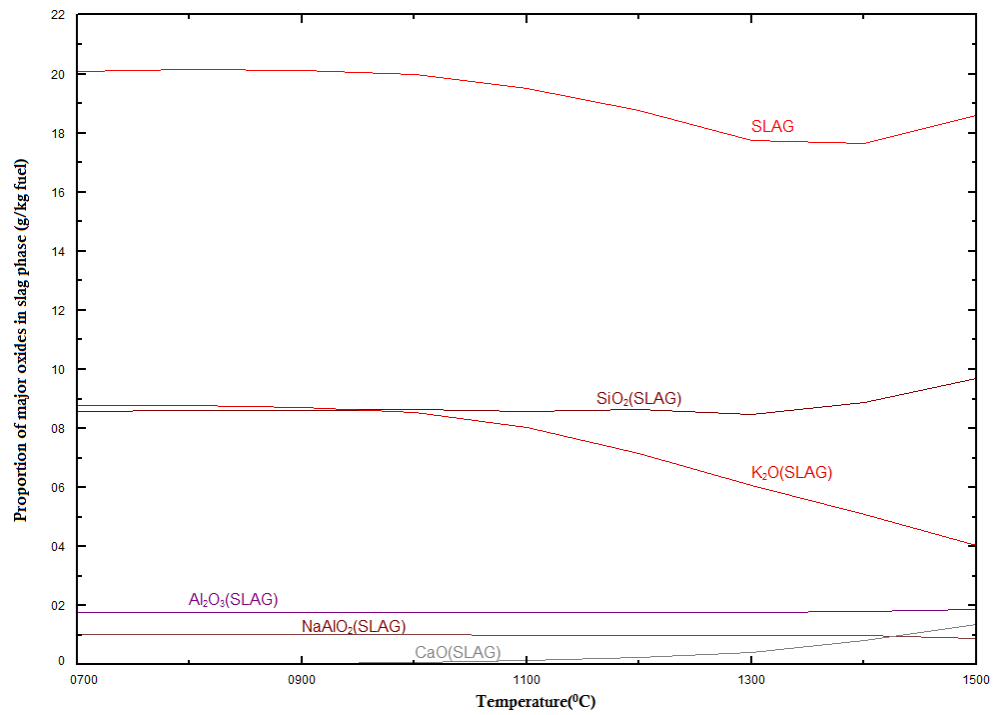
Figure 6.3(c). Proportion of major oxides in the slag phase for peanut ash.
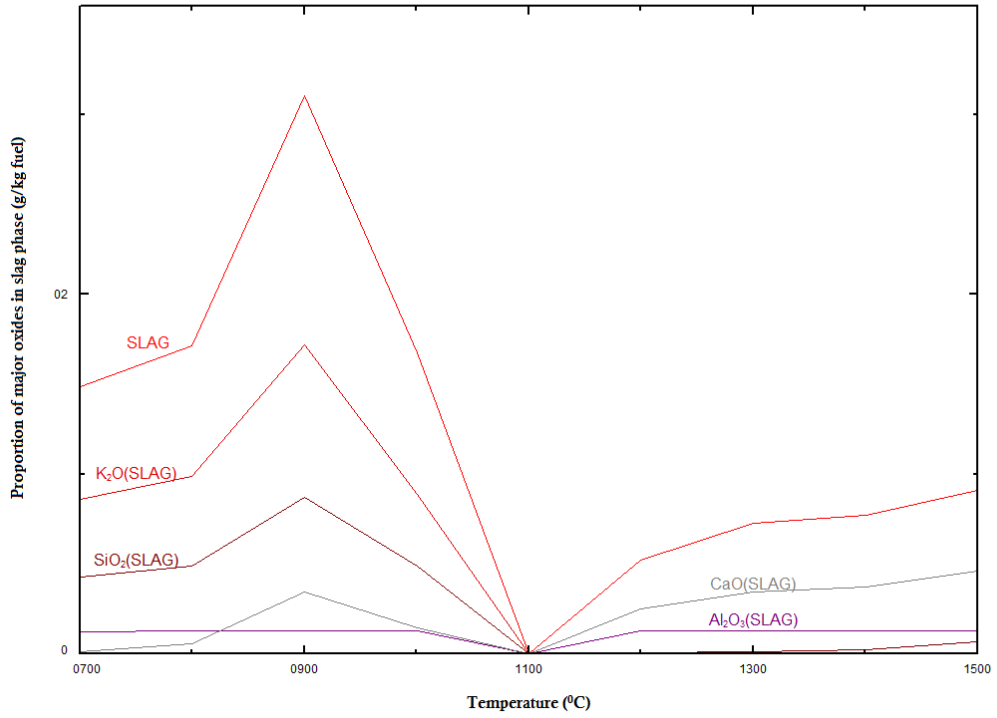
Figure 6.3(d) Proportion of major oxides in the slag phase for sunflower.
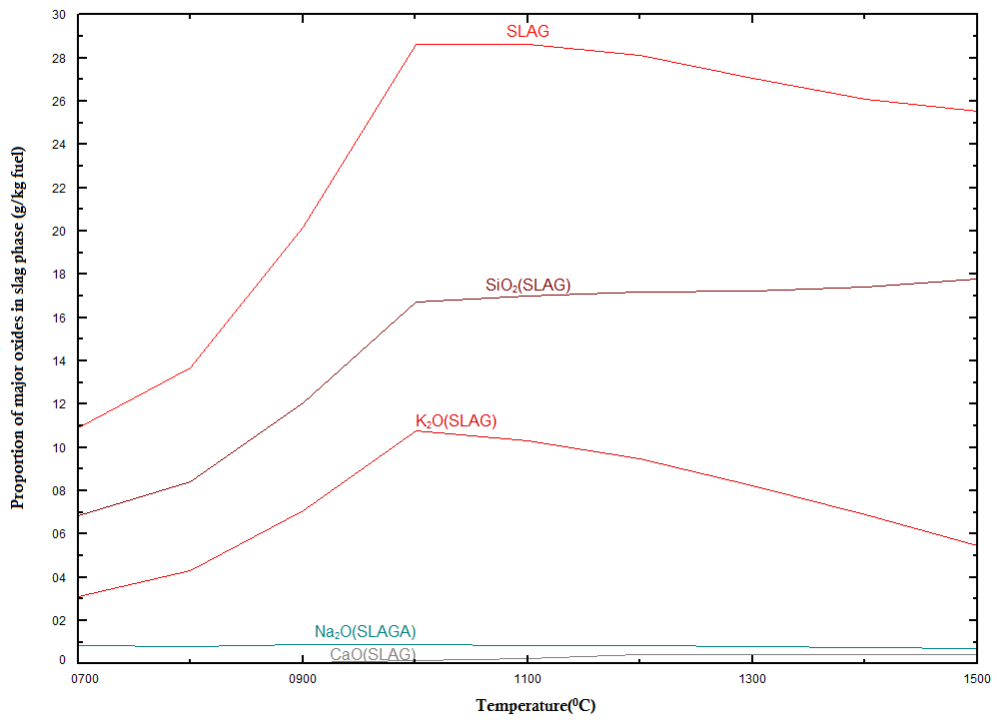
Figure 6.3(e) Proportion of major oxides in the slag phase for miscanthus ash.
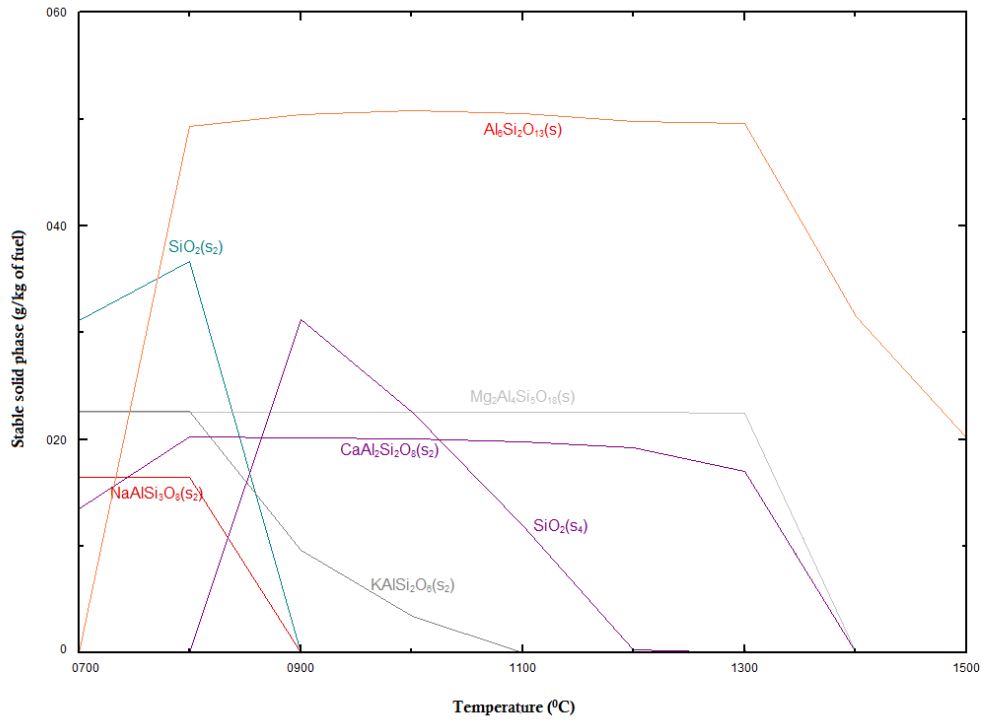
Figure 6.4(a). Stable solid phases in equilibrium with the slag phase for coal ash.
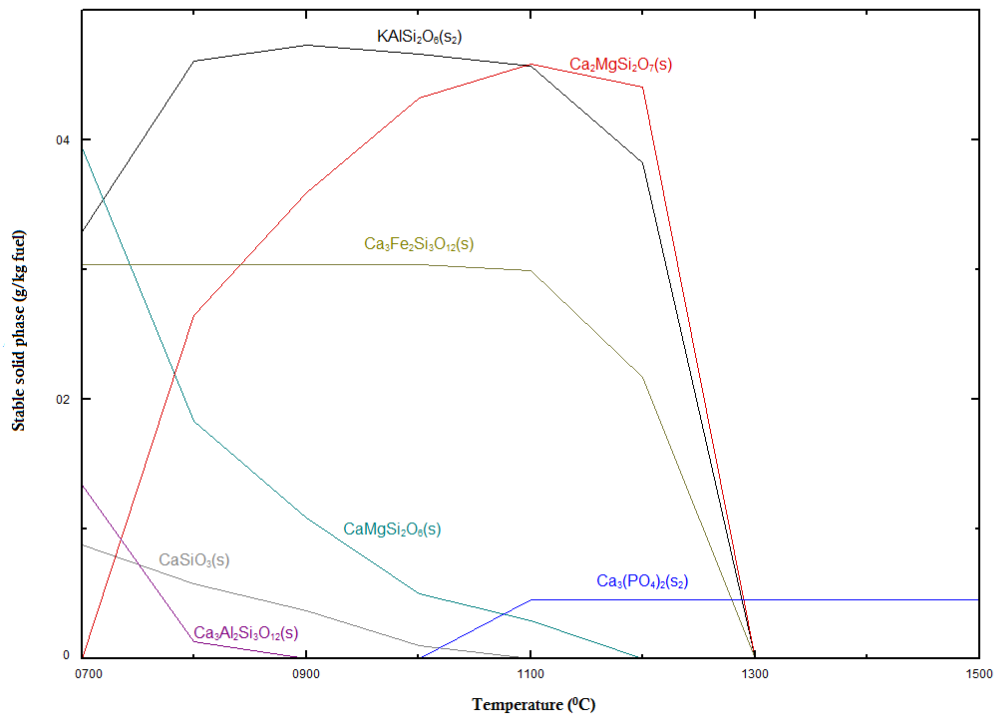
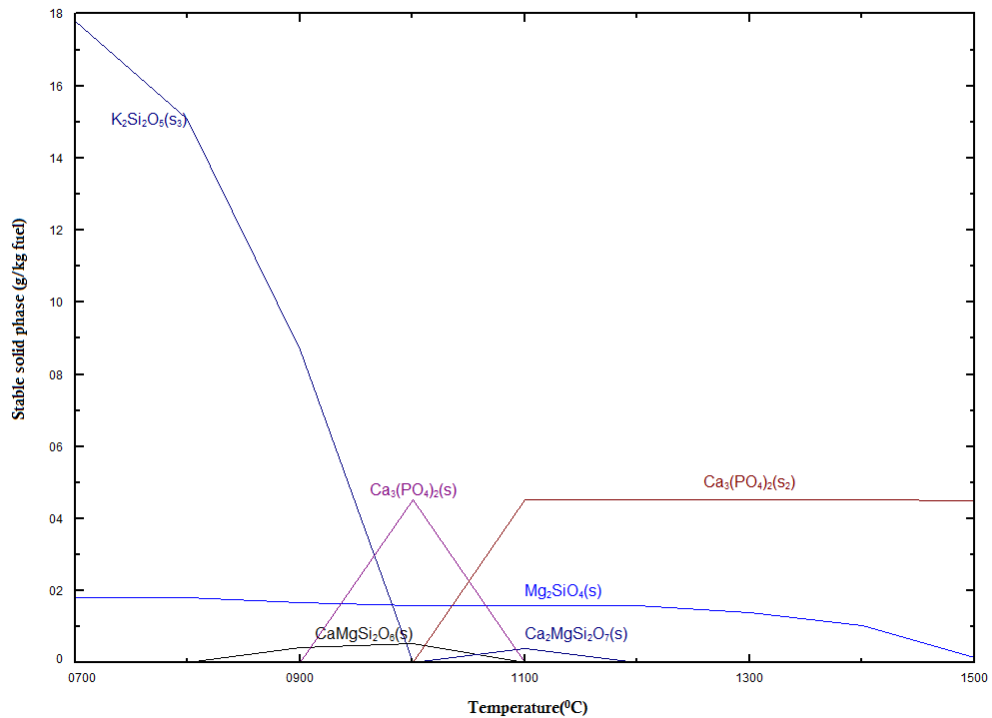Figure 6.4(b). Stable solid phases in equilibrium with the slag phase for wood ash.
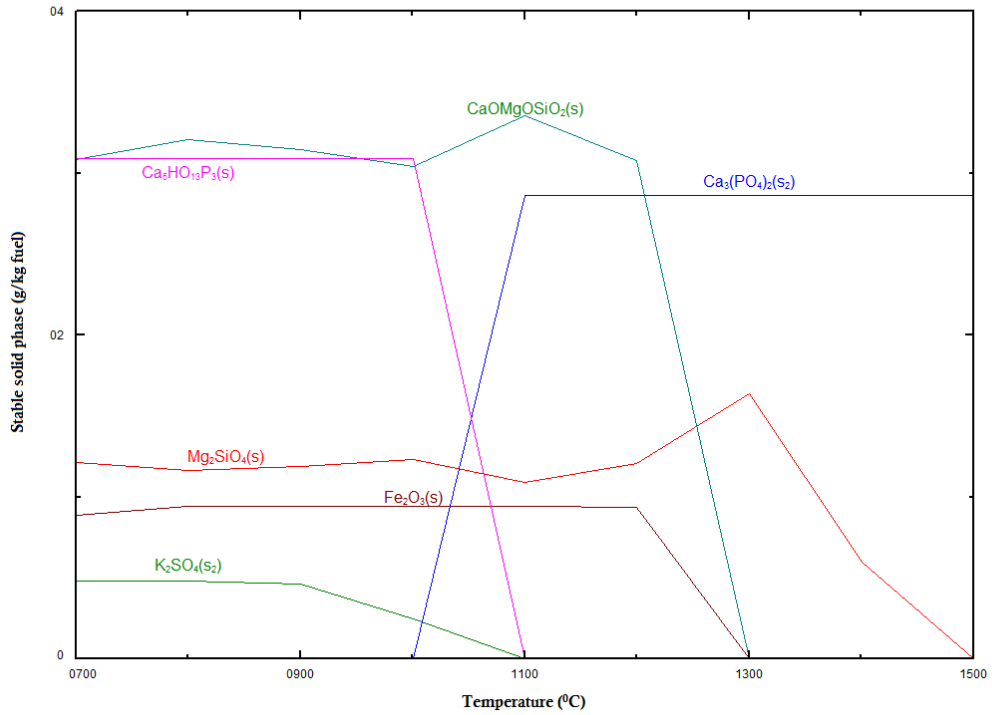
Figure 6.4(c). Stable solid phases in equilibrium with the slag phase for peanut ash.
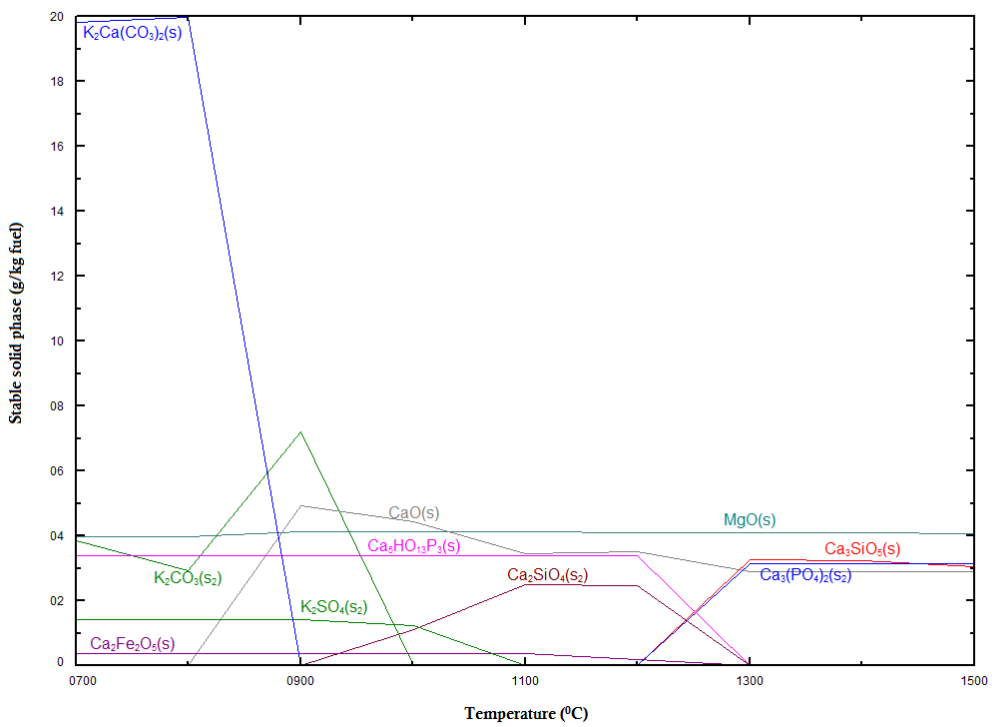
Figure 6.4(d). Stable solid phases in equilibrium with the slag phase for peanut ash.

Figure 6.4(e). Stable solid phases in equilibrium with the slag phase for miscanthus ash.

6.2.2 Ternary Phase diagrams

6.2.2.1 Background

Phase diagrams are graphical representations of the different phases that exist in equilibrium within a given system and provide information regarding the phase transformations that are expected to occur with a change in the values of thermodynamic variables such as temperature, pressure and composition. They can be classified as unary, binary or ternary depending on whether the system contains one, two or three components. To represent completely the phase equilibria at constant pressure in a ternary system, a three-dimensional model in the form of a

triangular prism is required where composition is represented on the base of the prism and the vertical axis represents temperature. However, due to the complexity involved in the use of 3-D ternary plots, the information from the diagrams is more commonly plotted in two dimensions which simplifies data interpretation. One such representation is a polythermal projection of the liquidus surface known as liquidus plots.

Liquidus plots can be useful for the prediction of fusion tendencies of ash of known composition. Huggins (1981) first demonstrated that the ash fusion temperatures for coal ashes correlated closely with liquidus temperatures for the appropriate Al_2O_3-SiO_2-XO (where X =Ca, K_2, Na_2) phase diagram and that the liquidus and ash fusion temperatures generally showed parallel compositional trends. Similar observations were made by (Hurst et al., 1996, Qiu et al., 1999, Gupta et al., 1998) and others who used the phase diagram approach for explaining the fusion behaviour of various coal ashes. However, little data is available in the literature to correlate fusion temperatures of biomass ash with the properties of ternary phase diagrams. The following section is based on an attempt to evaluate the relationship, if any, between fusion behaviour of ash (from ash fusion tests) and high temperature solid phases calculated using the Phase Diagram module and FToxide database in FactSage.

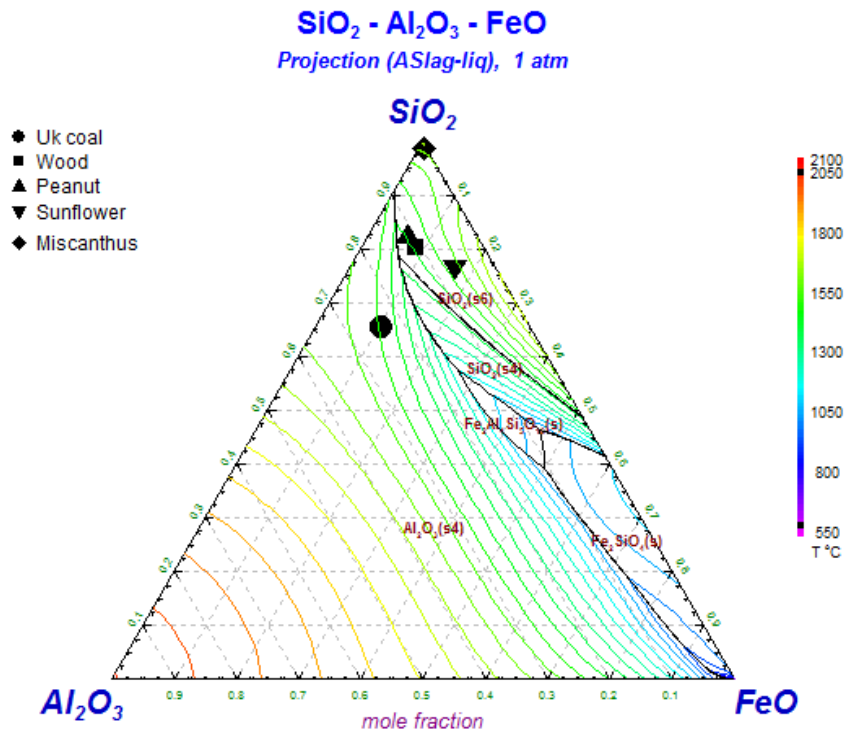### 6.2.2.4 Relation between liquidus plots and high temperature melting species

The liquidus projections for the three component system SiO_2-Al_2O_3-XO (where X = Ca, Fe, K_2) are shown in Figure 6.5(a-c) respectively. Furthermore, liquidus temperatures for SiO_2-K_2O system with third component as either Ca, Na_2, Fe were also computed and are shown in Figure 6.5(d-f). The reason for considering three component systems based on SiO_2-Al_2O_3 was that although silica and alumina are the major components of coals, this is not the case for biomass. With the exception of wood, silica and potassium are the major components for the biomasses used in this study.

Table 6.1 shows the liquidus temperatures of the five fuels obtained from the respective ternary plots along with the predicted high temperature solid phase. The solid phase represents the mineral species that are last to melt on heating and first to crystallize on cooling. For the coal ash, the SiO_2-K_2O-FeO phase diagram gives the closest approximation to the FT from ash fusion test with cristobalite [SiO_2 (s6)] as the high temperature solid. For wood ash, the SiO_2-Al_2O_3-CaO system gives the lowest liquidus closest to AFT with anorthite [$CaAl_2Si_2O_8$] the solid phase that persists at high temperatures. For peanut, the SiO_2-K_2O-CaO system seems most suitable with calcium silicate [$Ca_3Si_2O_7$] the high temperature melting compound. For sunflower the highest temperature solid is cristobalite [$SiO2(s6)$] according to SiO_2-Al_2O_3-FeO. For miscanthus, potassium silicate [$K_2Si_2O_5$] is the highest melting species with the SiO_2-K_2O-FeO system being that which agrees most closely to the flow temperature.
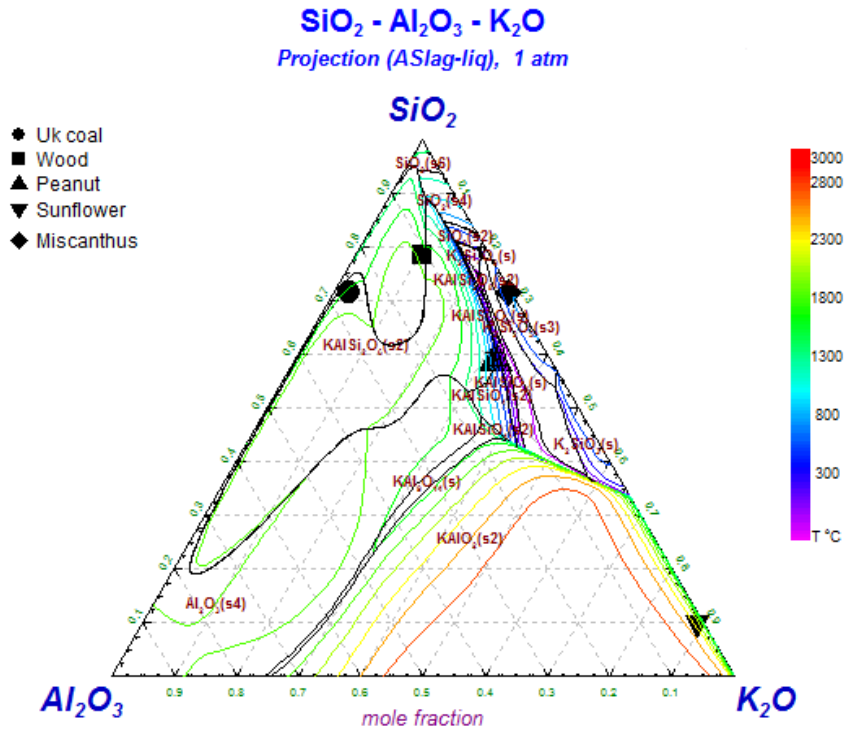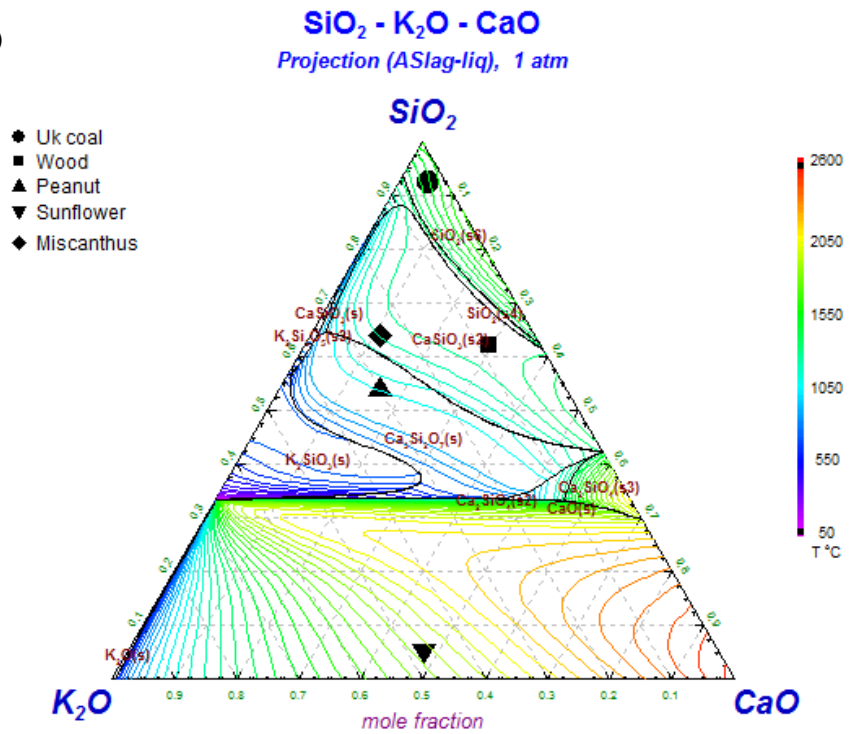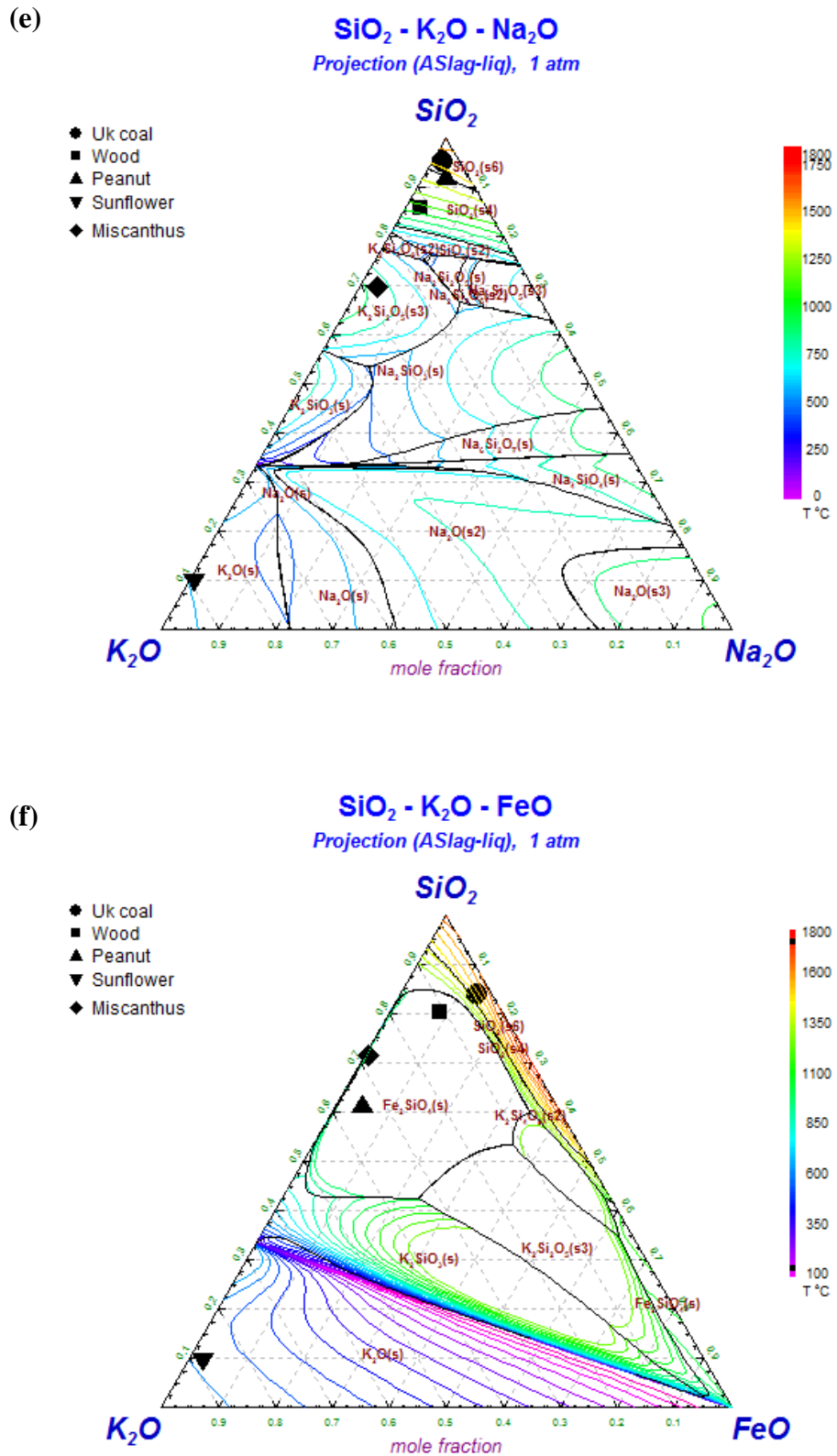
(a)

SiO₂ - Al₂O₃ - CaO
Projection (ASlag-liq), 1 atm

(b)

SiO₂ - Al₂O₃ - FeO
Projection (ASlag-liq), 1 atm

(c)

SiO₂ - Al₂O₃ - K₂O
Projection (ASlag-liq), 1 atm

(d)

SiO₂ - K₂O - CaO
Projection (ASlag-liq), 1 atm

(e)

(f)
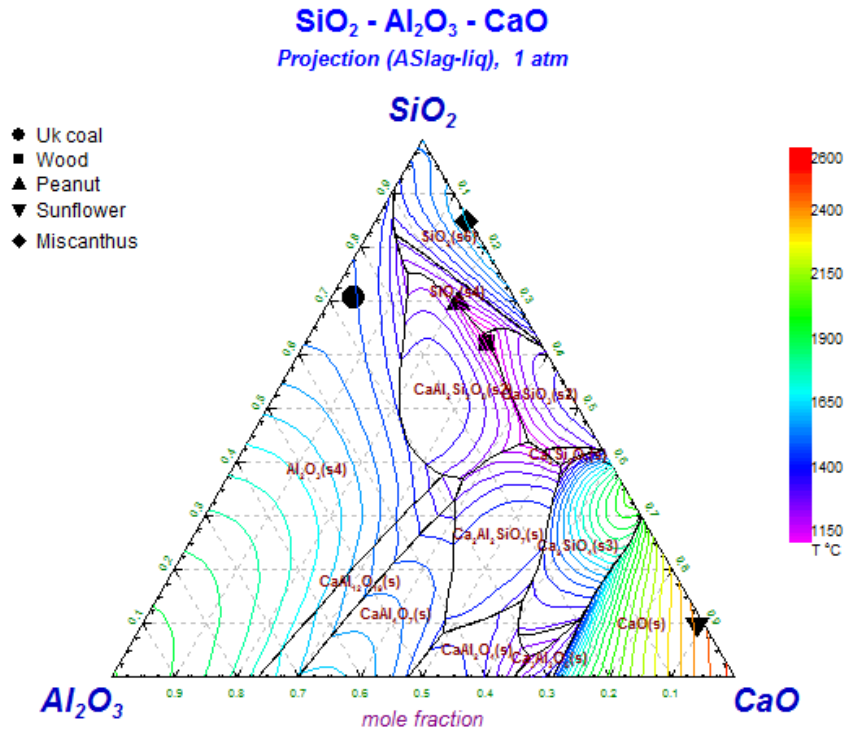
Figure 6. Ternary liquidus plots for (a) SiO_2-Al_2O_3-CaO, (b) SiO_2-Al_2O_3-FeO, (c) SiO_2-Al_2O_3- K_2O, (d) SiO_2-K_2O-CaO, (e) SiO_2-K_2O-Na_2, (f) SiO_2-K_2O-FeO

Table 6.1 Liquidus temperatures and predicted high temperature phases.

Sample	Liquidus temperature from ternary phase diagram (^{o}C) / High temperature solid phase					
	SiO_2-Al_2O_3-CaO	SiO_2-Al_2O_3-FeO	SiO_2-Al_2O_3-K_2O	SiO_2-K_2O-CaO	SiO_2-K_2O-FeO	SiO_2-K_2O-Na_2O
UK coal	1604/ Al_2O_3	1540/ Al_2O_3	1831/ $KAlSi_2O_6$	1576/ SiO2	1520/ SiO_2	1531/ SiO_2
Wood	1225/ $CaAl_2Si_2O_8$	1500/ SiO_2	1883/ Al_2O_3	1423/ $CaSiO_3$	1295/ Fe_2SiO_4	1178/ SiO_2
Peanut	1326 SiO_2	1498/ SiO_2	821/ $KAlSi_2O_6$	1206/ $Ca_3Si_2O_7$	1399/ K_2O	1463/ SiO_2
Sunflower	2472 CaO	1581/ SiO_2	2183/ $KAlO_2$	1935/ CaO	688/ K_2O	695/ K_2O
Miscanthus	1755/ SiO_2	1680/ SiO_2	962/ $K_2Si_2O_5$	1353/ $CaSiO_3$	972/ $K_2Si_2O_5$	946/ $K_2Si_2O_5$

This shows that there is no single phase diagram that can be used to predict the fusion behaviour of biomass and the difference in highest and lowest liquidus temperatures computed from the various ternary systems for individual samples is large. It might be possible to make better predictions regarding the fusion properties if the solidus temperatures could also be computed. Unfortunately this was not possible with the current version of Factsage due to regions of retrograde solubility exhibited by slags containing high potassium and calcium content. While it is difficult to express the properties of biomass based on a three component system due to the diversity in their composition, ternary plots such as those

presented here are useful in evaluating the relative melting tendencies of complex mineral and crystalline phases in ash. This data in conjunction with analytical techniques such as XRD analysis may prove useful for studying the phase mineral transformations in ashes at various temperatures.

6.3 Conclusions

Thermodynamic analysis carried out to assess the melting behaviour of ash, particularly biomass ash showed that biomass fuels demonstrate the existence of a melt phase even below 700^0C. Although this is much lower than the melting temperatures evaluated from laboratory techniques presented in Chapter 5, it offers a better explanation regarding the concerns associated with high rates of deposition in biomass boilers which could also lead to high rates of corrosion under deposits. Phase diagrams based on normalized three components systems showed that the complex behaviour of biomass ashes is difficult to explain with the help of a ternary system. On the whole, thermodynamic modelling is a useful tool that can aid in explaining the complex behaviour of fuel ash, in addition to laboratory techniques. However, the main limitation associated with this type of analysis is the assumption of equilibrium within the system which is associated with sufficiently high temperatures and long residence times.

Chapter 7

Conclusions and suggestions for future work

7.1 Conclusions

7.1.1 Corrosion experiments

A custom built laboratory corrosion equipment was set up to study the effect of varying different parameters on the corrosion rate of different boiler tube materials in a simulated oxy-fuel environment. A summary of the conclusions is as follows:

- Baseline experiments showed that substituting N_2 with CO_2 had little effect on the rate of corrosion if the concentration of all other gas components O_2, SO_2, HCl, H_2O were kept constant.

- Evaluating the effect of increasing the SO_2 content of the simulated oxy fuel gas mixture for three concentrations (1000ppm, 2000ppm, 3000ppm) while keeping the concentrations of remaining gas constituents fairly constant, showed a slight increase in the rate of corrosion for bare mild steel (A210) and austenitic steel (AISI 310) specimen.

- EDX analysis showed that the corrosion of bare specimen was primarily due to combined oxidation/sulphidation mechanism.

- For specimen coated with biomass (pine wood) ash, the measured rate of corrosion was much higher than the corresponding bare specimen for all concentrations of SO_2.

- A deposit of coal (Potland burn UK) ash on the surface of the specimen acted as a protective layer so that the coated specimen showed negligible metal loss under these conditions.

- Specimen coated with a 50% coal, 50% biomass ash (on a weight basis) showed higher rates of corrosion than bare specimen but lower than those observed for pure biomass ash.

- EDX analysis indicated the alkali components of the biomass ash as being the main cause of corrosion under deposits. This was owed to sulphation of alkali oxides in biomass ash by reacting with sulphur species in the gas and subsequent fluxing of the metal due to the formation of sulphate melt.

- The suggested increase in SO_3 formation with increase in SO_2 content was supported by chemical kinetic modelling.

- Similar trends of increase in the rate of corrosion were observed for both materials but the metal loss rates for mild steel were much higher than those for stainless steel.

- The effect of decreasing the concentration of HCl to a minimum (50ppm) corresponding to one of the test cases (2000ppm of SO_2), was to decrease slightly the observed metal loss for bare specimen but no change for biomass ash coated specimen was observed.

7.1.2 Fuel and ash characterisation

A UK sourced power station coal (Potland Burn) and four biomass samples namely wood (pine), miscanthus, peanut shells and sunflower husks were evaluated for their characteristics particularly in terms of their tendency to form deposits in boilers with the help of different laboratory based techniques and methods.

- The behaviour of the biomass samples differed considerably from that of the given coal in terms of ultimate and proximate content, ash melting behaviour and predicted tendency to form deposits.

- The biomass samples differed widely in their ash composition.

- The large variation in ash composition was also depicted in the wide variation of ash fusion temperatures.

- The ash fusion temperatures obtained from STA were considerably lower than those evaluated from the standard AFT.

- High to severe slagging and fouling consequences were predicted for all the biomasses which are likely to increase the risk of under deposit corrosion of boiler tubes.

7.1.3 Prediction of ash fusion behaviour using thermodynamic modelling

- Thermodynamic modelling showed that biomass ashes have a tendency to form a melt phase in combustion environments at much lower temperatures than those predicted by laboratory techniques.

- Thermodynamic predictions suggest that potassium, which is the main alkali component in biomass is most likely to prevail either in the gas phase or as melt in deposits during combustion.

- The fusion behaviour of biomass ash could not be related to ternary phase diagrams based on normalized three component systems.

7.2 Suggestions for future work

7.2.1 Corrosion rig

The current study can be expanded to include the effect of varying the following parameters on the rate of corrosion:

- gas and metal temperature

- type of ash deposits

- influence of varying the water vapour, HCl concentration in the gas

- different materials can be studied

The current work is based on evaluating the rate of corrosion based on thickness loss measurements. Future work could involve assessing the effect of corrosive environments on internal attack of the tube material. However, it should be noted that internal attack requires much longer test durations.

In addition, the corrosion rig can also be used to assess the efficacy of different corrosion control strategies such as corrosion inhibition coatings and claddings.

If a similar facility can be designed to accommodate a larger number of specimens, more variables can be studied at one time.

7.2.2 Ash characterisation

Ash characterization techniques (AFT and STA) could only be performed under oxidising conditions. Reducing conditions can be studied for comparison. In addition, the effect of ashing temperature on alkali retention of biomass ash could be useful in assessing its fusion and deposit forming tendencies.

Bibliography

ABANG, R., LISK, A. & KRAUTZ, H. J. 2013. Fireside Corrosion of Superheater Materials Under Oxy-coal Firing Conditions. *Energy Procedia,* 40**,** 304-311.

ABELS, J. M. & STREHBLOW, H. H. 1997. A surface analytical approach to the high temperature chlorination behaviour of inconel 600 at 700 °C. *Corrosion Science,* 39**,** 115-132.

AHN, J., OVERACKER, D., RYAN, O., FRY, A. & EDDINGS, E. G. 2010. SO3 formation during oxy-coal combustion. *35th International Technical Conference on Clean Coal and Fuel Systems.* Clearwater, Florida.

AKIYAMA, K., PAK, H., TAKUBO, Y., TADA, T., UEKI, Y., YOSHIIE, R. & NARUSE, I. 2011a. Ash deposition behavior of upgraded brown coal in pulverized coal combustion boiler. *Fuel Processing Technology,* 92**,** 1355-1361.

AKIYAMA, K., PAK, H., UEKI, Y., YOSHIIE, R. & NARUSE, I. 2011b. Effect of MgO addition to upgraded brown coal on ash-deposition behavior during combustion. *Fuel,* 90**,** 3230-3236.

AL-MANSOUR, F. & ZUWALA, J. 2010. An evaluation of biomass co-firing in Europe. *Biomass and Bioenergy,* 34**,** 620-629.

ANGıN, D. 2013. Effect of pyrolysis temperature and heating rate on biochar obtained from pyrolysis of safflower seed press cake. *Bioresource Technology,* 128**,** 593-597.

ANTUNES, R. A. & DE OLIVEIRA, M. C. L. 2013. Corrosion in biomass combustion: A materials selection analysis and its interaction with corrosion mechanisms and mitigation strategies. *Corrosion Science,* 76**,** 6-26.

BAKKER, W. T. 2003. The effect of deposits on waterwall corrosion in fossil fueled boilers. *Materials at High Temperatures,* 20**,** 161-168.

BAKKER, W. T. & KUNG, S. C. 2000. Waterwall Corrosion in Coal-Fired Boilers, A New Culprit, FeS. *CORROSION 2000.* Orlando, Fl: NACE International.

BALE, C. W., BÉLISLE, E., CHARTRAND, P., DECTEROV, S. A., ERIKSSON, G., HACK, K., JUNG, I. H., KANG, Y. B., MELANÇON, J., PELTON, A. D., ROBELIN, C. & PETERSEN, S. 2009. FactSage thermochemical software and databases — recent developments. *Calphad,* 33**,** 295-311.

BARROSO, J., BALLESTER, J. & PINA, A. 2007. Study of coal ash deposition in an entrained flow reactor: Assessment of traditional and alternative slagging indices. *Fuel Processing Technology,* 88**,** 865-876.

BARTLETT, E. P. 1927. THE CONCENTRATION OF WATER VAPOR IN COMPRESSED HYDROGEN, NITROGEN AND A MIXTURE OF THESE GASES IN THE PRESENCE OF CONDENSED WATER. *Journal of the American Chemical Society,* 49**,** 65-78.

BASU, P., BUTLER, J. & LEON, M. A. 2011. Biomass co-firing options on the emission reduction and electricity generation costs in coal-fired power plants. *Renewable Energy,* 36**,** 282-288.

BÉRANGER, G., HENRY, G. & SANZ, G. 1996. *The Book of the Steel*, Intercept Limited.

BILIRGEN, H. 2014. Slagging in PC boilers and developing mitigation strategies. *Fuel,* 115**,** 618-624.

BLOUGH, J. L. & KIHARA, S. 1988. Corrosion/88. NACE International.

BORDENET, B. 2008. Influence of novel cycle concepts on the high temperature corrosion of power plants. *Materials and Corrosion,* 59**,** 361-366.

BRAMFITT, B. L. & BENSCOTTER, A. O. 2002. *Metallographer's Guide: practices and procedures for irons and steels*, ASM International.

BRYERS, R. W. 1996. Fireside slagging, fouling, and high-temperature corrosion of heat-transfer surface due to impurities in steam-raising fuels. *Progress in Energy and Combustion Science,* 22**,** 29-120.

BUHRE, B. J. P., ELLIOTT, L. K., SHENG, C. D., GUPTA, R. P. & WALL, T. F. 2005. Oxy-fuel combustion technology for coal-fired power generation. *Progress in Energy and Combustion Science,* 31**,** 283-307.

BURCAT, A., GOOS, E. & RUSCIC, B. 2009. Third Millennium Ideal Gas and Condensed Phase Thermochemical Database for Combustion.

CAMPBELL, F. C. 2008. *Elements of Metallurgy and Engineering Alloys*, ASM International.

CHEN, L., YONG, S. Z. & GHONIEM, A. F. 2012. Oxy-fuel combustion of pulverized coal: Characterization, fundamentals, stabilization and CFD modeling. *Progress in Energy and Combustion Science,* 38**,** 156-214.

CLARKE, F. & MORRIS, C. W. 1983. Combustion aspects of furnace wall corrosion. *In:* MEADOWCROFT, D. B. & MANNING, M. I. (eds.) *Corrosion Resistant Materials in Coal Conversion Systems.* London Applied Science Publishers.

COUCH, G. 1994. *Understanding Slagging and Fouling in Pf Combustion*, IEA Coal Research.

COVINO, B. S., MATTHES, S. A. & BULLARD, S. J. 2008. Effect of Oxyfuel Combustion on Superheater Corrosion. NACE International.

CULLIS, C. F. & MULCAHY, M. F. R. 1972. The kinetics of combustion of gaseous sulphur compounds. *Combustion and Flame,* 18**,** 225-292.

DAVIS, J. R. 2000. *Corrosion: Understanding the Basics*, A S M International.

DEMIRBAS, A. 2004. Combustion characteristics of different biomass fuels. *Progress in Energy and Combustion Science,* 30**,** 219-230.

DU, S., YANG, H., QIAN, K., WANG, X. & CHEN, H. 2014. Fusion and transformation properties of the inorganic components in biomass ash. *Fuel,* 117, Part B**,** 1281-1287.

EIA. 2013. *International Energy Outlook* [Online]. U.S. Energy Information Administration. Available: http://www.eia.gov/forecasts/ieo/electricity.cfm [Accessed].

EMAMI-TABA, L., IRFAN, M. F., WAN DAUD, W. M. A. & CHAKRABARTI, M. H. 2013. Fuel blending effects on the co-gasification of coal and biomass – A review. *Biomass and Bioenergy,* 57**,** 249-263.

FONTANA, M. G. & GREENE, N. D. 1967. *Corrosion Engineering,* New York, McGraw-Hill.

FRANDSEN, F. J. 2009. Ash research from Palm Coast, Florida to Banff, Canada: Entry of biomass in modern power boilers. *Energy and Fuels,* 23**,** 3347-3378.

FRY, A., ADAMS, B., DAVIS, K., SWENSEN, D., MUNSON, S. & COX, W. 2011. An investigation into the likely impact of oxy-coal retrofit on fire-

side corrosion behavior in utility boilers. *International Journal of Greenhouse Gas Control,* 5**,** S179-S185.

FU, C. & GUNDERSEN, T. 2012. Carbon Capture and Storage in the Power Industry: Challenges and Opportunities. *Energy Procedia,* 16, Part C**,** 1806-1812.

GIBBINS, J. & CHALMERS, H. 2008. Carbon capture and storage. *Energy Policy,* 36**,** 4317-4322.

GRABKE, H. J., REESE, E. & SPIEGEL, M. 1995. The effects of chlorides, hydrogen chloride, and sulfur dioxide in the oxidation of steels below deposits. *Corrosion Science,* 37**,** 1023-1043.

GRABKE, H. J., SPIEGEL, M. & ZAHS, A. 2004. Role of alloying elements and carbides in the chlorine-induced corrosion of steels and alloys. *Materials Research,* 7**,** 89-95.

GUPTA, R., WALL, T. & BAXTER, L. 1999. *Impact of mineral impurities in solid fuel combustion*, Kluwer Academic/Plenum.

GUPTA, S. K., WALL, T. F., CREELMAN, R. A. & GUPTA, R. P. 1998. Ash fusion temperatures and the transformations of coal ash particles to slag. *Fuel Processing Technology,* 56**,** 33-43.

HARB, J. N. & SMITH, E. E. 1990. Fireside corrosion in pc-fired boilers. *Progress in Energy and Combustion Science,* 16**,** 169-190.

HOLCOMB, G. R., TYLCZAK, J., MEIER, G. H., JUNG, K. Y., MU, N., YANAR, N. & PETTIT, F. 2012. Fireside Corrosion in Oxy-Fuel Combustion of Coal. *ECS Transactions,* 41**,** 73-84.

HÖÖK, M. & TANG, X. 2013. Depletion of fossil fuels and anthropogenic climate change—A review. *Energy Policy,* 52**,** 797-809.

HSU, H. S. 1987. Review of the development and breakdown of protective oxide scales on alloys exposed to coal-derived atmospheres. *Oxidation of Metals,* 28**,** 213-235.

HUGGINS, F. E., KOSMACK, D. A. & HUFFMAN, G. P. 1981. Correlation between ash-fusion temperatures and ternary equilibrium phase diagrams. *Fuel,* 60**,** 577-584.

HUGHES, E. E. & TILLMAN, D. A. 1998. Biomass cofiring: status and prospects 1996. *Fuel Processing Technology,* 54**,** 127-142.

HUGHES, K. J., TURÁNYI, T., CLAGUE, A. R. & PILLING, M. J. 2001. Development and testing of a comprehensive chemical mechanism for the oxidation of methane. *International Journal of Chemical Kinetics,* 33**,** 513-538.

HURST, H. J., NOVAK, F. & PATTERSON, J. H. 1996. Phase Diagram Approach to the Fluxing Effect of Additions of CaCO3 on Australian Coal Ashes. *Energy & Fuels,* 10**,** 1215-1219.

IEA. 2012. *Key World Energy Statistics* [Online]. International Energy Agency. Available: http://www.iea.org/publications/ [Accessed].

JAMES, P. J. & PINDER, L. W. 1997. THE IMPACT OF COAL CHLORINE ON THE FIRESIDE CORROSION BEHAVIOUR OF BOILER TUBING: A UK PERSPECTIVE. NACE International.

KIHARA, S., NAKAGAWA, K., WOLOWODIUK, W., BLOUGH, J. L. & BAKKER, W. T. 1992. CORROSION RESISTANCE OF ADVANCED TUBE MATERIALS IN COAL-FIRED BOILERS. *In:* SAITO, Y., ÖNAY, B., T. MARUYAMAA2 - Y. SAITO, B. Ö. & MARUYAMA, T.

(eds.) *High Temperature Corrosion of Advanced Materials and Protective Coatings.* Oxford: Elsevier.

KORIPELLI, R. S., CROWE, D. C., FRENCH, D. N. & BRAND, J. 2010. The Role of Fireside Corrosion on Boiler Tube Failures, Part 1. *Coal Power.* Hong Kong: TradeFair Group.

KUNG, S. C. 1997. Prediction of corrosion rate for alloys exposed to reducing/sulfidizing combustion gases. *Materials Performance,* 36**,** 36-40.

KUNG, S. C. 2006. Fireside Corrosion in Coal and Oil-fired Boilers. *In:* CRAMER, S. D. & COVINO, B. S. (eds.) *Corrosion:Environments and Industries.* ASM International.

LABUDA, E., CLINE, D. A. & SHIELDS, K. J. 2000. Fireside Corrosion in Coal and Oil Fired Units: Failure Mechanisms and Methods of Prevention. *CORROSION 2000.* Orlando, Fl: NACE International.

LACKNER, M., WINTER, F. & AGARWAL, A. K. 2010. *Handbook of Combustion*, Wiley.

LAI, G. Y. 1990. *High-temperature corrosion of engineering alloys*, ASM International.

LAI, G. Y. 2007. *High-temperature Corrosion and Materials Applications*, ASM International.

LANDOLT, D. 2007. *Corrosion and surface chemistry of metals.*, EPFL Press.

LEES, D. J. & WHITEHEAD, M. E. 1983. Influence of gas and deposit chemistry on the fireside corrosion of furnace wall tubes in coal-fired boilers. *In:* BRYERS, R. W. (ed.) *Fouling of Heat Exchanger Surfaces.*

LI, H., YOSHIHIKO, N., DONG, Z. & ZHANG, M. 2006. Application of the FactSage to Predict the Ash Melting Behavior in Reducing Conditions. *Chinese Journal of Chemical Engineering,* 14**,** 784-789.

LLORENTE, M. J. F. & GARCÍA, J. E. C. 2006. Concentration of elements in woody and herbaceous biomass as a function of the dry ashing temperature. *Fuel,* 85**,** 1273-1279.

LUTZ, A. E., KEE, R. J. & MILLER, J. A. 1988. SENKIN: A FORTRAN program for predicting homogeneous gas phase chemical kinetics with sensitivity analysis. *Sandia National Laboratories Report SAND87-8248.*

MALMGREN, A. & RILEY, G. 2012. 5.04 - Biomass Power Generation. *In:* EDITOR-IN-CHIEF: ALI, S. (ed.) *Comprehensive Renewable Energy.* Oxford: Elsevier.

MANNY, E. H., BARTOK, W., CRAWFORD, A. R., HALL, R. E. & VATSKY, J. 1978. Studies of waterwall corrosion with staged combustion of coal. *In:* BRYERS, R. W. (ed.) *Ash Deposits and Corrosion Due to Impurities in Combustion Gases.* Washington: Hemisphere Publishing.

MAYORAL, M. C., IZQUIERDO, M. T., ANDRÉS, J. M. & RUBIO, B. 2001. Different approaches to proximate analysis by thermogravimetry analysis. *Thermochimica Acta,* 370**,** 91-97.

MEADOWCROFT, D. B. & MANNING, M. I. 1983. *Corrosion resistant materials for coal conversion systems*, Applied Science Publishers.

MEETHAM, G. W., VAN DE VOORDE, H. & VOORDE, M. H. 2000. *Materials for High Temperature Engineering Applications*, Springer.

MILES, T. R., MILES JR, T. R., BAXTER, L. L., BRYERS, R. W., JENKINS, B. M. & ODEN, L. L. 1996. Boiler deposits from firing biomass fuels. *Biomass and Bioenergy,* 10**,** 125-138.

MIMMO, T., PANZACCHI, P., BARATIERI, M., DAVIES, C. A. & TONON, G. 2014. Effect of pyrolysis temperature on miscanthus (Miscanthus × giganteus) biochar physical, chemical and functional properties. *Biomass and Bioenergy,* 62**,** 149-157.

NIELSEN, H. P., FRANDSEN, F. J., DAM-JOHANSEN, K. & BAXTER, L. L. 2000. The implications of chlorine-associated corrosion on the operation of biomass-fired boilers. *Progress in Energy and Combustion Science,* 26**,** 283-298.

NIST. 2013. NIST Standard Reference Database 17. Available: http://kinetics.nist.gov/

NIU, Y., DU, W., TAN, H., XU, W., LIU, Y., XIONG, Y. & HUI, S. 2013. Further study on biomass ash characteristics at elevated ashing temperatures: The evolution of K, Cl, S and the ash fusion characteristics. *Bioresource Technology,* 129**,** 642-645.

OBERNBERGER, I., BRUNNER, T. & BÄRNTHALER, G. 2006. Chemical properties of solid biofuels—significance and impact. *Biomass and Bioenergy,* 30**,** 973-982.

OTSUKA, N. 2002. Effects of fuel impurities on the fireside corrosion of boiler tubes in advanced power generating systems—a thermodynamic calculation of deposit chemistry. *Corrosion Science,* 44**,** 265-283.

PANG, C. H., HEWAKANDAMBY, B., WU, T. & LESTER, E. 2013. An automated ash fusion test for characterisation of the behaviour of ashes from biomass and coal at elevated temperatures. *Fuel,* 103**,** 454-466.

PANSU, M. & GAUTHEYROU, J. 2007. *Handbook of Soil Analysis: Mineralogical, Organic and Inorganic Methods*, Springer London, Limited.

PARIKH, J., CHANNIWALA, S. A. & GHOSAL, G. K. 2005. A correlation for calculating HHV from proximate analysis of solid fuels. *Fuel,* 84**,** 487-494.

PETTERSSON, R., FLYG, J. & VIKLUND, P. 2009. HIGH TEMPERATURE CORROSION UNDER SIMULATED BIOMASS DEPOSIT CONDITIONS. *CORROSION 2009.* Atlanta, GA: NACE International.

PIRES, J. C. M., MARTINS, F. G., ALVIM-FERRAZ, M. C. M. & SIMÕES, M. 2011. Recent developments on carbon capture and storage: An overview. *Chemical Engineering Research and Design,* 89**,** 1446-1460.

POHJANNE, P., YLI-OLLI, S., AUERKARI, P., TUURNA, S., JAUHIAINEN, P., TURUNEN, E., VARIS, T., RUUSUVUORI, K. & MAKIPAA, M. Year. Fireside corrosion of superheater materials in oxyfuel combustion. *In:* Corrosion 2010, March 14, 2010 - March 18, 2010, 2010 San Antonio, TX, United states. National Assoc. of Corrosion Engineers International.

PRONOBIS, M. 2005. Evaluation of the influence of biomass co-combustion on boiler furnace slagging by means of fusibility correlations. *Biomass and Bioenergy,* 28**,** 375-383.

QIU, J. R., LI, F., ZHENG, Y., ZHENG, C. G. & ZHOU, H. C. 1999. The influences of mineral behaviour on blended coal ash fusion characteristics. *Fuel,* 78**,** 963-969.

RAPP, R. & ZHANG, Y.-S. 1994. Hot corrosion of materials: Fundamental studies. *JOM,* 46**,** 47-55.

REID, W. T. 1971. *External Corrosion and deposits: boilers and gas turbines,* New York, American Elsevier Company.

REIDL, R., DAHL, J., OBERNBERGER, I. & NARODOSLAWSKY, M. 1999. Corrosion in fire tube boilers of biomass combustion plants. *Proceedings of the China International Corrosion Control Conference.* Beijing.

REVIE, R. W. 2011. *Uhlig's Corrosion Handbook*, Wiley.

REVIE, R. W. & UHLIG, H. H. 2008. *Corrosion and Corrosion Control*, John Wiley and Sons.

ROBERGE, P. R. 2000. *Handbook of Corrosion Engineering*, McGraw-Hill.

ROBERT, J. 1989. Chemkin-II: A Fortran chemical kinetics package for the analysis of gas-phase chemical kinetics. *Sandia National Laboratories Report***,** SAND89-8009B.

SAMI, M., ANNAMALAI, K. & WOOLDRIDGE, M. 2001. Co-firing of coal and biomass fuel blends. *Progress in Energy and Combustion Science,* 27**,** 171-214.

SAMUELSSON, R., NILSSON, C. & BURVALL, J. 2006. Sampling and GC-MS as a method for analysis of volatile organic compounds (VOC) emitted during oven drying of biomass materials. *Biomass and Bioenergy,* 30**,** 923-928.

SAVOLAINEN, K. 2003. Co-firing of biomass in coal-fired utility boilers. *Applied Energy,* 74**,** 369-381.

SCHEFFKNECHT, G., AL-MAKHADMEH, L., SCHNELL, U. & MAIER, J. 2011. Oxy-fuel coal combustion—A review of the current state-of-the-art. *International Journal of Greenhouse Gas Control,* 5, Supplement 1**,** S16-S35.

SEGGIANI, M. 1999. Empirical correlations of the ash fusion temperatures and temperature of critical viscosity for coal and biomass ashes. *Fuel,* 78**,** 1121-1125.

SHAFIEE, S. & TOPAL, E. 2009. When will fossil fuel reserves be diminished? *Energy Policy,* 37**,** 181-189.

SHARMA, C. P. 2005. *Engineering materials Properties and Applications of Metals and Alloys*

Prentice-Hall.

SHIM, H.-S., VALENTINE, J. R., DAVIS, K., SEO, S.-I. & KIM, T.-H. 2008. Development of fireside waterwall corrosion correlations using pilot-scale test furnace. *Fuel,* 87**,** 3353-3361.

SHREIR, L. L. (ed.) 1976. *Corrosion Metal/Environment Reactions*: Newnes-Butterworths.

SKRIFVARS, B.-J., BACKMAN, R. & HUPA, M. 1996. 96/05936 Ash chemistry and sintering. *Fuel and Energy Abstracts,* 37**,** 422.

SKRIFVARS, B. J., BACKMAN, R., HUPA, M., SALMENOJA, K. & VAKKILAINEN, E. 2008. Corrosion of superheater steel materials under alkali salt deposits Part 1: The effect of salt deposit composition and temperature. *Corrosion Science,* 50**,** 1274-1282.

SPLIETHOFF, H. & HEIN, K. R. G. 1998. Effect of co-combustion of biomass on emissions in pulverized fuel furnaces. *Fuel Processing Technology,* 54**,** 189-205.

SRIVASTAVA, S. C., GODIWALLA, K. M. & BANERJEE, M. K. 1997. Fuel ash corrosion of boiler and superheater tubes. *Journal of Materials Science,* 32**,** 835-849.

STAM, A. F., LIVINGSTON, W. R., CREMERS, M. F. & BREM, G. 2009. Review of Models and Tools for Slagging and Fouling prediction for biomass co-combustion. Netherland: KEMA.

STANGER, R. & WALL, T. 2011. Sulphur impacts during pulverised coal combustion in oxy-fuel technology for carbon capture and storage. *Progress in Energy and Combustion Science,* 37**,** 69-88.

STEIN-BRZOZOWSKA, G., MAIER, J. & SCHEFFKNECHT, G. 2011. Impact of the oxy-fuel combustion on the corrosion behavior of advanced austenitic superheater materials. *Energy Procedia,* 4**,** 2035-2042.

SYED, A. U., SIMMS, N. J. & OAKEY, J. E. 2012. Fireside corrosion of superheaters: Effects of air and oxy-firing of coal and biomass. *Fuel,* 101**,** 62-73.

THY, P., LESHER, C. E. & JENKINS, B. M. 2000. Experimental determination of high-temperature elemental losses from biomass slag. *Fuel,* 79**,** 693-700.

TILLMAN, D. A., DUONG, D. & MILLER, B. 2009. Chlorine in Solid Fuels Fired in Pulverized Fuel Boilers - Sources, Forms, Reactions, and Consequences: a Literature Review. *Energy & Fuels,* 23**,** 3379-3391.

TOFTEGAARD, M. B., BRIX, J., JENSEN, P. A., GLARBORG, P. & JENSEN, A. D. 2010. Oxy-fuel combustion of solid fuels. *Progress in Energy and Combustion Science,* 36**,** 581-625.

TOMECZEK, J. & WACŁAWIAK, K. 2009. Two-dimensional modelling of deposits formation on platen superheaters in pulverized coal boilers. *Fuel,* 88**,** 1466-1471.

UN. 1998. *Kyoto Protocol to the United Nations Framework Convention On Climate Change* [Online]. United Nations. Available: http://unfccc.int/kyoto_protocol/items/2830.php [Accessed].

UUSITALO, M. A., VUORISTO, P. M. J. & MÄNTYLÄ, T. A. 2002. High temperature corrosion of coatings and boiler steels in reducing chlorine-containing atmosphere. *Surface and Coatings Technology,* 161**,** 275-285.

UUSITALO, M. A., VUORISTO, P. M. J. & MÄNTYLÄ, T. A. 2003. High temperature corrosion of coatings and boiler steels in oxidizing chlorine-containing atmosphere. *Materials Science and Engineering A,* 346**,** 168-177.

VALENTE, T. 2001. Fireside corrosion of superheater materials in chlorine containing flue gas. *Journal of Materials Engineering and Performance,* 10**,** 608-613.

VAN DYK, J. C., MELZER, S. & SOBIECKI, A. 2006. Mineral matter transformation during Sasol-Lurgi fixed bed dry bottom gasification – utilization of HT-XRD and FactSage modelling. *Minerals Engineering,* 19**,** 1126-1135.

VASSILEV, S. V., BAXTER, D., ANDERSEN, L. K. & VASSILEVA, C. G. 2010. An overview of the chemical composition of biomass. *Fuel,* 89**,** 913-933.

VASSILEV, S. V., BAXTER, D. & VASSILEVA, C. G. 2014. An overview of the behaviour of biomass during combustion: Part II. Ash fusion and ash formation mechanisms of biomass types. *Fuel,* 117, Part A**,** 152-183.

WALL, T., LIU, Y., SPERO, C., ELLIOTT, L., KHARE, S., RATHNAM, R., ZEENATHAL, F., MOGHTADERI, B., BUHRE, B., SHENG, C., GUPTA, R., YAMADA, T., MAKINO, K. & YU, J. 2009. An overview on

oxyfuel coal combustion—State of the art research and technology development. *Chemical Engineering Research and Design,* 87**,** 1003-1016.

WALL, T. F., CREELMAN, R. A., GUPTA, R. P., GUPTA, S. K., COIN, C. & LOWE, A. 1998. Coal ash fusion temperatures—New characterization techniques, and implications for slagging and fouling. *Progress in Energy and Combustion Science,* 24**,** 345-353.

WALL, T. F., LOWE, A., WIBBERLEY, L. J. & MCC. STEWART, I. 1979. Mineral matter in coal and the thermal performance of large boilers. *Progress in Energy and Combustion Science,* 5**,** 1-29.

WERTHER, J., SAENGER, M., HARTGE, E. U., OGADA, T. & SIAGI, Z. 2000. Combustion of agricultural residues. *Progress in Energy and Combustion Science,* 26**,** 1-27.

YIN, J. & WU, Z. 2009. Corrosion Behavior of TP316L of Superheater in Biomass Boiler with Simulated Atmosphere and Deposit. *Chinese Journal of Chemical Engineering,* 17**,** 849-853.

YOUNG, D. J. 2008. *High Temperature Oxidation and Corrosion of Metals*, Elsevier.

YU, L. Y., WANG, L. W. & LI, P. S. 2014. Study on prediction models of biomass ash softening temperature based on ash composition. *Journal of the Energy Institute*.

ZEP 2010. CO2 Capture and Storage (CCS). 2010 ed.: ZEP.

ZHANG, J., ZHAO, Y., WEI, C., YAO, B. & ZHENG, C. 2010. Mineralogy and microstructure of ash deposits from the Zhuzhou coal-fired power plant in China. *International Journal of Coal Geology,* 81**,** 309-319.

ZHANG, Q., LIU, H., QIAN, Y., XU, M., LI, W. & XU, J. 2013. The influence of phosphorus on ash fusion temperature of sludge and coal. *Fuel Processing Technology,* 110**,** 218-226.

ZHAO, Y., ZHANG, Y., BAO, S., CHEN, T. & HAN, J. 2013. Calculation of mineral phase and liquid phase formation temperature during roasting of vanadium-bearing stone coal using FactSage software. *International Journal of Mineral Processing,* 124**,** 150-153.

Appendices

Appendix I

Simplified scheme for the computations using Senkin.

```
                          ┌─────────────┐
                          │   Chem.inp  │
                          └─────────────┘
                                 │
                                 ▼
                    ┌──────────────────────────┐
                    │   Chemkin Interpreter    │
                    │       (chem.exe)         │
                    └──────────────────────────┘
                       │            │           │
                       ▼            ▼           ▼
              ┌──────────┐  ┌──────────┐  ┌──────────┐
              │ Chem.out │  │ Chem.bin │  │ Chem.out │
              └──────────┘  └──────────┘  └──────────┘
                   │              │
                   ▼              ▼
              ┌──────────────────────────────┐
              │     Senkin Interpreter       │
              │        (senk.exe)            │
              └──────────────────────────────┘
                  │          │            │
                  ▼          ▼            ▼
            ┌──────────┐ ┌──────────┐ ┌──────────┐
            │ senk.out │ │ save.bin │ │ tign.out │
            └──────────┘ └──────────┘ └──────────┘
```
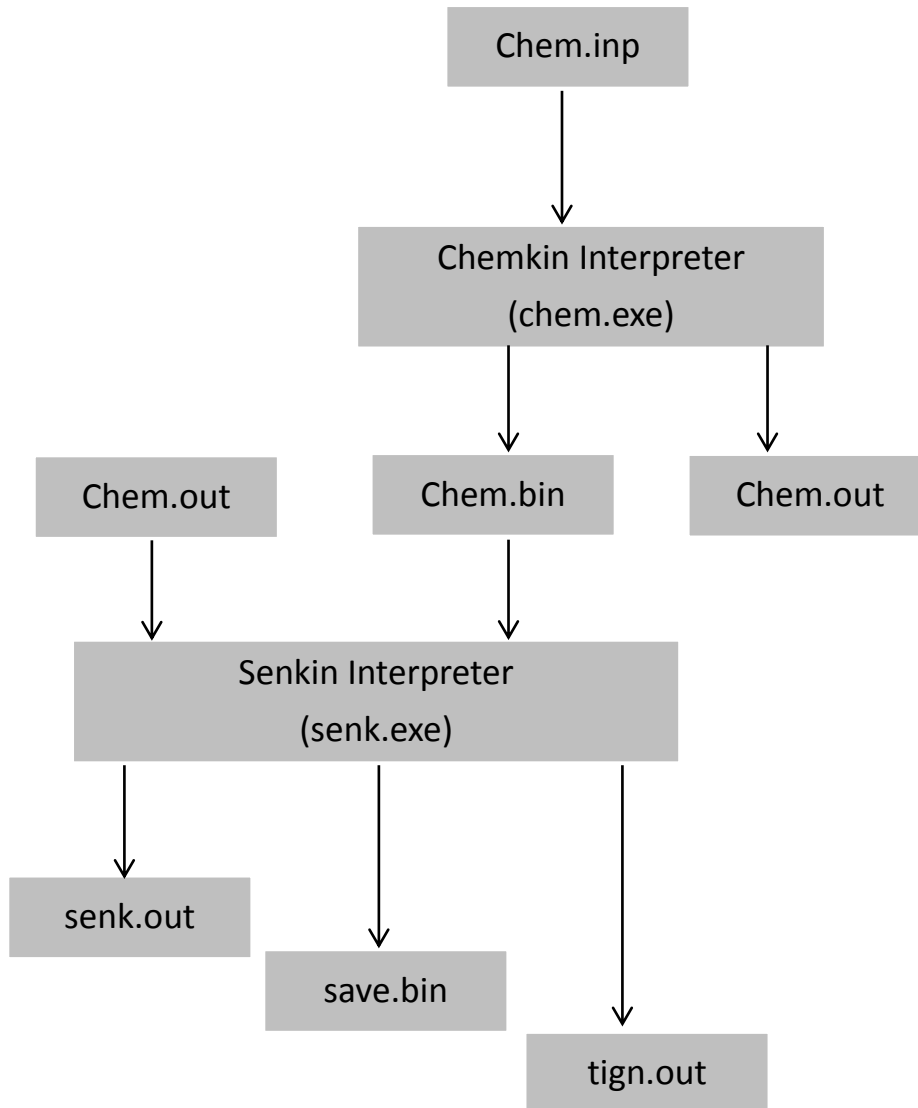
Appendix II.

Modified Leeds SOx mechanism used in gas phase modelling work.

```
ELEMENTS  H   O   C   N   S   CL   AR   END
SPECIES
H2        CH4       C2H2      C2H4      C2H6      C3H4      C3H6      C4H2
O2        H2O
H2O2      CO        CO2       CH2O      CH2CO     C         H         CH
CH2       CH2(S)
CH3       C2H       C2H3      C2H5      C3H2      H2CCCH    H2CCCCH O
OH        HO2
HCO       CH3O      CH2OH     HCCO      CH2HCO    N2        AR        CN
HCN       N
NH        NO        HNO       NH2       H2NO      NCO       N2O       NO2
N2H2      HOCN
H2CN      NNH       NH3       N2H3      C2N2      HNCO      S         SH
H2S       SO
SO2       SO3       HSO2      HOSO      HOSO2     SN        S2        CS
COS       HSNO
HSO       HOS       HSOH      H2SO      HOSHO     HS2       H2S2
H2SO4     CL        HCL
END
THERMO ALL
   300.000   1000.000   5000.000
H2                       H   2    0    0    0G     200.00
6000.00 1000.00    0 1
 2.93283050E+00 8.26598020E-04-1.46400570E-07 1.54098510E-
11-6.88796150E-16    2
-8.13055820E+02-1.02431640E+00 2.34430290E+00 7.98042480E-
03-1.94779170E-05    3
 2.01569670E-08-7.37602890E-12-9.17924130E+02 6.83002180E-01
4
CH4                      H   4C   1    0    0G     200.00
6000.00 1000.00    0 1
 1.63542560E+00 1.00844310E-02-3.36923690E-06 5.34972800E-
10-3.15528170E-14    2
-1.00056030E+04 9.99369530E+00 5.14987920E+00-1.36710080E-02
4.91801300E-05    3
-4.84744030E-08 1.66694410E-11-1.02466480E+04-4.64132440E+00
4
C2H2                     H   2C   2    0    0G     200.00
6000.00 1000.00    0 1
 4.65870470E+00 4.88409490E-03-1.60835630E-06 2.46987870E-
10-1.38615050E-14    2
 2.56632180E+04-3.99790740E+00 8.08691080E-01 2.33613950E-
02-3.55166360E-05    3
 2.80145660E-08-8.50044590E-12 2.63327640E+04 1.39396710E+01
4
C2H4                     H   4C   2    0    0G     300.00
5000.00 1000.00    0 1
 4.39854530E+00 9.62286070E-03-3.16637760E-06 4.57476280E-
10-2.36594060E-14    2
```

```
  4.11532030E+03-2.46274380E+00 1.21766000E+00 1.30026750E-02
3.50374470E-06    3
-1.11555140E-08 4.72032220E-12 5.33738280E+03 1.54801690E+01
4
C2H6              H   6C   2   0    0G   300.00
5000.00 1000.00    0 1
  4.70288470E+00 1.40426350E-02-4.64693770E-06 6.74737380E-
10-3.50893120E-14    2
-1.26719880E+04-4.54339500E+00 1.53952600E+00 1.50408410E-02
6.68471150E-06    3
-1.33829480E-08 4.85613980E-12-1.12487660E+04 1.41073750E+01
4
C3H4              H   4C   3   0    0G   200.00
6000.00 1000.00    0 1
  6.31687220E+00 1.11337280E-02-3.96293780E-06 6.35642380E-
10-3.78755400E-14    2
  2.01174950E+04-1.09957660E+01 2.61304450E+00 1.21225750E-02
1.85398800E-05    3
-3.45251490E-08 1.53350790E-11 2.15415670E+04 1.02261390E+01
4
C3H6              H   6C   3   0    0G   300.00
5000.00 1000.00    0 1
  6.72139740E+00 1.49317570E-02-4.96523530E-06 7.25107530E-
10-3.80014760E-14    2
-9.24531490E+02-1.21556170E+01 1.45751570E+00 2.11422630E-02
4.04680120E-06    3
-1.63190030E-08 7.04751530E-12 1.07402080E+03 1.73994600E+01
4
C4H2              H   2C   4   0    0G   200.00
6000.00 1000.00    0 1
  8.66700350E+00 6.71663710E-03-2.35449950E-06 3.73830790E-
10-2.21189140E-14    2
  4.98569330E+04-2.11142050E+01-3.95185080E-01 5.19558130E-
02-9.17866160E-05    3
  8.05239290E-08-2.69170880E-11 5.14517090E+04 2.09691010E+01
4
O2                O   2   0   0    0G   200.00
6000.00 1000.00    0 1
  3.66096083E+00 6.56365523E-04-1.41149485E-07 2.05797658E-
11-1.29913248E-15    2
-1.21597725E+03 3.41536184E+00 3.78245636E+00-2.99673415E-03
9.84730200E-06    3
-9.68129508E-09 3.24372836E-12-1.06394356E+03 3.65767573E+00
4
H2O               H   2O   1   0    0G   200.00
6000.00 1000.00    0 1
  2.67703890E+00 2.97318160E-03-7.73768890E-07 9.44335140E-
11-4.26899910E-15    2
-2.98858940E+04 6.88255000E+00 4.19863520E+00-2.03640170E-03
6.52034160E-06    3
-5.48792690E-09 1.77196800E-12-3.02937260E+04-8.49009010E-01
4
H2O2              H   2O   2   0    0G   200.00
6000.00 1000.00    0 1
  4.57333537E+00 4.04984070E-03-1.29479479E-06 1.97281710E-
10-1.13402846E-14    2
```

```
-1.80040975E+04 7.04278488E-01 4.27611269E+00-5.42822417E-04
1.67335701E-05    3
-2.15770813E-08 8.62454363E-12-1.77035843E+04 3.43505074E+00
4
CO                      O   1C   1    0    0G    200.00
6000.00 1000.00    0 1
 3.04848590E+00 1.35172810E-03-4.85794050E-07 7.88536440E-
11-4.69807460E-15    2
-1.42661170E+04 6.01709770E+00 3.57953350E+00-6.10353690E-04
1.01681430E-06    3
 9.07005860E-10-9.04424490E-13-1.43440860E+04 3.50840930E+00
4
CO2                     O   2C   1    0    0G    200.00
6000.00 1000.00    0 1
 4.63651110E+00 2.74145690E-03-9.95897590E-07 1.60386660E-
10-9.16198570E-15    2
-4.90249040E+04-1.93489550E+00 2.35681300E+00 8.98412990E-
03-7.12206320E-06    3
 2.45730080E-09-1.42885480E-13-4.83719710E+04 9.90090350E+00
4
CH2O                    H   2O   1C   1    0G    200.00
6000.00 1000.00    0 1
 3.16948070E+00 6.19327420E-03-2.25059810E-06 3.65982450E-
10-2.20154100E-14    2
-1.44784250E+04 6.04235330E+00 4.79370360E+00-9.90815180E-03
3.73214590E-05    3
-3.79279020E-08 1.31770150E-11-1.43089550E+04 6.02887020E-01
4
CH2CO                   H   2O   1C   2    0G    200.00
6000.00 1000.00    0 1
 5.75779010E+00 6.34965070E-03-2.25844070E-06 3.62084620E-
10-2.15690300E-14    2
-8.20537635E+03-6.10640370E+00 2.14011650E+00 1.80883680E-
02-1.73242160E-05    3
 9.27674770E-09-1.99150110E-12-7.26981595E+03 1.21986990E+01
4
C                       C   1    0    0    0G    200.00
6000.00 1000.00    0 1
 2.60558300E+00-1.95934340E-04 1.06737220E-07-1.64239400E-11
8.18705800E-16    2
 8.54117420E+04 4.19238680E+00 2.55423950E+00-3.21537720E-04
7.33792230E-07    3
-7.32234870E-10 2.66521440E-13 8.54426810E+04 4.53130850E+00
4
H                       H   1    0    0    0G    200.00
6000.00 1000.00    0 1
 2.50000000E+00 0.00000000E+00 0.00000000E+00 0.00000000E+00
0.00000000E+00    2
 2.54736600E+04-4.46682850E-01 2.50000000E+00 0.00000000E+00
0.00000000E+00    3
 0.00000000E+00 0.00000000E+00 2.54736600E+04-4.46682850E-01
4
CH                      H   1C   1    0    0G    200.00
6000.00 1000.00    0 1
 2.52090620E+00 1.76537260E-03-4.61475810E-07 5.92885670E-
11-3.34732090E-15    2
```

```
  7.10230206E+04 7.40532230E+00 3.48981660E+00 3.23835540E-
04-1.68899060E-06    3
  3.16217330E-09-1.40609070E-12 7.06888776E+04 2.08401110E+00
4
CH2                     H   2C   1    0    0G    200.00
6000.00 1000.00    0 1
  2.53871220E+00 3.82254910E-03-1.28613040E-06 1.98003080E-
10-1.14657430E-14    2
  4.61292530E+04 8.10546480E+00 4.17936550E+00-2.21785530E-03
7.96536020E-06    3
 -6.91273390E-09 2.24753180E-12 4.57508570E+04-7.61137030E-03
4
CH2(S)                  H   2C   1    0    0G    300.00
4000.00 1000.00    0 1
  3.55288800E+00 2.06678800E-03-1.91411600E-07-1.10467330E-10
2.02134900E-14    2
  5.02544011E+04 1.68657000E+00 3.97126500E+00-1.69908800E-04
1.02536890E-06    3
  2.49255000E-09-1.98126600E-12 5.02983211E+04 5.75320700E-02
4
CH3                     H   3C   1    0    0G    200.00
6000.00 1000.00    0 1
  2.96697350E+00 5.79366720E-03-1.96948090E-06 3.05569360E-
10-1.77678430E-14    2
  1.65131329E+04 4.79188030E+00 3.67333750E+00 2.00205590E-03
5.78531350E-06    3
 -6.98730540E-09 2.60555990E-12 1.64161969E+04 1.60183150E+00
4
C2H                     H   1C   2    0    0G    200.00
6000.00 1000.00    0 1
  3.66459586E+00 3.82189487E-03-1.36509398E-06 2.13253692E-
10-1.23098939E-14    2
  6.69367375E+04 3.91355399E+00 2.90180321E+00 1.32859725E-
02-2.80508233E-05    3
  2.89300812E-08-1.07446930E-11 6.68300042E+04 6.17234595E+00
4
C2H3                    H   3C   2    0    0G    200.00
6000.00 1000.00    0 1
  4.70253100E+00 7.26422830E-03-2.58019920E-06 4.13199440E-
10-2.45914920E-14    2
  3.40296750E+04-1.42937140E+00 3.00196020E+00 3.03043540E-03
2.44443150E-05    3
 -3.58102420E-08 1.51087000E-11 3.48681730E+04 9.33044950E+00
4
C2H5                    H   5C   2    0    0G    200.00
6000.00 1000.00    0 1
  4.28788140E+00 1.24338930E-02-4.41391190E-06 7.06541020E-
10-4.20351360E-14    2
  1.23269670E+04 8.46025830E-01 4.30585800E+00-4.18336380E-03
4.97072700E-05    3
 -5.99058740E-08 2.30484780E-11 1.31122260E+04 4.71002360E+00
4
C3H2                    H   2C   3    0    0G    200.00
6000.00 1000.00    0 1
  5.69445684E+00 6.53821901E-03-2.35907266E-06 3.82037384E-
10-2.29227460E-14    2
```

```
 5.49264274E+04-6.96163733E+00 3.18167129E+00-3.37611741E-04
3.95343765E-05    3
-5.49792422E-08 2.28335240E-11 5.61816758E+04 9.06482468E+00
4
H2CCCH                  H   3C   3    0    0G     200.00
6000.00 1000.00    0 1
 7.14221880E+00 7.61902005E-03-2.67459950E-06 4.24914801E-
10-2.51475415E-14    2
 3.80693414E+04-1.25848435E+01 1.35110927E+00 3.27411223E-
02-4.73827135E-05    3
 3.76309808E-08-1.18540923E-11 3.92663770E+04 1.52058924E+01
4
H2CCCCH                 H   3C   4    0    0G     298.15
6000.00 1000.00    0 1
 8.47620790E+00 8.87823270E-03-3.03284120E-06 4.73583020E-
10-2.77166270E-14    2
 5.47565400E+04-1.71705510E+01 2.41732470E+00 2.41047820E-
02-1.28134700E-05    3
-2.86062370E-09 3.91945270E-12 5.65064760E+04 1.44711070E+01
4
O                       O   1    0    0    0G     200.00
6000.00 1000.00    0 1
 2.54363697E+00-2.73162486E-05-4.19029520E-09 4.95481845E-
12-4.79553694E-16    2
 2.92260120E+04 4.92229457E+00 3.16826710E+00-3.27931884E-03
6.64306396E-06    3
-6.12806624E-09 2.11265971E-12 2.91222592E+04 2.05193346E+00
4
OH                      H   1O   1    0    0G     200.00
6000.00 1000.00    0 1
 2.83864607E+00 1.10725586E-03-2.93914978E-07 4.20524247E-
11-2.42169092E-15    2
 3.68599690E+03 5.84452662E+00 3.99201543E+00-2.40131752E-03
4.61793841E-06    3
-3.88113333E-09 1.36411470E-12 3.35711894E+03-1.03925458E-01
4
HO2                     H   1O   2    0    0G     200.00
6000.00 1000.00    0 1
 4.17226590E+00 1.88120980E-03-3.46292970E-07 1.94685160E-11
1.76091530E-16    2
 2.13222508E+02 2.95779740E+00 4.30178800E+00-4.74902010E-03
2.11579530E-05    3
-2.42759610E-08 9.29206700E-12 4.46212417E+02 3.71670100E+00
4
HCO                     H   1O   1C   1    0G     200.00
6000.00 1000.00    0 1
 3.64896209E+00 3.08090819E-03-1.12429876E-06 1.86308085E-
10-1.13951828E-14    2
 3.71209048E+03 5.06147406E+00 4.22118584E+00-3.24392532E-03
1.37799446E-05    3
-1.33144093E-08 4.33768865E-12 3.83956496E+03 3.39437243E+00
4
CH3O                    H   3O   1C   1    0G     200.00
6000.00 1000.00    0 1
 4.26533080E+00 7.85764060E-03-2.84104380E-06 4.60451900E-
10-2.76319060E-14    2
```

```
      1.65605687E+02 3.93099470E-01 3.26523370E+00 3.30316650E-03
1.70488010E-05    3
-2.27096300E-08 8.80717680E-12 8.38550421E+02 7.42573570E+00
4
CH2OH             H   3O  1C   1    0G   200.00
6000.00 1000.00     0 1
 4.72398695E+00 6.50832540E-03-2.24240605E-06 3.51742805E-
10-2.06424726E-14    2
-3.81156740E+03 1.47350104E+00 4.73864580E+00 1.27132491E-03
1.46005656E-05    3
-1.83666166E-08 7.07708694E-12-3.56200591E+03 2.65277676E+00
4
HCCO              H   1O  1C   2    0G   200.00
6000.00 1000.00     0 1
 5.84690060E+00 3.64059600E-03-1.29590070E-06 2.07969190E-
10-1.24000220E-14    2
 1.92484960E+04-5.29165330E+00 2.33501180E+00 1.70100830E-
02-2.20188670E-05    3
 1.54064470E-08-4.34550970E-12 2.00502990E+04 1.19767290E+01
4
CH2HCO            H   3O  1C   2    0G   300.00
5000.00 1000.00     0 1
 5.97566990E+00 8.13059140E-03-2.74362450E-06 4.07030410E-
10-2.17601710E-14    2
-1.26585075E+03-5.03208790E+00 3.40906240E+00 1.07385740E-02
1.89149250E-06    3
-7.15858310E-09 2.86738510E-12-2.34695926E+02 9.57145350E+00
4
N2                N   2   0   0    0G   200.00
6000.00 1000.00     0 1
 2.95254070E+00 1.39688380E-03-4.92625770E-07 7.86000910E-
11-4.60749780E-15    2
-9.23937530E+02 5.87182210E+00 3.53096280E+00-1.23659500E-
04-5.02993390E-07    3
 2.43527680E-09-1.40879540E-12-1.04696370E+03 2.96743910E+00
4
AR                AR  1   0   0    0G   200.00
6000.00 1000.00     0 1
 2.50000000E+00 0.00000000E+00 0.00000000E+00 0.00000000E+00
0.00000000E+00    2
-7.45375000E+02 4.37967490E+00 2.50000000E+00 0.00000000E+00
0.00000000E+00    3
 0.00000000E+00 0.00000000E+00-7.45375000E+02 4.37967490E+00
4
CN                C   1N   1   0    0G   300.00
5000.00 1000.00     0 1
 3.72012000E+00 1.51835100E-04 1.98738100E-07-3.79837100E-11
1.32823000E-15    2
 5.11162600E+04 2.88859700E+00 3.66320400E+00-1.15652900E-03
2.16340900E-06    3
 1.85420800E-10-8.21469500E-13 5.12811800E+04 3.73901600E+00
4
HCN               H   1C   1N   1    0G   300.00
4000.00 1000.00     0 1
 3.42645700E+00 3.92419000E-03-1.60113800E-06 3.16196600E-
10-2.43285000E-14    2
```

```
 1.48555200E+04 3.60779500E+00 2.41778700E+00 9.03185600E-
03-1.10772700E-05    3
 7.98014100E-09-2.31114100E-12 1.50104400E+04 8.22289100E+00
4
N                 N   1    0    0    0G    300.00
5000.00 1000.00    0 1
 2.45026800E+00 1.06614600E-04-7.46533700E-08 1.87965200E-
11-1.02598400E-15    2
 5.61160400E+04 4.44875800E+00 2.50307100E+00-2.18001800E-05
5.42052900E-08    3
-5.64756000E-11 2.09990400E-14 5.60989000E+04 4.16756600E+00
4
NH                H   1N   1    0    0G    300.00
5000.00 1000.00    0 1
 2.76024900E+00 1.37534600E-03-4.45191400E-07 7.69279200E-
11-5.01759200E-15    2
 4.20782800E+04 5.85719900E+00 3.33975800E+00 1.25300900E-
03-3.49164600E-06    3
 4.21881200E-09-1.55761800E-12 4.18504700E+04 2.50718100E+00
4
NO                O   1N   1    0    0G    300.00
5000.00 1000.00    0 1
 3.24543500E+00 1.26913800E-03-5.01589000E-07 9.16928300E-
11-6.27541900E-15    2
 9.80084000E+03 6.41729400E+00 3.37654200E+00 1.25306300E-
03-3.30275100E-06    3
 5.21781000E-09-2.44626300E-12 9.81796100E+03 5.82959000E+00
4
HNO               H   1O   1N   1    0G    300.00
5000.00 1000.00    0 1
 3.61514400E+00 3.21248600E-03-1.26033700E-06 2.26729800E-
10-1.53623600E-14    2
 1.06619100E+04 4.81026400E+00 2.78440300E+00 6.60964600E-
03-9.30022300E-06    3
 9.43798000E-09-3.75314600E-12 1.09187800E+04 9.03562900E+00
4
NH2               H   2N   1    0    0G    300.00
5000.00 1000.00    0 1
 2.96131100E+00 2.93269900E-03-9.06360000E-07 1.61725700E-
10-1.20420000E-14    2
 2.19197700E+04 5.77787800E+00 3.43249300E+00 3.29954000E-
03-6.61360000E-06    3
 8.59094700E-09-3.57204700E-12 2.17722800E+04 3.09011100E+00
4
H2NO              H   2O   1N   1    0G    300.00
4000.00 1500.00    0 1
 5.67334600E+00 2.29883700E-03-1.77444600E-07-1.10348200E-10
1.85976200E-14    2
 5.56932500E+03-6.15354000E+00 2.53059000E+00 8.59603500E-
03-5.47103000E-06    3
 2.27624900E-09-4.64807300E-13 6.86803000E+03 1.12665100E+01
4
NCO               O   1C   1N   1    0G    300.00
4000.00 1400.00    0 1
 6.07234600E+00 9.22782900E-04-9.84557400E-08-4.76412300E-11
9.09044500E-15    2
```

1.35982000E+04-8.50729300E+00 3.35959300E+00 5.39323900E-
03-8.14458500E-07   3
-1.91286800E-09 7.83679400E-13 1.46280900E+04 6.54969400E+00
4
N2O   O 1N 2 0   0G   300.00
5000.00 1000.00   0 1
 4.71897700E+00 2.87371400E-03-1.19749600E-06 2.25055200E-
10-1.57533700E-14   2
 8.16581100E+03-1.65725000E+00 2.54305800E+00 9.49219300E-
03-9.79277500E-06   3
 6.26384500E-09-1.90182600E-12 8.76510000E+03 9.51122200E+00
4
NO2   O 2N 1 0   0G   300.00
5000.00 1000.00   0 1
 4.68285900E+00 2.46242900E-03-1.04225900E-06 1.97690200E-
10-1.39171700E-14   2
 2.26129200E+03 9.88598500E-01 2.67060000E+00 7.83850100E-
03-8.06386500E-06   3
 6.16171500E-09-2.32015000E-12 2.89629100E+03 1.16120700E+01
4
N2H2   H 2N 2 0   0G   300.00
5000.00 1000.00   0 1
 3.37118500E+00 6.03996800E-03-2.30385400E-06 4.06278900E-
10-2.71314400E-14   2
 2.41817200E+04 4.98058500E+00 1.61799900E+00 1.30631200E-
02-1.71571200E-05   3
 1.60560800E-08-6.09363900E-12 2.46752600E+04 1.37946700E+01
4
HOCN   H 1O 1C 1N 1G   300.00
4000.00 1400.00   0 1
 6.02211200E+00 1.92953000E-03-1.45502900E-07-1.04581100E-10
1.79481400E-14   2
-4.04032100E+03-5.86643300E+00 3.78942400E+00 5.38798100E-
03-6.51827000E-07   3
-1.42016400E-09 5.36796900E-13-3.13533500E+03 6.66705200E+00
4
H2CN   H 2C 1N 1 0G   300.00
4000.00 1000.00   0 1
 5.20970300E+00 2.96929100E-03-2.85558900E-07-1.63555000E-10
3.04325900E-14   2
 2.76771100E+04-4.44447800E+00 2.85166100E+00 5.69523300E-03
1.07114000E-06   3
-1.62261200E-09-2.35110800E-13 2.86378200E+04 8.99275100E+00
4
NNH   H 1N 2 0   0G   250.00
4000.00 1000.00   0 1
 4.41534200E+00 1.61438800E-03-1.63289400E-07-8.55984600E-11
1.61479100E-14   2
 2.78802900E+04 9.04288800E-01 3.50134400E+00 2.05358700E-03
7.17041000E-07   3
 4.92134800E-10-9.67117000E-13 2.83334700E+04 6.39183700E+00
4
NH3   H 3N 1 0   0G   300.00
5000.00 1000.00   0 1
 2.46190400E+00 6.05916600E-03-2.00497700E-06 3.13600300E-
10-1.93831700E-14   2

```
-6.49327000E+03 7.47209700E+00 2.20435200E+00 1.01147600E-
02-1.46526500E-05    3
 1.44723500E-08-5.32850900E-12-6.52548800E+03 8.12713800E+00
4
N2H3              H  3N  2  0   0G   300.00
5000.00 1000.00    0 1
 4.44184600E+00 7.21427100E-03-2.49568400E-06 3.92056500E-
10-2.29895000E-14    2
 1.66422100E+04-4.27520500E-01 3.17420400E+00 4.71590700E-03
1.33486700E-05    3
-1.91968500E-08 7.48756400E-12 1.72727000E+04 7.55722400E+00
4
C2N2              C  2N  2  0   0G   300.00
5000.00 1000.00    0 1
 6.54800300E+00 3.98470700E-03-1.63421600E-06 3.03859700E-
10-2.11106900E-14    2
 3.49071600E+04-9.73579000E+00 4.26545900E+00 1.19225700E-
02-1.34201400E-05    3
 9.19229700E-09-2.77894200E-12 3.54788800E+04 1.71321200E+00
4
HNCO              H  1O  1C  1N  1G   300.00
4000.00 1400.00    0 1
 6.54530700E+00 1.96576000E-03-1.56266400E-07-1.07431800E-10
1.87468000E-14    2
-1.66477300E+04-1.00388000E+01 3.85846700E+00 6.39034200E-
03-9.01662800E-07    3
-1.89822400E-09 7.65138000E-13-1.56234300E+04 4.88249300E+00
4
S                 S  1  0  0   0G   300.00
5000.00 1000.00    0 1
 2.90214800E+00-5.48454600E-04 2.76457600E-07-5.01711500E-11
3.15068500E-15    2
 3.24942300E+04 3.83847100E+00 3.18732900E+00-1.59577600E-03
2.00553100E-06    3
-1.50708100E-09 4.93128200E-13 3.24225900E+04 2.41444100E+00
4
SH                H  1S  1  0   0G   300.00
5000.00 1000.00    0 1
 3.05381000E+00 1.25888400E-03-4.24916900E-07 6.92959100E-
11-4.28169100E-15    2
 1.58822500E+04 5.97355100E+00 4.13332700E+00-3.78789300E-
04-2.77785400E-06    3
 5.37011200E-09-2.39400600E-12 1.55586200E+04 1.61153500E-01
4
H2S               H  2S  1  0   0G   300.00
5000.00 1000.00    0 1
 2.88314700E+00 3.82783500E-03-1.42339800E-06 2.49799900E-
10-1.66027300E-14    2
-3.48074300E+03 7.25816200E+00 3.07102900E+00 5.57826100E-
03-1.03096700E-05    3
 1.20195300E-08-4.83837000E-12-3.55982600E+03 5.93522600E+00
4
SO                O  1S  1  0   0G   300.00
5000.00 1000.00    0 1
 4.02107800E+00 2.58485600E-04 8.94814200E-08-3.58014500E-11
3.22843000E-15    2
```

-7.11962000E+02 3.45252300E+00 3.08040100E+00 1.80310600E-03
6.70502200E-07   3
-2.06900500E-09 8.51465700E-13-3.98616300E+02 8.58102800E+00
4
SO2   O 2S 1   0   0G   300.00
5000.00 1000.00   0 1
 5.25449800E+00 1.97854500E-03-8.20422600E-07 1.57638300E-
10-1.12045100E-14   2
-3.75688600E+04-1.14605600E+00 2.91143900E+00 8.10302200E-
03-6.90671000E-06   3
 3.32901600E-09-8.77712100E-13-3.68788200E+04 1.11174000E+01
4
SO3   O 3S 1   0   0G   300.00
5000.00 1000.00   0 1
 7.05066800E+00 3.24656000E-03-1.40889700E-06 2.72153500E-
10-1.94236500E-14   2
-5.02066800E+04-1.10644300E+01 2.57528300E+00 1.51509200E-
02-1.22987200E-05   3
 4.24025700E-09-5.26681200E-13-4.89441100E+04 1.21951200E+01
4
HSO2   H 1O 2S 1   0G   300.00
1500.00 1500.00   0 1
 1.56273740E+00 2.06913890E-02-2.31120730E-05 1.26702030E-
08-2.72741760E-12   2
-1.82148240E+04 1.75568200E+01 1.56273740E+00 2.06913890E-
02-2.31120730E-05   3
 1.26702030E-08-2.72741760E-12-1.82148240E+04 1.75568200E+01
4
HOSO   H 1O 2S 1   0G   300.00
2000.00 1000.00   0 1
 9.60146992E+00-2.53592657E-02 6.76829409E-05-6.34954136E-08
1.95893537E-11   2
-3.12540147E+04-1.56740934E+01 9.60146992E+00-2.53592657E-02
6.76829409E-05   3
-6.34954136E-08 1.95893537E-11-3.12540147E+04-1.56740934E+01
4
HOSO2   H 1O 3S 1   0G   300.00
2000.00 1000.00   0 1
 7.62277304E+00-4.19908990E-03 3.52054969E-05-4.12715317E-08
1.40006629E-11   2
-4.69478133E+04-7.80787503E+00 7.62277304E+00-4.19908990E-03
3.52054969E-05   3
-4.12715317E-08 1.40006629E-11-4.69478133E+04-7.80787503E+00
4
SN   N 1S 1   0   0G   300.00
5000.00 1000.00   0 1
 3.88828700E+00 6.77842700E-04-2.72530900E-07 5.13592700E-
11-3.59383600E-15   2
 3.04449600E+04 4.19429100E+00 3.40734600E+00 1.79788700E-
03-2.01897000E-06   3
 2.10785700E-09-9.52759200E-13 3.06237300E+04 6.82148100E+00
4
S2   S 2   0   0   0G   300.00
5000.00 1000.00   0 1
 3.90444300E+00 6.92573300E-04-1.23309700E-07 8.78380900E-13
1.37466200E-15   2

```
   1.42569300E+04 4.95683400E+00 3.15767300E+00 3.09948000E-
03-1.56074600E-06    3
-1.35789100E-09 1.13744400E-12 1.43918700E+04 8.59606200E+00
4
CS                   C  1S   1   0    0G     300.00
5000.00 1000.00    0 1
 3.73743100E+00 8.18045100E-04-3.17891800E-07 5.35680100E-
11-2.88619500E-15    2
 3.24772500E+04 3.57655700E+00 2.93862300E+00 2.72435200E-
03-2.39770700E-06    3
 1.68950100E-09-6.66505000E-13 3.27399200E+04 7.84872000E+00
4
COS                  O  1C   1S   1    0G     300.00
5000.00 1000.00    0 1
 5.19192500E+00 2.50612300E-03-1.02439600E-06 1.94391400E-
10-1.37080000E-14    2
-1.84621000E+04-2.82575500E+00 2.85853100E+00 9.51545800E-
03-8.88491500E-06    3
 4.22099400E-09-8.55734000E-13-1.78514500E+04 9.08198900E+00
4
HSNO                 H  1O   1N   1S   1G     300.00
5000.00 1000.00    0 1
 2.90214800E+00-5.48454600E-04 2.76457600E-07-5.01711400E-11
3.15068400E-15    2
 3.24942300E+04 3.83847100E+00 3.18732900E+00-1.59577630E-03
2.00553100E-06    3
-1.50708140E-09 4.93128200E-13 3.24225900E+04 2.41444100E+00
4
HSO                  H  1O   1S   1    0G     300.00
1500.00 1500.00    0 1
 2.58075930E+00 7.99109020E-03-5.15359720E-06 7.42028010E-10
2.44456910E-13    2
-3.79766780E+03 1.22267030E+01 2.58075930E+00 7.99109020E-
03-5.15359720E-06    3
 7.42028010E-10 2.44456910E-13-3.79766780E+03 1.22267030E+01
4
HOS                  H  1O   1S   1    0G     300.00
1500.00 1500.00    0 1
 2.63736730E+00 7.89119090E-03-8.11726030E-06 4.24833820E-
09-8.57901160E-13    2
-1.07268870E+03 1.17096820E+01 2.63736730E+00 7.89119090E-
03-8.11726030E-06    3
 4.24833820E-09-8.57901160E-13-1.07268870E+03 1.17096820E+01
4
HSOH                 H  2O   1S   1    0G     300.00
1500.00 1500.00    0 1
 2.56764410E+00 1.13805210E-02-5.86673240E-06-5.94700410E-10
8.74383290E-13    2
-1.55712560E+04 1.17663990E+01 2.56764410E+00 1.13805210E-
02-5.86673240E-06    3
-5.94700410E-10 8.74383290E-13-1.55712560E+04 1.17663990E+01
4
H2SO                 H  2O   1S   1    0G     300.00
1500.00 1500.00    0 1
 1.95805190E+00 9.72652010E-03 6.84131700E-07-6.23437200E-09
2.41665770E-12    2
```

```
-6.67708890E+03 1.47834510E+01 1.95805190E+00 9.72652010E-03
6.84131700E-07    3
-6.23437200E-09 2.41665770E-12-6.67708890E+03 1.47834510E+01
4
HOSHO             H   2O   2S   1    0G    300.00
1500.00 1500.00    0 1
 1.19038220E+00 2.56447350E-02-2.66228420E-05 1.34796650E-
08-2.64746290E-12    2
-3.37448860E+04 1.90954940E+01 1.19038220E+00 2.56447350E-
02-2.66228420E-05    3
 1.34796650E-08-2.64746290E-12-3.37448860E+04 1.90954940E+01
4
HS2               H   1S   2    0    0G    300.00
5000.00 1395.00    0 1
 5.10949802E+00 1.61440788E-03-5.59150857E-07 8.75419872E-
11-5.10877907E-15    2
 1.07861033E+04 4.66519398E-01 3.24915375E+00 6.72607196E-
03-6.12427074E-06    3
 2.88457020E-09-5.42122152E-13 1.13627566E+04 1.01981642E+01
4
H2S2              H   2S   2    0    0G    300.00
5000.00 1395.00    0 1
 6.23682403E+00 3.17137220E-03-1.08859887E-06 1.69375472E-
10-9.84045085E-15    2
-4.06812922E+02-6.92943476E+00 3.15971698E+00 1.19631659E-
02-1.11173543E-05    3
 5.43915901E-09-1.06004978E-12 5.26704992E+02 9.07002520E+00
4
H2SO4             H   2O   4S   1    0G    200.00
6000.00 1000.00    0 1
 1.14077640E+01 6.47450160E-03-2.26841850E-06 3.60607600E-
10-2.13733800E-14    2
-9.23511920E+04-3.21413070E+01 1.58786610E+00 4.08823660E-
02-4.88457630E-05    3
 2.90145030E-08-6.68589150E-12-9.00400150E+04 1.66877800E+01
4
CL                CL  1    0    0    0G    200.000
6000.000 1000.         1
 2.94658358E+00-3.85985408E-04 1.36139388E-07-2.17032923E-11
1.28751025E-15    2
 1.36970327E+04 3.11330136E+00 2.26062480E+00 1.54154399E-
03-6.80283622E-07    3
-1.59972975E-09 1.15416636E-12 1.38552986E+04 6.57020799E+00
1.45891941E+04    4
HCL               H   1CL  1    0    0G    200.000
6000.000 1000.         1
 0.27575767E+01 0.14538737E-02-0.47964697E-06 0.77790943E-
10-0.47957377E-14    2
-0.11913766E+05 0.65219722E+01 0.34637647E+01 0.47648423E-
03-0.20030122E-05    3
 0.33171437E-08-0.14495818E-11-0.12144352E+05
0.26642828E+01-0.11102278E+05    4
END
REACTIONS   MOLECULES  KELVINS
!
!    1
```

```
H2+CH2(S) =  CH3+H                  1.200E-10   0.0000        0.00
!
!      2
H2+O =  OH+H                        8.501E-20   2.6700     3159.73
!
!      3
H2O+H =  H2+O                       7.505E-16   1.6000     9271.11
!
!      4
CH4+O2 =                            6.591E-11   0.0000    28631.22
!
!      5
CH4+C =  CH+CH                      8.302E-11   0.0000    12085.64
!
!      6
CH4+H =  CH3+H2                     2.192E-20   3.0000     4044.98
!
!      7
CH4+CH =  C2H4                      4.998E-11   0.0000     -199.66
!
!      8
CH4+CH2 =  2CH3                     7.139E-12   0.0000     5051.72
!
!      9
CH4+CH2(S) =  2CH3                  1.162E-10   0.0000        0.00
!
!     10
CH4+C2H =  CH3+C2H2                 3.005E-12   0.0000        0.00
!
!     11
CH4+O =  CH3+OH                     1.200E-15   1.5600     4269.91
!
!     12
CH4+OH =  CH3+H2O                   2.607E-17   1.8300     1400.05
!
!     13
CH4+HO2 =  CH3+H2O2                 1.499E-11   0.0000    12440.46
!
!     14
2C2H2 =  H2CCCCH+H                  3.321E-15   0.0000    29107.53
!
!     15
C2H2+O2 =  C2H+HO2                  1.992E-11   0.0000    37527.06
!
!     16
H2+C2H =  C2H2+H                    1.793E-11   0.0000     1089.73
!
!     17
C2H2+H(+M) =  C2H3(+M)             1.400E-11   0.0000     1300.22
 N2/0.4/ O2/0.4/ CO/0.75/ CO2/1.5/ H2O/6.5/ CH4/3/ C2H6/3/
AR/0.35/
    LOW /  9.455E-30   0.00       739.72 /
    TROE /   1.0000E+00  1.0000E+00  1.0000E+00  1.2310E+03
/
!
!     18
```

```
C2H2+CH =  C2H+CH2                3.503E-10   0.0000     -61.34
!
!    19
C2H2+CH2 =  C3H4                  1.992E-11   0.0000    3330.53
!
!    20
C2H2+CH2(S) =  H2CCCH+H           2.906E-10   0.0000       0.00
!
!    21
C2H2+C2H =  C4H2+H                1.499E-10   0.0000       0.00
!
!    22
C2H2+O =  CH2+CO                  3.603E-18   2.1000     790.23
!
!    23
C2H2+O =  HCCO+H                  8.401E-18   2.1000     790.23
!
!    24
C2H2+OH =  C2H+H2O                9.962E-11   0.0000    6499.88
!
!    25
C2H2+M =  C2H+H+M                 1.893E-07   0.0000   53764.73
 N2/0.4/ O2/0.4/ CO/0.75/ CO2/1.5/ H2O/6.5/ CH4/3/ C2H6/3/
AR/0.35/
!
!    26
C2H4+H =  C2H3+H2                 8.999E-10   0.0000    7500.60
!
!    27
C2H4+H(+M) =  C2H5(+M)            6.591E-15   1.2800     649.51
 N2/0.4/ O2/0.4/ CO/0.75/ CO2/1.5/ H2O/6.5/ CH4/3/ C2H6/3/
AR/0.35/
     LOW /  3.721E-29   0.00      380.08 /
     TROE /   7.6000E-01  4.0000E+01  1.0250E+03 /
!
!    28
C2H4+CH =  C3H4+H                 2.192E-10   0.0000    -173.20
!
!    29
C2H4+CH2(S) =  C3H6               1.601E-10   0.0000       0.00
!
!    30
C2H4+CH3 =  CH4+C2H3              6.907E-12   0.0000    5600.19
!
!    31
C2H4+O =  H+CH2HCO                7.870E-18   1.8800      90.21
!
!    32
C2H4+O =  CH3+HCO                 1.350E-17   1.8800      90.21
!
!    33
C2H4+O =  CH2CO+H2               1.129E-18   1.8800      90.21
!
!    34
C2H4+OH =  C2H3+H2O               3.404E-11   0.0000    2990.14
!
```

```
!    35
C2H4+M =  C2H2+H2+M              1.655E-07   0.0000   36001.92
 N2/0.4/ O2/0.4/ CO/0.75/ CO2/1.5/ H2O/6.5/ CH4/3/ C2H6/3/
AR/0.35/
!
!    36
C2H4+M =  C2H3+H+M               1.229E-06   0.0000   48603.56
 N2/0.4/ O2/0.4/ CO/0.75/ CO2/1.5/ H2O/6.5/ CH4/3/ C2H6/3/
AR/0.35/
!
!    37
C2H6+H =  C2H5+H2               2.407E-15   1.5000    3729.85
!
!    38
C2H6+CH =  C2H4+CH3            1.793E-10   0.0000    -132.31
!
!    39
C2H6+CH2(S) =  CH3+C2H5        3.985E-10   0.0000       0.00
!
!    40
C2H6+CH3 =  C2H5+CH4           2.507E-31   6.0000    3043.06
!
!    41
C2H6+O =  C2H5+OH              1.660E-15   1.5000    2920.38
!
!    42
C2H6+OH =  C2H5+H2O            1.200E-17   2.0000     435.41
!
!    43
C2H6+HO2 =  H2O2+C2H5          2.192E-11   0.0000   10299.49
!
!    44
C4H2+O =  C3H2+CO              1.310E-11   0.0000     678.37
!
!    45
C4H2+OH =  C3H2+HCO            1.109E-11   0.0000    -205.68
!
!    46
O2+CO =  CO2+O                 2.092E-11   0.0000   23682.94
!
!    47
O2+CH2O =  HCO+HO2             9.995E-11   0.0000   20460.67
!
!    48
O2+C =  CO+O                   1.992E-10   0.0000    2009.86
!
!    49
O2+H+M =  HO2+M                                      5.789E-30
-0.8000       0.00
 N2/0.67/ O2/0.4/ CO/0.75/ CO2/1.5/ H2O/0/ CH4/3/ C2H6/3/
AR/0.28/
!
!    50
O2+H+H2O =  HO2+H2O            1.899E-32   0.0000   -1050.04
!
!    51
```

```
O2+H =  OH+O                    1.620E-10   0.0000    7470.53
!
!      52
O2+CH =  CO+OH                  2.756E-11   0.0000       0.00
!
!      53
O2+CH =  CO2+H                  2.756E-11   0.0000       0.00
!
!      54
O2+CH2 =  CO2+H2               9.015E-12   0.0000     750.54
!
!      55
O2+CH2 =  CO2+2H              9.015E-12   0.0000     750.54
!
!      56
O2+CH2 =  CO+OH+H            1.353E-11   0.0000     750.54
!
!      57
O2+CH2 =  CO+H2O             2.457E-12   0.0000     750.54
!
!      58
O2+CH2 =  CH2O+O              6.973E-12   0.0000     750.54
!
!      59
O2+CH2(S) =  CO+OH+H         5.197E-11   0.0000       0.00
!
!      60
O2+CH3 =  CH2O+OH            5.496E-13   0.0000    4500.84
!
!      61
O2+C2H =  HCCO+O             1.503E-11   0.0000       0.00
!
!      62
O2+C2H =  CO2+CH             1.503E-11   0.0000       0.00
!
!      63
O2+C2H3 =  C2H2+HO2         8.999E-12   0.0000       0.00
!
!      64
O2+C2H5 =  C2H4+HO2         1.694E-14   0.0000   -1100.55
!
!      65
O2+C3H2 =  HCO+HCCO         1.660E-11   0.0000       0.00
!
!      66
O2+H2CCCH =  CH2CO+HCO      4.998E-14   0.0000    1443.35
!
!      67
O2+HCO =  HO2+CO             4.998E-12   0.0000       0.00
!
!      68
O2+CH3O =  CH2O+HO2          3.603E-14   0.0000     880.44
!
!      69
O2+CH2OH =  CH2O+HO2         2.607E-09  -1.0000       0.00
DUPLICATE
```

```
!
!     70
O2+CH2OH  =  CH2O+HO2            1.200E-10   0.0000   1800.58
DUPLICATE
!
!     71
O2+HCCO  =  2CO+OH               2.706E-12   0.0000    430.60
!
!     72
H2O2+H  =  HO2+H2                2.806E-12   0.0000   1889.58
!
!     73
H2O2+H  =  OH+H2O                1.694E-11   0.0000   1800.58
!
!     74
H2O2+O  =  OH+HO2                1.099E-12   0.0000   2000.24
!
!     75
H2O2+OH  =  H2O+HO2              1.300E-11   0.0000    669.95
!
!     76
2OH(+M)  =  H2O2(+M)             1.200E-10  -0.3700      0.00
 N2/0.4/ O2/0.4/ CO/0.75/ CO2/1.5/ H2O/6.5/ CH4/3/ C2H6/3/
AR/0.35/
    LOW /  1.524E-28  -0.76       0.00 /
    TROE /   1.0000E+00  1.0000E+00  1.0000E+00  1.0400E+03
/
!
!     77
CO+O+M  =  CO2+M                 4.245E-33   0.0000   1510.70
 N2/0.4/ O2/0.4/ CO/0.75/ CO2/1.5/ H2O/6.5/ CH4/3/ C2H6/3/
AR/0.35/
!
!     78
CO+OH  =  CO2+H                  2.756E-17   1.3000   -384.89
!
!     79
CO+HO2  =  CO2+OH                2.507E-10   0.0000  11910.03
!
!     80
CO+CH  =  HCCO                   4.599E-13   0.0000   -860.00
!
!     81
CO2+CH  =  HCO+CO                5.695E-12   0.0000    345.20
!
!     82
CO2+CH2  =  CH2O+CO              3.902E-14   0.0000      0.00
!
!     83
CH2O+H  =  HCO+H2                2.092E-16   1.6200   1089.73
!
!     84
CH2O+CH  =  CH2+HCO              1.601E-10   0.0000   -259.80
!
!     85
CH2O+CH3  =  CH4+HCO             1.300E-31   6.1000    989.90
```

```
!
!    86
CH2O+O =  HCO+OH                6.907E-13   0.5700    1390.43
!
!    87
CH2O+OH =  HCO+H2O              5.695E-15   1.1800    -224.92
!
!    88
CH2O+HO2 =  H2O2+HCO            4.998E-12   0.0000    6580.47
!
!    89
CH2O+M =  HCO+H+M               2.324E+12  -5.5400   48662.50
 N2/0.4/ O2/0.4/ CO/0.75/ CO2/1.5/ H2O/6.5/ CH4/3/ C2H6/3/
AR/0.35/
!
!    90
CH2O+M =  H2+CO+M               5.413E+12  -5.5400   48662.50
 N2/0.4/ O2/0.4/ CO/0.75/ CO2/1.5/ H2O/6.5/ CH4/3/ C2H6/3/
AR/0.35/
!
!    91
CH2CO+H =  CH3+CO               3.005E-11   0.0000    1699.54
!
!    92
CH2CO+O =  CH2+CO2             2.208E-12   0.0000     679.58
!
!    93
CH2CO+O =  CH2O+CO             7.604E-13   0.0000     679.58
!
!    94
CH2CO+O =  HCO+H+CO            4.184E-13   0.0000     679.58
!
!    95
CH2CO+O =  2HCO               4.184E-13   0.0000     679.58
!
!    96
CH2CO+OH =  CH3+CO2            4.184E-12   0.0000       0.00
!
!    97
CH2CO+OH =  CH2OH+CO          7.770E-12   0.0000       0.00
!
!    98
CH2CO+M =  CH2+CO+M           1.091E-08   0.0000   28990.86
 N2/0.4/ O2/0.4/ CO/0.75/ CO2/1.5/ H2O/6.5/ CH4/3/ C2H6/3/
AR/0.35/
!
!    99
CH2CO+M =  HCCO+H+M           1.893E-15   0.0000       0.00
 N2/0.4/ O2/0.4/ CO/0.75/ CO2/1.5/ H2O/6.5/ CH4/3/ C2H6/3/
AR/0.35/
!
!   100
C+CH2 =  C2H+H                8.302E-11   0.0000       0.00
!
!   101
C+CH3 =  C2H2+H               8.302E-11   0.0000       0.00
```

```
!
!   102
C+OH =  CO+H                      8.302E-11   0.0000      0.00
!
!   103
2H+M =  H2+M                      5.155E-30  -1.0000      0.00
 N2/0.4/ O2/0.4/ CO/0.75/ CO2/1.5/ H2O/6.5/ CH4/3/ H2/0/
C2H6/3/ AR/0.35/
!
!   104
2H+H2 =  2H2                      2.699E-31  -0.6000      0.00
!
!   105
H+CH =  C+H2                      1.400E-11   0.0000      0.00
!
!   106
H+CH2 =  CH+H2                    9.995E-12   0.0000   -899.69
!
!   107
H+CH2(S) =  CH2+H                 3.321E-10   0.0000      0.00
!
!   108
H+CH3(+M) =  CH4(+M)              2.803E-10   0.0000      0.00
 N2/0.4/ O2/0.4/ CO/0.75/ CO2/1.5/ H2O/6.5/ CH4/3/ C2H6/3/
AR/0.35/
    LOW /  3.881E-24  -1.80        0.00 /
    TROE /   3.7000E-01  3.3150E+03  6.1000E+01 /
!
!   109
H+C2H3 =  C2H2+H2                 1.992E-11   0.0000      0.00
!
!   110
2CH3 =  C2H5+H                    4.998E-11   0.0000   6800.58
!
!   111
H+O+M =  OH+M                     3.253E-29  -1.0000      0.00
 N2/0.4/ O2/0.4/ CO/0.75/ CO2/1.5/ H2O/6.5/ CH4/3/ C2H6/3/
AR/0.35/
!
!   112
H+OH+M =  H2O+M                   1.524E-25  -2.0000      0.00
 N2/0.4/ O2/0.4/ CO/0.75/ CO2/1.5/ H2O/2.54/ CH4/3/ C2H6/3/
AR/0.15/
!
!   113
H+HO2 =  H2+O2                    7.106E-11   0.0000    709.65
!
!   114
H+HO2 =  2OH                      2.806E-10   0.0000    440.22
!
!   115
H+HO2 =  H2O+O                    4.998E-11   0.0000    866.01
!
!   116
H+HCO =  CO+H2                    1.499E-10   0.0000      0.00
!
```

```
!   117
H+CH3O =  CH2O+H2              3.005E-11  0.0000       0.00
!
!   118
H+CH2OH =  CH3+OH              1.694E-11  0.0000       0.00
!
!   119
H+CH2OH =  CH2O+H2             5.114E-11  0.0000       0.00
!
!   120
H+HCCO =  CH2+CO               2.507E-10  0.0000       0.00
!
!   121
CH+CH2 =  C2H2+H               6.641E-11  0.0000       0.00
!
!   122
CH+CH3 =  C2H3+H               4.981E-11  0.0000       0.00
!
!   123
CH+C2H3 =  CH2+C2H2            8.302E-11  0.0000       0.00
!
!   124
CH+O =  CO+H                   6.591E-11  0.0000       0.00
!
!   125
CH+OH =  HCO+H                 4.981E-11  0.0000       0.00
!
!   126
CH+HCCO =  C2H2+CO             8.302E-11  0.0000       0.00
!
!   127
2CH2 =  C2H2+H2                1.992E-11  0.0000     400.53
!
!   128
2CH2 =  C2H2+2H                1.793E-10  0.0000     400.53
!
!   129
CH2+CH3 =  C2H4+H              7.006E-11  0.0000       0.00
!
!   130
CH2+C2H3 =  C2H2+CH3           3.005E-11  0.0000       0.00
!
!   131
CH2+O =  CO+2H                 1.195E-10  0.0000       0.00
!
!   132
CH2+O =  CO+H2                 7.969E-11  0.0000       0.00
!
!   133
CH2+OH =  CH2O+H               3.005E-11  0.0000       0.00
!
!   134
CH2+HCO =  CH3+CO              3.005E-11  0.0000       0.00
!
!   135
CH2+HCCO =  C2H3+CO            4.981E-11  0.0000       0.00
```

```
!
!    136
CH2+HCCO =  C2H+CH2O              1.660E-11   0.0000     1006.74
!
!    137
CH2(S)+M =  CH2+M                 2.507E-11   0.0000        0.00
 N2/0.4/ O2/.4/ CO/.75/ CO2/1.5/ H2O/6.5/ CH4/.48/ C2H2/3.2/
C2H4/1.6/
 C2H6/1.44/ AR/.24/
!
!    138
2CH3(+M) =  C2H6(+M)             5.994E-11   0.0000        0.00
 N2/0.4/ O2/0.4/ CO/0.75/ CO2/1.5/ H2O/6.5/ CH4/3/ C2H6/3/
AR/0.35/
    LOW /  1.001E-06  -7.00    1390.43 /
    TROE /  6.2000E-01  7.3000E+01  1.1800E+03 /
!
!    139
CH3+O =  CH2O+H                   1.400E-10   0.0000        0.00
!
!    140
CH3+OH =  CH2(S)+H2O              1.200E-10   0.0000     1400.05
!
!    141
CH3+HO2 =  CH3O+OH               2.989E-11   0.0000        0.00
!
!    142
CH3+HCO =  CH4+CO                1.992E-10   0.0000        0.00
!
!    143
CH3+M =  CH2+H+M                  4.831E-08   0.0000    45602.60
 N2/0.4/ O2/0.4/ CO/0.75/ CO2/1.5/ H2O/6.5/ CH4/3/ C2H6/3/
AR/0.35/
!
!    144
C2H+C2H3 =  2C2H2                 3.155E-11   0.0000        0.00
!
!    145
C2H+O =  CH+CO                    1.660E-11   0.0000        0.00
!
!    146
C2H+OH =  HCCO+H                  3.321E-11   0.0000        0.00
!
!    147
C2H+OH =  CH2+CO                  3.005E-11   0.0000        0.00
!
!    148
C2H3+O =  CO+CH3                  4.981E-11   0.0000        0.00
!
!    149
C2H3+OH =  C2H2+H2O               8.302E-12   0.0000        0.00
!
!    150
C2H5+O =  CH2O+CH3                1.099E-10   0.0000        0.00
!
!    151
```

```
H2CCCH+O =  C2H2+CO+H              2.308E-10   0.0000        0.00
!
!    152
H2CCCH+OH =  C3H2+H2O              3.321E-11   0.0000        0.00
!
!    153
H2CCCCH+M =  C4H2+H+M              1.860E-08   0.0000    23408.71
 N2/0.4/ O2/0.4/ CO/0.75/ CO2/1.5/ H2O/6.5/ CH4/3/ C2H6/3/
AR/0.35/
!
!    154
2O+M =  O2+M                      1.489E-34   0.0000     -899.69
 N2/0.4/ O2/0.4/ CO/0.75/ CO2/1.5/ H2O/6.5/ CH4/3/ C2H6/3/
AR/0.35/
!
!    155
O+HO2 =  O2+OH                    5.296E-11   0.0000        0.00
!
!    156
O+HCO =  CO+OH                    4.998E-11   0.0000        0.00
!
!    157
O+HCO =  CO2+H                    4.998E-11   0.0000        0.00
!
!    158
O2+CH3 =  CH3O+O                  7.305E-11   0.0000    15801.06
!
!    159
O+CH3O =  CH2O+OH                 3.005E-12   0.0000        0.00
!
!    160
O+CH2OH =  CH2O+OH                1.499E-10   0.0000        0.00
!
!    161
O+HCCO =  H+2CO                   1.601E-10   0.0000        0.00
!
!    162
2OH =  O+H2O                      2.507E-15   1.1400       50.52
!
!    163
OH+HO2 =  H2O+O2                  4.798E-11   0.0000     -250.18
!
!    164
OH+HCO =  H2O+CO                  1.694E-10   0.0000        0.00
!
!    165
OH+CH3O =  CH2O+H2O               3.005E-11   0.0000        0.00
!
!    166
OH+CH2OH =  CH2O+H2O              4.001E-11   0.0000        0.00
!
!    167
OH+HCCO =  2HCO                   1.660E-11   0.0000        0.00
!
!    168
OH+HCCO =  CH2O+CO                1.660E-11   0.0000        0.00
```

```
!
!   169
2HO2 =  H2O2+O2                  7.006E-10   0.0000    6030.79
DUPLICATE
!
!   170
2HO2 =  H2O2+O2                  2.192E-13   0.0000    -820.30
DUPLICATE
!
!   171
2HCO =  CH2O+CO                  4.998E-11   0.0000       0.00
!
!   172
HCO+M =  H+CO+M                  7.455E-10   0.0000    7930.00
 N2/0.4/ O2/0.4/ CO/0.75/ CO2/1.5/ H2O/6.5/ CH4/3/ C2H6/3/
AR/0.35/
!
!   173
CH3O+M =  CH2O+H+M               2.573E-10   0.0000    6790.95
 N2/0.4/ O2/0.4/ CO/0.75/ CO2/1.5/ H2O/6.5/ CH4/3/ C2H6/3/
AR/0.35/
!
!   174
CH2OH+M =  CH2O+H+M              2.092E-08   0.0000   15107.05
 N2/0.4/ O2/0.4/ CO/0.75/ CO2/1.5/ H2O/6.5/ CH4/3/ C2H6/3/
AR/0.35/
!
!   175
2HCCO =  C2H2+2CO                1.660E-11   0.0000       0.00
!
!   176
H2+CN =  HCN+H                   3.204E-20   2.8700     820.06
!
!   177
CH4+N =  NH+CH3                  1.660E-11   0.0000   12076.02
!
!   178
CH4+CN =  HCN+CH3               1.499E-19   2.6400    -149.99
!
!   179
O2+N =  NO+O                     1.499E-14   1.0000    3270.27
!
!   180
O2+NH =  HNO+O                   6.492E-11   0.0000    9000.36
!
!   181
O2+NH =  NO+OH                   1.260E-13   0.0000     769.79
!
!   182
O2+NH2 =  HNO+OH                 2.507E-12  -0.3900   18166.95
!
!   183
O2+NH2 =  H2NO+O                 1.826E-06  -1.3400   16908.83
!
!   184
O2+CN =  NCO+O                   1.200E-11   0.0000    -210.01
```

```
!
!    185
O2+NCO =  NO+CO2                2.856E-17  0.0000    -369.26
!
!    186
CO+N2O =  CO2+N2                1.622E-13  0.0000    8780.37
!
!    187
CO2+N =  NO+CO                  3.155E-13  0.0000    1710.01
!
!    188
N2+CH =  HCN+N                  2.607E-12  0.0000    9030.31
!
!    189
N2+CH2 =  HCN+NH               1.660E-11  0.0000   37240.80
!
!    190
NO+N2O =  N2+NO2               1.660E-10  0.0000   25000.00
!
!    191
NO+N2H2 =  N2O+NH2             4.981E-12  0.0000       0.00
!
!    192
NO+C =  CN+O                   3.204E-11  0.0000       0.00
!
!    193
NO+C =  CO+N                   4.798E-11  0.0000       0.00
!
!    194
NO+H => N+OH                   3.603E-10  0.0000   24909.79
!
!    195
N+OH => NO+H                   4.699E-11  0.0000       0.00
!
!    196
NO+CH =  CO+NH                 1.992E-11  0.0000       0.00
!
!    197
NO+CH =  CN+OH                 1.992E-11  0.0000       0.00
!
!    198
NO+CH =  HCN+O                 1.594E-10  0.0000       0.00
!
!    199
NO+CH2 =  HOCN+H              2.308E-12  0.0000    -553.28
!
!    200
NO+CH2(S) =  HCN+OH          1.601E-10  0.0000       0.00
!
!    201
NO+CH3 =  HCN+H2O             1.540E-12  0.0000    8409.31
!
!    202
NO+CH3 =  H2CN+OH             1.540E-12  0.0000    8409.31
!
!    203
```

```
NO+HO2 =  NO2+OH                 3.470E-12   0.0000    -240.56
!
!   204
NO+HO2 =  HNO+O2                 3.321E-13   0.0000     999.52
!
!   205
NO+HCCO =  HOCN+CO               3.321E-11   0.0000       0.00
!
!   206
NO+N => N2+O                     7.106E-11   0.0000     790.23
!
!   207
N2+O => NO+N                     3.005E-10   0.0000   38300.46
!
!   208
NO+NH =  N2+OH                   5.313E-11   0.0000    6400.05
!
!   209
NO+NH =  N2O+H                   6.910E-10  -0.4500       0.00
!
!   210
NO+NH2 =  NNH+OH                 4.001E-09  -1.1700       0.00
!
!   211
NO+NH2 =  N2+H2O                 9.098E-09  -1.1700       0.00
!
!   212
NO+NNH =  N2+HNO                 8.302E-11   0.0000       0.00
!
!   213
NO+HNO =  N2O+OH                 4.900E-19   0.0000       0.00
!
!   214
NO+NCO =  N2O+CO                 2.308E-06  -1.7300     380.08
!
!   215
NO+M =  N+O+M                    6.019E-09   0.0000   74648.78
 CH4/3/ H2O/6.5/ CO2/1.5/ CO/0.75/ O2/0.4/ N2/0.4/ AR/0.35/
!
!   216
2NO2 =  2NO+O2                   3.321E-12   0.0000   13500.12
!
!   217
NO2+H =  NO+OH                   5.761E-10   0.0000     739.72
!
!   218
NO2+O =  NO+O2                   1.660E-11   0.0000     301.90
!
!   219
NO2+N =  2NO                     1.340E-12   0.0000       0.00
!
!   220
NO2+N =  N2O+O                   1.660E-12   0.0000       0.00
!
!   221
NO2+NH =  HNO+NO                 1.660E-13   0.5000    2000.24
```

```
!
!   222
NO2+NH =  N2O+OH              1.612E-11   0.0000       0.00
!
!   223
NO2+NH2 =  N2O+H2O            3.370E-07  -1.7000       0.00
!
!   224
NO2+CN =  NCO+NO              4.981E-11   0.0000       0.00
!
!   225
NO2+M =  NO+O+M               5.202E-08   0.0000   32999.76
 CH4/3/ H2O/6.5/ CO2/1.5/ CO/0.75/ O2/0.4/ N2/0.4/ AR/0.35/
!
!   226
N2O+C =  CN+NO               8.501E-12   0.0000       0.00
!
!   227
N2O+H =  N2+OH               7.256E-10   0.0000    9499.64
!
!   228
N2O+O =  N2+O2               1.660E-10   0.0000   14100.31
!
!   229
N2O+O =  2NO                 1.149E-10   0.0000   13400.29
!
!   230
N2O+OH =  N2+HO2             1.048E-12   0.0000    5000.00
!
!   231
N2O+N =  N2+NO               1.660E-11   0.0000   10000.00
!
!   232
N2O+NH =  HNO+N2             3.321E-12   0.0000    2999.76
!
!   233
N2O+CN =  NCO+N2             1.660E-11   0.0000       0.00
!
!   234
N2O+M =  N2+O+M              4.743E-09   0.0000   30190.04
 CH4/3/ H2O/6.5/ CO2/1.5/ CO/0.75/ O2/0.4/ N2/0.4/ AR/0.35/
!
!   235
NH3+H =  NH2+H2              8.999E-19   2.4000    4990.38
!
!   236
NH3+O => NH2+OH             1.601E-11   0.0000    3669.71
!
!   237
NH3+OH =  NH2+H2O            5.247E-12   0.0000    1010.34
!
!   238
NH3+HO2 =  NH2+H2O2          4.167E-12   0.0000   12000.24
!
!   239
NH3+NH2 =  N2H3+H2           1.318E-12   0.5000   10850.37
```

```
!
!   240
NH3(+M) =  NH2+H(+M)              8.300E+15  0.0000  55169.59
 CH4/3/ H2O/6.5/ CO2/1.5/ CO/0.75/ O2/0.4/ N2/0.4/ AR/0.35/
    LOW / 2.115E-08   0.00   41562.42 /
    TROE /  4.2000E-01  4.5810E+03  1.0200E+02 /
!
!   241
NH3+M =  NH+H2+M                  2.994E-09  0.0000  47001.44
 CH4/3/ H2O/6.5/ CO2/1.5/ CO/0.75/ O2/0.4/ N2/0.4/ AR/0.35/
!
!   242
N2H2+H =  NNH+H2                  1.660E-11  0.0000    500.36
!
!   243
N2H2+O =  NH2+NO                  1.660E-11  0.0000      0.00
!
!   244
N2H2+O =  NNH+OH                  1.660E-13  0.5000      0.00
!
!   245
N2H2+OH =  NNH+H2O                1.660E-11  0.0000   1000.00
!
!   246
N2H2+NH =  NNH+NH2               1.660E-11  0.0000    500.36
!
!   247
N2H2+NH2 =  NH+N2H3             1.660E-13  0.5000  16995.43
!
!   248
N2H2+NH2 =  NH3+NNH             1.660E-11  0.0000   2000.24
!
!   249
N2H2+M =  NNH+H+M                 4.151E-08  0.0000  24993.99
 CH4/3/ H2O/6.5/ CO2/1.5/ CO/0.75/ O2/0.4/ N2/0.4/ AR/0.35/
!
!   250
N2H2+M =  2NH+M                   1.313E-07  0.0000  50000.00
 CH4/3/ H2O/6.5/ CO2/1.5/ CO/0.75/ O2/0.4/ N2/0.4/ AR/0.35/
!
!   251
C2N2+O =  NCO+CN                  2.142E-10  0.0000   7130.14
!
!   252
C2N2+OH =  HOCN+CN               3.105E-13  0.0000   1447.80
!
!   253
HCN+O =  NCO+H                    1.403E-18  2.1000   3075.54
!
!   254
HCN+O =  NH+CO                    5.296E-19  2.1000   3075.54
!
!   255
HCN+O =  CN+OH                    3.686E-19  2.1000   3075.54
!
!   256
```

```
HCN+OH  =   CN+H2O                  1.499E-11   0.0000    5400.53
!
!    257
HCN+OH  =   HOCN+H                  9.713E-20   2.4000    6290.59
!
!    258
HCN+OH  =   HNCO+H                  3.287E-27   4.0000     502.77
!
!    259
HCN+CN  =   C2N2+H                  6.309E-17   1.5700      49.31
!
!    260
HOCN+H  =   H2O+CN                  1.660E-12   0.0000       0.00
!
!    261
HOCN+H  =   H2+NCO                  1.660E-12   0.0000       0.00
!
!    262
HOCN+H  =   HNCO+H                  1.660E-11   0.0000       0.00
!
!    263
HNCO+H  =   NCO+H2                  3.404E-10  -0.2700   10190.04
!
!    264
HNCO+H  =   NH2+CO                  1.826E-10   0.0000    6398.85
!
!    265
HNCO+O  =   NH+CO2                  3.321E-11   0.0000    6550.40
!
!    266
HNCO+O  =   HNO+CO                  3.155E-12   0.0000    5184.03
!
!    267
HNCO+O  =   OH+NCO                  3.321E-10   0.0000   11599.71
!
!    268
HNCO+OH  =   NCO+H2O                3.304E-12   0.0000    2788.07
!
!    269
HNCO+OH  =   NH2+CO2                1.099E-12   0.0000    2788.07
!
!    270
HNCO+HO2  =   NCO+H2O2             4.981E-11   0.0000   14594.66
!
!    271
HNCO+N  =   NH+NCO                  6.608E-11   0.0000   17999.76
!
!    272
HNCO+NH  =   NH2+NCO                4.981E-11   0.0000   11926.87
!
!    273
HNCO+NH2  =   NH3+NCO               1.660E-12   0.0000    3500.12
!
!    274
HNCO+M  =   NH+CO+M                 3.990E-08   0.0000   42641.33
 CH4/3/ H2O/6.5/ CO2/1.5/ CO/0.75/ O2/0.4/ N2/0.4/ AR/0.35/
```

```
!
!   275
HNCO+M =  H+NCO+M                  4.743E-07  0.0000   56402.45
 CH4/3/ H2O/6.5/ CO2/1.5/ CO/0.75/ O2/0.4/ N2/0.4/ AR/0.35/
!
!   276
H+NH =  N+H2                       1.694E-11  0.0000      0.00
!
!   277
H+NH2 =  NH+H2                     9.995E-12  0.0000      0.00
!
!   278
H+NNH =  N2+H2                     6.608E-11  0.0000   1499.88
!
!   279
H+N2H3 =  2NH2                     2.623E-12  0.0000      0.00
!
!   280
H+N2H3 =  NH+NH3                   1.660E-13  0.0000      0.00
!
!   281
H+N2H3 =  N2H2+H2                  1.660E-12  0.0000   1000.00
!
!   282
H+HNO =  H2+NO                     2.092E-11  0.0000   2000.24
!
!   283
H+NCO =  NH+CO                     8.700E-11  0.0000      0.00
!
!   284
CH+N =  CN+H                       2.092E-11  0.0000      0.00
!
!   285
CH+NH =  HCN+H                     8.302E-11  0.0000      0.00
!
!   286
CH+NH2 =  HCN+2H                   4.981E-11  0.0000      0.00
!
!   287
CH2+N =  HCN+H                     8.302E-11  0.0000      0.00
!
!   288
CH2+NH =  HCN+2H                   4.981E-11  0.0000      0.00
!
!   289
CH3+N =  H2CN+H                    4.300E-10  0.0000    419.77
!
!   290
C2H3+N =  HCN+CH2                  3.321E-11  0.0000      0.00
!
!   291
H2CCCH+N =  HCN+C2H2              1.660E-11  0.0000      0.00
!
!   292
O+NH =  N+OH                       6.176E-11  0.0000      0.00
!
```

```
!   293
O+NH =   NO+H                        9.132E-11   0.0000       0.00
!
!   294
O+NH2 =   NH+OH                      1.146E-12   0.3500    -101.03
!
!   295
O+NH2 =   HNO+H                      1.483E-09  -0.4890     163.58
!
!   296
O+NNH =   N2+OH                      1.660E-11   0.0000    2500.60
!
!   297
O+NNH =   N2O+H                      1.660E-11   0.0000    1499.88
!
!   298
O+NNH =   NH+NO                      2.739E-10  -0.2300    -509.98
!
!   299
O+HNO =   OH+NO                      8.318E-13   0.5000     999.52
!
!   300
O+CN =   CO+N                        1.694E-11   0.0000       0.00
!
!   301
O+NCO =   NO+CO                      5.250E-11   0.0000       0.00
!
!   302
OH+NH =   HNO+H                      1.660E-12   0.5000    1000.00
!
!   303
OH+NH =   N+H2O                      8.321E-13   0.5000    1000.00
!
!   304
OH+NH2 => O+NH3                      3.304E-14   0.4050     250.18
!
!   305
OH+NH2 =   NH+H2O                    8.318E-13   0.5000    1000.00
!
!   306
OH+NNH =   N2+H2O                    5.247E-11   0.0000       0.00
!
!   307
OH+HNO =   NO+H2O                    1.793E-11   0.0000       0.00
!
!   308
OH+CN =   NCO+H                      1.000E-10   0.0000       0.00
!
!   309
OH+NCO =   NO+HCO                    8.302E-12   0.0000    7548.71
!
!   310
OH+NCO =   NO+CO+H                   1.660E-11   0.0000       0.00
!
!   311
HO2+NH2 =   HNO+H2O                  2.607E-11   0.0000       0.00
```

```
!
!    312
HCCO+N =  HCN+CO                    8.302E-11   0.0000        0.00
!
!    313
2N+M =  N2+M                        1.799E-32   0.0000        0.00
 CH4/3/ H2O/6.5/ CO2/1.5/ CO/0.75/ O2/0.4/ N2/0.4/ AR/0.35/
!
!    314
N+NH =  N2+H                        1.048E-12   0.5000        0.00
!
!    315
N+NH2 =  N2+2H                      1.150E-10   0.0000        0.00
!
!    316
N+NNH =  NH+N2                      5.247E-11   0.0000     1000.00
!
!    317
N+CN => C+N2                        3.005E-10   0.0000        0.00
!
!    318
C+N2 => N+CN                        8.700E-11   0.0000    22600.43
!
!    319
N+H2CN =  N2+CH2                    3.321E-11   0.0000        0.00
!
!    320
N+NCO =  NO+CN                      4.599E-06  -0.9900     8690.16
!
!    321
N+NCO =  N2+CO                      3.304E-11   0.0000        0.00
!
!    322
2NH =  N2+2H                        8.517E-11   0.0000        0.00
!
!    323
NH+NH2 =  N2H2+H                    2.507E-09  -0.5000        0.00
!
!    324
NH+NNH =  N2+NH2                    3.321E-13   0.5000      999.52
!
!    325
NH+M =  N+H+M                       1.257E-09   0.0000    37999.76
 CH4/3/ H2O/6.5/ CO2/1.5/ CO/0.75/ O2/0.4/ N2/0.4/ AR/0.35/
!
!    326
2NH2 =  N2H2+H2                     6.608E-11   0.0000     5999.52
!
!    327
2NH2 =  NH3+NH                      8.302E-11   0.0000     5032.48
!
!    328
NH2+M =  NH+H+M                     1.313E+00  -2.0000    45994.71
 CH4/3/ H2O/6.5/ CO2/1.5/ CO/0.75/ O2/0.4/ N2/0.4/ AR/0.35/
!
!    329
```

```
NH2+NNH =  N2+NH3                 1.660E-11   0.0000      0.00
!
!   330
NH2+HNO =  NH3+NO                 8.318E-13   0.5000    500.36
!
!   331
NNH =  N2+H                       3.000E+08   0.0000      0.00
!
!   332
NNH+M =  N2+H+M                   4.151E-11   0.5000   1539.57
CH4/3/ H2O/6.5/ CO2/1.5/ CO/0.75/ O2/0.4/ N2/0.4/ AR/0.35/
!
!   333
NNH+O2 =  N2+HO2                  8.302E-12   0.0000      0.00
!
!   334
N2H3+M =  N2H2+H+M                4.151E-08   0.0000  25000.00
 CH4/3/ H2O/6.5/ CO2/1.5/ CO/0.75/ O2/0.4/ N2/0.4/ AR/0.35/
!
!   335
N2H3+M =  NH2+NH+M                4.151E-08   0.0000  21000.72
 CH4/3/ H2O/6.5/ CO2/1.5/ CO/0.75/ O2/0.4/ N2/0.4/ AR/0.35/
!
!   336
HNO+M =  H+NO+M                   8.451E-08   0.0000  24499.64
 CH4/3/ H2O/6.5/ CO2/1.5/ CO/0.75/ O2/0.4/ N2/0.4/ AR/0.35/
!
!   337
H2CN+M =  HCN+H+M                 1.245E-09   0.0000  11071.69
 CH4/3/ H2O/6.5/ CO2/1.5/ CO/0.75/ O2/0.4/ N2/0.4/ AR/0.35/
!
!   338
NCO+M =  N+CO+M                   4.838E-09   0.0000  23500.12
 CH4/3/ H2O/6.5/ CO2/1.5/ CO/0.75/ O2/0.4/ N2/0.4/ AR/0.35/
!
!   339
H2O+CH =  CH2O+H                  9.497E-12   0.0000   -380.08
!
!   340
H2S+M =  S+H2+M                   2.656E+00  -2.6100  44800.00
 N2/1.5/ SO2/10/ H2O/10/
!
!   341
H2S+H =  SH+H2                    1.992E-17   2.1000    350.00
!
!   342
H2S+O =  SH+OH                    1.245E-16   1.7500   1460.00
!
!   343
H2S+OH =  SH+H2O                  4.483E-12   0.0000      0.00
!
!   344
H2S+S =  2SH                      1.378E-10   0.0000   3700.00
!
!   345
H2S+S =  HS2+H                    3.321E-11   0.0000   3723.84
```

```
!
!   346
S+H2 =  SH+H                    2.324E-10   0.0000    9700.00
!
!   347
SH+O =  H+SO                    1.660E-10   0.0000       0.00
!
!   348
SH+OH =  S+H2O                  1.660E-11   0.0000       0.00
!
!   349
SH+HO2 =  HSO+OH                1.660E-12   0.0000       0.00
!
!   350
SH+O2 =  HSO+O                  3.155E-11   0.0000    9000.00
!
!   351
S+OH =  H+SO                    6.641E-11   0.0000       0.00
!
!   352
S+O2 =  SO+O                    8.634E-18   1.8100    -600.00
!
!   353
2SH =  S2+H2                    1.660E-12   0.0000       0.00
!
!   354
SH+S =  S2+H                    1.660E-11   0.0000       0.00
!
!   355
S2+M =  2S+M                    7.969E-11   0.0000   38800.00
!
!   356
S2+H+M =  HS2+M                 2.757E-32   0.0000       0.00
 N2/1.5/ SO2/10/ H2O/10/
!
!   357
S2+O =  SO+S                    1.660E-11   0.0000       0.00
!
!   358
HS2+H =  S2+H2                  1.992E-17   2.1000     352.42
!
!   359
HS2+O =  S2+OH                  1.245E-16   1.8000    1460.00
!
!   360
HS2+OH =  S2+H2O                4.483E-12   0.0000       0.00
!
!   361
HS2+S =  S2+SH                  1.378E-10   0.0000    3700.00
!
!   362
HS2+H+M =  H2S2+M               2.757E-32   0.0000       0.00
 N2/1.5/ SO2/10/ H2O/10/
!
!   363
H2S2+H =  HS2+H2                1.992E-17   2.1000     360.00
```

```
!
!    364
H2S2+O =  HS2+OH               1.245E-16   1.8000    1460.00
!
!    365
H2S2+OH =  HS2+H2O             4.483E-12   0.0000       0.00
!
!    366
H2S2+S =  HS2+SH               1.378E-10   0.0000    3700.00
!
!    367
SO3+H =  HOSO+O                4.151E-19   2.9200   25300.00
!
!    368
SO3+O =  SO2+O2                3.321E-12   0.0000   10000.00
!
!    369
SO3+SO =  2SO2                 1.660E-12   0.0000    5000.00
!
!    370
SO+O(+M) =  SO2(+M)            5.313E-11   0.0000       0.00
 N2/1.5/ SO2/10/ H2O/10/
     LOW / 3.308E-27  -1.54       0.00 /
     TROE /  5.5000E-01  1.0000E-30  1.0000E+30 /
!
!    371
SO2+O(+M) =  SO3(+M)           1.527E-13   0.0000    1200.00
     LOW / 6.616E-20  -4.00   2640.00 /
!
!    372
SO2+OH(+M) =  HOSO2(+M)        8.406E-12  -0.2500       0.00
     LOW / 4.653E-21  -4.09       0.00 /
     TROE /  1.0000E+00  1.0000E+30  4.1200E+02 /
!
!    373
SO2+OH =  HOSO+O               6.475E-16   1.8900   38200.00
!
!    374
SO2+OH =  SO3+H                8.135E-22   2.6900   12000.00
!
!    375
SO2+CO =  SO+CO2               4.483E-12   0.0000   24300.00
!
!    376
SO+M =  S+O+M                  6.641E-10   0.0000   54000.00
 N2/1.5/ SO2/10/ H2O/10/
!
!    377
SO+H+M =  HSO+M                1.378E-32   0.0000       0.00
 N2/1.5/ SO2/10/ H2O/10/
!
!    378
HOSO(+M) =  SO+OH(+M)          9.940E+21  -2.5400   38190.00
     LOW / 1.919E+22  -9.02   26647.00 /
     TROE /  9.5000E-01  2.9890E+03  1.1000E+00 /
!
```

```
!   379
SO+OH =  SO2+H                    1.788E-07  -1.3500      0.00
!
!   380
SO+O2 =  SO2+O                    1.262E-20   2.3700   1500.00
!
!   381
2SO =  SO2+S                      3.321E-12   0.0000   2000.00
!
!   382
HSO+H =  HSOH                     4.151E-04  -3.1400    460.00
!
!   383
HSO+H =  SH+OH                    8.135E-05  -1.8600    785.00
!
!   384
HSO+H =  S+H2O                    2.656E-15   1.3700   -170.00
!
!   385
HSO+H =  H2SO                     2.989E-07  -2.4700     25.00
!
!   386
HSO+H =  H2S+O                    1.826E-18   1.0300   5230.00
!
!   387
HSO+H =  SO+H2                    1.660E-11   0.0000      0.00
!
!   388
HSO+O+M =  HSO2+M                 3.032E-29  -1.7300    -25.00
 N2/1.5/ SO2/10/ H2O/10/
!
!   389
HSO+O =  SO2+H                    7.471E-10  -0.4000      0.00
!
!   390
HSO+O+M =  HOSO+M                 1.902E-28  -1.6100    800.00
 N2/1.5/ SO2/10/ H2O/10/
!
!   391
HSO+O =  O+HOS                    7.969E-16   1.0200   2700.00
!
!   392
HSO+O =  OH+SO                    2.324E-11   0.1500    150.00
!
!   393
HSO+OH =  HOSHO                   8.634E+04  -5.4400   1600.00
!
!   394
HSO+OH =  HOSO+H                  8.800E-17   1.5700   1900.00
!
!   395
HSO+OH =  SO+H2O                  2.823E-15   1.0300    235.00
!
!   396
HSO+O2 =  SO2+OH                  1.660E-12   0.0000   5000.00
!
```

```
!   397
HSOH =  SH+OH                    2.800E+39  -8.7500   37800.00
!
!   398
HSOH =  S+H2O                    5.800E+29  -5.6000   27400.00
!
!   399
HSOH =  H2S+O                    9.800E+16  -3.4000   43500.00
!
!   400
H2SO =  H2S+O                    4.900E+28  -6.6600   36000.00
!
!   401
H+SO2(+M) =  HOSO(+M)            5.178E-16   1.6100    3606.00
    LOW /  7.338E-10  -6.43    5577.00 /
    TROE /   8.2000E-01  1.3088E+05  2.6600E+02 /
!
!   402
HOSO+M =  O+HOS+M                4.151E+06  -4.8000   60000.00
!
!   403
HOSO+H =  SO2+H2                 4.981E-11   0.0000       0.00
!
!   404
HOSO+H =  SO+H2O                 1.046E-33   6.2900    -960.00
!
!   405
HOSO+OH =  SO2+H2O               1.660E-12   0.0000       0.00
!
!   406
HOSO+O2 =  HO2+SO2               1.660E-12   0.0000     500.00
!
!   407
HSO2+H =  SO2+H2                 4.981E-11   0.0000       0.00
!
!   408
HSO2+OH =  SO2+H2O               1.660E-11   0.0000       0.00
!
!   409
HSO2+O2 =  HO2+SO2               1.660E-11   0.0000       0.00
!
!   410
H+SO2(+M) =  HSO2(+M)            1.760E-15   1.4800     594.60
    LOW /  3.449E-17  -5.17    1563.00 /
    TROE /   4.5000E-01  9.3550E+02  4.2700E+01 /
!
!   411
HOSO2 =  HOSO+O                  5.400E+18  -2.3400   53500.00
!
!   412
HOSO2 =  SO3+H                   1.400E+18  -2.9100   27600.00
!
!   413
HOSO2+H =  SO2+H2O               1.660E-12   0.0000       0.00
!
!   414
```

```
HOSO2+O  =  SO3+OH              8.302E-12   0.0000        0.00
!
!    415
HOSO2+OH =  SO3+H2O             1.660E-12   0.0000        0.00
!
!    416
HOSO2+O2 =  HO2+SO3            1.295E-12   0.0000       330.00
!
!    417
HOSHO  =  HOSO+H               6.400E+30  -5.8900     37100.00
!
!    418
HOSHO  =  SO+H2O               1.200E+24  -3.5900     30000.00
!
!    419
HOSHO+H  =  HOSO+H2            1.660E-12   0.0000        0.00
!
!    420
HOSHO+O  =  HOSO+OH            8.302E-12   0.0000        0.00
!
!    421
HOSHO+OH =  HOSO+H2O           1.660E-12   0.0000        0.00
!
!    422
C+SO2  =  CO+SO                6.900E-11   0.0000        0.00
!
!    423
HOSO2+H  =  SO3+H2             1.660E-12   0.0000        0.00
!
!    424
S+CH4  =  SH+CH3               9.962E-10   0.0000     12078.42
!
!    425
H2S+CH3 =  CH4+SH              2.989E-13   0.0000      1177.53
!
!    426
SH+O  =  S+OH                  1.046E-12   0.5000      4030.55
!
!    427
C+H2S  =  CH+SH                1.992E-10   0.0000      4450.32
!
!    428
O+COS  =  CO+SO                3.204E-11   0.0000      2328.60
!
!    429
O+CS  =  CO+S                  2.700E-10   0.0000       760.16
!
!    430
COS+M  =  CO+S+M               2.374E-10   0.0000     30700.02
!
!    431
O+COS  =  CO2+S                8.302E-11   0.0000      5530.43
!
!    432
SH+O2  =  SO+OH                1.660E-12   0.0000      5032.48
!
```

```
!    433
CH+SO  =  CO+SH                1.660E-11   0.0000        0.00
!    434
SO3+S  =  SO+SO2               8.501E-13   0.0000        0.00
!    435
SH+NO  =  SN+OH                1.660E-11   0.0000     8900.65
!    436
S+NO  =  SN+O                  1.660E-12   0.5000    17500.60
!    437
SH+NH  =  SN+H2                1.660E-10   0.0000        0.00
!    438
N+SO  =  NO+S                  1.048E-12   0.5000     1010.34
!    439
N+SH  =  SN+H                  1.048E-12   0.5000     4030.55
!    440
SN+NO  =  N2+SO                3.000E-14   0.0000        0.00
!    441
SN+O2  =  SO+NO                4.981E-16   0.0000        0.00
!    442
SN+NO2  =  S+2NO              6.754E-09  -0.9805        0.00
!    443
N+SN  =  N2+S                  1.046E-12   0.5000        0.00
!    444
SO2+NO2  =  NO+SO3            7.056E-43   8.9000     3797.21
!    445
SO+NO2  =  SO2+NO             1.400E-11   0.0000        0.00
!    446
SN+O  =  SO+N                  1.048E-12   0.5000     4030.55
!    447
S+NH  =  SH+N                  1.660E-11   0.0000        0.00
!    448
NH+SO  =  NO+SH               5.001E-11   0.0000        0.00
!    449
HSO+NO2  =  HOSO+NO           9.630E-12   0.0000        0.00
!    450
SO3+H2O  =  H2SO4             1.200E-15   0.0000        0.00
!    451
HCL+OH  =  H2O+CL             4.491E-17   1.6500     -111.85
```

```
!
!  452
HCL+O =  OH+CL                    5.603E-21   2.8700    1770.00
END
```

Appendix III

Simplified scheme for the computations using FactSage.

```
┌─────────────────────────────────┐
│      EQUILIB/PHASE DIAGRAM       │
└─────────────────────────────────┘
                 │
                 ▼
      ┌─────────────────────┐
      │   Select Database   │
      └─────────────────────┘
                 │
                 ▼
      ┌─────────────────────┐
      │   Enter Reactants   │
      └─────────────────────┘
                 │
                 ▼
     ┌───────────────────────┐
     │ Define solution species│
     └───────────────────────┘
                 │
                 ▼
      ┌─────────────────────┐
      │   Specify variables  │
      └─────────────────────┘
                 │
                 ▼
      ┌─────────────────────┐
      │   Select parameters  │
      └─────────────────────┘
                 │
                 ▼
        ┌─────────────────┐
        │    Calculate    │
        └─────────────────┘
```